

THE SPATIAL RESPONSE  
OF A MULTIPLYING SYSTEM TO  
A PERIODIC NEUTRON SOURCE

By

Alvaro GIL RAMOS, M.Sc., D.I.C.

A thesis submitted to the UNIVERSITY OF ASTON  
IN BIRMINGHAM for the Degree of

DOCTOR OF PHILOSOPHY

THESIS  
539-17  
GIL

176298 - 4 SEP 1974

July, 1974

DEPARTMENT OF PHYSICS

## SUMMARY

The source transfer function has been measured in a natural uranium-light water moderated sub-critical assembly as a function of source frequency and position. A square wave input of fast neutrons from the D-T reaction was supplied by a SAMES type J accelerator suitably modified for the purpose. Thermal neutrons inside the assembly were detected with lithium glass scintillation counters and the time variation of the detector outputs was recorded on a multi-channel analyser used in the time sequence storage mode and synchronised with the source pulsing frequency. By Fourier analysing the recorded waveform the source transfer function was found. An attempt was also made to determine the source transfer function by detecting the prompt gamma radiation from fission.

Two theoretical models were used to determine the spatially dependent source transfer function for a system similar to the experimental one. The first was a multigroup, multi-region two dimensional approach based on diffusion theory and Telegrapher's equation which used a standard static computer code(SNAP) to obtain the transfer function at chosen frequencies. The other was based on the time-dependent Fermi Age and diffusion theory and was limited to a single region description of the system. Both methods

gave good agreement with each other and with experiment but the first method showed an upper frequency limit of 400 Hz due to solution methods used in the code.

## ACKNOWLEDGMENTS

I should like to thank my supervisor, Dr. P.N. Cooper for his invaluable guidance and help throughout the course of this work.

Thanks are also due to Professor S.E. Hunt for his interest in this study.

I wish to express my gratitude to the technical staff of the main workshop and the nuclear laboratory. I am particularly indebted to Messrs. H. Arrowsmith, F. Lane, J. Phull and H. Biggs.

Finally, I would like to express my appreciation for the one year research studentship awarded by the British Council.

Birmingham, 1974.

A. Gil Ramos

## TABLE OF CONTENTS

	<u>Page</u>
SUMMARY	i
ACKNOWLEDGMENTS	iii
LIST OF FIGURES	vii
LIST OF TABLES	xv
 Chapter	
1. INTRODUCTION	1
2. EXPERIMENTAL EQUIPMENT	7
2.1 Nuclear System	7
2.2 Neutron Generating System	8
2.2.1 The SAMES accelerator	9
2.2.2 Neutron source modulation	12
2.3 Detection and data acquisition systems	17
2.3.1 Neutron detectors	19
2.3.2 Gamma detectors	24
2.3.2.1 Gamma detector shielding	27
2.3.3 Data acquisition system	29
3. ANALYSIS OF EXPERIMENTAL DATA AND EXPERIMENTAL RESULTS	44
3.1 Loss of data due to analyser	44
3.2 Harmonic Analysis	47
3.2.1 Numerical determination of Fourier Coefficients	48
3.3 Computer Program DATACOR	51
3.4 Experimental results	53

Chapter	<u>Page</u>
4. THEORY	66
4.1 Complex Source Method	66
4.1.1 Two-group diffusion treatment	69
4.1.2 Two-group Telegrapher's treatment	71
4.1.3 Method of solution	74
4.2 Fermi Age-Diffusion method	80
5. RESULTS	87
5.1 Complex Source Method	87
5.2 Fermi Age - Diffusion method	92
5.3 Comparison between theoretical methods	101
5.4 Comparison between theoretical and experimental results	115
5.5 Lumped parameter approximation	125
6. GAMMA MEASUREMENTS	128
6.1 Experimental arrangement	130
6.2 Results and Conclusions	131
7. CONCLUSIONS AND RECOMMENDATIONS	138
7.1 Conclusions	138
7.2 Recommendations for future work	140

	<u>Page</u>
Appendix	
1      Published work	141
2      Computer program DATACOR	143
3      Computer program FERMI	168
REFERENCES	180

## LIST OF FIGURES

<u>Figure</u>		<u>Page</u>
2.1	The SAMES accelerator	10
2.2	Diagram of the SAMES accelerator	11
2.3	Driver and Transmitter circuit	15
2.4	Receiver and Pulsing System Circuit	15
2.5	SAMES 100 MHz. R.F. oscillator showing link with pulsing system	18
2.6	Neutron detectors located inside the subcritical assembly	23
2.7	Gamma detector located outside the subcritical assembly	30
2.8	Block diagram of the experimental set-up	
2.9	Dual input gate circuit	33
2.10	Start and reset unit circuit	35
2.11	Neutron detectors response at 1 Hz	38
2.12	Neutron detectors response at 50 Hz	38
2.13	Neutron detectors response at 150 Hz	38
2.14	Neutron detectors response at 250 Hz	38
2.15	Neutron detectors response at 500 Hz	39
2.16	Neutron detectors response at 1000 Hz	39
2.17	Neutron detectors response at 1500 Hz	39
2.18	Neutron detectors response at 2000 Hz	39
2.19	Neutron and gamma detectors response at 1 Hz	40
2.20	Neutron and gamma detectors response at 50 Hz	40
2.21	Neutron and gamma detectors response at 150 Hz	40

<u>Figure</u>	<u>Page</u>
2.22 Neutron and gamma detectors response at 200 Hz	40
2.23 Neutron and gamma detectors response at 250 Hz	41
2.24 Neutron and gamma detectors response at 500 Hz	41
2.25 Neutron and gamma detectors response at 1000 Hz	41
2.26 Data acquisition system and associated equipment	43
3.1 Experimental transfer function showing the contribution of different harmonics	55
3.2 Experimental transfer function showing the contribution of different harmonics	56
3.3 Amplitude response for different axial positions	58
3.4 Amplitude response for different axial positions	58
3.5 Amplitude response for different radial positions	59
3.6 Amplitude response for different radial positions	59
3.7 Measured variation in amplitude with axial position	60
3.8 Measured variation in amplitude with axial position	60
3.9 Measured variation in amplitude with axial position	61

<u>Figure</u>	<u>Page</u>
3.10 Measured variation in amplitude with axial position	61
3.11 Measured variation in amplitude with radial position	63
3.12 Measured variation in amplitude with radial position	63
3.13 Measured variation in amplitude with radial position	64
3.14 Measured variation in amplitude with radial position	64
3.15 Phase response for different axial positions	65
3.16 Phase response for different radial positions	65
5.1 Schematic diagram of the subcritical assembly as considered by both theoretical models	89
5.2 Comparison between Diffusion and Telegrapher's treatments	90
5.3 Comparison between Diffusion and Telegrapher's treatments	90
5.4 Theoretical amplitude response for different axial positions	91
5.5 Theoretical amplitude response for different axial positions	91
5.6 Theoretical amplitude response for different radial positions	93

<u>Figure</u>		<u>Page</u>
5.7	Theoretical amplitude response for different radial positions	93
5.8	Theoretical phase response for different axial positions	94
5.9	Theoretical phase response for different axial positions	94
5.10	Theoretical phase response for different radial positions	95
5.11	Theoretical phase response for different radial positions	95
5.12	Theoretical amplitude response for different axial positions	97
5.13	Theoretical amplitude response for different axial positions	97
5.14	Theoretical amplitude response for different axial positions	98
5.15	Theoretical amplitude response for different axial positions	98
5.16	Theoretical amplitude response for different radial positions	99
5.17	Theoretical amplitude response for different radial positions	99
5.18	Theoretical amplitude response for different radial positions	100
5.19	Theoretical amplitude response for different radial positions	100
5.20	Theoretical phase response for different axial positions	102

<u>Figure</u>		<u>Page</u>
5.21	Theoretical phase response for different axial positions	102
5.22	Theoretical phase response for different radial positions	103
5.23	Theoretical phase response for different radial positions	103
5.24	Comparison between the amplitude responses of the different theoretical models	109
5.25	Comparison between the amplitude responses of the different theoretical models	109
5.26	Comparison between the amplitude responses of the different theoretical models	110
5.27	Comparison between the amplitude responses of the different theoretical models	110
5.28	Comparison between the phase responses of the different theoretical models	111
5.29	Comparison between the phase responses of the different theoretical models	111
5.30	Comparison between the phase responses of the different theoretical models	112

<u>Figure</u>		<u>Page</u>
5.31	Comparison between the phase responses of the different theoretical models	112
5.32	Variation of the -3dB amplitude with thermal lifetime	114
5.33	Comparison between experimental and theoretical (Telegrapher's) results	116
5.34	Comparison between experimental and theoretical (Telegrapher's) results	116
5.35	Comparison between experimental and theoretical (Telegrapher's) results	117
5.36	Comparison between experimental and theoretical (Telegrapher's) results	117
5.37	Comparison between experimental and theoretical (Telegrapher's) results	118
5.38	Comparison between experimental and theoretical (Telegrapher's) results	118
5.39	Comparison between experimental and theoretical (Telegrapher's) results	119
5.40	Comparison between experimental and theoretical (Telegrapher's) results	119
5.41	Comparison between experimental and theoretical (Fermi-Diffusion) results	121
5.42	Comparison between experimental and theoretical (Fermi-Diffusion) results	121
5.43	Comparison between experimental and theoretical (Fermi-Diffusion) results	122

<u>Figure</u>		<u>Page</u>
5.44	Comparison between experimental and theoretical (Fermi-Diffusion) results	122
5.45	Comparison between experimental and theoretical (Fermi-Diffusion) results	123
5.46	Comparison between experimental and theoretical (Fermi-Diffusion) results	123
5.47	Comparison between experimental and theoretical (Fermi-Diffusion) results	124
5.48	Comparison between experimental and theoretical (Fermi-Diffusion) results	124
5.49	Comparison between lumped parameter and space dependent transfer function	127
5.50	Comparison between lumped parameter and space dependent transfer function	127
6.1	Experimental amplitude response	132
6.2	Comparison between neutron and gamma responses	133
6.3	Comparison between neutron and gamma responses	133
6.4	Experimental amplitude response for different axial positions	134

<u>Figure</u>		<u>Page</u>
6.5	Gamma detector response at 1 Hz	137
6.6	Gamma detector response at 250 Hz	137
6.7	Gamma detector response at 500 Hz	137
6.8	Gamma detector response at 1000 Hz	137

LIST OF TABLES

<u>Table</u>		<u>Page</u>
1	Summary of Nuclear Parameters of the Subcritical Assembly	8
2	Numerical values of the Amplitude as given by the different theoretical models and experiments. (H= 15 CMS.)	104
3	Numerical values of the Amplitude as given by the different theoretical models and experiments. (H= 30 CMS.)	105
4	Numerical values of the Amplitude as given by the different theoretical models and experiments. (H= 45 CMS.)	106
5	Numerical values of the Amplitude as given by the different theoretical models and experiments. (H= 60 CMS.)	107

CHAPTER 1

INTRODUCTION

Historically, subcritical assemblies have been used as static devices in which an equilibrium condition is maintained between the neutrons supplied by an external source, the neutrons produced in fission, the neutrons absorbed in the various materials of the assembly, and the neutrons that escape from the assembly. Such experiments give information about the infinite multiplication constant and diffusion parameters. However, the variation of the source strength in a pulsed manner has also been used extensively in determining neutron diffusion parameters since its early application by Manley et al (1)<sup>+</sup> in 1942. Moderators, in particular, have been studied repeatedly with this technique (2 to 6). Pulsed-neutron techniques have also been extensively used towards the determination of subcritical reactivities in Nuclear Systems as reported elsewhere (7, 8).

A supplement to the pulsed neutron experiments has been the neutron wave technique in which the neutron source strength varies in a regular periodic manner. The propagation of neutron waves in both moderating and multiplying media has been discussed by Weinberg and Schweinler (9) and Weinberg and Wigner (10). Experimental

---

<sup>+</sup> Underlined numbers in parenthesis refer to corresponding numbers in the list of references.

measurements of diffusion parameters in graphite and heavy water were performed by Raievski and Horowitz (11) and preliminary experiments in graphite and in water moderated subcritical assemblies have been performed by Uhrig (12, 13). Later, the propagation of a sinusoidal disturbance introduced into the neutron distribution of homogeneous and heterogeneous nuclear systems has been investigated experimentally by several workers and surveys of the relevant literature are available (14, 15).

The essential contribution to the field of Reactor Physics from these investigations is that the relative attenuation and phase shift of neutron waves excited by an external modulated-neutron source are strongly dependent upon the physical and nuclear properties of the medium through which the waves propagate. Such neutron wave experiments have been used to obtain information regarding the diffusion, absorption and thermalization properties of the media. Also, many elaborate theoretical works have been carried out for the understanding of the neutron-wave problem. Particular mention in this respect should be made of the work of Mortensen (16), Moore (17), Williams (18), Wood (19), Brehm (20) and Kunaish (21).

The general opinion is that there is no fundamental difference between neutron-wave propagation and neutron-pulse propagation from the point of view of the time-dependent diffusion and thermalization phenomena (22). However, the neutron wave technique

provides the advantage, compared with the pulsed-neutron experiments, that the method allows for two independent quantities to be measured, attenuation and phase shift.

From the standpoint of reactor control, the dynamic behaviour of a reactor (or indeed of any system) is customarily described by its response to small disturbances. This response as a function of the frequency of the disturbance is called the transfer function of the reactor.

The purpose of the present work is to study both theoretically and experimentally, the space-dependent transfer function of a nuclear system. The term transfer function is used here in its classical electrical-engineering sense as a relation between input and output. No connection is implied with the familiar reactivity transfer function of space-independent kinetics. Since reactivity is an integral or whole-reactor parameter, specification of the reactivity effect of an input does not uniquely specify the input in a space-dependent situation. (That is, a large number of different configuration changes could give rise to the same reactivity change, and yet induce completely different dynamic effects (23)). Therefore there is no such thing as a space-dependent reactivity transfer function.

The early studies on reactor transfer functions were derived from the time-dependent diffusion equation, after the spatial dependence had been removed by assuming that the flux shape was the fundamental spatial mode. The reactor was then treated as a lumped parameter model

(24, 25).

A reactor, however is not a lumped parameter system. The distance between the input and output devices, as well as their relative locations in the system, can have a large effect on the measured attenuation and phase shift of a disturbance as it propagates through the system. As higher frequencies are present and of interest, as in neutron wave and random noise experiments, the time and spatially dependent solution of the neutron flux behaviour is needed to adequately describe experimental results. The dispersive nature of the neutron wave propagation phenomena in both multiplying and non-multiplying media was observed in the late fifties by Uhrig (12). Later, Kylstra (26) and Cohn (27) provided further evidence, both theoretically and experimentally, of the space-dependent nature of the reactor transfer function.

The principal objective of this work was to select suitable models for the determination of the transfer function in a subcritical Nuclear System and then to test the validity of these models in a situation of practical interest. To accomplish this objective, two different theories were applied to determine analytically the source transfer functions for a nuclear system and special instrumentation was developed in order to correlate the theoretical results with those obtained experimentally.

Considerable effort was expended in improving the method for pulsing externally the S.A.M.E.S.

accelerator to produce a square beam current waveform with an operating frequency range from 1 Hz to about 2 kHz. This was used to produce a constant amplitude square-waveform source of fast neutrons from the D-D and D-T reactions. Since the square wave can be Fourier analysed into an infinite number of harmonics of the fundamental it can be considered as the superposition of harmonically related sinusoidal inputs and therefore the methods of analysis can be based on a sinusoidal input.

A natural uranium-light water moderated subcritical assembly was supplied with the square wave of fast neutrons produced by the S.A.M.E.S. accelerator. By varying the input frequency and by Fourier analyzing the system response at different locations, the transfer function of the subcritical assembly was measured as a function of frequency and space. Both neutron and gamma signals were detected by scintillation counters with lithium glass and NaI(Tl) scintillators respectively. These signals were fed into a multichannel pulse-height analyzer used in the time sequence storage mode. The experimental results, after analysis, have been compared with those obtained by both theoretical models.

This work has been organised as follows. In Chapter 2 a detailed description of the experimental equipment used is presented. Chapter 3 contains the methods developed for the analysis of the experimental data, also including some experimental results. The two different theoretical methods used to evaluate the spatially dependent transfer functions are presented in

Chapter 4. In Chapter 5 the theoretical results are summarized and compared with those obtained experimentally. Chapter 6 refers to an attempt made to determine experimentally the system transfer functions via photon observation. Finally, in Chapter 7, the principal conclusions drawn from this work are given. Also in this Chapter, a number of additional experiments and analytical studies are suggested to extend and complement the present work.

## CHAPTER 2

### EXPERIMENTAL EQUIPMENT

#### 2.1 Nuclear System.

The Nuclear System consisted of a light-water moderated, natural Uranium subcritical assembly. The natural Uranium was in the form of 196 cylindrical bars of outside diameter 29.2 mm., 813 mm. long and 10 kg. weight. These were inserted in aluminium cans 0.9 mm. thick and supported inside a stainless steel tank by two perspex fuel grids. The core shape was almost hexagonal with a triangular pitch of 45.2 mm.

The water level was the same height as the fuel rods, thus the core was unreflected on the top horizontal face. The vertical faces were reflected by water with thicknesses varying between 100 mm. and 270 mm. Water was periodically purified by means of an ion-exchange column. The stainless steel tank was placed on the top of a graphite pedestal 533 mm. high. This provided both slowing down material for the source neutrons and a bottom reflector for the subcritical assembly.

This arrangement had an effective core radius of 333 mm. and infinite multiplication factor of 0.996, calculated for a water to uranium volume ratio of 1.5:1. The volume fractions were,

$$U = 0.379, \quad Al = 0.048, \quad H_2O = 0.573$$

A summary of some of the most relevant nuclear parameters of the subcritical assembly is presented in Table 1.

Table 1: Summary of Nuclear Parameters

Parameter	Value	Units
K	0.996 <sup>+</sup>	--
B <sup>2</sup>	0.004135 <sup>+</sup>	cm <sup>-2</sup>
L <sup>2</sup>	3.61	cm <sup>2</sup>
L <sub>s</sub>	0.000013 <sup>+</sup>	secs.
P	0.729	--
β	0.0064 <sup>+++</sup>	--
λ	0.0079 <sup>+++</sup>	sec <sup>-1</sup>
ε	1.076 <sup>++</sup>	--
η	2.07	--
τ	40.6	cm <sup>2</sup>
T	20.0	eC

+ ref. 22

++ ref. 27

+++ ref. 28

A more comprehensive description of the subcritical assembly can be found in ref. (22).

## 2.2 Neutron Generating System.

Neutrons, at energies of 14 Mev or 2.5 Mev were produced using the T(d,n)He<sup>4</sup> and D(d,n)He<sup>3</sup> reactions with a deuteron beam of energy up to 150 Kev incident on a titanium-tritide target type TRT51 or a titanium-deuteride target type TRD51.

### 2.2.1 The S.A.M.E.S. accelerator.

The deuterium beam was furnished by the S.A.M.E.S. type J accelerator shown in Fig. (2.1). The accelerating voltage, produced by an electrostatic generator hermetically sealed in a hydrogen atmosphere can be varied from 0-160 Kv.

Fig. (2.2) shows details of the acceleration and beam electrodes together with the extraction system and ion source. Deuterium gas, from a reservoir, is admitted to the ion source through a thermally activated palladium leak. The ion source is excited by a 100 MHz oscillator and can produce currents on a target up to about 200  $\mu$ A under favourable conditions of steady running. Extraction into the acceleration system is effected by applying a 0-6 Kv repelling voltage to the electrode shown in Fig. (2.2). The ions are concentrated at the entrance of the extraction canal by the magnetic field of the coil located at the base of the ion source bottle. An oil immersed Cockcroft-Walton multiplier circuit supplies the 0-45 Kv required for beam focussing. These units, which are situated inside the high voltage terminal, are controlled through a system of isolation transformers that are fed from variable transformers.

The target assembly, which was inserted into the graphite pedestal and centrally placed 155 mm. below the base of the core, was coupled with the S.A.M.E.S. accelerator by means of a flight tube. A more detailed description of the flight tube is given in ref. (29).

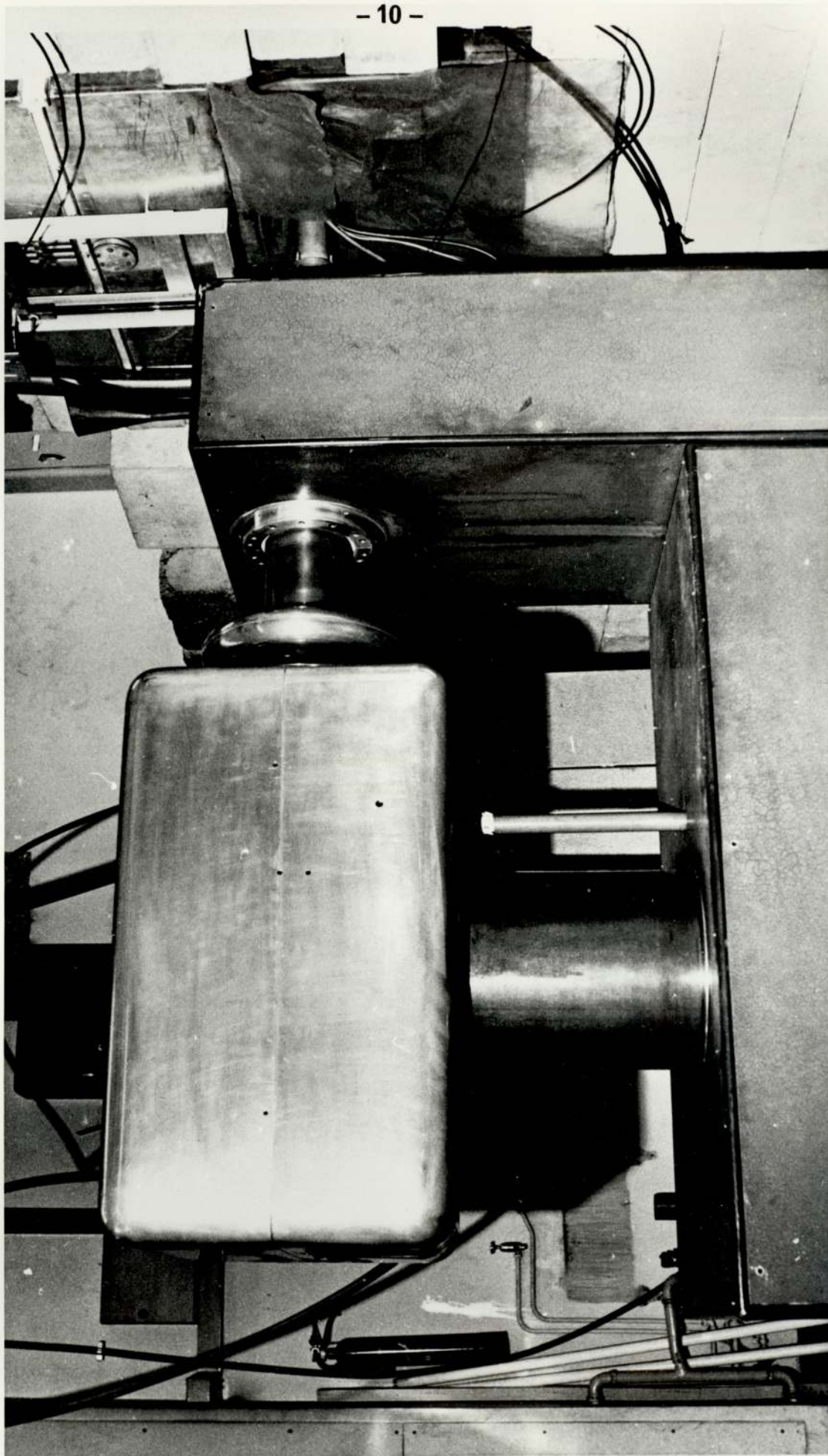


FIG. 2.1 THE SAMES ACCELERATOR

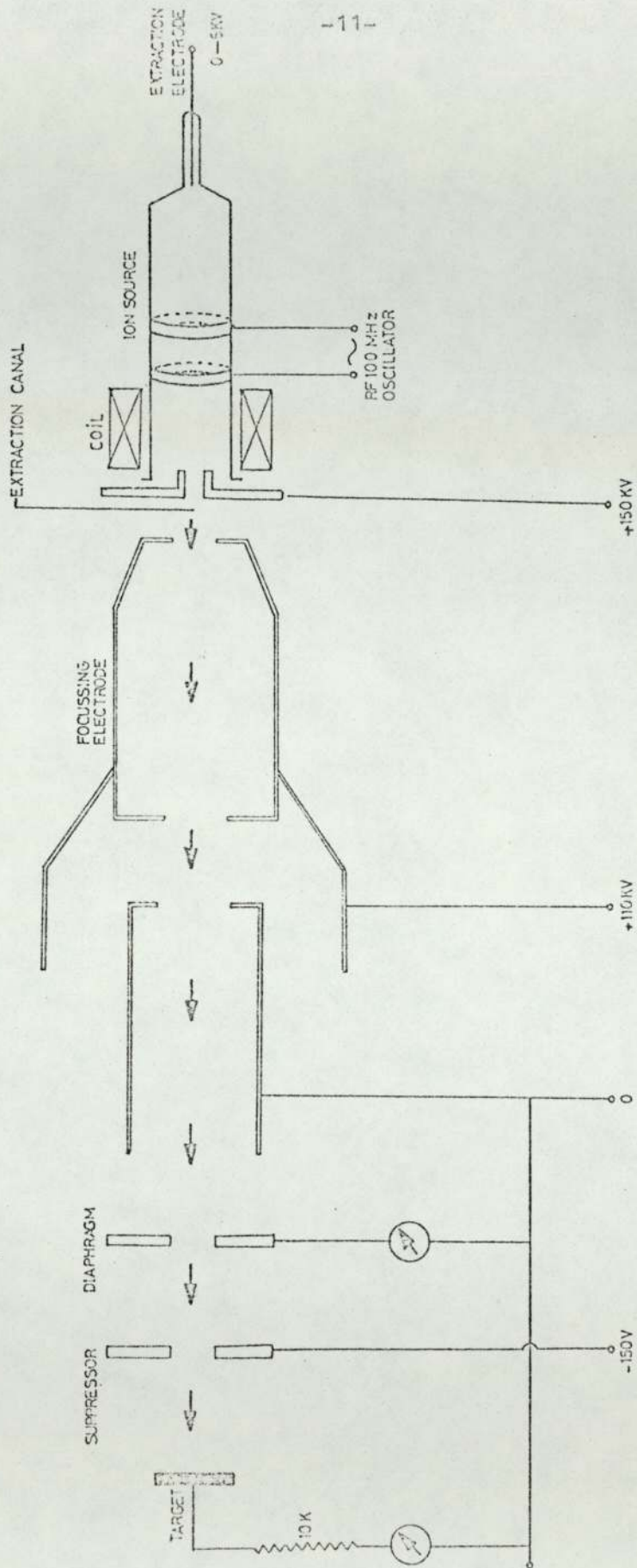


FIG. 2.2 DIAGRAM OF THE SAMES ACCELERATOR (NOT TO SCALE)

### 2.2.2 Neutron source modulation.

The nature of the present work, concerning the measurement of the transfer function in a subcritical assembly, requires a neutron population varying periodically with time. A sinusoidal variation would be best for analysis but for neutrons produced at an accelerator target, the nearest easily obtained waveform is a square wave.

One important aspect of the present measurement is that the output from the radiation detectors had to be sampled by a multiscaler at regular intervals during each cycle of the neutron pulse. Therefore the pulsing frequency had to be a submultiple of that controlling the channel-advance command of the analyzer. Therefore it was necessary to pulse the accelerator with an externally supplied signal in order to maintain synchronism.

Two main methods exist for producing a pulsed accelerator beam (30): post acceleration beam deflection and ion source pulsing. The latter can be achieved either by switching the radio frequency exciter or by pulsing the extraction electrode. Post-acceleration deflection was impossible with the present experimental arrangement due to lack of space.

Ion source pulsing involves transmitting a signal to the high voltage terminal containing the ion source through a potential difference of 150 Kv. This has been achieved by others (31) with a radio frequency signal but the risk of creating stray rf fields made it necessary to use a different method.

The method adopted was to transmit a light beam across the potential barrier, a technique previously proved to be successful when used with a 4 Mev Van de Graaff accelerator (32) and later when used with the S.A.M.E.S. accelerator in a previous experiment (22, 30). In the latter, a sharp light signal correspondent to the leading edge of a square pulse was produced by a gallium arsenide diode type MGA 100 and transmitted to the high voltage terminal of the accelerator to a light sensitive diode type LS400. This was done by means of a rigid, tight PVC tube which contained two lenses to improve light collection and provide adequate focusing to the LS 400 detector. This tube ran parallel to the main insulating column of the accelerator as can be seen in Fig. (2.1). The signal from the receiver diode was amplified and used to drive a bistable circuit which alternately rendered a power pentode type EL 84 conducting and nonconducting. This pentode was then used to ground the screen grid of the oscillator double tetrode type QQV06-40A and so switch the radio frequency.

For the present work, the modulated light beam was still used to transmit the signal to the high voltage terminal. Since the light emitting diode MGA 100 was obsolete, it was replaced by the more efficient type 1A48 which has an output of 40  $\mu$ w at 100 mA and a peak wave length of 930 nm. and which can be modulated at frequencies up to approximately 500 KHz. Also modifications have been made to the driving circuit so that the transmitted light pulse follows the shape of the driving pulse instead of producing a short light signal

coincident with the leading edge. The final circuit is given in fig. (2.3). Driving signals were taken directly from the output of a dividing circuit network constructed from SN 7490N and SN 7493N integrated circuits.

The bistable circuits, originally used to drive the switching pentode was found to be over-sensitive to supply voltage variations when run for long periods. Consequently it did not always respond to the trigger pulse. In order to overcome this, the bistable circuit and the switching pentode were replaced by a single high voltage n-p-n transistor type BU 105. The base of this was driven by a square wave voltage signal derived from the transmitted light signal which was received by the n-p-n planar silicon photo-device LS 400 and subsequently amplified by means of the SN 72748P integrated circuit. The complete circuit diagram is shown in fig. (2.4). It was found necessary to include adequate screening and filtering against the intense radio frequency signals produced by the ion-source oscillator. One advantage of this method is that the beam pulse is always in phase with the transmitted pulse whereas previously the phases could differ by  $180^\circ$ , depending on the initial state of the bistable.

When the base of the BU105 is made positive the transistor conducts. In this mode, two different ways can be followed to shut off the ion source radio frequency. The first method, which was used in the original S.A.M.E.S pulsing unit, consists in reducing the voltage of the oscillator screen grid to near earth. This leaves the full high tension on the anode and on the coupling straps

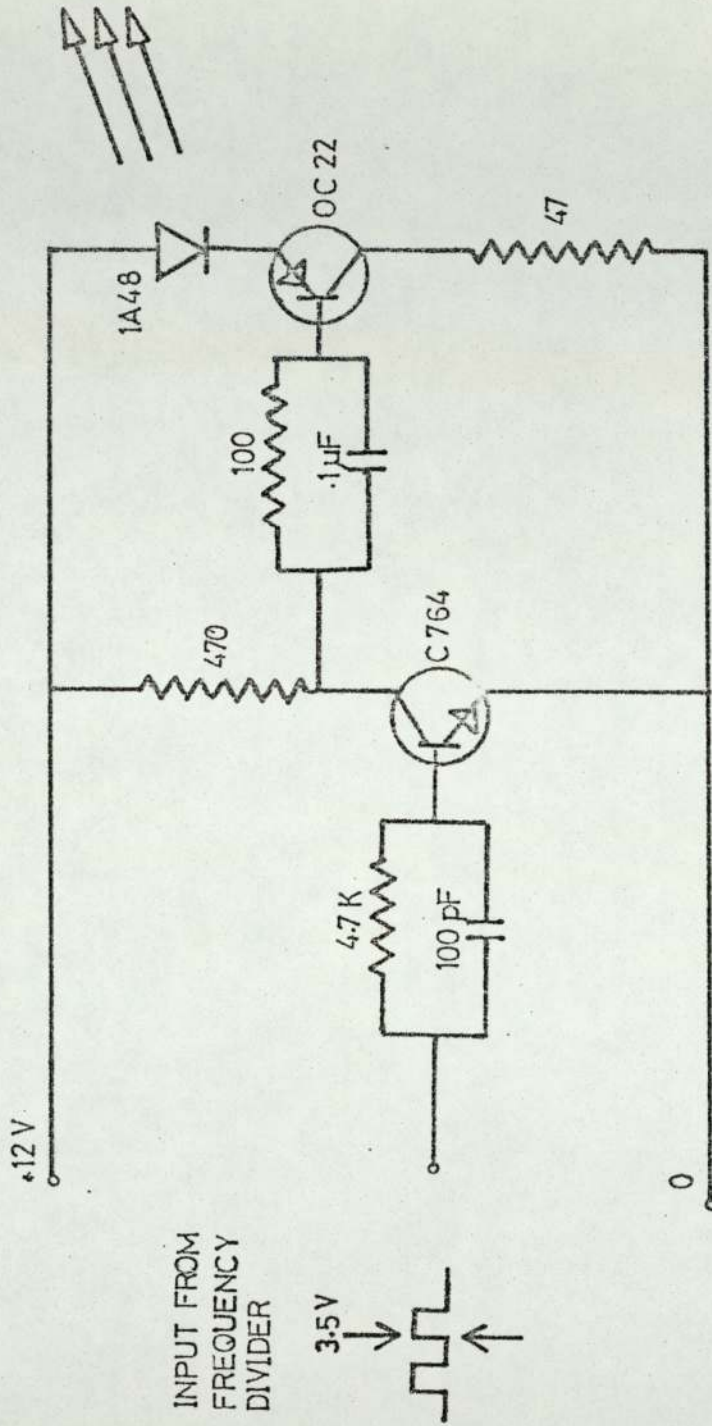


FIG.2.3 DRIVER AND TRANSMITTER CIRCUIT



of the ion source bottle. In consequence, the plasma, under certain combinations of gas pressure and high tension voltage, may not always extinguish completely thus giving some ion current during the off period of the cycle. An alternative which has proved to be consistently reliable, was to use the BU 105 to short the high tension supply to the whole oscillator to ground. As shown in fig. (2.5) a 2k 100 W wirewound resistor was inserted into the high tension lead between the power pack and the BU 105 to act as a current limiter.

This method of pulsing can be easily adapted to any desired rectangular waveform where the on period differs from the off period, simply by applying the appropriate waveform to the input of the transmitter. For an applied square wave the system has been found to operate reliably in the range of frequencies 1HZ to 2000 HZ.

Since this method of pulsing the accelerator no longer includes the pulsing unit designed by S.A.M.E.S., it can be adapted to other accelerators.

Details of the pulsing system have been published (33) as shown in Appendix 1.

### 2.3 Detection and data acquisition systems.

The variation of the neutron and gamma populations of the subcritical assembly were monitored by means of the detection and data acquisition systems. The major components of these were the radiation detectors with their associated amplifiers and discriminators and the data acquisition unit.

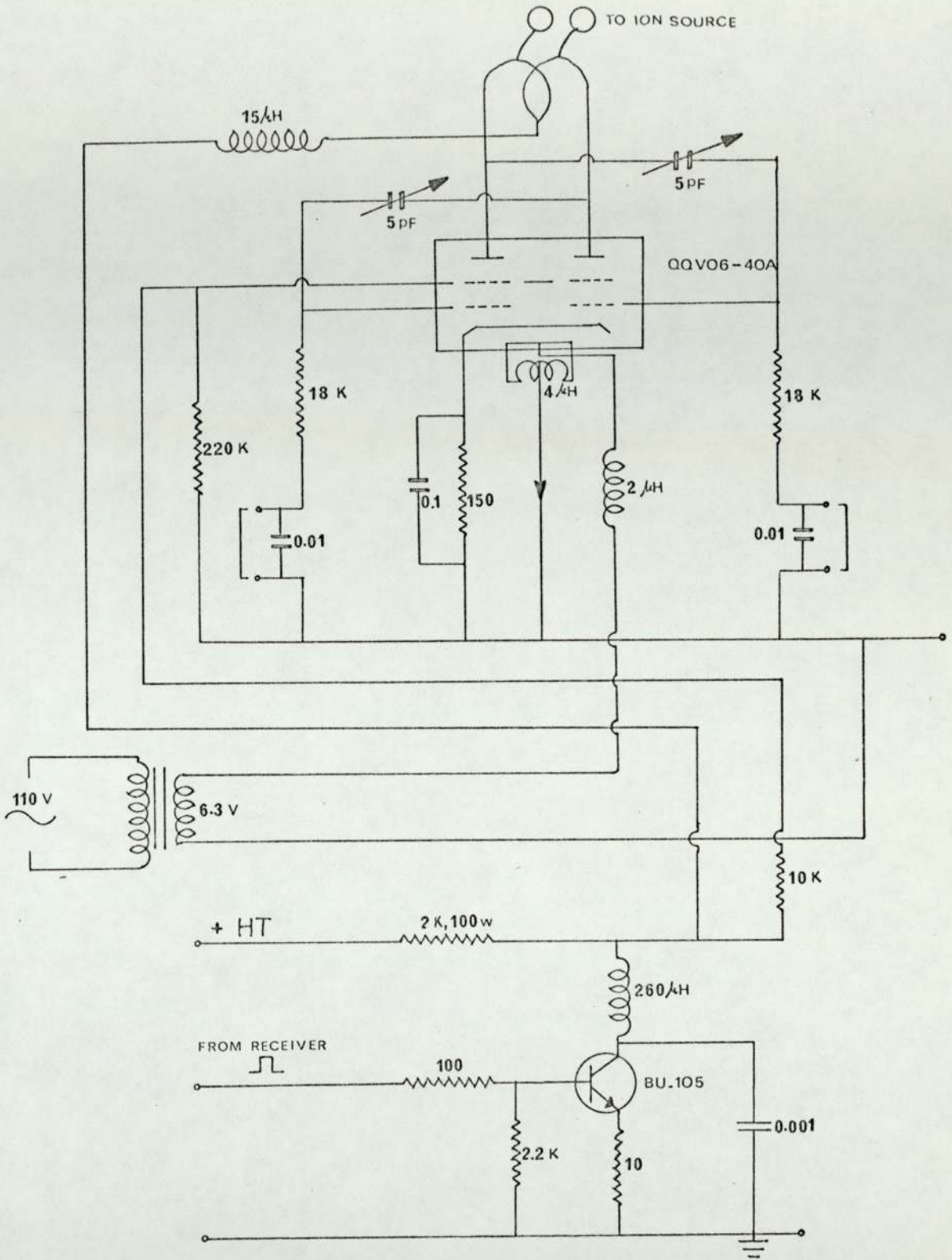


FIG. 2.5 SAMES 100 MHZ R.F. OSCILLATOR SHOWING LINK WITH PULSING SYSTEM

An important feature of the detection system was that two detectors were used simultaneously. One of them, a neutron detector, was always placed at different heights in the central line of the assembly. The other one, either a neutron or a gamma detector, was placed in the same plane but at different radial positions. This permitted the direct comparison of phase and amplitude between different detector positions and the repeated centreline measurements also were a good measure of reproducibility of the results.

A good consistency was achieved; both amplitude and phase lag correspondent to different runs were found to be in a range of  $\pm 2$  per cent. This deviation would be in part due to the detection system itself and the statistical nature of the data, and in part also to the different running conditions of the accelerator.

### 2.3.1 Neutron detectors.

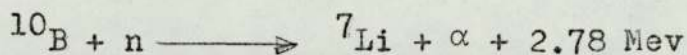
The main requirements for the neutron detectors were:

- (i) High thermal neutron efficiency.
- (ii) Very low efficiency for other types of radiation, i.e. fast neutrons and gamma rays.
- (iii) Small volume.

In order to achieve this, the following detectors were considered.

(1) BF<sub>3</sub> Counter.

The reaction



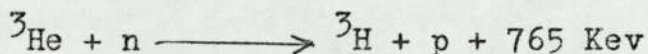
is widely used for thermal neutron detection (34). The cross section of the reaction is 3840 barns at  $2.2 \times 10^3$  m/sec. and follows the  $1/v$  law for energies less than 30 Kev (35). The reaction is easy to detect even in the presence of high gamma fluxes because of the high specific ionization and the large energy of the charged particles which are released.

Because of the drop in the cross section for the  $\text{B}^{10} (\text{n}, \alpha)$  reaction with an increase in neutron energy, the sensitivity of this detector is very small for fast neutrons.

The main disadvantage of the  $\text{BF}_3$  detector is that large volumes of active counter are required in order to obtain a reasonable efficiency.

(2)  $^3\text{He}$  detector chamber.

$^3\text{He}$  undergoes the following reaction,



This reaction has rather ideal properties for neutron detection and particularly for neutron spectroscopy (34). The cross section, starting at 5400 barns for thermal neutrons, varies smoothly over the entire energy range, having no resonances. The efficiency for thermal neutrons (36) is up to 20 times that of a  $\text{BF}_3$  counter of the same size. The major disadvantage, apart from the size, arises from the elastic

scattering of neutrons by  $\text{He}^3$ , which has a cross section approximately twice that of the  $\text{He}^3$  (n,p) reaction.

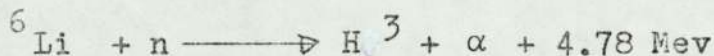
(3) Fission chamber.

The fission reaction is important in nuclear-radiation detection by using either the kinetic energy of the fission products or their resulting radioactivity.

Fission chambers containing the thermal fissionable nuclei  $^{233}\text{U}$ ,  $^{235}\text{U}$  or  $^{239}\text{Pu}$  are efficient thermal-neutron detectors. Their cross sections follow more or less a  $\frac{1}{v}$  dependence in the thermal neutron region. Also, the large energy released per reaction makes it possible to discriminate against much larger fluxes of gamma rays than with detectors employing the (n,  $\alpha$ ) or similar reactions (37). On the other hand, their sensitivity is rather low, for example (38), a  $\text{B}^{10}$  counter can be built to have a sensitivity of one to two orders of magnitude higher than that of a fission chamber of the same physical dimensions.

(4)  $^6\text{Li}$  Glass scintillator.

$^6\text{Li}$  undergoes the following reaction:



The cross section for this reaction is 936 barn at  $2.2 \times 10^5$  cm/sec and follows the  $\frac{1}{v}$  law up to 1Kev. The scattering cross section for thermal neutrons is 1.4 barn.

The main advantage of lithium detectors is that they are highly efficient. For example (32), a 1 cm. thick crystal made from natural lithium has an efficiency of 69% for thermal neutrons. The major disadvantage is that the scintillator has about the same efficiency for both

electrons and alpha particles, thus the pile-up of gamma ray pulses can give serious trouble at high gamma ray levels. This disadvantage can be avoided by using very thin crystals highly enriched in  $\text{Li}^6$ .

As a result of compromise between efficiency, size and gamma and fast neutron discrimination,  $\text{Li}^6$  glass scintillators were selected for the present measurements. They consisted of Cerium activated lithium silicate glass (type NE 905) containing 6.6% lithium enriched in  $\text{Li}^6$  to 95%, size 25.4 mm. x 3 mm. They were optically coupled to EMI 9524B photomultipliers and housed inside tight aluminium tubes identical to those used for canning the natural uranium. They could thus be inserted in place of a fuel rod. Neutron streaming was minimized by filling the aluminium tube with a solid, centrally hollowed polypropylene rod. Both high tension and signal were conveyed through the central hole with a coaxial cable.

Fig. (2.6) shows the neutron detectors located in different axial and radial positions inside the system. They were suspended by a sliding aluminium collar resting on the top of the fuel elements and fixed parallel to them by means of perspex rings.

The signals from the photomultipliers were fed into charge sensitive amplifier-discriminator units type NM 115. High tension was provided by two NM 120 units.

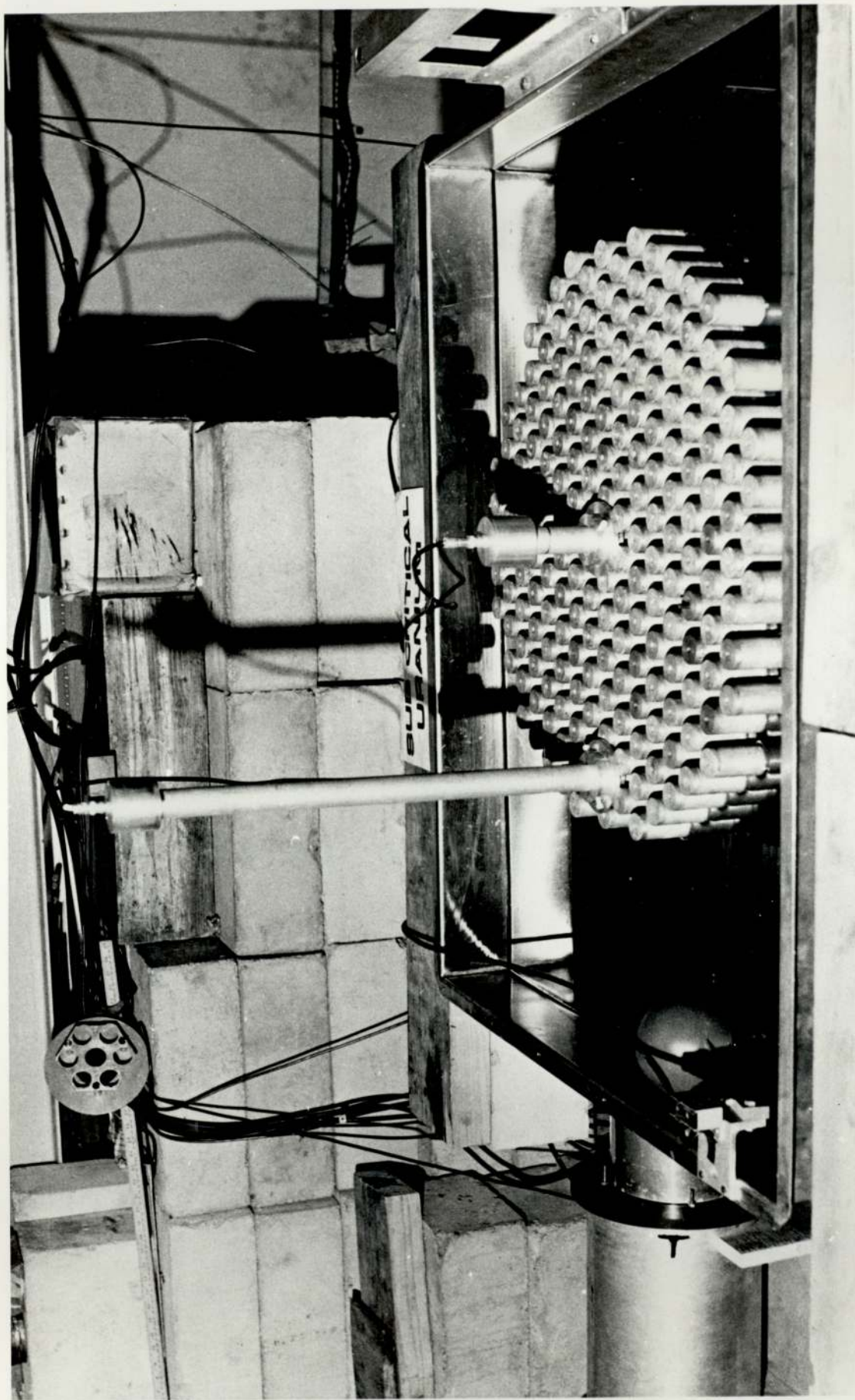


FIG. 2.6 NEUTRON DETECTORS LOCATED INSIDE THE SUBCRITICAL ASSEMBLY

### 2.3.2 Gamma detectors.

The two major properties considered in the choice of the detector were the detector efficiency and the neutron response.

The two more useful detectors for  $\gamma$ -ray detection are the lithium germanium (Ge(Li)) semiconductor detector and the NaI(Tl) scintillator detector.

#### (a) The Ge(Li) semiconductor detector.

The interaction processes producing secondary ionizing electrons are the photoelectric effect, Compton scattering and pair production ( $E \geq 1.02$  Mev). The probability of these processes increases with the atomic number. Germanium has an atomic number of 32 and consequently the detector has a poor efficiency for gamma ray detection. The great advantage of the Ge(Li) detector is its excellent energy resolution. This is unimportant in the present measurements because we are concerned with a very broad spectrum.

The main disadvantage is that the detector is very sensitive to neutrons, particularly fast neutrons. The main detection mechanism for slow neutrons, i.e. energies below about 0.5 Mev is the radioactive capture process. The  $(n, \gamma)$  cross section for Germanium is 2.4 barn for thermal neutrons (41). The main fast neutron processes are the  $(n, n'\gamma)$ ,  $(n, p)$  and  $(n, \alpha)$  reactions. Both the  $(n, p)$  and  $(n, \alpha)$  reactions, besides causing prompt neutron detection, generally produce unstable reaction products (42).

The Ge(Li) detector is very susceptible to damage caused by continued exposure to fast neutrons. Fast neutrons produce crystal defects such as the displacement of atoms from their equilibrium sites leaving vacancies and interstitial atoms in the lattice. Radiation damage mainly affects the energy resolution of the detector. Ortec, manufacturers of Ge(Li) detectors state that a rapid deterioration is produced by a fast neutron exposure of more than  $10^8$  neutrons/cm<sup>2</sup>. The figure given by Mann (43) is of  $10^{11}$  neutrons/cm<sup>2</sup>.

(b) The Na I(Tl) scintillator detector.

Iodine has an atomic number of 127. This makes the Na I (Tl) a very good  $\gamma$ -ray absorbing material relative to the Ge(Li). For this reason, and as NaI is a very dense material, 3670 kg. m<sup>-3</sup>, it has a very good intrinsic  $\gamma$ -ray detection efficiency.

On the other hand, the NaI(Tl) detector is sensitive to neutrons.

Because of the variation of neutron reaction cross section with energy, the neutron response is very energy dependent. For slow neutrons, the major response is from capture in the iodine. This reaction has a cross section of 7.0 barn (39) for neutrons of 2200 m.s<sup>-1</sup>. The resulting  $\gamma$ -ray energy spectrum correspondent to <sup>128</sup>I is almost continuous with a maximum at 6.71 Mev which is the binding energy of a neutron in <sup>128</sup>I. Neutron capture in iodine also leads to an increase in the background due to 25 min. decay of <sup>128</sup>I to <sup>128</sup>Xe.

The predominant neutron detection mechanism in the

fast neutron energy range (0.5 Mev - 14.5 Mev) is by inelastic scattering (40). In the lower energy end, the induced activity is mainly due to the (n, $\gamma$ ) reaction with the iodine, and at the high energy end of the range, the induced activity results mainly from the (n,2n) and (n,p) reactions with the iodine. These reactions, which lead to an increase in background, have a cross section of 1.3b and 230 mb. for neutrons of 14.5 Mev (39).

As a result of compromise between detection efficiency and neutron response, Na I(Tl) scintillator detectors were used for the present measurements.

Three different detectors were used. They were the following:

- (i) Size 12.7 mm. dia. x 19.05 thickness  
optically coupled to an EMI 9524B  
photomultiplier.
- (ii) Size 44.5 mm. dia. x 38.1 mm. thickness  
together with a 6097B photomultiplier.
- (iii) Size 101.6 mm. dia. x 101.6 mm. thickness.  
It was optically coupled to an EMI  
9530 B photomultiplier.

The first two scintillators were used in connection with charge sensitive amplifier-discriminator units type NM 115. The high tension was provided by NM 120 units.

The signals from the third detector were fed into Nuclear Enterprises units type NE 5259 and NE 5159C. High tension was provided by a NE 5353 unit.

### 2.3.2.1 Gamma detector shielding.

Because of the sensitivity of NaI(Tl) scintillator to neutrons, adequate detector-shielding was needed.

The detector shield should provide:

- (i) absorption of slow neutrons
- (ii) absorption of secondary penetrating radiation, e.g.  $\gamma$  rays.

There are three widely used materials for slow neutron absorption which are cadmium, lithium and boron. Moderation of fast neutrons was already provided by the water and graphite reflectors.

Cadmium is a very efficient thermal neutron absorber. The absorption is by radioactive capture but the many hard  $\gamma$ -rays emitted in a single capture process make it unacceptable for use in a neutron shield requiring a low  $\gamma$ -ray background.

The cross section for the  ${}^6\text{Li}(n, \alpha){}^3\text{H}$  reaction is 945 barns at thermal neutron energies (0.0025 eV). The unstable tritium decays, by  $\beta$ -emission with a 12.3 year half life, to helium again without  $\gamma$  emission. Also, the lithium neutron-scattering cross-section is negligible. A disadvantage of the use of lithium is that  ${}^6\text{Li}$  has an isotopic abundance of only 7 per cent.

The dominant neutron reaction on boron in the thermal range is the  $(n, \alpha)$  reaction on  ${}^{10}\text{B}$ . Its cross section is 3840 barns for 0.0025 eV neutrons. The product nucleus for this reaction is  ${}^7\text{Li}$ . In 94% of the reactions, the nucleus is formed in an excited state

giving rise to a 0.424 Mev  $\gamma$  ray.  $^{10}\text{B}$  has an isotopic abundance of 19.7%.

A boron compound was chosen in preference to a lithium compound because of the larger cross-section and isotopic abundance of the relevant isotope. The 0.47 Mev  $\gamma$ -rays produced in the  $^{10}\text{B}(n, \alpha)^7\text{Li}$  reaction can largely be absorbed by the  $\gamma$ -ray shield.

The inner part of the shield consists of a suitable  $\gamma$ -ray absorbing material. Almost invariably lead is used for this purpose because of its density and high atomic number. It shields the detector from  $\gamma$ -rays produced by reactions in the shielding material and from the general background such as the X rays generated by the decay of thorium.

The lead shield was 10 mm. thick at the side of the detector and had a maximum thickness of 15 mm. in the front side of the crystal. This thickness corresponds to the half thickness for 3.5 Mev gamma rays which are the most penetrating  $\gamma$ -rays in lead (44).

The lead shield was surrounded by a 24.5 mm. thick layer of boric oxide powder. This thickness absorbs nearly 100% of a neutron flux up to a neutron energy of over 1eV (39).

The small NaI(Tl) crystal was used for inside core measurements. It was located inside an aluminium rod identical to those used for canning the fuel elements.

The other two detectors were used for measurements outside the system. They were placed horizontally in a central position in either the front or

the back side of the subcritical assembly. Different axial positions were achieved by sliding the detectors upwards and downwards. Fig. (2.7) shows a gamma detector in position outside the system.

In order to monitor the neutron population inside the subcritical facility, a neutron detector was used simultaneously with the gamma detector. The latter was always placed in the center of the system and in the same plane as the gamma detector.

### 2.3.3 Data acquisition system.

Fig. (2.8) shows a block diagram of the experimental set-up, including the detection and pulsing networks together with the data acquisition system.

The data acquisition system was built around a RIDL (Nuclear Chicago) model 24.2, 400 channel analyzer used in the time sequence storage (T.S.S) mode. In this mode, each channel counts the number of pulses delivered into it during a fixed time interval. The analyzer required the following input signals:

- (i) Channel-advance address signal, and
- (ii) Signal Input from the detectors.

In the T.S.S. mode, each channel records the number of counts between time  $t$  and  $t + \Delta t$ , where  $\Delta t$  is the channel width. Each channel address advance signal triggers a programme cycle which transfers the accumulated counts from the scaler into the memory core for the assigned channel, resets the scaler and changes the address channel to the next sequentially higher one.

The total time required for going once through

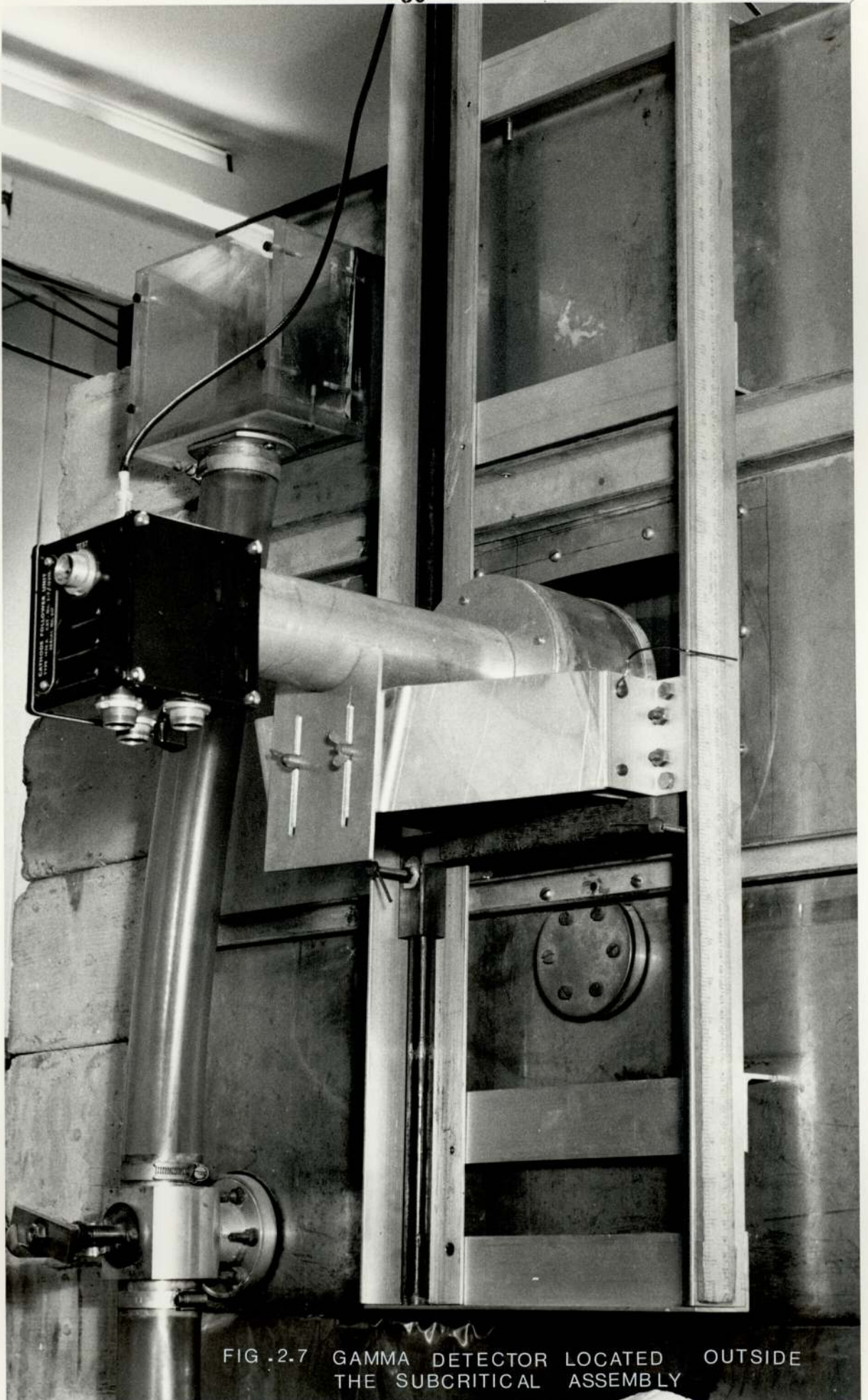


FIG .2.7 GAMMA DETECTOR LOCATED OUTSIDE THE SUBCRITICAL ASSEMBLY

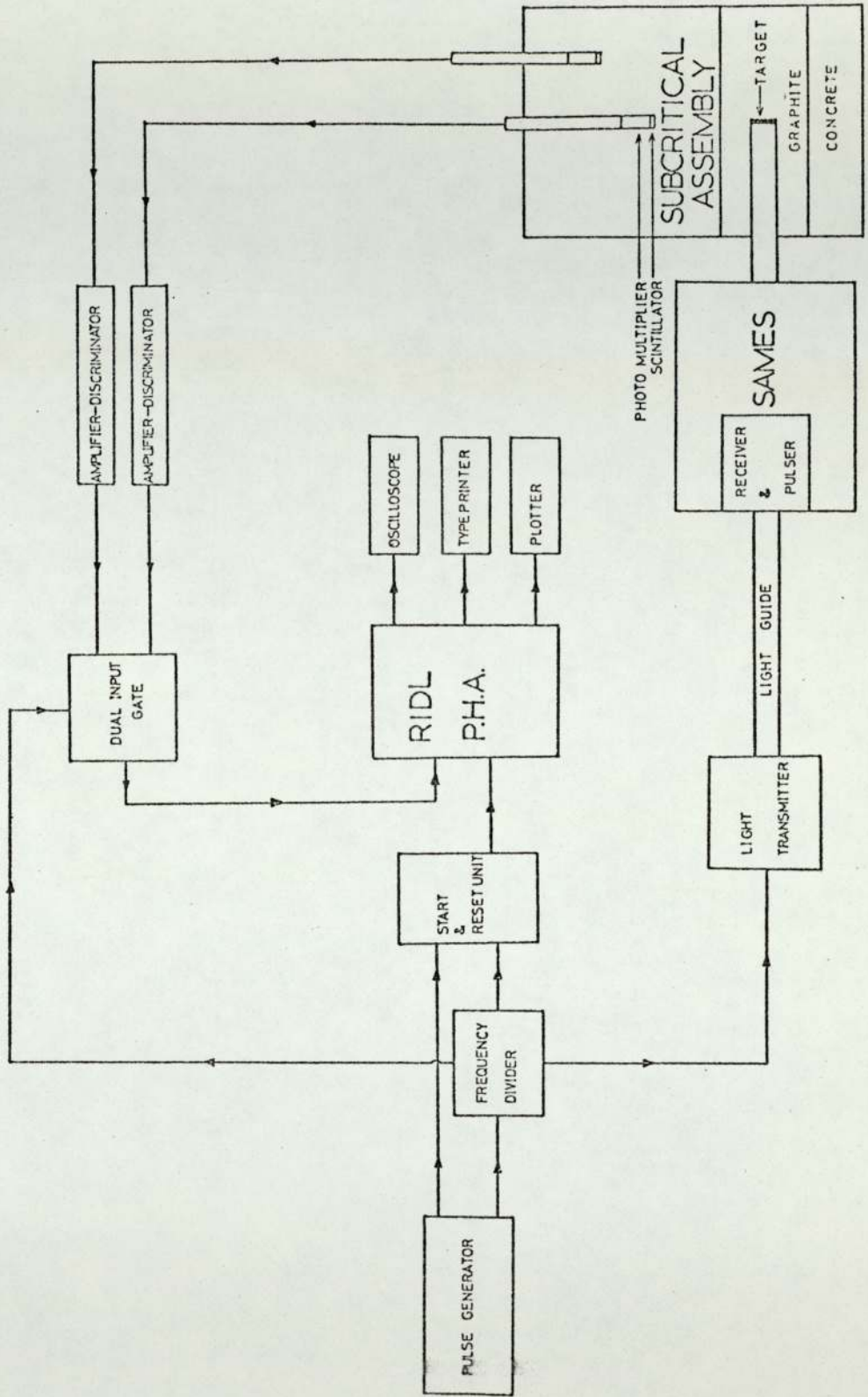


FIG. 2.8 BLOCK DIAGRAM OF THE EXPERIMENTAL SET-UP

each channel was then  $400 \Delta t$ . As two detectors were used simultaneously, the signals from each of them were fed into the analyzer for alternate periods of  $200 \Delta t$ . By following this procedure, each half of the analyzer memory was always storing information corresponding to the same detector.

A Farnell modular pulse generator was used to produce the required signals to control the whole experimental arrangement. It was assembled to provide simultaneously two signals identical in frequency but different in width and height.

One of the signals, of 6V amplitude,  $1 \mu$  sec duration and frequency  $F(\text{Hz})$  was fed into a frequency divider network. This unit was built from SN 7490N and SN 7493N integrated circuits. It produced square pulses of 3.5 volt amplitude which were used to control the following networks:

- (i) Driver and transmitter for the ion source pulsing as described in section 2.2.
- (ii) Dual Input gate, and,
- (iii) Start and reset unit.

The other signal from the pulse generator, negative, of 10 volt amplitude and  $1 \mu$  sec duration, was used to trigger the channel-advance address command of the P.H.A.

Fig. (2.9) shows a diagram of the dual input gate. A bistable circuit based on BC 107 npn transistors was used to gate the input pulses coming from one of the



detectors while the pulses from the other detector were allowed to pass through. When a positive voltage is applied to the base of one of the transistors, it conducts and the signal is earthed through the diode OA 200. At the same time, the other transistor is not conducting and a positive voltage is being applied to the anode of the diode, thus allowing the pulses to be transmitted.

The P.H.A memory input requires signals of + 12 volts in amplitude and around  $1 \mu$  sec duration. So, the pulses had to be amplified and shaped to match the analyzer requirements. The amplification and pulse shaping stages can also be seen in figure 2.9.

The bistable was triggered by 3.5 volt signals coming from the frequency divider with a frequency of  $F/200$  ( $H_z$ ). Therefore, the signals from each detector passed through the gate for alternative periods of  $200 \Delta t$ .

The P.H.A. starts recording when a pushbutton is pressed. So, there was a complete uncertainty about which 200 channels corresponded to each detector. In order to overcome this, the first channel address advance signal reaching the P.H.A. was synchronized with the detector gate triggering pulse. This eliminated the random starting of the P.H.A. and provided the first 200 channels for one detector and the rest of them for the other.

This synchronization was achieved by using the network represented in Fig. (2.10).

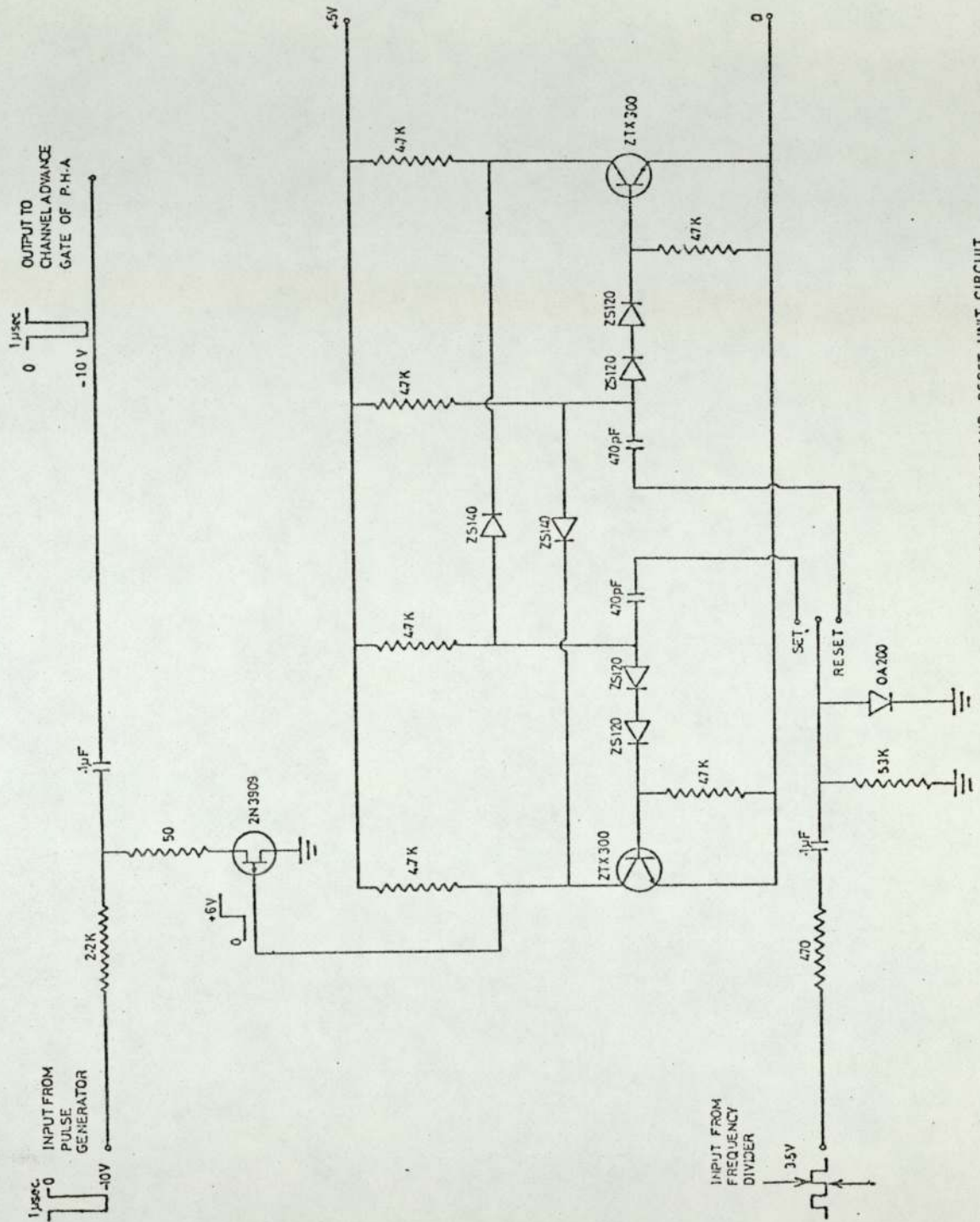


FIG. 2.10 START AND RESET UNIT CIRCUIT

When a positive voltage is applied to the base of the pnp channel  $\text{EETB909}$ , it does not conduct and it has a resistance of several megohms. So, the negative pulses go through. On the other hand, if no voltage is applied to its base, its resistance is of the order of a few hundred ohms and the pulses are driven to earth.

The base voltage was supplied by a set-reset bistable based on XTX 300 npn transistor which was triggered by the leading edge of a square pulse produced by the frequency divider network. This pulse was exactly the same as that used for changing over the dual input gate bistable. Its frequency was, therefore, of  $F/200$  (Hz).

The following procedure had to be followed in every measurement:

- (i) The set-reset unit was reset. Therefore no pulses reached the channel advance command of the P.H.A.
- (ii) The P.H.A. was started by pressing the start pushbutton. As the channel advance signal was not reaching the P.H.A., all pulses reaching the analyzer from the detector, were stored in the first channel.
- (iii) The set-reset unit was set automatically by a signal from the frequency divider. Therefore, the channel-advance pulses could then reach the channel advance command of the P.H.A.

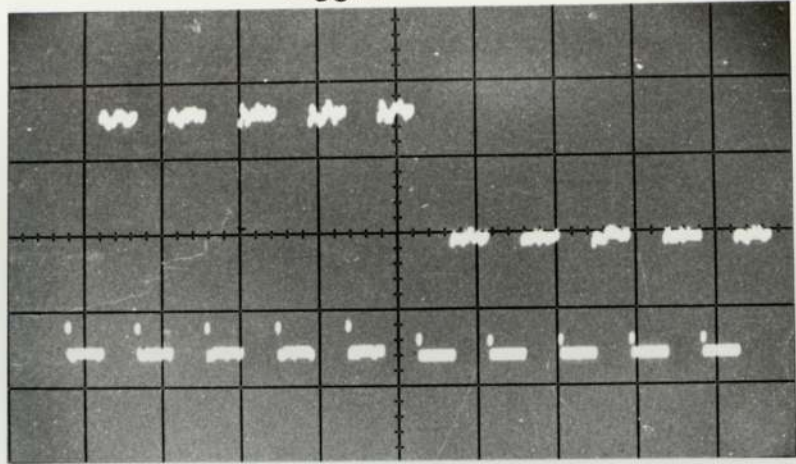
- (iv) The recording of pulses was stopped when required either by stopping the P.H.A. or by resetting the set-reset unit.
- (v) Finally, the output from the measuring system was displayed on an oscilloscope and also recorded on a typewriter. Also, coupled to the analyzer, was a graph plotter unit.

Figs. (2.11) to (2.18) show photographs of the oscilloscope for different frequencies. They correspond to two neutron detectors located in the same plane but in different radial positions and they show the main range of frequencies covered in the present measurements.

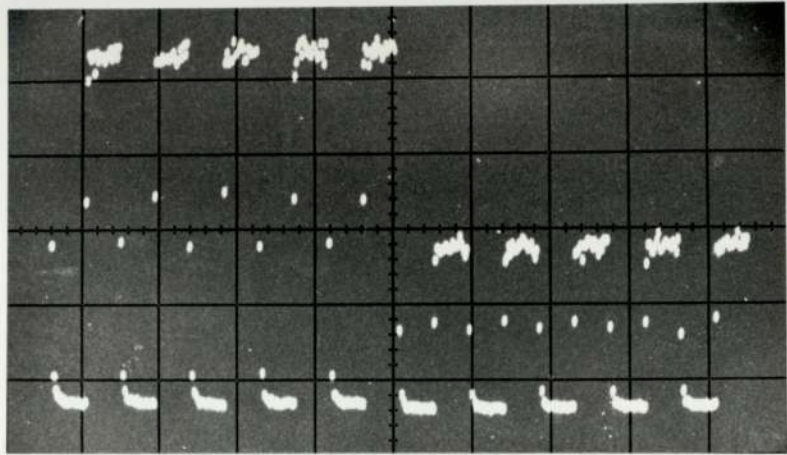
It can be seen from the photographs how at low frequencies, the neutron population follows source variations closely. At higher frequencies, however, the neutron variation within the assembly approaches more closely the fundamental oscillatory component of the source distribution. Also, the photographs show clearly how half of the memory of the analyzer was storing information corresponding to each detector.

Figs. (2.19) to (2.25) show the neutron and gamma populations of the system. The gamma detector was located outside the subcritical assembly in the same plane as the neutron detector. The latter was placed in the central line of the system.

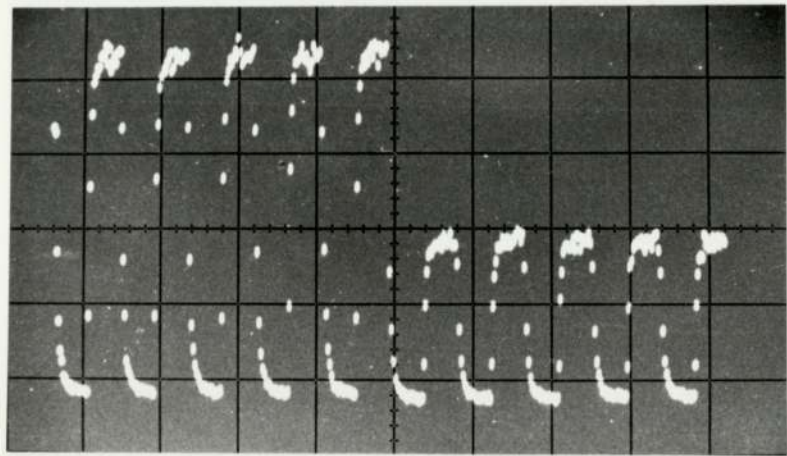
At low frequencies, the gamma population follows



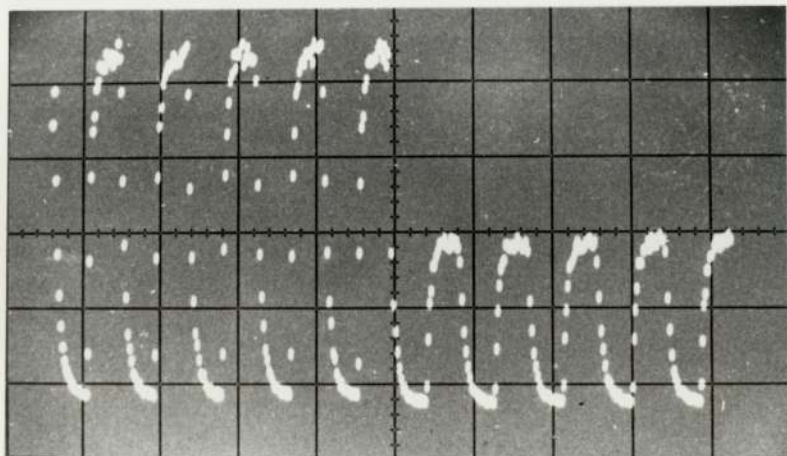
1 Hz.



50 Hz.

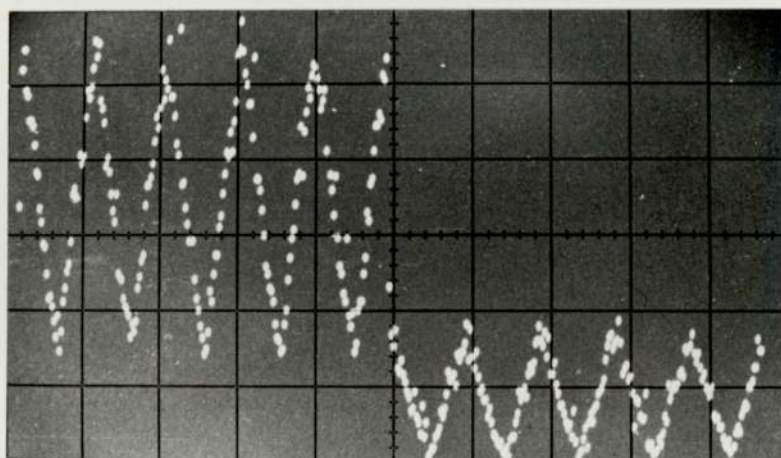
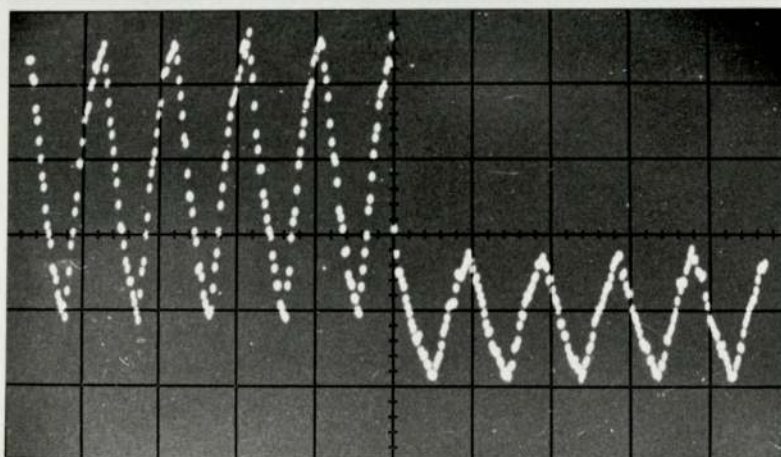
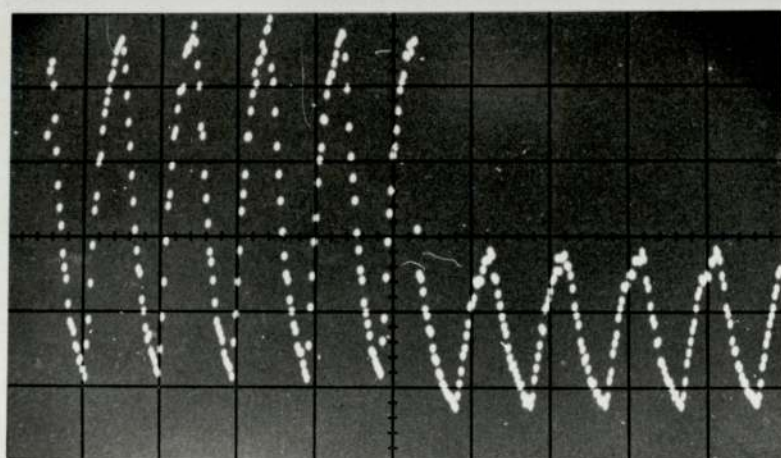
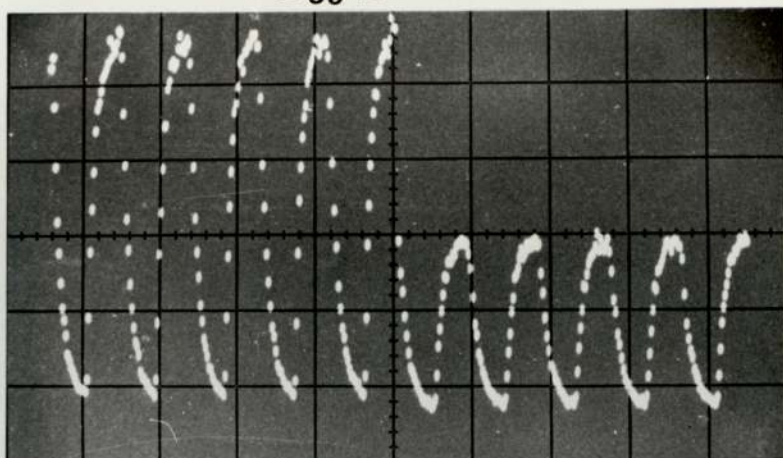


150 Hz.

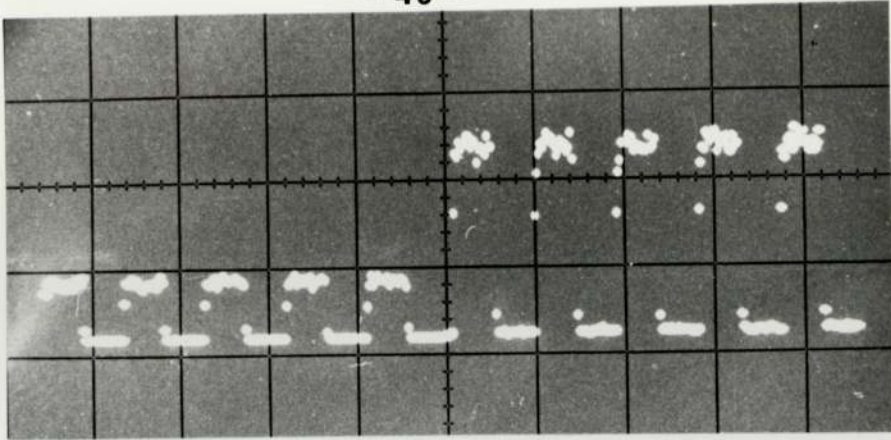


250 Hz.

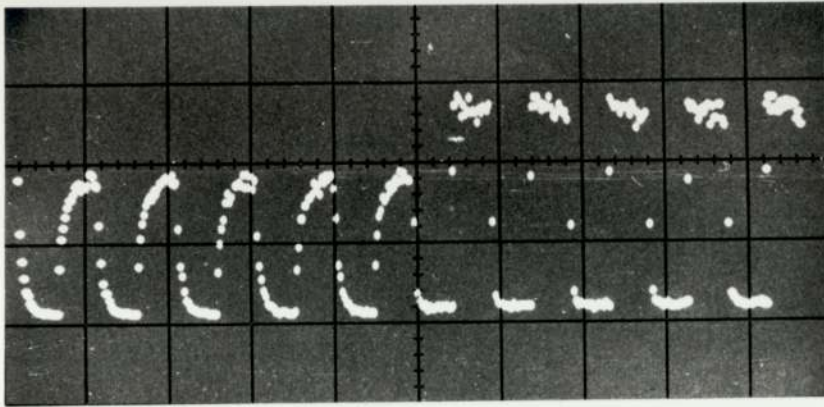
FIGS. 2-11 to 2-14 NEUTRON DETECTORS RESPONSE



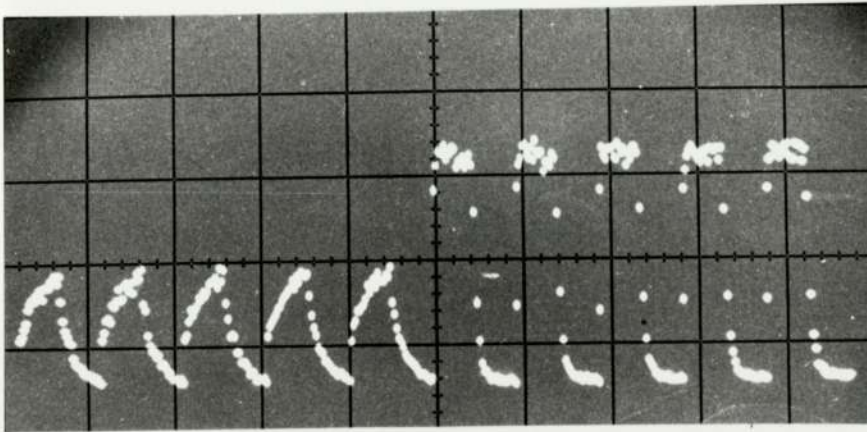
FIGS. 2.15 to 2.18 NEUTRON DETECTORS RESPONSE



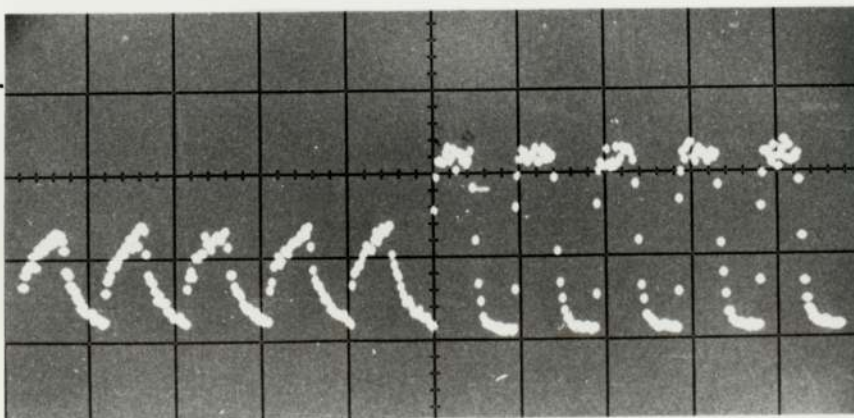
1 Hz.



50 Hz.

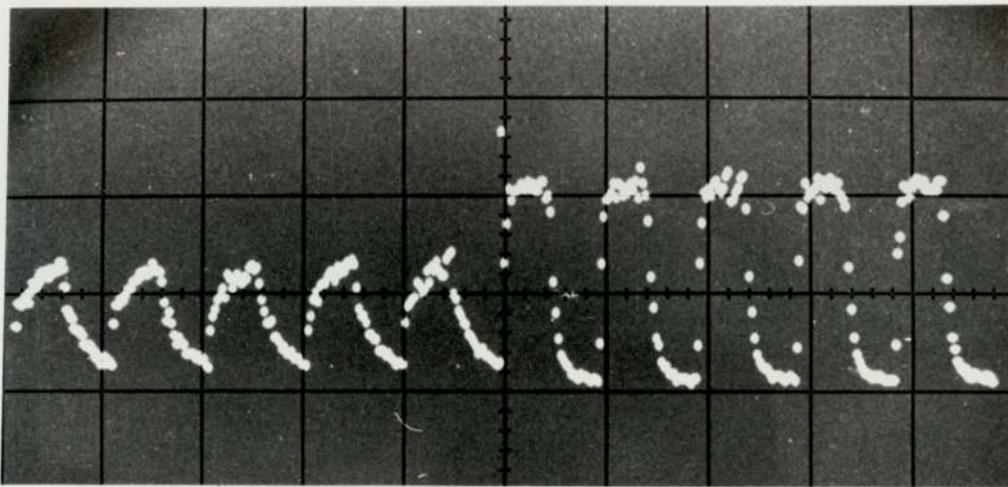


150 Hz.

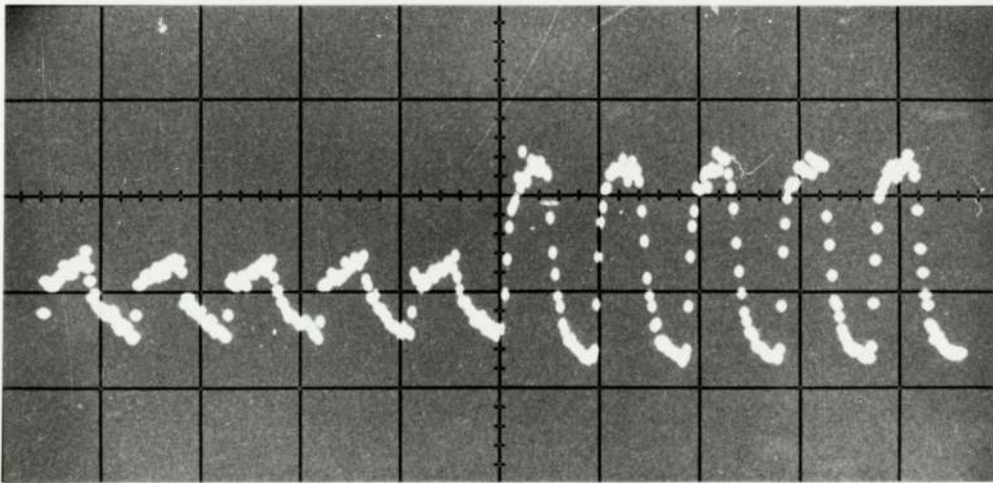


200 Hz.

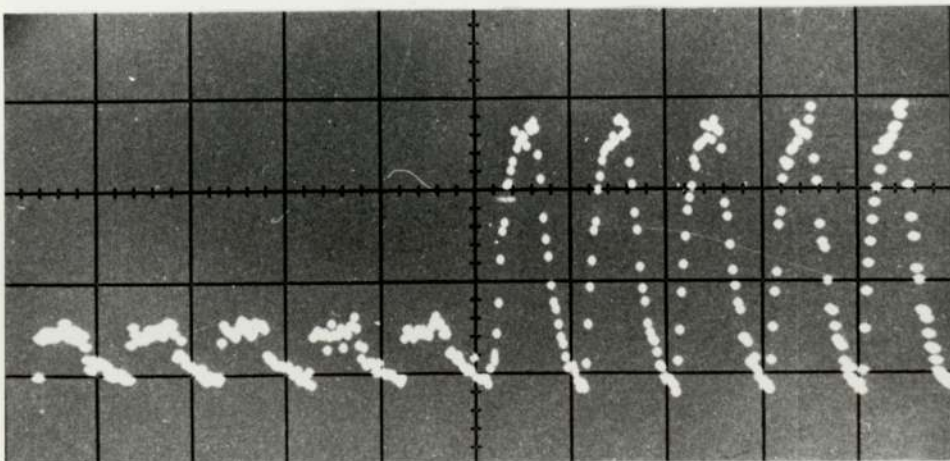
FIGS. 2.19 to 2.22 NEUTRON AND GAMMA DETECTORS RESPONSE



250 Hz.



500 Hz.



1000 Hz.

FIGS. 2.23 to 2.25 NEUTRON AND GAMMA DETECTORS AND RESPONSE

the same trend as that of the neutrons. At higher frequencies, however, the gamma population varies in a completely different way from the neutron one. This effect will be discussed in Chapter 6.

Finally, a photograph of the data acquisition system and associated equipment, is shown in Fig. (2.26).

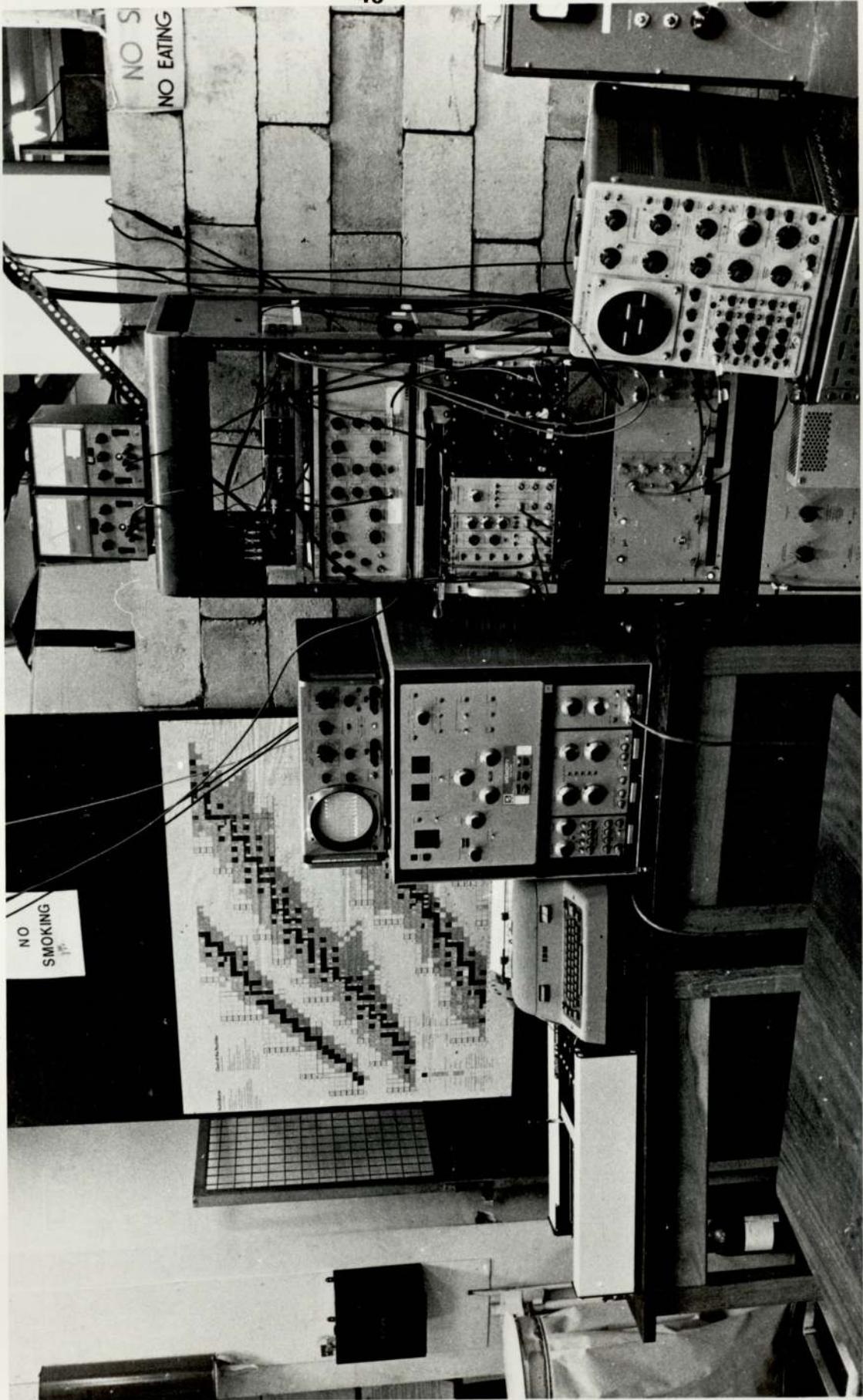


FIG.2.26 DATA ACQUISITION SYSTEM AND ASSOCIATED EQUIPMENT

### CHAPTER 3

#### ANALYSIS OF EXPERIMENTAL DATA

#### AND EXPERIMENTAL RESULTS.

In this Chapter, the method used to obtain the frequency response characteristics of the subcritical assembly from the experimental data is presented. The method includes firstly raw data corrections for the effects of losses due to the analyser and background. Next, by Fourier analyzing the corrected data, the output response of the system is resolved into components harmonically related to the fundamental period. Finally, the amplitude and phase angle both for the fundamental period and its related harmonics are determined from the Fourier analysis.

#### 3.1 Loss of data due to analyser.

As described in Chapter 2, each channel of the analyser records the number of pulses delivered into it during a controlled period of time. Thus, each channel records the number of counts between time  $t$  and  $t + T$ , where  $T$  is the dwell time per channel (channel width).

After a recording period of time, the true counts  $Q$  that should be in a given channel is given by:

$$Q = NcT \quad \dots\dots (3.1)$$

where  $c$  is the average true count rate per cycle and  $N$  represents the number of neutron cycles.

In practice, the recorded counts per channel,  $Q^1$  are somewhat smaller than the true counts that should

be in that channel. In this section, a relationship between  $Q$  and  $Q^1$  is found by taking into account the analyzer memory transfer time ( $\tau$ ) and dead time ( $\delta$ ).

The probability of  $n$  counts being recorded into the same channel in time  $t$  is given by the Poisson distribution,

$$p(n,t) = \frac{(ct)^n e^{-ct}}{n!} \dots\dots (3.2)$$

where  $ct$ , the average count rate in time  $t$  is given by the expression

$$ct = 0xp(0,t) + 1 \times p(1,t) + 2 \times p(2,t) + \dots\dots (3.3)$$

The analyzer memory transfer time is 12.5  $\mu$ sec. There is a temporary store which records one event occurring in this time. Therefore, the recorded counts in time  $\tau$  averaged over many cycles are given by the expression,

$$\begin{aligned} r(\tau) &= 1xp(1,\tau) + 1xp(2,\tau) + \dots = \\ &= c\tau e^{-c\tau} + \frac{(c\tau)^2 e^{-c\tau}}{2!} + \frac{(c\tau)^3 e^{-c\tau}}{3!} + \dots = \\ &= e^{-c\tau} \left[ -1 + 1 + c\tau + \frac{(c\tau)^2}{2!} + \frac{(c\tau)^3}{3!} + \dots \right] = \\ &= e^{-c\tau} [ e^{c\tau} - 1 ] = \\ &= 1 - e^{-c\tau} \dots\dots (3.4) \end{aligned}$$

The fraction of counts occurring in time  $\tau$  that is recorded is  $\frac{1 - e^{-c\tau}}{c\tau}$

Therefore, the recorded counts per channel are given by the expression,

$$Q^1 = Nc \left[ (T - \tau) + \tau \left( \frac{1 - e^{-c\tau}}{c\tau} \right) \right] =$$

$$= NcT \left[ \left( 1 - \frac{\tau}{T} \right) + \frac{\tau}{T} \left( \frac{1 - e^{-c\tau}}{c\tau} \right) \right] \quad \dots (3.5)$$

If each event (or count) processed has an associated dead time  $\delta$ , then, neglecting memory transfer time  $\tau$  the "true" count rate  $c$  is related to the observed count rate  $c^1$  by the expression,

$$c = \frac{c^1}{1 - c^1 \delta} \quad \text{or,} \quad c^1 = \frac{c}{1 + c \delta} \quad \dots (3.6)$$

This applies to the counts received in the interval  $T - \tau$  but not in the memory transfer time. Hence, equation (3.5) becomes,

$$Q^1 = Q \left[ \frac{\left( 1 - \frac{\tau}{T} \right)}{1 + c \delta} + \left( \frac{\tau}{T} \right) \left( \frac{1 - e^{-c\tau}}{c\tau} \right) \right] \quad \dots (3.7)$$

and therefore,

$$Q = \frac{Q^1}{\left[ \frac{\left( 1 - \frac{\tau}{T} \right)}{1 + c \delta} + \left( \frac{\tau}{T} \right) \left( \frac{1 - e^{-c\tau}}{c\tau} \right) \right]} \quad \dots (3.8)$$

This expression was used to correct each channel content recorded by the analyzer. This was done by means of subroutine CORRECT (computer program DATACOR) in which an iterative technique was used to evaluate an approximate value of the true count rate  $c$ . This value became nearly constant ( $\pm 0.001$ ) after two or three iterations. The initial value taken for  $c$  was the uncorrected count rate.

### 3.2 Harmonic Analysis.

Conventionally, the frequency response of a nuclear system is measured by applying a sinusoidal wave of known frequency to the input and measuring the amplitude and relative phase of the output. The process is repeated for all frequencies of interest. This is tedious and prompts one to seek other forms of excitation that are rich in harmonics and apply many sinusoidal frequencies simultaneously to the system input. One such form of excitation is the injection of a neutron source whose time variation is a square waveform. Since the square wave can be Fourier analyzed (45) into an infinite number of odd harmonics of the fundamental frequency, it can be considered as the superposition of sinusoidal inputs and therefore may be used in a similar manner to a sinusoidal input.

By definition (46), any arbitrarily defined function  $f(x)$  in the interval  $-\pi < x < \pi$  can be represented by a trigonometric series of the type,

$$\begin{aligned} f(x) &= \frac{a_0}{2} + a_1 \cos x + a_2 \cos 2x + \dots + b_1 \sin x + \\ &\quad + b_2 \sin 2x + \dots = \\ &= \frac{a_0}{2} + \sum_{r=1}^{\infty} (a_r \cos rx + b_r \sin rx) \end{aligned} \quad \dots (3.9)$$

where the coefficients  $a_0$ ,  $a_r$  and  $b_r$  are defined as,

$$a_0 = \frac{1}{\pi} \int_{-\pi}^{\pi} f(x) dx \quad \dots (3.10)$$

$$a_r = \frac{1}{\pi} \int_{-\pi}^{\pi} f(x) \cos rx \, dx, \quad (r = 1, 2, 3, \dots) \quad \dots(3.11)$$

$$b_r = \frac{1}{\pi} \int_{-\pi}^{\pi} f(x) \sin rx \, dx, \quad (r = 1, 2, 3, \dots) \quad \dots(3.12)$$

The resulting series is called the Fourier series of  $f(x)$  and the coefficients so defined are the Fourier coefficients.

In the present work, the channel content for each of the  $2N$  channels contained in a cycle was expanded in a series of sine and cosine terms as in equation (3.9).

This procedure permitted the calculation of the Fourier coefficients  $a_r$  and  $b_r$  which were used to determine the amplitude  $A_r$  and phase angle  $\epsilon_r$  for the different  $r$  harmonics by using the relationship,

$$a_r \cos rx + b_r \sin rx = A_r \sin (rx + \epsilon_r) \quad \dots(3.13)$$

By equating equivalent terms,

$$A_r = (a_r^2 + b_r^2)^{\frac{1}{2}} \quad \dots(3.14)$$

and,

$$\epsilon_r = \arctan (a_r/b_r) \quad \dots(3.15)$$

### 3.2.1 Numerical determination of Fourier Coefficients.

In this section, the method used to determine the Fourier coefficients is presented.

The values  $f_n$  taken by a function  $f(x)$  at the points  $X_n = \frac{n\pi}{N}$ , ( $n = 0, 1, \dots, 2N - 1$ ) can be Fourier expanded (47) in such a way that the equations,

$$f_n = \frac{a_0}{2} + \sum_{r=1}^{N-1} \left( a_r \cos \frac{\pi nr}{N} + b_r \sin \frac{\pi nr}{N} \right) + \frac{a_N}{2} \cos \pi n \quad \dots (3.16)$$

are satisfied. Thus, by making  $f_n$  correspond to the content of the  $2N$  channels contained in a cycle, the Fourier coefficients  $a_r$  and  $b_r$  could be used to determine the amplitude and phase angle for up to  $r$  ( $r = 0, 1, \dots, N-1$ ) different harmonics.

The solution of the system (3.16) is well known (48-50),

$$a_r = \frac{1}{N} \sum_{n=0}^{2N-1} f_n \cos \frac{\pi nr}{N} \quad \dots (3.17)$$

$$b_r = \frac{1}{N} \sum_{n=0}^{2N-1} f_n \sin \frac{\pi nr}{N} \quad \dots (3.18)$$

In order to calculate the values of  $a_r$  and  $b_r$ , let us consider, for each  $r = 0, 1, \dots, N-1$ , the numbers  $U_{n,r}$  defined by

$$U_{n,r} = f_n + 2 \cos \frac{\pi r}{N} U_{n+1,r} - U_{n+2,r} \quad \dots (3.19)$$

where,

$$U_{2N+1,r} = U_{2N,r} = 0 \quad \dots (3.20)$$

It is found following reference (51), that

$$a_r = \frac{1}{N} \left( f_0 + U_{1,r} \cos \frac{\pi r}{N} - U_{2,r} \right) \quad \dots (3.21)$$

$$b_r = \frac{1}{N} U_{1,r} \sin \frac{\pi r}{N} \quad \dots (3.22)$$

To see this, suppose (dropping the subscript  $r$ ) that,

$$U_{n+1} \sin x = \sum_{j=n+1}^{2N-1} f_j \sin (j-n)x = \sum_{j=n}^{2N-1} f_j \sin (j-n)x$$

.... (3.23)

then,

$$\begin{aligned} & (f_n + 2 \cos x U_{n+1} - U_{n+2}) \sin x = \\ & = f_n \sin x + \sum_{j=n+1}^{2N-1} f_j [ 2 \cos x \sin (j-n)x - \sin (j-n-1)x ] \\ & = f_n \sin x + \sum_{j=n+1}^{2N-1} f_j (j-n+1)x = \\ & = \sum_{j=n}^{2N-1} f_j \sin (j-n+1)x = \\ & = U_n \sin x \end{aligned}$$

.... (3.24)

which yields (3.19) and (3.20).

The value of  $a_r$  (3.21) can be found as follows,

$$\begin{aligned} & (f_n + U_{n+1} \cos x - U_{n+2}) \sin x = \\ & = f_n \sin x + \sum_{j=n+1}^{2N-1} f_j [ \cos x \sin (j-n)x - \sin(j-n-1)x ] \\ & = [ f_n + \sum_{j=n+1}^{2N-1} f_j \cos (j-n)x ] \sin x = \\ & = [ \sum_{j=n}^{2N-1} f_j \cos (j-n)x ] \sin x \end{aligned}$$

.... (3.25)

By making  $n = 0$ , equation (3.25) yields the value of  $a_r$  as given by equation (3.21). Also, by making  $n = 0$  in equation (3.23), the value of  $b_r$  as given by equation (3.22), is obtained.

Therefore, by following this simple numerical procedure, the Fourier coefficients can be evaluated from equations (3.21) and (3.22) by using only one sine and cosine function per harmonic and by evaluating  $U_0$ ,  $U_1$  and  $U_2$  from the recurrence relationship (equation 3.19) working from  $n = 2N-1$  to 0. This involves much less computational work than the direct evaluation of equations (3.17) and (3.18).

This method was applied to develop the computer program subroutine FOURIER which evaluates the constants  $a_r$  and  $b_r$  and computes the values of the amplitude and phase angle for every one of the  $N-1$  harmonics. In practice, it was found that reliable information could be found up to and including the fifth harmonic. The subroutine FOURIER is listed in Appendix 2 as part of the computer program DATACOR.

This method of calculation was also successfully used by other workers with both an odd and an even number of data points as described in reference (52).

### 3.3 Computer Program DATACOR.

The experimental frequency response characteristics of the subcritical assembly were analyzed by means of the computer program DATACOR. The code, which was written in Algol for an ICL-1905 system, includes the calculations discussed in the previous sections of this Chapter and provides a graphical output of the amplitude response of the system for every input frequency and its corresponding harmonics.

The output from the analyzer was fed into the

program which performs the following major operations:

- 1 - Corrections for dead time and memory transfer time.

- 2 - Background corrections.

- 3 - Fourier analysis of the corrected input data.

This includes the determination of both the amplitude and phase shift responses of the nuclear system for any input frequency and its different harmonics.

Before making any corrections, the input data is reduced to one neutron cycle by adding-up the time-equivalent contents from each cycle and then calculating the average content per channel. This is performed by subroutines `BACKGROU`P and `ARRANGE`.

Corrections for dead time and memory transfer times are performed by subroutine `CORRECT`. This subroutine is based on the scheme discussed in section 3.1.

Once the data has been corrected for losses due to the analyzer and the background content per channel has been subtracted, a Fourier analysis (as discussed in the previous sections) is carried out by subroutine `FOURIER`.

Subroutine `FOUREXIT` provides both numerical and graphical output for subroutine `FOURIER`. The numerical output includes both amplitude and phase shift and was limited to the first seven harmonics. The graphical output was limited to the first, third and fifth harmonic contents. The graphical output is based on subroutines `PLOT`CROSS, `PLOT`ROMB and `PLOT`SQUARE.

Subroutine FOURHEAD provides the heading for the lineprinter output of subroutine FOURIER.

The program can be used with data corresponding to either one or two detectors. In case of two detectors, subroutine BACKORDER and DATAORDER are used to prepare the background and experimental data in such a way that each half of the values always correspond to the same detector.

Subroutine LINEPRIN provides with an optional graphical display of the raw data on the lineprinter.

Subroutine PLOTBULK commands the graphplotter for drawing the axis and titles for the graphical output.

Subroutines OPENPLOT, CLOSEPLOT, HGPLOT, HGPSCALE, HGPAXISV, STRARR, HGPLOGAXIS, HGPSYMBL and HGPWHERE, are standard subroutines for the ICL 1934/4 graphplotter (53).

Finally, a listing of the program together with an input and output examples is presented in Appendix 2. A schematic block diagram of the code is also shown in Appendix 2.

### 3.4 Experimental results.

The space-dependent transfer functions for different source-frequency configurations were measured by varying the frequency of the square wave modulated neutron source and observing the amplitude and phase shift of the resultant fluctuating component of the detector response as a function of source frequency. The neutron source frequency was varied within the working limits of the pulsing system, i.e., between 1 Hz and

2 Khz. The techniques used for analysing the detectors response were those discussed in the previous sections.

Figures (3.1) and (3.2) show the amplitudes of the frequency response functions of the subcritical assembly for a particular detector location as given by the computer program DATACOR. It can be seen how by Fourier analyzing the detector response, it was possible to extract additional data from any set of measurements for every source frequency. The results obtained over a wide range of frequencies shown that, up to and including the fifth harmonic, the data obtained from higher harmonics is seen to be in good agreement with that computed from the fundamental component of the detector response. Furthermore, data corresponding to the seventh harmonic proved to be reliable for source frequencies included in the range of 10 Hz. to 500 Hz., being unrealistic and showing significant variations for source frequencies outside this range.

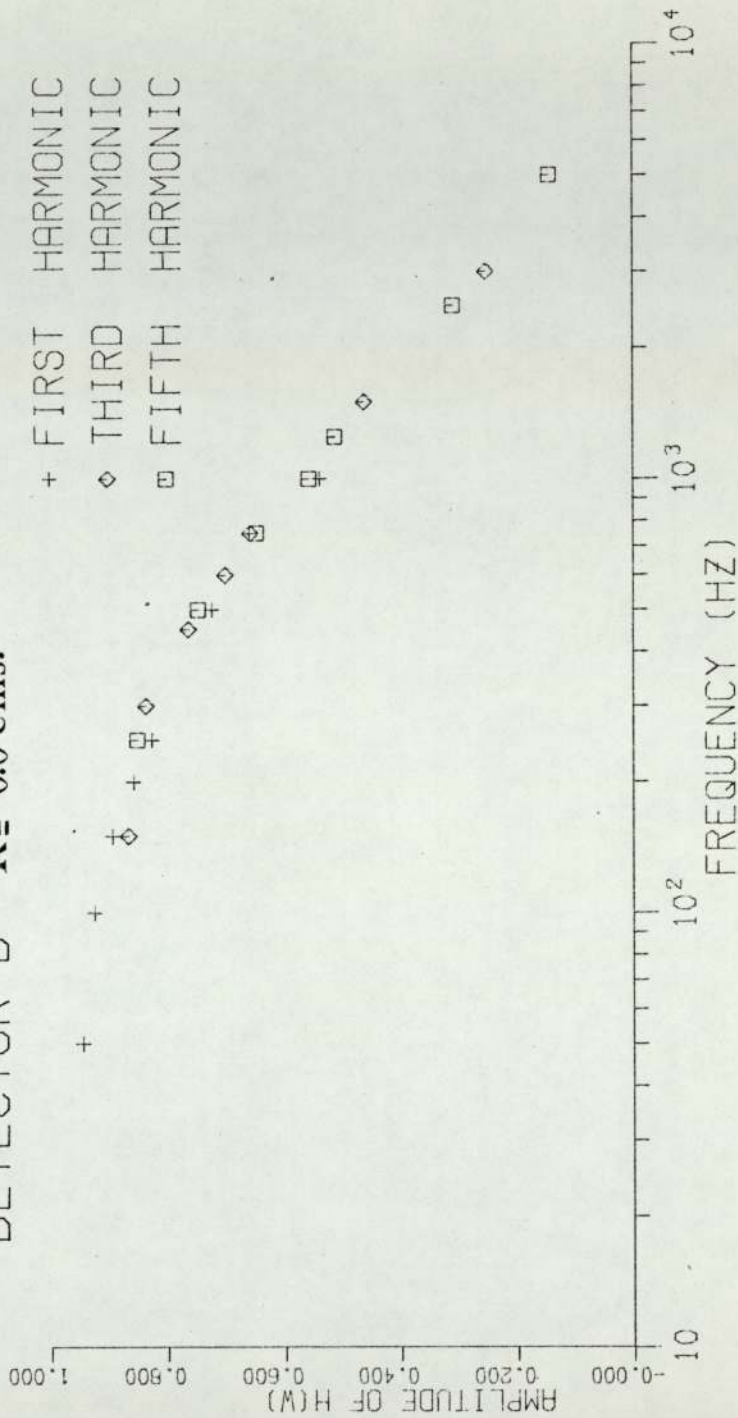
Figures (3.1) and (3.2), as well as all the experimentally obtained figures presented in this work, correspond to measurements carried out with source neutrons produced from D-T reactions. The reasons for using the D-T instead of the D-D reaction can be summarized as follows:

(i) Much higher neutron yield (approximately 100 times). This was of vital importance in the present experiments where the oscillator R.F. and ion source extraction voltage had to be kept as low as possible in order to provide a reliable and steady operation of the pulsing system.

# EXPERIMENTAL TRANSFER FUNCTION

H = 15.0 cms.

DETECTOR B R = 0.0 cms.

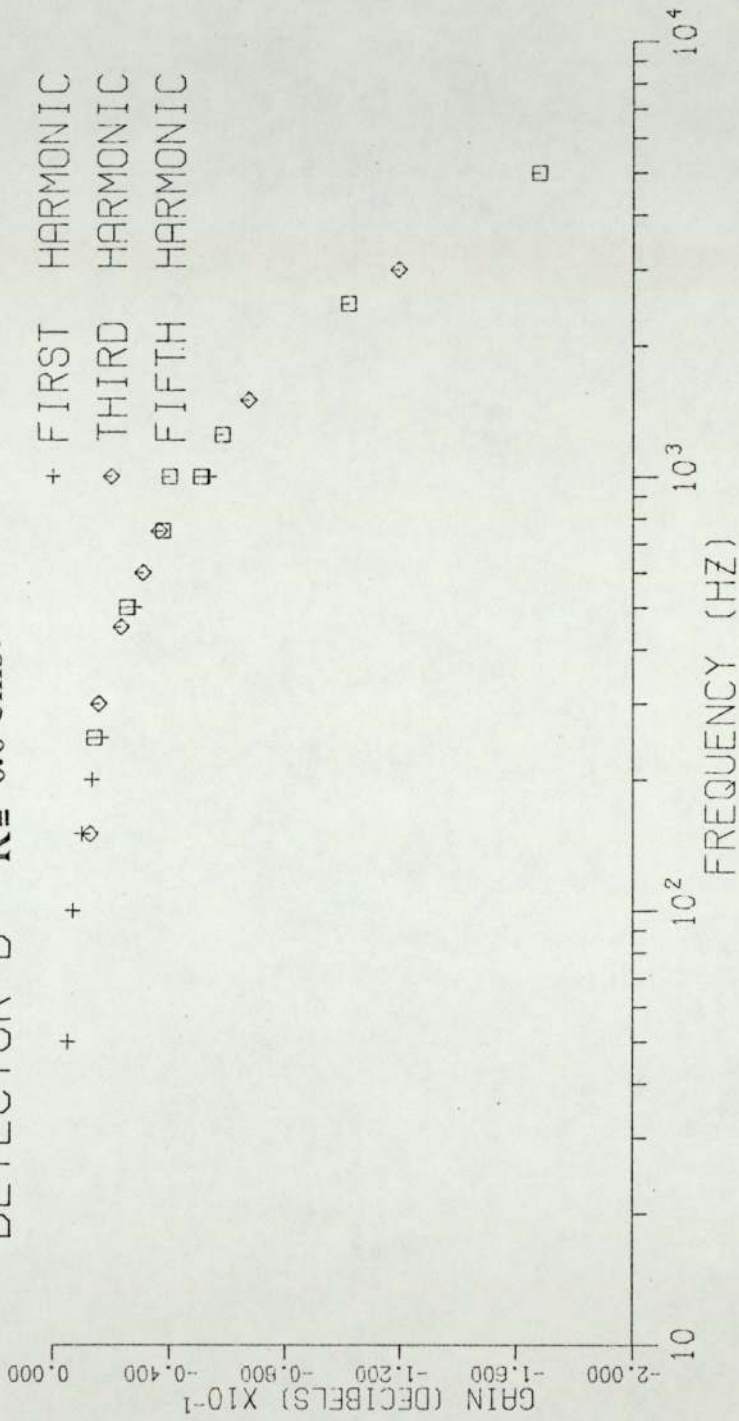


FIG(3.1) EXPERIMENTAL TRANSFER FUNCTION SHOWING THE CONTRIBUTION OF DIFFERENT HARMONICS

# EXPERIMENTAL TRANSFER FUNCTION

H = 15.0 cms.

DETECTOR B R = 0.0 cms.



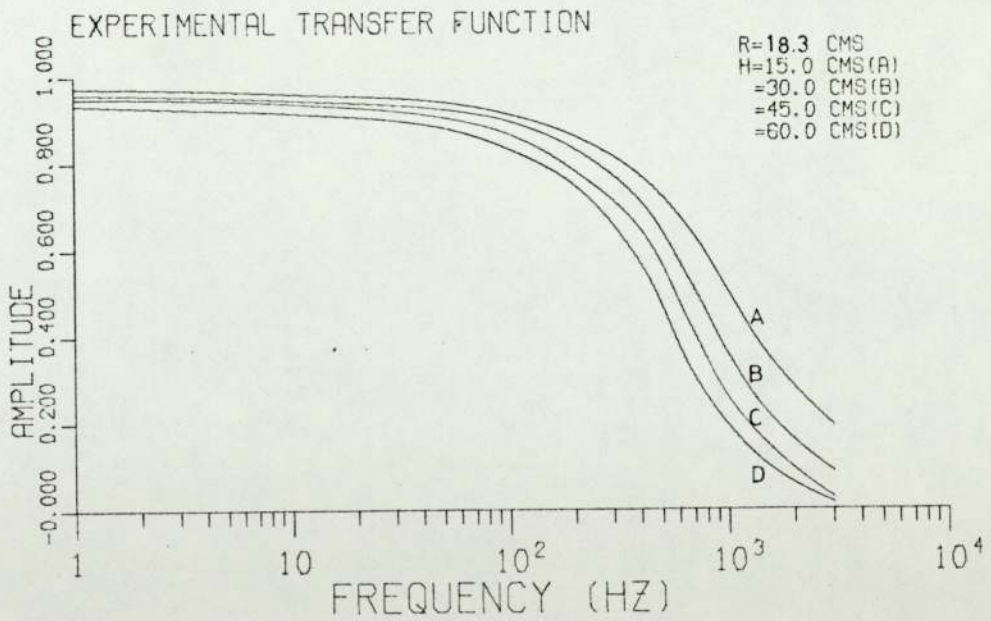
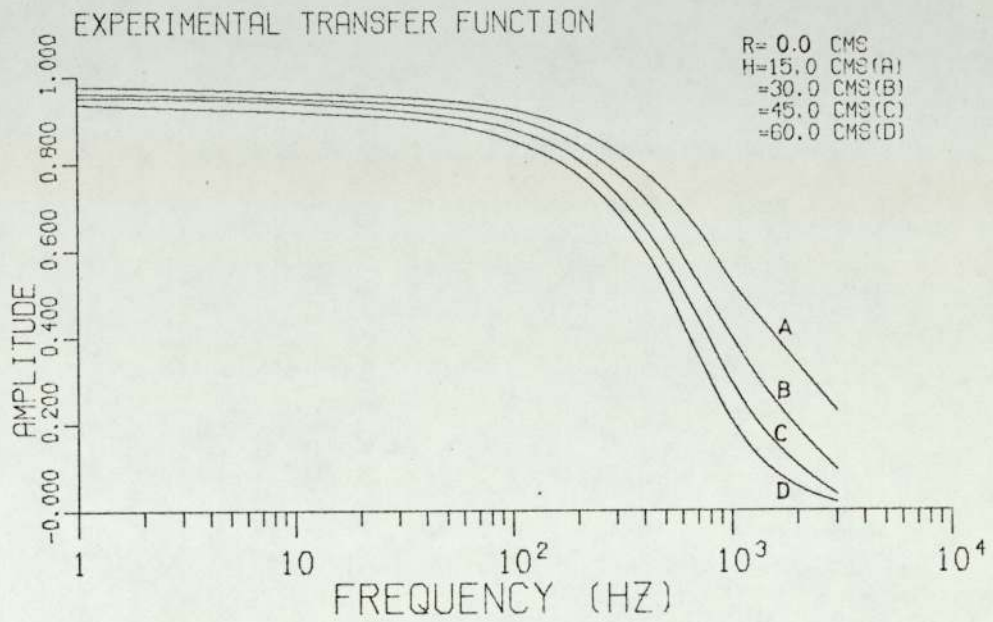
FIG(3.2) EXPERIMENTAL TRANSFER FUNCTION SHOWING THE CONTRIBUTION OF DIFFERENT HARMONICS

(ii) Experimental measurements have shown how the system response characteristics (transfer functions) do not depend either on the neutron source intensity or its strength.

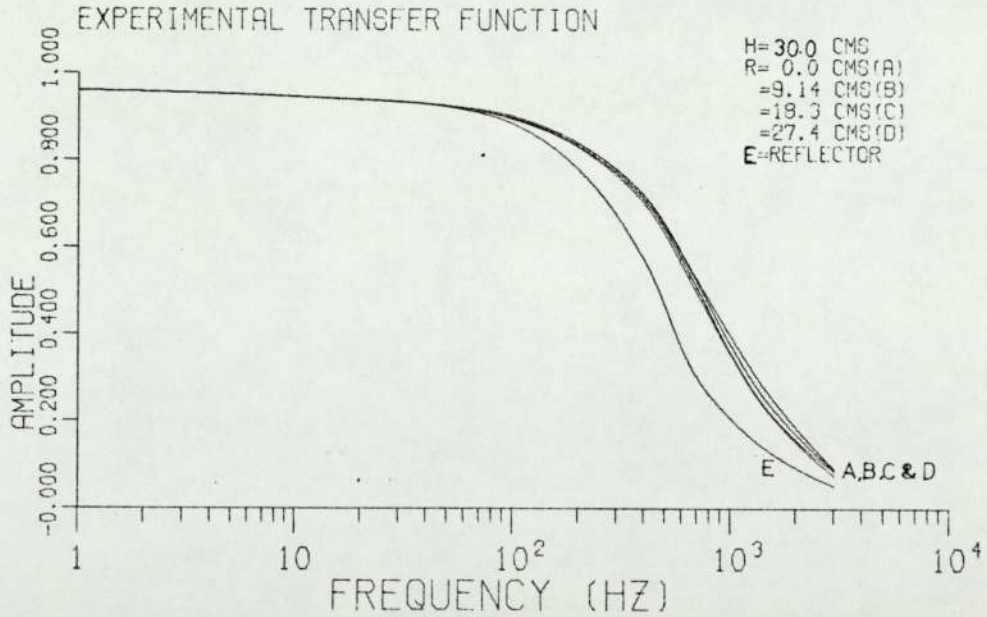
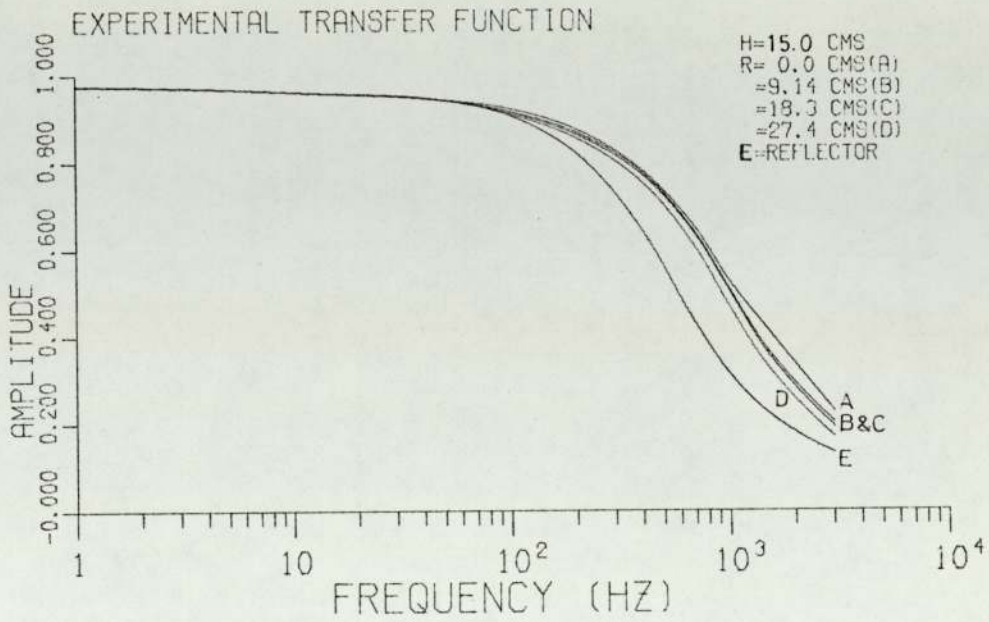
The response of the nuclear system proved to be very sensitive to different output locations. Measurements were taken for different radial and axial detector positions. Figs. (3.3) and (3.4) show typical examples of the neutron detector responses over a number of different axial locations. Measurements correspondent to different radial positions are presented in Figs. (3.5) and (3.6).

These curves are the result of a least squares fitting performed by means of the computer code UA01 (54). It can clearly be seen from graphs (3.3) and (3.4) how for frequencies of up to 100 Hz the amplitude decreases very slowly. For higher frequencies, the amplitude decreases much more rapidly and the spatial differences become more noticeable. It can also be seen how the spatial differences are more noticeable for points closer to the external source. All these effects can be observed very clearly in Figs. (3.7) to (3.10) which represent the variation in amplitude with respect to the axial position for a wide range of frequencies.

Figs. (3.5) and (3.6) represent the amplitude response for different radial positions inside the subcritical assembly. Here no spatial differences are noticeable for frequencies below approximately 100 Hz, and below this frequency, the differences are rather

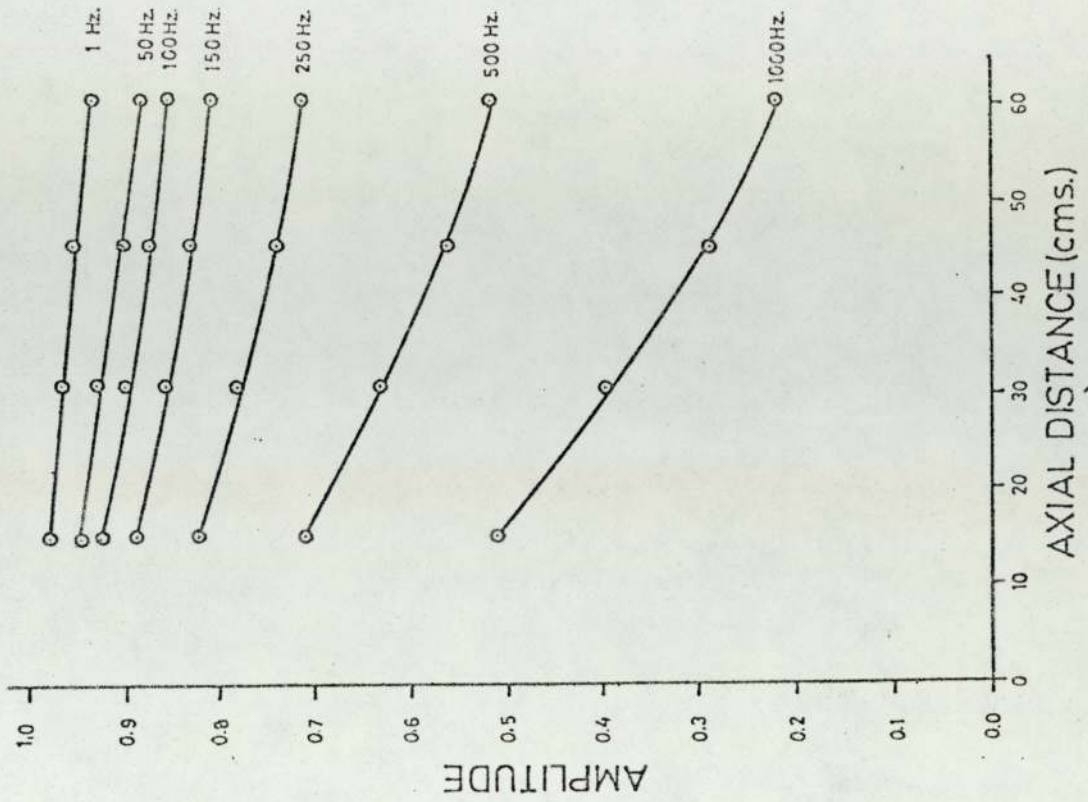


FIGS(3.3) AND (3.4) AMPLITUDE RESPONSE FOR DIFFERENT AXIAL POSITIONS

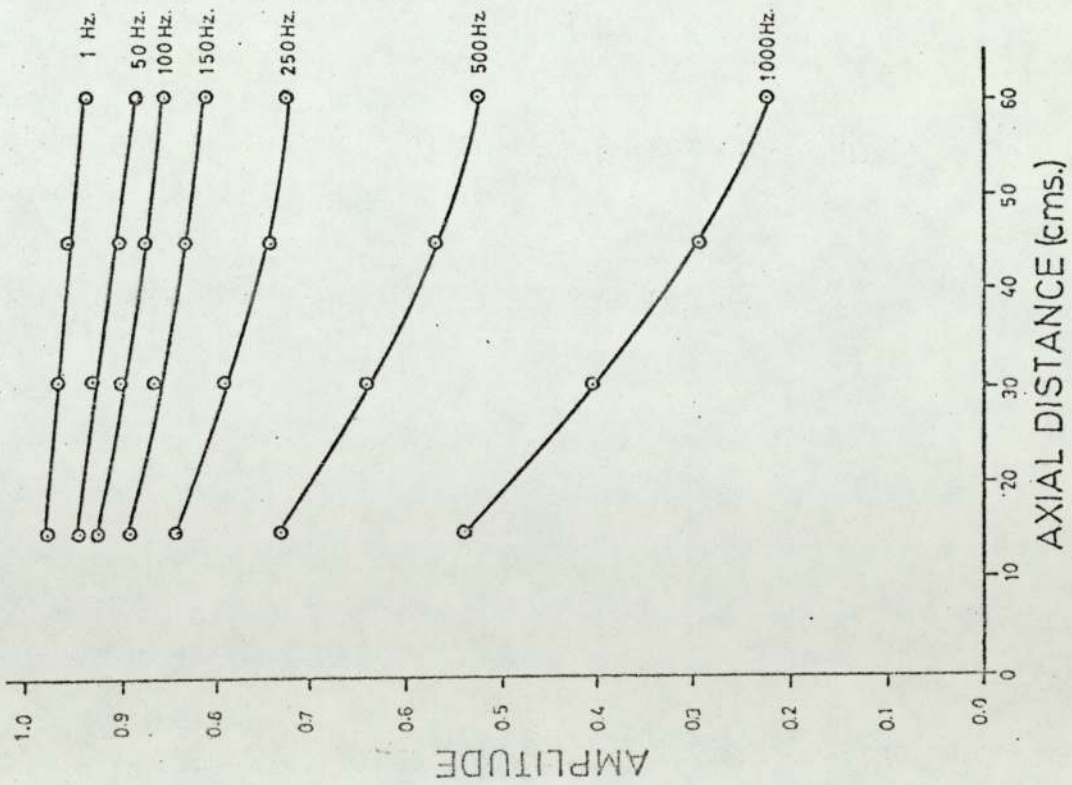


FIGS(3.5) AND (3.6) AMPLITUDE RESPONSE FOR DIFFERENT RADIAL POSITIONS

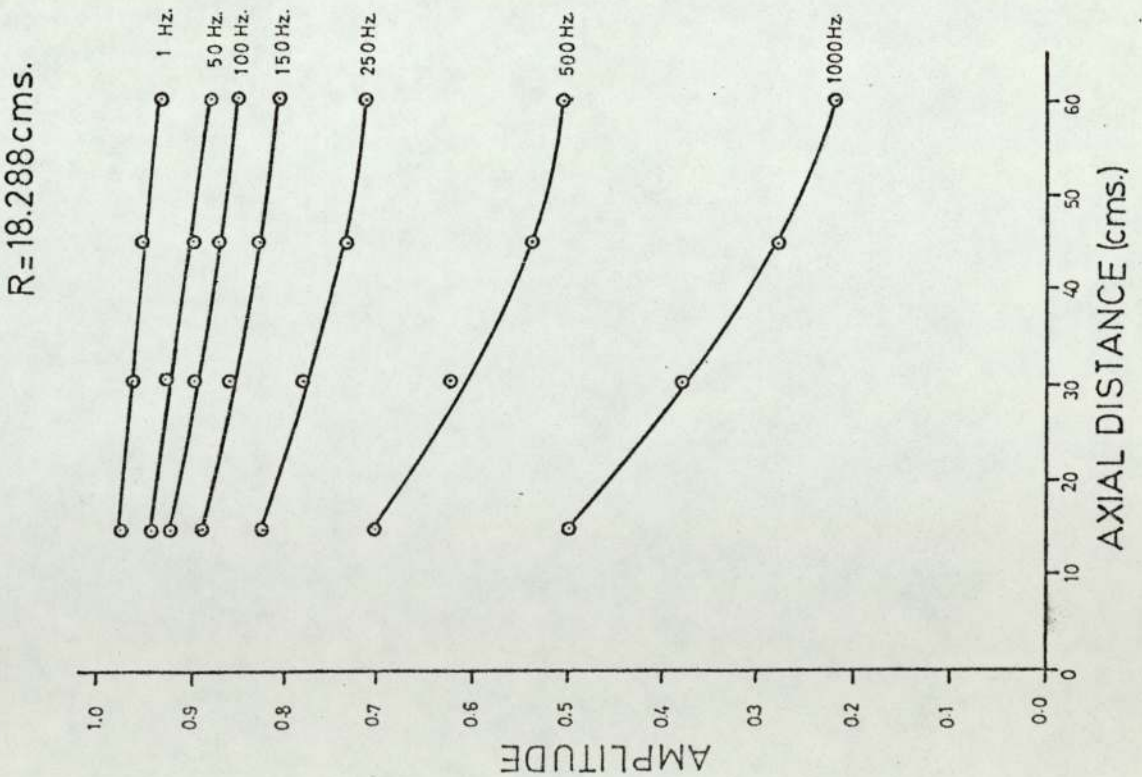
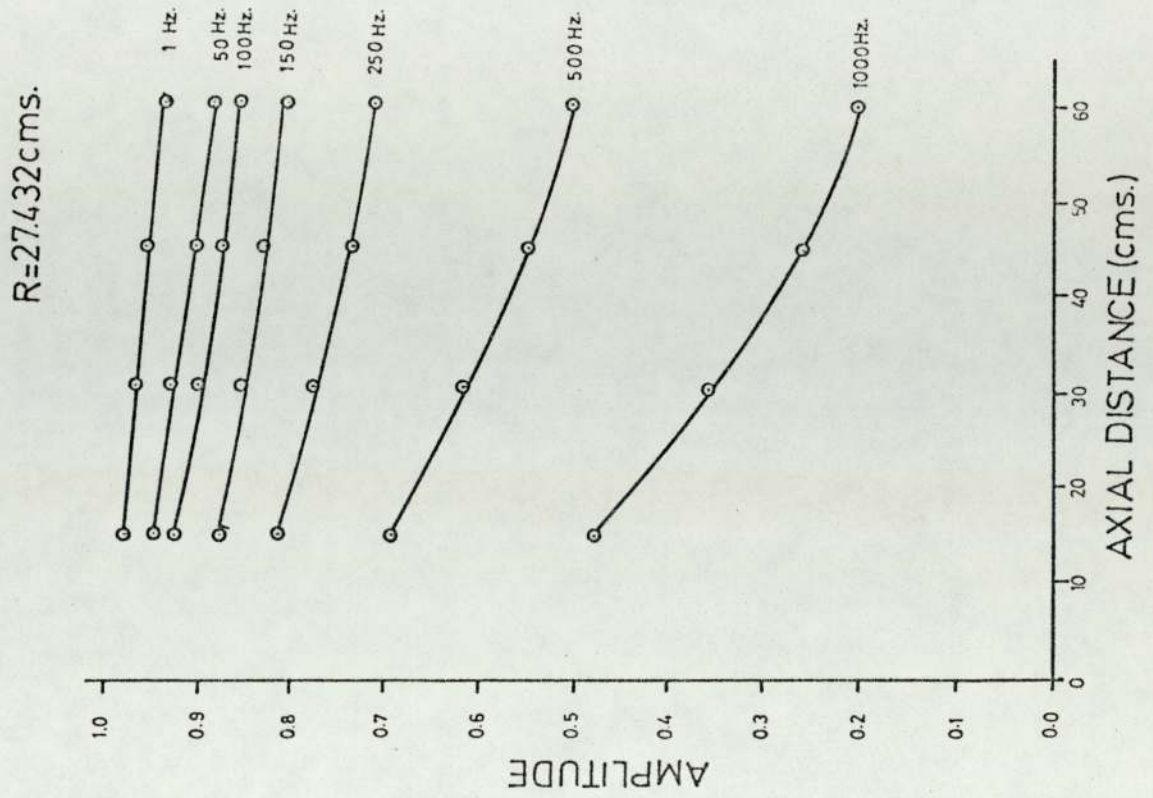
R=9.144 cms.



R=0



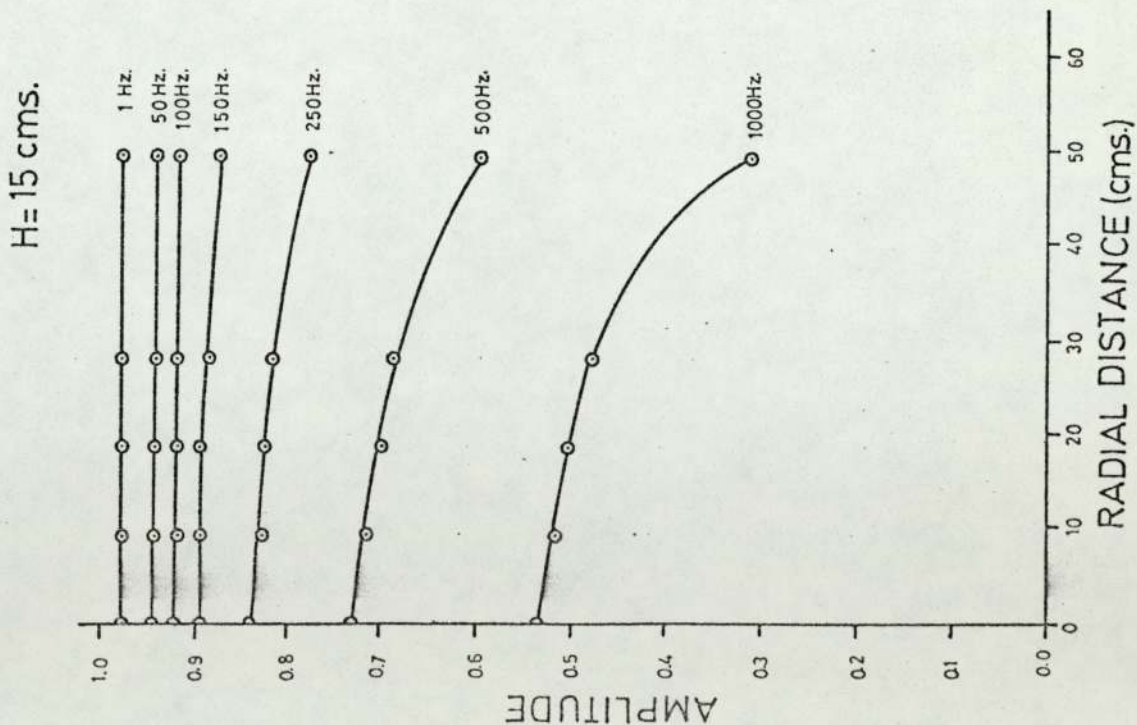
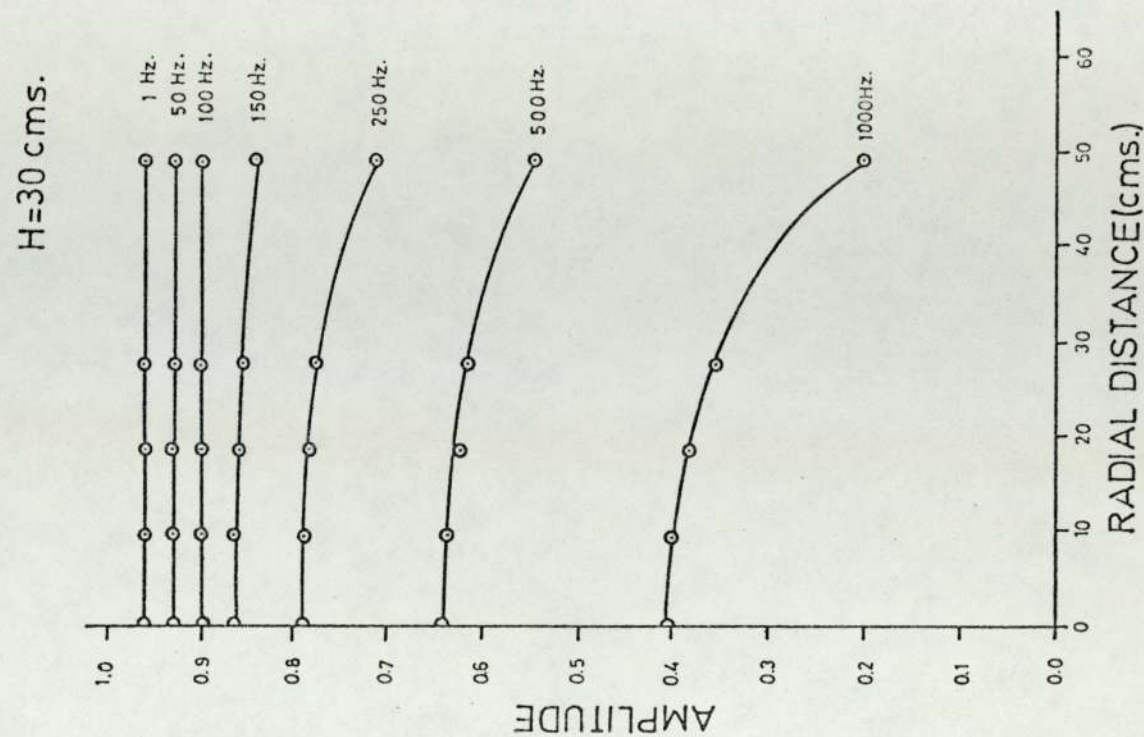
FIGS. (3.7) AND (3.8) MEASURED VARIATION IN AMPLITUDE WITH AXIAL POSITION



FIGS. (3.9) AND (3.10) MEASURED VARIATION IN AMPLITUDE WITH AXIAL POSITION

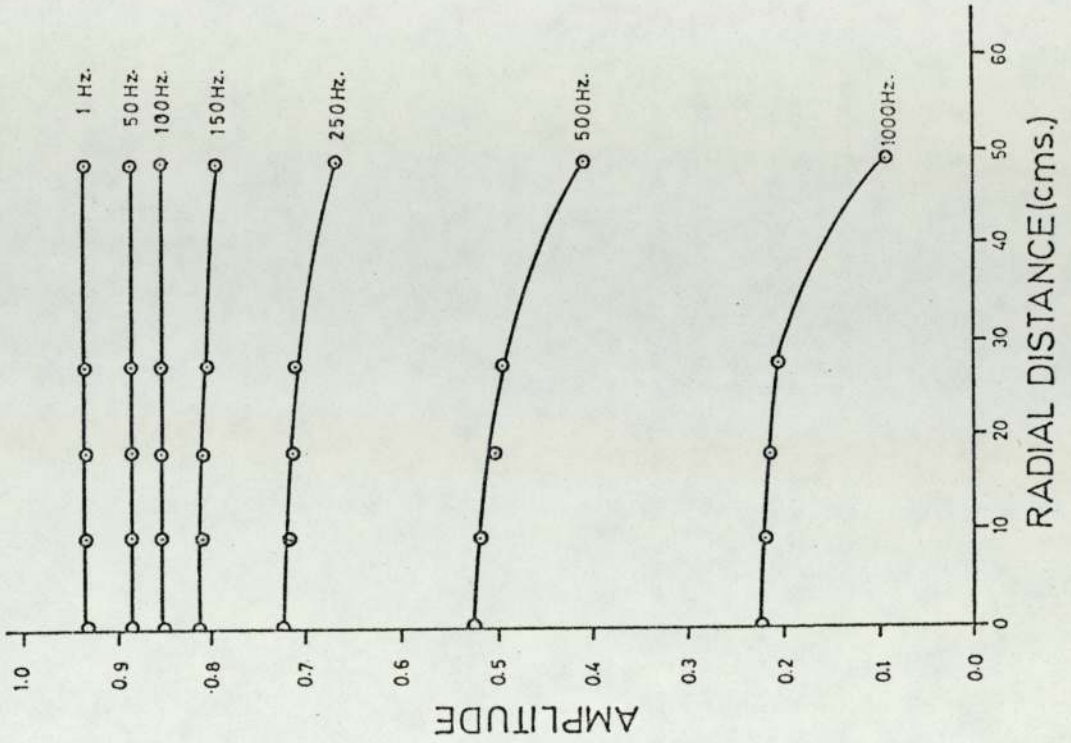
small. This effect could be explained due to the fact that the neutrons produced in an almost point source are spread out inside the graphite pedestal which supports the system and enter the system in a broad beam. However, a much bigger spatial difference is found in the reflector where the response is more attenuated due to the much longer neutron lifetime in the water reflector. The same effects are seen even more clearly in Figs. (3.11) to (3.14) which show the variation in amplitude with respect to the radial position for different frequencies.

With regard to the phase response characteristics of the subcritical assembly, a very similar pattern is observed as shown in graphs (3.15) and (3.16). Here again the spatial differences observed in an axial distribution are much bigger than those correspondent to a radial distribution. Also, the higher attenuation of the phase response in the reflector can be clearly noticed.

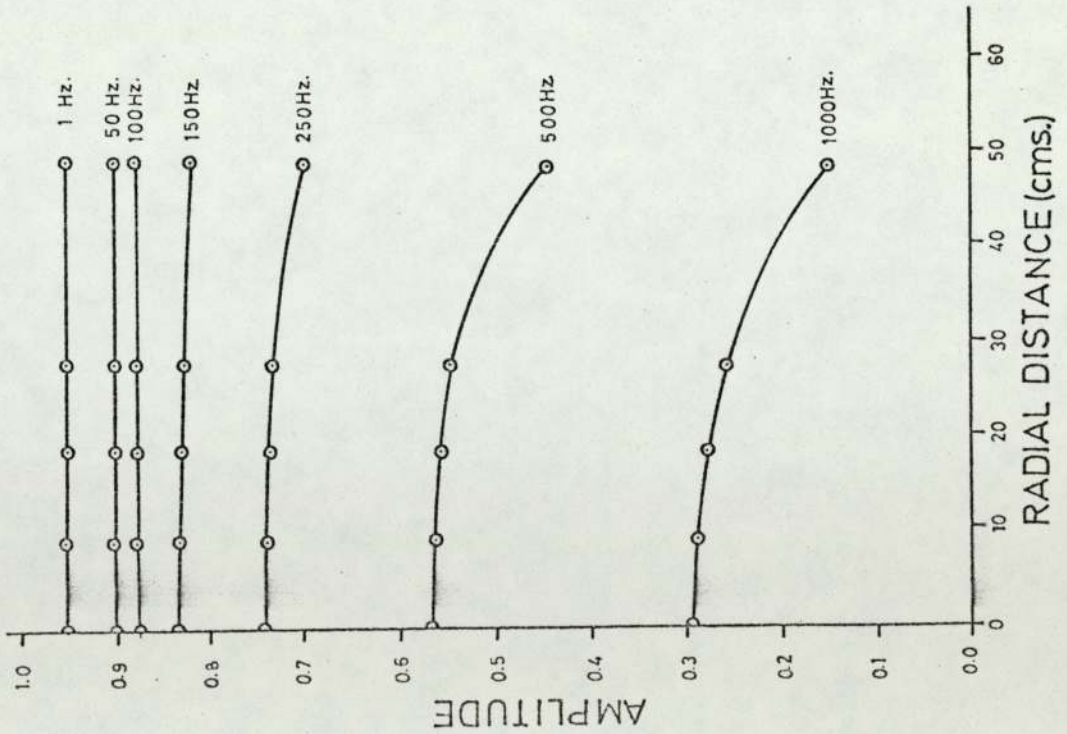


FIGS. (3.11) AND (3.12) MEASURED VARIATION IN AMPLITUDE WITH RADIAL POSITION

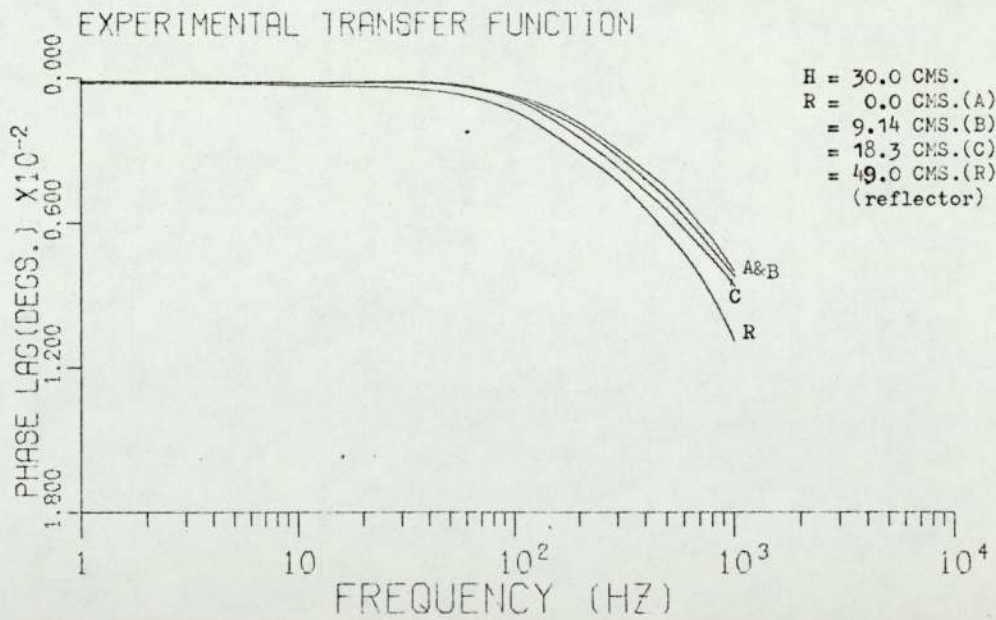
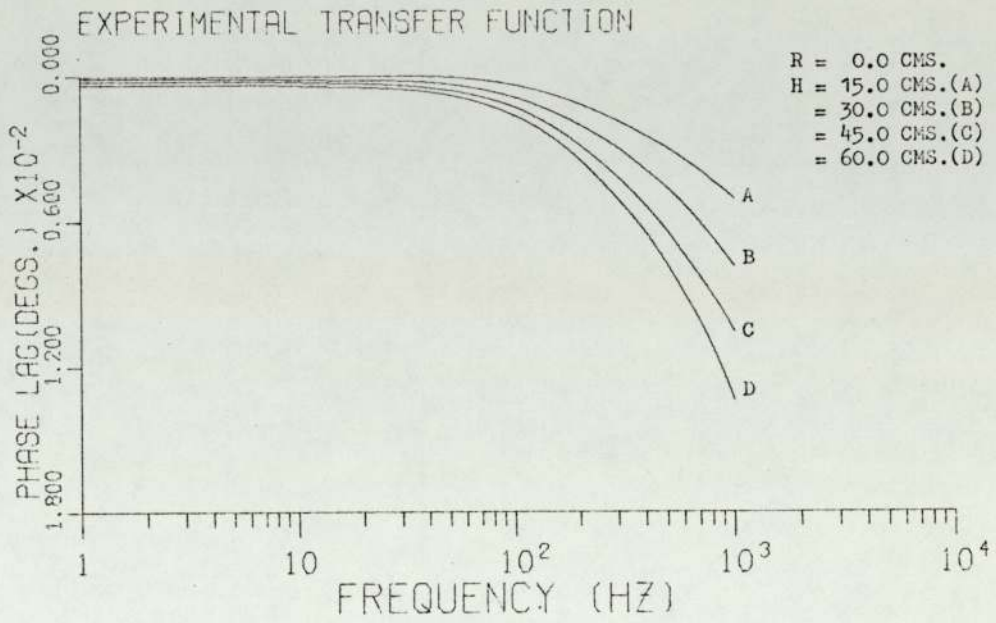
H=60 cms.



H=45 cms.



FIGS. (313) AND (314) MEASURED VARIATION IN AMPLITUDE WITH RADIAL POSITION



FIGS(3.15) AND (3.16) PHASE RESPONSE FOR DIFFERENT AXIAL AND RADIAL POSITIONS

## CHAPTER 4

### THEORY

The methods used to obtain the spatially dependent transfer functions for a nuclear system are presented in this Chapter. First, a multigroup, multidimensional approximation is developed, then an alternative method based on the time-dependent Fermi Age and diffusion theories is considered. In both methods, the time-dependent equations describing the kinetic behaviour of the nuclear system are solved using well known static techniques.

#### 4.1 Complex source method.

This method is based in the transformation of the time-dependent equations describing the kinetic behaviour of a nuclear system into a set of complex equations dependent on space and frequency but independent of time. Once the time-dependence has been removed, the equations can be solved for the real and imaginary components of the fluxes using static techniques. It will be shown how the method presents no problems if the external source and the flux response are assumed to be sinusoidal.

Consider first a one group diffusion approximation. The kinetic behaviour of a nuclear system can be described by,

$$D \nabla^2 \phi(x,t) - \Sigma_r \phi(x,t) + (1 - \beta) \nu \Sigma_f \phi(x,t) + \Sigma_i \lambda_i C_i(x,t) + S(x,t) = \frac{1}{v} \frac{\partial \phi(x,t)}{\partial t} \quad \dots (4.1)$$

where  $S(t)$  is a source term which represents the external disturbance. The other terms have their usual meanings.

The precursor densities  $C_i(x,t)$  are given by:

$$\frac{\partial C_i(x,t)}{\partial t} = \beta_i \nu \Sigma_f \epsilon \phi(x,t) - \lambda_i C_i(x,t) \quad \dots (4.2)$$

If we consider an external sinusoidal disturbance and we assume that the flux response is also sinusoidal, we can express  $\phi(x,t)$  as

$$\phi(x,t) = \phi(x) e^{j\omega t} \quad \dots (4.3)$$

where  $\phi(x)$  is a complex amplitude dependent on frequency and position. In a similar manner we can assume that

$$\begin{aligned} C_i(x,t) &= C_i(x) e^{j\omega t}, \text{ and} \\ S(x,t) &= S(x) e^{j\omega t} \end{aligned} \quad \dots (4.4)$$

Where  $C_i(x)$  and  $S(x)$  are also complex amplitudes. By substituting these in equation (4.1) and eliminating  $e^{j\omega t}$  the following expression is obtained,

$$\begin{aligned} D \nabla^2 \phi(x) - (\Sigma_r + \frac{j\omega}{v}) \phi(x) + \\ + (1 - \beta) \nu \Sigma_f \phi(x) + \nu \Sigma_f \phi(x) \Sigma_i \frac{(\lambda_i - j\omega) \lambda_i^\beta}{\lambda_i^2 + \omega^2} \\ + S(x) = 0 \end{aligned} \quad \dots (4.5)$$

Since  $\phi(x)$  and  $S(x)$  are complex amplitudes, their real and imaginary components must satisfy equation (4.5) separately. This yields two intercoupled equations in terms of  $\phi_R$  and  $\phi_I$ , the in-phase and quadrature components of  $\phi(x)$ . They can be written as follows,

$$\begin{aligned}
 D \nabla^2 \phi_R - \Sigma_r \phi_R + \frac{\omega}{V} \phi_I + v \Sigma_f \left( \phi_R \Sigma_i \frac{\lambda_i \beta_i}{\omega^2 + \lambda_i^2} + \right. \\
 \left. + \phi_I \Sigma_i \frac{\omega \lambda_i \beta_i}{\omega^2 + \lambda_i^2} \right) + (1 - \beta) v \Sigma_f \phi_R + S_R = 0
 \end{aligned}$$

..... (4.6)

$$\begin{aligned}
 D \nabla^2 \phi_I - \Sigma_r \phi_I - \frac{\omega}{V} \phi_R + v \Sigma_f \left( -\phi_R \Sigma_i \frac{\omega \lambda_i \beta_i}{\omega^2 + \lambda_i^2} + \right. \\
 \left. + \phi_I \Sigma_i \frac{\lambda_i^2 \beta_i}{\omega^2 + \lambda_i^2} \right) + (1 - \beta) v \Sigma_f \phi_I + S_I = 0
 \end{aligned}$$

..... (4.7)

These inhomogeneous differential equations can be solved using static techniques for the real and imaginary components,  $\phi_R$  and  $\phi_I$ , of the complex flux amplitude. This will in turn yield the gain and phase shift characteristics of the nuclear system for every frequency of interest.

This method was first applied by C.E. Cohn et al (23). It was later used by other workers (55, 56) in the study of source transfer functions in critical systems. The method is being applied here to a very subcritical system.

In the present work, this treatment was extended to a multigroup model. Both two-group diffusion and two-group Telegrapher's equations were selected for the present calculations.

4.1.1 Two-group diffusion treatment.

The two-group diffusion equations can be written as;

Fast group:

$$D_1 \nabla^2 \phi_1(x,t) - \Sigma r_1 \phi_1(x,t) + S_p(x,t) + S_D(x,t) + S_1(x,t) = \frac{1}{V_1} \frac{\partial \phi_1(x,t)}{\partial t} \dots\dots(4.8)$$

Thermal group:

$$D_2 \nabla^2 \phi_2(x,t) - \Sigma r_2 \phi_2(x,t) + \Sigma_{12} \phi_1(x,t) + S_2(x,t) = \frac{1}{V_2} \frac{\partial \phi_2(x,t)}{\partial t} \dots\dots(4.9)$$

where  $S_p$  and  $S_D$ , the prompt and delayed fissions source terms respectively, are given by:

$$S_p(x,t) = (1-\beta) \sum_j \nu \Sigma_{fj} \phi_j(x,t) \dots\dots(4.10)$$

$$S_D(x,t) = \sum_i \lambda_i C_i(x,t) \dots\dots(4.11)$$

where  $j$  refers to the group number and  $i$  to the precursor number.  $S_1$  and  $S_2$  are the external source terms.

As before, equations (4.8) and (4.9) can be separated into real and imaginary components by making substitutions similar to equations (4.3) and (4.4), yielding four coupled inhomogeneous equations. These can be written as follows:

Fast imaginary:

$$\begin{aligned}
 -D_1 \nabla^2 \phi_1 + \Sigma_1 \phi_1 &= \frac{-\omega}{v_1} \phi_3 + \nu \left( 1 - \sum_i \frac{\omega^2 \beta_i}{\omega^2 + \lambda_i^2} \right) \cdot (\Sigma_{f_1} \phi_1 + \Sigma_{f_2} \phi_2) + \\
 + \nu \sum_i \frac{\omega \lambda_i \beta_i}{\omega^2 + \lambda_i^2} & \cdot (\Sigma_{f_1} \phi_3 + \Sigma_{f_2} \phi_4) + S_1
 \end{aligned}$$

..... (4.12)

Thermal imaginary:

$$-D_2 \nabla^2 \phi_2 + \Sigma_2 \phi_2 = \frac{-\omega}{v_2} \phi_4 + \Sigma_{12} \phi_1 + S_2$$

..... (4.13)

Fast real:

$$\begin{aligned}
 -D_1 \nabla^2 \phi_3 + \Sigma_1 \phi_3 &= \frac{\omega}{v_1} \phi_1 + \left( 1 - \sum_i \frac{\omega^2 \beta_i}{\omega^2 + \lambda_i^2} \right) \cdot (\Sigma_{f_1} \phi_3 + \Sigma_{f_2} \phi_4) + \\
 + \nu \sum_i \frac{\omega \lambda_i \beta_i}{\omega^2 + \lambda_i^2} & \cdot (\Sigma_{f_1} \phi_1 + \Sigma_{f_2} \phi_2) + S_3
 \end{aligned}$$

..... (4.14)

Thermal real:

$$-D_2 \nabla^2 \phi_4 + \Sigma_2 \phi_4 = \frac{\omega}{v_2} \phi_2 + \Sigma_{12} \phi_3 + S_4$$

..... (4.15)

It can be noticed how the equations for each group are identical except for an interchange in the flux subscripts and a sign change in the coupling term between real and imaginary flux components.

The gain and phase characteristics of the nuclear system can then be obtained from the complex fluxes as in one group diffusion approximation.

The two-group diffusion analysis developed in this

section was programmed for a two dimensional cylindrical geometry similar in shape and nuclear characteristics to the subcritical assembly described previously in Chapter 2. Both the method of solution of equations (4.12) to (4.15) and results will be considered in a later section.

#### 4.1.2 Two-group Telegrapher's treatment.

In many cases the conditions required in order to apply diffusion theory can not be met. These conditions include the neglect of the absorption cross-section in comparison to the scattering cross-section, the avoidance of proximity to sources and boundaries, the assumption that the flux is isotropic and that it does not change rapidly with position. Besides, in diffusion theory a disturbance initiated at any point within or on a boundary of a system at steady state is instantaneously sensed everywhere within the system. That is, the initial part of the perturbation propagates with an infinite velocity.

Physically, when a wavelike disturbance is introduced at some point in the system, the neutron field in the proximity of the point is perturbed and the disturbance begins to move outwards. Since neutrons move with a finite velocity, an initially well defined wavefront must be expected and therefore any equation describing a time-dependent neutron phenomena should allow for this. Furthermore, some residual disturbance effects remain within the system even after the passage of the wavefront.

The Telegrapher's equation was selected for the present calculations because it describes the time-

dependent neutron phenomena which exhibits both wavelike properties and residual disturbance effects.

In contrast to the diffusion equation, which can be derived directly from a balance of neutrons within the system, the Telegrapher's equation is obtained from the direction and time-dependent Boltzman transport equation (57, 10).

The two-group Telegrapher's equations can be written (23) as follows;

Fast group:

$$\begin{aligned}
 & D_1 \nabla^2 \phi_1(x, t) - \Sigma_1 \phi_1(x, t) + S_p(x, t) + S_D(x, t) \\
 & + S_1(x, t) = \left( \frac{1 + 3D_1 \Sigma_1}{V_1} \right) \frac{\partial \phi_1(x, t)}{\partial t} + \frac{3D_1}{V_1^2} \frac{\partial^2 \phi_2(x, t)}{\partial t^2} \\
 & \dots\dots (4.16)
 \end{aligned}$$

Thermal group:

$$\begin{aligned}
 & D_2 \nabla^2 \phi_2(x, t) - \Sigma_2 \phi_2(x, t) + \Sigma_{12} \phi_1(x, t) + \\
 & + S_2(x, t) = \left( \frac{1 + 3D_2 \Sigma_2}{V_2} \right) \frac{\partial \phi_2(x, t)}{\partial t} + \\
 & + \frac{3D_2}{V_2^2} \frac{\partial^2 \phi_2(x, t)}{\partial t^2} \\
 & \dots\dots (4.17)
 \end{aligned}$$

The presence of the second order time derivative of flux  $\frac{\partial^2 \phi}{\partial t^2}$  introduces into the analysis a finite velocity for propagation of a disturbance which decays as determined by the term  $\frac{\partial \phi}{\partial t}$ .

Equations (4.16) and (4.17) can be separated, as

before, into real and imaginary components. This yields the following,

Fast imaginary:

$$\begin{aligned}
 -D_1 \nabla^2 \phi_1 + \left( \sum r_1 \frac{-3D_1 \omega^2}{v_1^2} \right) \phi_1 &= \frac{-\omega}{v} (1 + 3D_1 \sum r_1) \phi_3 + \\
 + v \left( 1 - \sum_i \frac{\omega^2 \beta_i}{\omega^2 + \lambda_i^2} \right) \cdot (\sum_{f_1} \phi_1 + \sum_{f_2} \phi_2) + \\
 + v \sum_i \frac{\omega \lambda_i \beta_i}{\omega^2 + \lambda_i^2} \left( \sum_{f_1} \phi_3 + \sum_{f_2} \phi_4 \right) + S_1 &\dots\dots (4.18)
 \end{aligned}$$

Thermal imaginary:

$$\begin{aligned}
 -D_2 \nabla^2 \phi_2 + \left( \sum r_2 - \frac{3D_2 \omega^2}{v_2^2} \right) \phi_2 &= \frac{-\omega}{v_2} (1 + 3D_1 \sum r_2) \phi_4 + \\
 + \sum_{12} \phi_1 + S_2 &\dots\dots (4.19)
 \end{aligned}$$

Fast real:

$$\begin{aligned}
 -D_1 \nabla^2 \phi_3 + \left( \sum r_1 \frac{-3D_1 \omega^2}{v_1^2} \right) \phi_3 &= \frac{-\omega}{v_1} (1 + 3D_1 \sum r_1) \phi_3 + \\
 + v \left( 1 - \sum_i \frac{\omega^2 \beta_i}{\omega^2 + \lambda_i^2} \right) \cdot (\sum_{f_1} \phi_3 + \sum_{f_2} \phi_4) + \\
 + v \sum_i \frac{\omega \lambda_i \beta_i}{\omega^2 + \lambda_i^2} \left( \sum_{f_1} \phi_1 + \sum_{f_2} \phi_2 \right) + S_3 &\dots\dots (4.20)
 \end{aligned}$$

Thermal real:

$$-D_2 \nabla^2 \phi_4 + \left( \Sigma_{r_2} - \frac{3D_2 \omega^2}{v_2^2} \right) \phi_4 = \frac{-\omega}{v_2} \left( 1 + 3D_2 \Sigma_{r_2} \right) \phi_2 + \Sigma_{12} \phi_3 + S_4 \quad \dots (4.21)$$

As in the case of the two-group diffusion analysis, these equations were solved for a two-dimensional cylindrical geometry.

In the next section, the method used for solving both the telegrapher's and diffusion equation is presented in detail.

#### 4.1.3 Method of solution.

Both the diffusion and Telegrapher's equations were solved by means of the computer program SNAP (58, 59). The code is a Fortran IV program that solves the finite difference form of the group diffusion equations in one or two dimensions (\*). The program can handle up to 60 energy groups and fixed source problems are allowed.

The code solves for each group the following pair of equations,

$$-\nabla \cdot D_g(r) \nabla \phi_g(r) + \Sigma_g(r) \phi_g(r) = Q \quad \dots (4.22)$$

$$Q = \sum_{n=1}^G \Sigma_{ng}(r) \phi_n(r) + \frac{1}{k} \sum_{m=1}^M X_{mg}(r) \cdot$$

$$\cdot \sum_{n=1}^G [\nu \Sigma_f(r)]_{mn} \phi_n(r) + S_g(r) \quad \dots (4.23)$$

---

(\* ) there is now available a three dimensional version of the code (60).

Where,

$g$  = energy group.

$G$  = total number of groups.

$M$  = number of fissionable materials or nuclides.

$r$  = two-dimensional position vector.

$\Sigma_g$  = effective removal cross section.

$\Sigma_{hg}$  = scatter cross section.

$X$  = emergence spectrum of fission neutrons.

$K$  = unknown positive eigenvalue greater than the modules of all other eigenvalues.

$\phi$  = neutron flux (positive eigenfunction corresponding to  $K$ ).

Now, let us consider a four group problem with only one fissionable nuclide. Equations (4.22) and (4.23) can be rewritten as,

Group 1,

$$\begin{aligned}
 & -\nabla \cdot D_1 \nabla \phi_1 + \Sigma_1 \phi_1 = \\
 & = \Sigma_{11} \phi_1 + \Sigma_{21} \phi_2 + \Sigma_{31} \phi_3 + \Sigma_{41} \phi_4 + \\
 & + \frac{X_1}{K} \left[ (\nu \Sigma_f)_1 \phi_1 + (\nu \Sigma_f)_2 \phi_2 + (\nu \Sigma_f)_3 \phi_3 + \right. \\
 & \qquad \qquad \qquad \left. + (\nu \Sigma_f)_4 \phi_4 \right] + S_1 \quad \dots \dots (4.24)
 \end{aligned}$$

Group 2,

$$\begin{aligned}
 & -\nabla \cdot D_2 \nabla \phi_2 + \Sigma_2 \phi_2 = \\
 & = \Sigma_{12} \phi_1 + \Sigma_{22} \phi_2 + \Sigma_{32} \phi_3 + \Sigma_{42} \phi_4 + \\
 & + \frac{X_2}{K} \left[ (\nu \Sigma_f)_1 \phi_1 + (\nu \Sigma_f)_2 \phi_2 + (\nu \Sigma_f)_3 \phi_3 + (\nu \Sigma_f)_4 \phi_4 \right] + \\
 & \qquad \qquad \qquad + S_2 \quad \dots \dots (4.25)
 \end{aligned}$$

Group 3,

$$\begin{aligned}
 & -\nabla \cdot D_3 \nabla \phi_3 + \Sigma_3 \phi_3 = \\
 & = \Sigma_{13} \phi_1 + \Sigma_{23} \phi_2 + \Sigma_{33} \phi_3 + \Sigma_{43} \phi_4 + \\
 & + \frac{\lambda_3}{K} \left[ (\nu \Sigma_f)_1 \phi_1 + (\nu \Sigma_f)_2 \phi_2 + (\nu \Sigma_f)_3 \phi_3 + (\nu \Sigma_f)_4 \phi_4 \right] + S_3 \\
 & \dots\dots (4.26)
 \end{aligned}$$

Group 4,

$$\begin{aligned}
 & -\nabla \cdot D_4 \nabla \phi_4 + \Sigma_4 \phi_4 = \\
 & = \Sigma_{14} \phi_1 + \Sigma_{24} \phi_2 + \Sigma_{34} \phi_3 + \Sigma_{44} \phi_4 + \\
 & + \frac{\lambda_4}{K} \left[ (\nu \Sigma_f)_1 \phi_1 + (\nu \Sigma_f)_2 \phi_2 + (\nu \Sigma_f)_3 \phi_3 + \right. \\
 & \quad \left. + (\nu \Sigma_f)_4 \phi_4 \right] + S_4 \\
 & \dots\dots (4.27)
 \end{aligned}$$

In the present calculations, where only one fissionable nuclide is considered, the emergence spectrum of fissionable neutrons is (58) (1,0,0,0); that is, all fast neutrons from fission are assumed to appear in the first group.

The scatter fission and removal cross sections necessary to run the program, are obtained by comparing equations (4.24) to (4.27) with those describing either theoretical model, diffusion or Telegrapher's. Thus, by comparison with equations (4.18) to (4.21),

$$\Sigma_{ij} = \begin{pmatrix} 0 & \Sigma_{12} & \frac{\omega(1+3D_1 \Sigma_{r1})}{V_1} & 0 \\ 0 & 0 & \left(\frac{\omega\lambda\beta}{\omega^2 + \lambda^2}\right)v\Sigma_{f_2} & \frac{(1+3D_2 \Sigma_{r2})}{V_2} \\ -\frac{\omega(1+3D_1 \Sigma_{r1})}{V_1} & 0 & 0 & \Sigma_{12} \\ -\left(\frac{\omega\lambda\beta}{\omega^2 + \lambda^2}\right)v\Sigma_{f_2} & -\frac{\omega(1+3D_2 \Sigma_{r2})}{V_2} & \left(1 - \frac{\omega^2\beta}{\omega^2 + \lambda^2}\right)v\Sigma_{f_2} & 0 \end{pmatrix}$$

..... (4.28)

$$\left(v\Sigma_f\right)_i = \begin{pmatrix} 0 \\ \left(1 - \frac{\omega^2\beta}{\omega^2 + \lambda^2}\right)v\Sigma_{f_2} \\ 0 \\ 0 \end{pmatrix}$$

..... (4.29)

$$\Sigma_{i} = \begin{pmatrix} \Sigma_{r_1} - \frac{3D_1 \omega^2}{v_1^2} \\ \Sigma_{r_2} - \frac{3D_2 \omega^2}{v_2^2} \\ \Sigma_{r_1} - \frac{3D_1 \omega^2}{v_1^2} \\ \Sigma_{r_2} - \frac{3D_2 \omega^2}{v_2^2} \\ \dots \end{pmatrix} \quad (4.30)$$

where  $\beta = \sum_i \beta_i$ ,  $\frac{\partial}{\partial \lambda} = \sum_i \frac{\partial}{\partial \lambda_i}$  and  $\Sigma_{f_1}$  has been neglected in comparison with  $\Sigma_{f_2}$ .

In the same way, the cross-sections corresponding to the diffusion model are,

$$\Sigma_{ij} = \begin{pmatrix} 0 & \Sigma_{12} & \frac{\omega}{v_1} & 0 \\ 0 & 0 & \left( \frac{\omega \lambda \beta}{\omega^2 + \lambda^2} \right) v \Sigma_{f_2} & \frac{\omega}{v_2} \\ \frac{-\omega}{v_1} & 0 & 0 & \Sigma_{12} \\ \left( \frac{\omega \lambda \beta}{\omega^2 + \lambda^2} \right) v \Sigma_{f_2} & -\frac{\omega}{v_2} & \left( 1 - \frac{\omega^2 \beta}{\omega^2 + \lambda^2} \right) v \Sigma_{f_2} & 0 \\ \dots \end{pmatrix} \quad (4.31)$$

$$\Sigma_i = \begin{pmatrix} \Sigma_{r_1} \\ \Sigma_{r_2} \\ \Sigma_{r_1} \\ \Sigma_{r_2} \\ \dots \end{pmatrix} \dots \dots (4.32)$$

The fission cross sections for the diffusion treatment are the same as those of the Telegrapher's treatment (4.29).

These frequency dependent constants were used to calculate the fluxes for different frequencies in a two dimensional cylindrical geometry very similar to the subcritical system under study. The values of the fluxes were computed in 250 different positions inside the system.

Programming details referring SNAP can be found in refs. (58, 59, 61 and 62).

Calculations were performed for frequencies ranging from 0 up to 400 Hz. Beyond 400 Hz the code was unable to find a solution. For low frequencies, the convergence of the problem was very uniform and only around 25 iterations were required. This rate of convergence was approximately constant up to 200 Hz. At higher frequencies the rate of convergence became completely non-uniform. For instance, no convergence was achieved after 100 iterations at 225 Hz while at 250 Hz convergence was achieved after 24 iterations and 82 iterations were necessary at 275 Hz. This behaviour seems to indicate that the iteration scheme followed by SNAP is somewhat unstable when the off diagonal elements of the coefficient matrix reach a limiting negative

value which in our case seems to correspond to around 225 Hz. The same unstable behaviour was also observed by Cohn when using CRAM (63) an older code which has many features in common with SNAP. Cohn was unable to use CRAM for frequencies greater than 50 Hz when trying to calculate the transfer functions in a D<sub>2</sub>O moderated critical system in a one-dimensional geometry. It seems therefore that the successive over-relaxation techniques (SOR) used by SNAP (64) represent an improvement over the PDQ method used by CRAM. A definite conclusion can not be drawn, however, without testing SNAP in a critical system. It should also be desirable to test the latest version of SNAP which includes the possibility of using a three dimensional geometry (60).

It was possible, however, to perform calculations beyond 400 Hz by considering a simplified nuclear system which consisted of the equivalent unreflected system in which the negative upscatter terms corresponding to the graphite were assumed to be equal to zero. By using this approximation most of the off diagonal elements of the coefficient matrix with negative values were eliminated. With this arrangement it was possible to perform calculations for frequencies going up to 1500 Hz.

Results are presented and discussed in the next Chapter.

#### 4.2 Fermi Age - Diffusion method.

An alternative method of calculating the spatially dependent transfer function in a nuclear system

is being considered in this section. As in the previous theoretical model, the transfer function refers to the relationship between the thermal neutron density fluctuations at a point in the nuclear system and the fluctuations of an artificial source of fast neutrons having a known spatial distribution.

The method, based on the Fermi Age and diffusion theories was first applied by C.D. Kylstra and R.E. Uhrig (65), (66) and (26). The method of analysis to obtain the spatially dependent transfer function is very cumbersome and therefore is not presented in detail in the present work.

Let us consider an isotropic and homogeneous, single-region multiplying nuclear system. The driving function or input to the system is a time-varying source of fast neutrons. These undergo a slowing down phase represented by the time-dependent Fermi Age theory. Upon reaching thermal energy, the neutrons enter a diffusion phase at constant velocity represented by the time-dependent diffusion theory. Additional neutrons are created by fission and join the source of neutrons in the slowing down process.

It is also assumed for simplicity that the neutrons from the artificial source, the prompt neutrons from fission and the delayed neutrons have the same energy at birth. This energy is defined as the zero point on the lethargy scale.

In order to determine the spatially dependent transfer function in the system under consideration, the

following procedure is followed:

(1) The dynamic behaviour of the system is represented by three linear differential equations. These are the Fermi Age equation for continuous slowing down, absorption and leakage, the time dependent diffusion equation and the equation of the delayed neutron precursors.

They can be written as follows:

The time dependent Fermi Age equation for continuous slowing down, absorption and leakage (25)

$$\frac{1}{v(u)} \frac{\partial \phi(r, u, t)}{\partial t} = -\frac{\partial q(r, u, t)}{\partial u} - \Sigma_a(u) \phi(r, u, t) +$$

$$+ D(u) \nabla^2 \phi(r, u, t) + S_a(r, t) \delta(u) + \nu \Sigma_f \epsilon (1-\beta) \phi_t(r, t) \delta(u) +$$

$$+ \sum_{i=1}^m \lambda_i C_i(r, t) \delta(u)$$

$$u \geq 0 \qquad \dots (4.33)$$

Neutrons from prompt fission  $\nu \Sigma_f (1-\beta) \phi_t(r, t)$ , from the decay of the neutron precursors  $\sum_{i=1}^m \lambda_i C_i(r, t)$ , and from the artificial source  $S_a(r, t)$ , start the slowing down at zero lethargy. The slowing down neutron flux is  $\phi(r, u, t)$  and the thermal flux which is not a function of lethargy is  $\phi_t(r, t)$ . The slowing down density is represented by  $q(r, u, t)$ . The other terms have their usual meaning.

The Dirac delta function  $\delta(u)$  in the source terms is necessary since the source neutrons have zero lethargy by definition.

The time-dependent diffusion equation is,

$$\frac{1}{v_t} \frac{\partial \phi_t(r,t)}{\partial t} = \Sigma_{at} \phi_t(r,t) + D_t \nabla^2 \phi_t(r,t) + q(r, u_t, t) \dots (4.34)$$

and finally, the equations for the delayed neutron precursors are,

$$\frac{\partial C_i(r,t)}{\partial t} = \beta_i \nu \Sigma_f \phi_t(r,t) - \lambda_i C_i(r,t) \dots (4.35)$$

$i = 1 \dots \dots \dots m$

Equations (4.33), (4.34) and (4.35) are coupled; equation (4.33) is coupled to equation (4.34) by  $q(r, u_t, t)$ , equation (4.34) is coupled to equation (4.35) by  $\beta_i \nu \Sigma_f \phi_t(r,t)$  and equation (4.33) is coupled to equation (4.34) and (4.35) by  $\left[ \nu \Sigma_f \epsilon (1-\beta) \phi_t(r,t) + \sum_{i=1}^m \lambda_i C_i(r,t) \right] \delta(u)$ .

(2) These equations are separated in terms of the steady-state and time-dependent components. This produces three linear, time dependent equations in terms of the change in the thermal neutron density, the slowing down density, the precursors and the artificial source.

(3) These equations are Laplace transformed. This eliminates the time derivatives from the equations and produces a change from the time to the frequency domain.

(4) The slowing down density, thermal neutron density, precursor density and the artificial source are expanded in a series of spatial harmonics. This yields the expression which gives the perturbation in the neutron density at any point inside the system, caused by an

artificial source.

Let us now consider a homogeneous, cylindrical, multiplying nuclear system with the artificial source located at the centre of the bottom face which represents the origin of the system. The spatially dependent transfer function is given by the expression (65, 66)

$$\begin{aligned}
 T(r, \omega) = & P(u_t) l_s \exp(-j\omega l_T) \sum_{n=1}^{\infty} \frac{J_0(\nu_n \rho)}{J_1^2(\nu_n)} \cdot \\
 & \cdot \sum_{i=1}^{\infty} \frac{\exp(-\tau B_n^2 + \tau R_i^2)}{R_i [L^2 + \tau(1 + L^2 B_n^2 - L^2 R_i^2 + j\omega l_s)]} \\
 & \cdot \left[ \exp(-R_i Z) + \sum_{m=1}^{\infty} (-1)^m \left\{ \exp[-R_i (Z + Hm)] + \exp[R_i (Z - Hm)] \right\} \right]
 \end{aligned}
 \tag{4.36}$$

where

$P(u_t)$  = resonance scape probability

$l_s$  = thermal lifetime

$l_T$  = slowing down time

$\nu$  = n'th zero of the  $J_0$  Bessel function

$\rho$  = radial co-ordinate divided by the system radius, R

H = height of the assembly

Z = axial co-ordinate

$R_i$  represents the roots of the following,

$$(1 + L^2 B_n^2 - L^2 R_i^2 + j\omega L_s) \exp(j\omega L_s + \tau B_n^2 - \tau R_i^2) -$$

$$-K_\infty \left( 1 - \beta + \sum_{i=1}^m \frac{\beta_i \lambda_i}{j\omega + \lambda_i} \right) = 0 \quad \dots (4.37)$$

Equation(4.36) was numerically solved by means of the computer program FERMI (written by the author) which uses essentially the same numerical techniques as SPAT (65, 66). The program, written in standard FORTRAN IV is listed in appendix 3 together with input and output examples. The main differences from SPAT include (apart from the language itself), a complete change of most machine subroutines which were incompatible with any modern ICL or IBM compiler and a change in the whole structure of the program including the input and output channels. General graphplotter options were also introduced in the program. They allow the user to obtain a graphical display of the change of amplitude with frequency. A graphical comparison between the calculated and experimentally obtained amplitudes can also be done with the program. Details of the input requirements and output options are given in Appendix 3.

The code was used to calculate the source transfer function for an homogeneous cylinder of 81.3 cms. high and 39.0 cms. radius which are the extrapolated dimensions of the subcritical assembly used in the present experiments. Calculations were performed for different output locations and for frequencies ranging from 0 up to 3,000 Hz.

Results, which are shown in the next Chapter, were compared with those obtained both with the lumped parameter model and the complex source method described in the previous section. They were also compared with those obtained experimentally.

## CHAPTER 5

### RESULTS

In this Chapter, the results obtained with both theoretical models described in the previous Chapter, are presented and discussed. Also, in order to test the validity of both methods, the theoretical results are compared with those obtained experimentally. No reference is made in this Chapter to the measurements of the transfer function performed via gamma detection. Those measurements are discussed in the next Chapter.

By definition both theoretical models give an amplitude of 1 and a phase shift of 0 at zero frequency. This is also assumed in the experimental analysis. Therefore, the values plotted in the theoretical graphs of this Chapter, are directly comparable.

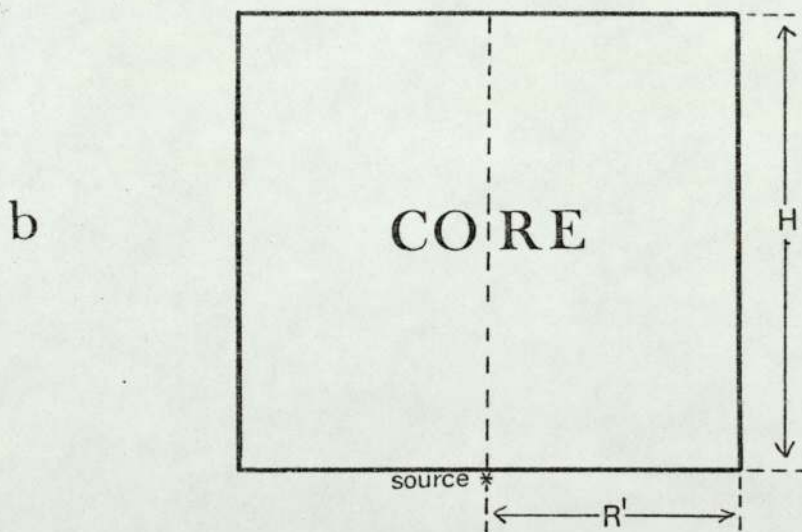
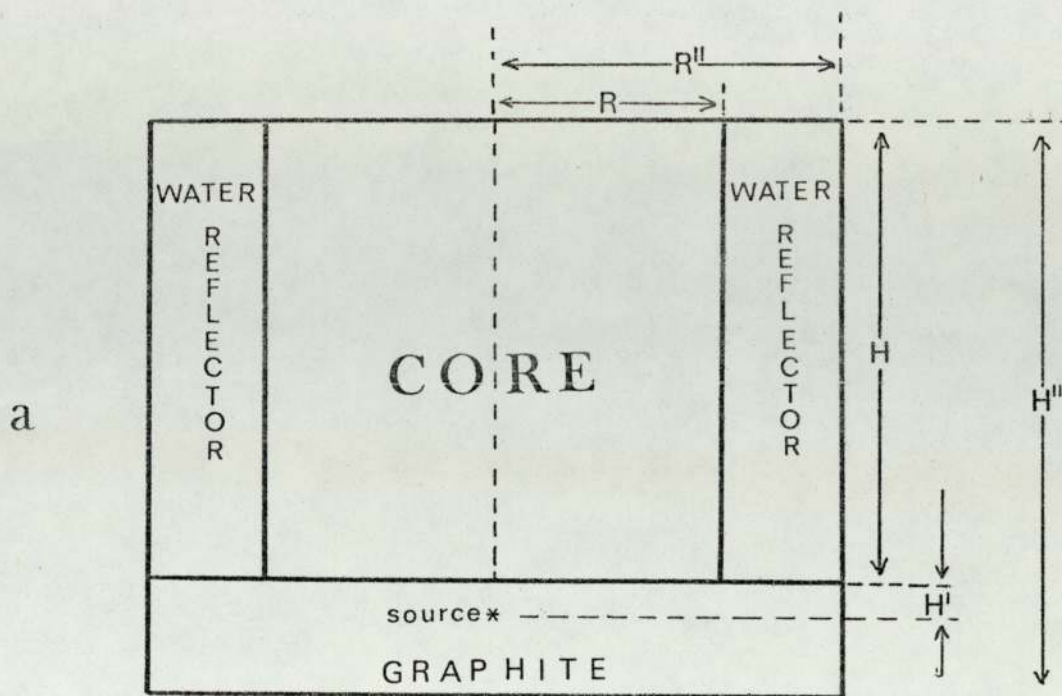
#### 5.1 Complex Source Method.

As described in the previous Chapter, both the amplitude and phase shift characteristics of the Nuclear System were calculated by means of the computer program SNAP. The code was used to determine the fluxes corresponding to the solution of both the Diffusion and Telegrapher's equations. These fluxes were calculated for frequencies ranging from 0 to up to 400 Hz for a two dimensional geometry similar in size and nuclear characteristics to the subcritical system used to test the validity of the theoretical method. The values of the fluxes, which represent the real and imaginary

components of the complex amplitude, were computed in 250 different positions inside the nuclear system, including several points inside the reflector. The values of the real and imaginary components of the complex amplitude were then used to determine the amplitude and phase shift for every frequency and position of interest. A cross section of the nuclear system as assumed in this theoretical model is given in Figure (5.1) which also shows the nuclear system assumed for the Fermi Age diffusion method.

Figures (5.2) and (5.3) show a comparison between amplitude and phase response for the two-group diffusion and the two-group Telegrapher's equations. It can be seen from these figures how the response is practically identical for both theoretical approaches, at least for the range of frequencies in which SNAP was able to find a solution. A comparison between the theoretical results and the experimental ones, showed that the experimental results follow slightly better the Telegrapher's than the diffusion approach. For this reason, all graphs shown in this Chapter referring to the complex source method, will correspond to the Telegrapher's approach.

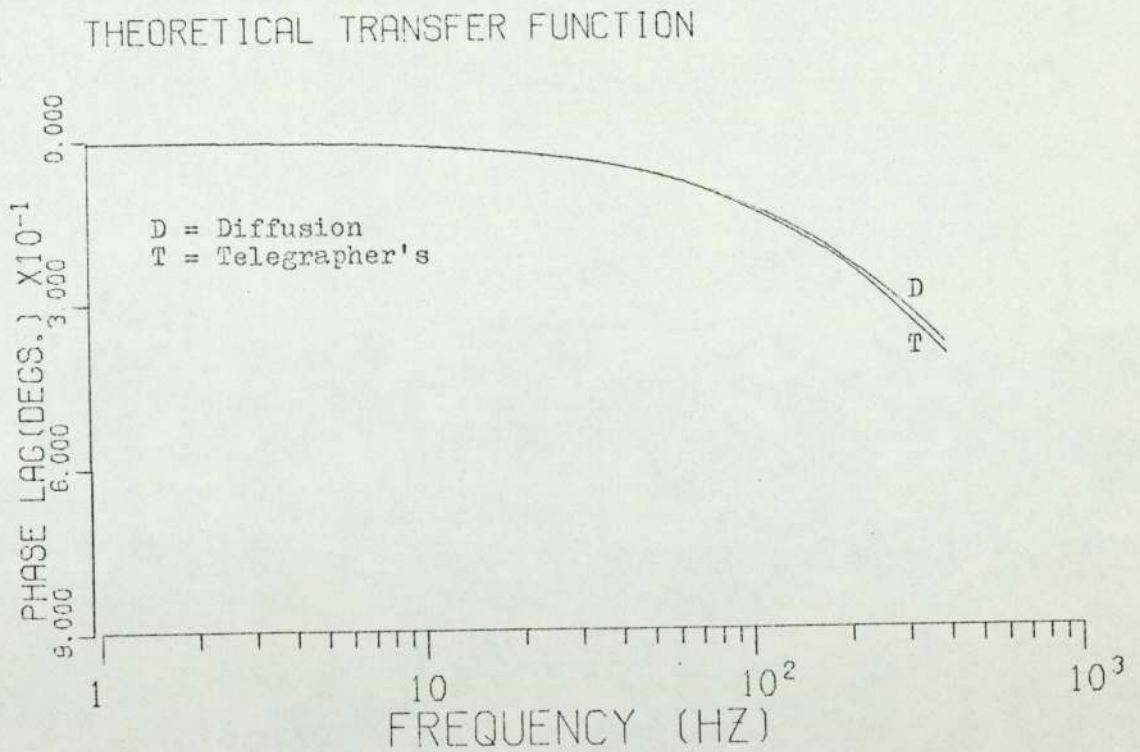
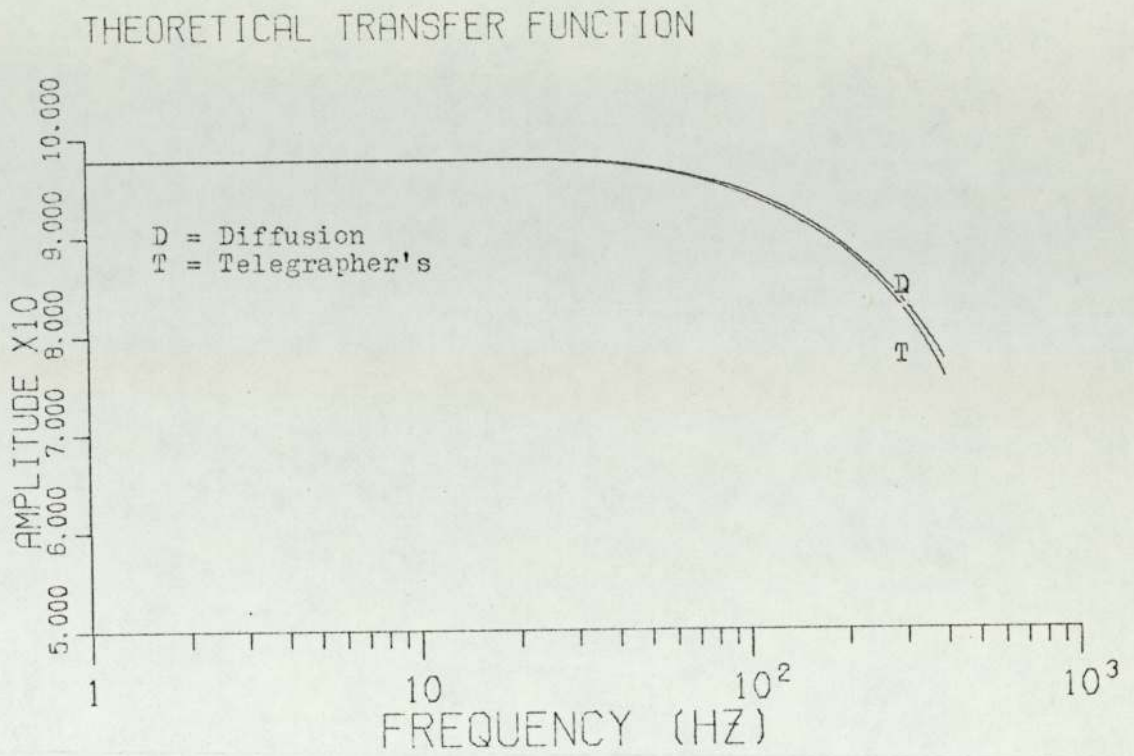
The theoretical amplitude response of the nuclear system for different axial positions is shown in Figures (5.4) and (5.5). These two figures show how for each output position, the amplitude and therefore the spatial differences remain practically constant for frequencies of up to nearly 100 Hz. At the higher end of the system, however, the amplitude starts falling down before this



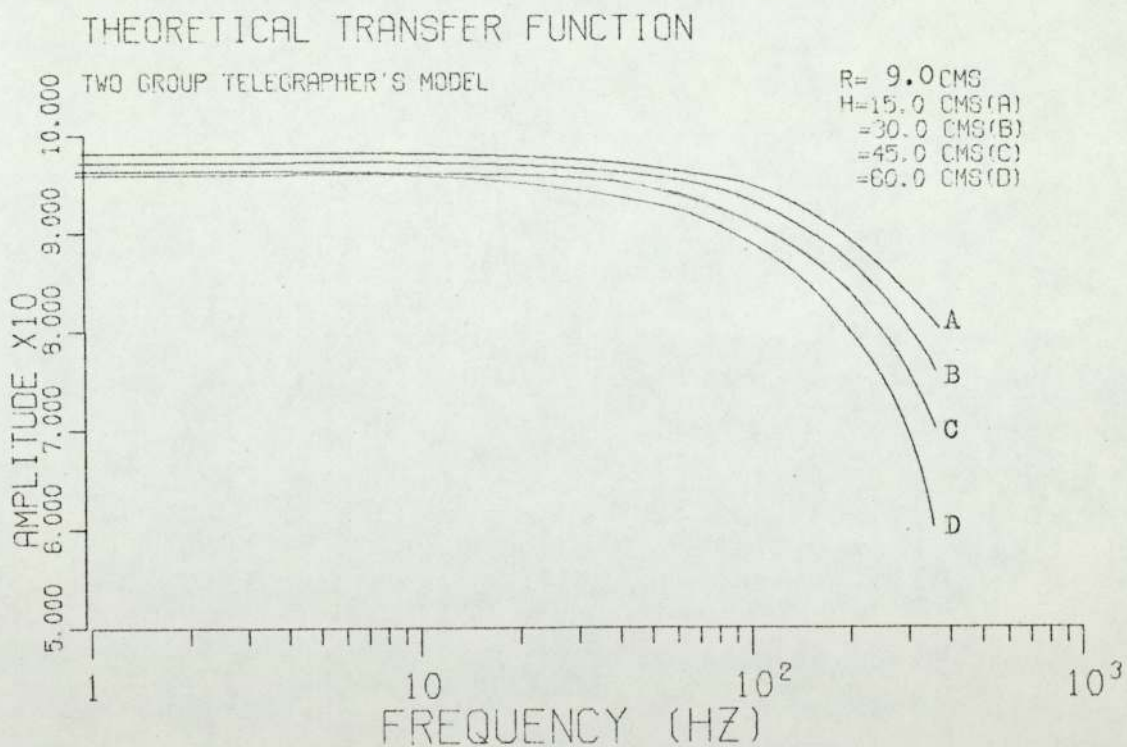
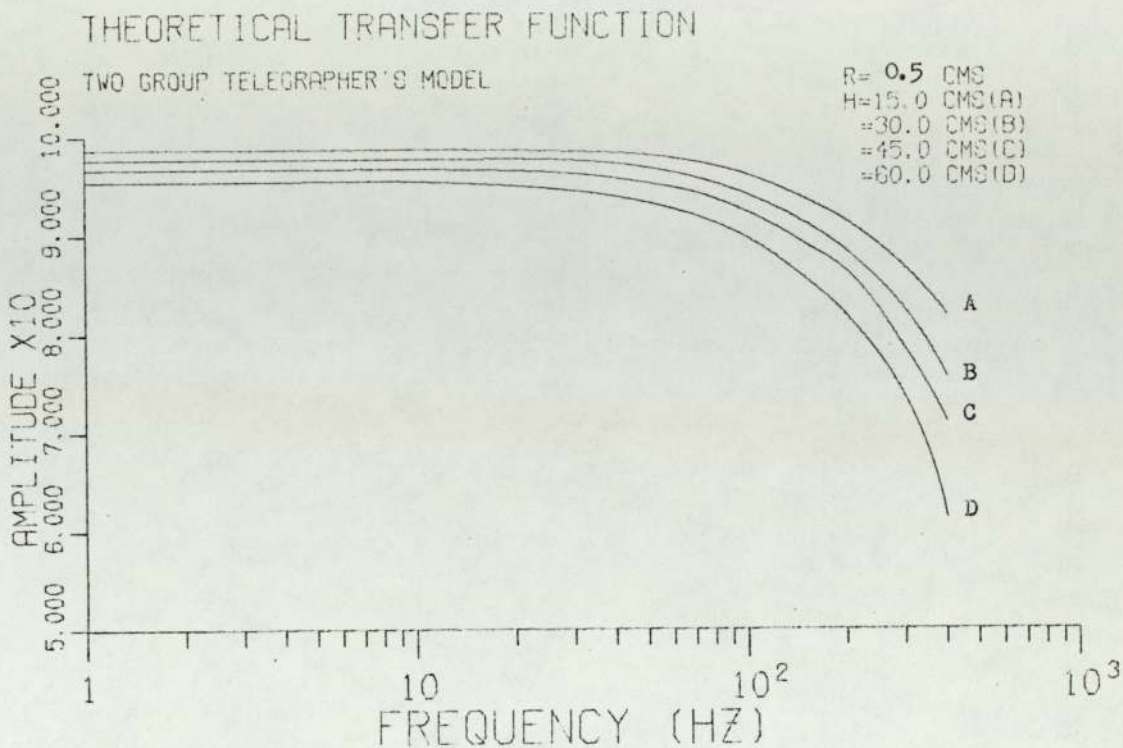
$H = 81.3$  CMS  
 $H' = 15.0$  CMS  
 $H'' = 126.3$  CMS

$R = 33.3$  CMS  
 $R' = 39.0$  CMS  
 $R'' = 45.3$  CMS

FIG.(5.1) SCHEMATIC DIAGRAM OF THE SUBCRITICAL ASSEMBLY AS CONSIDERED BY BOTH THEORETICAL MODELS  
 a- COMPLEX SOURCE  
 b- FERMI AGE - DIFFUSION



FIGS. (5.2) and (5.3) COMPARISON BETWEEN DIFFUSION AND TELEGRAPHER'S TREATMENTS



FIGS.(5.4)and (5.5) THEORETICAL AMPLITUDE RESPONSE FOR DIFFERENT AXIAL POSITIONS

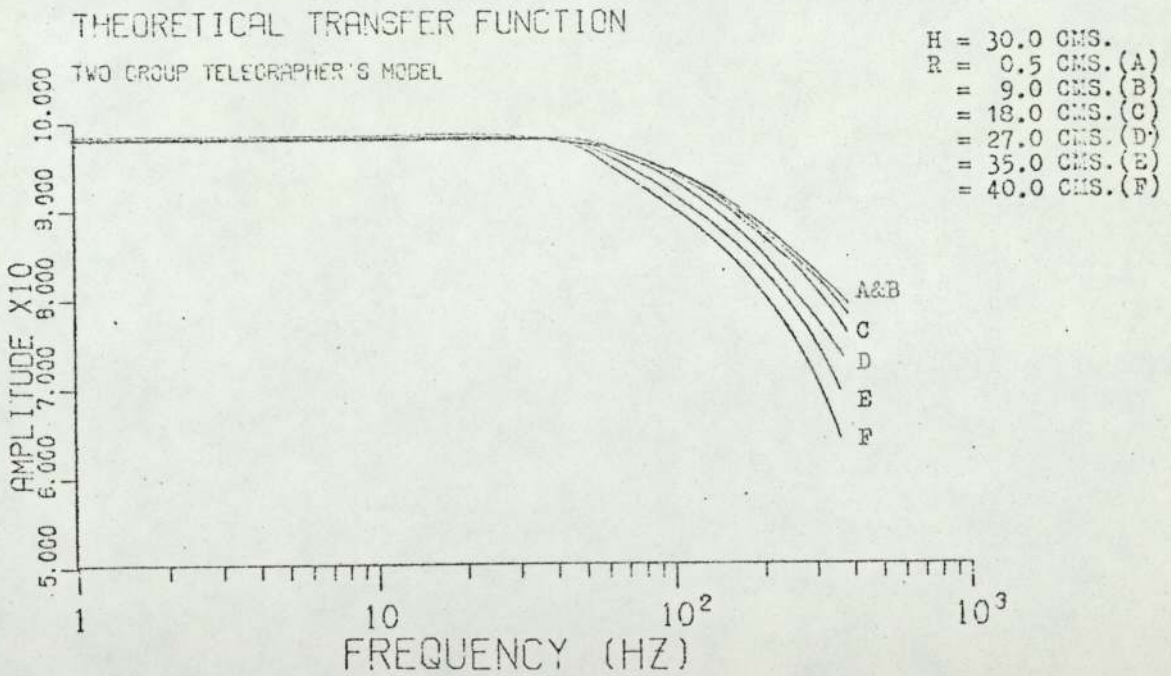
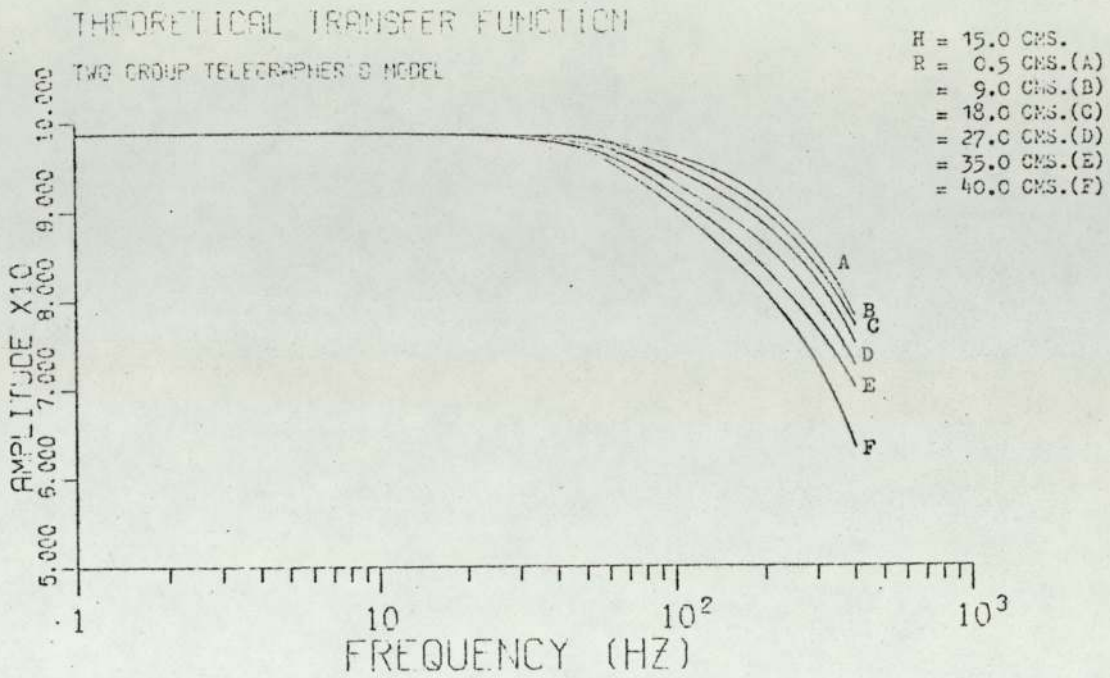
frequency. Beyond 100 Hz, the amplitude decreases rather rapidly and the spatial differences become much more noticeable.

The response varied markedly for different radial positions as shown in Figures (5.6) and (5.7). Here, no spatial differences are noticeable for frequencies of up to nearly 50 Hz, and above this frequency, the differences are rather small. This effect could be explained, as already seen in Chapter 3, by the fact that the neutrons produced in an almost point source, are spread out inside the graphite pedestal which supports the nuclear system and enter the system in a broad beam. Also, from Figures (5.6) and (5.7) it can be seen how the spatial differences are much higher in the reflector, where the response is more attenuated due to the much longer neutron lifetime in the water reflector.

The theoretical phase response of the nuclear system for different axial and radial positions is shown in Figures (5.8) to (5.11). Here, again, the spatial differences are much more noticeable in the case of an axial distribution. Also, the reflector effect is very marked.

## 5.2 Fermi Age - Diffusion Method.

The equation representing the spatially dependent transfer function (4.36) was numerically solved by means of the computer program FERMI which has already been described in Chapter 4 and which is listed in Appendix 3.

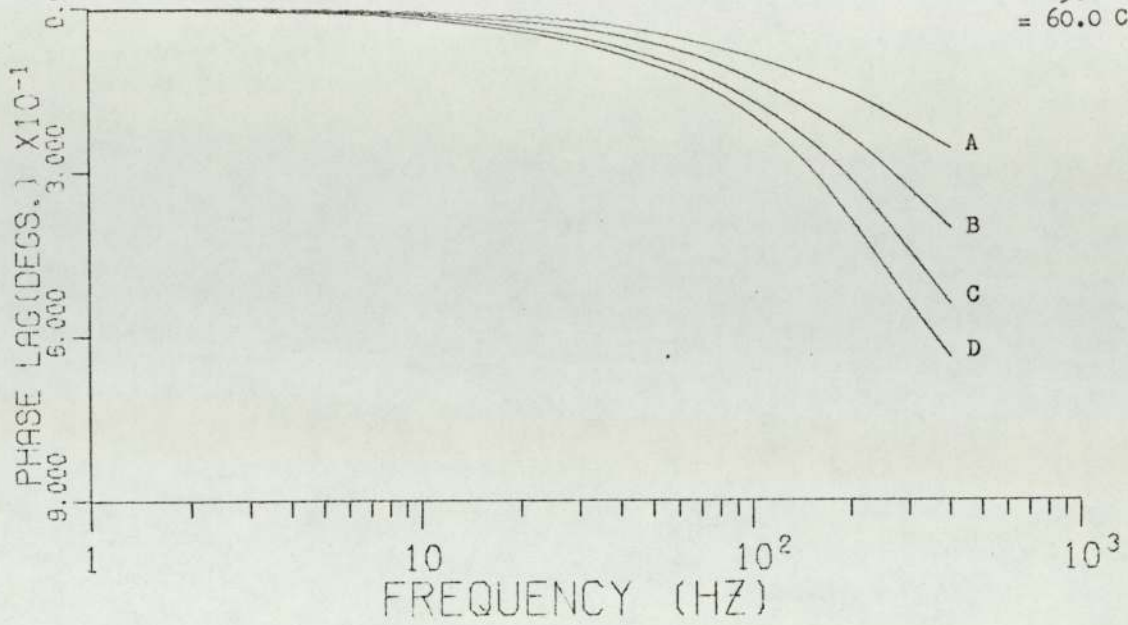


FIGS. (5.6) and (5.7) THEORETICAL AMPLITUDE RESPONSE FOR DIFFERENT RADIAL POSITIONS

### THEORETICAL TRANSFER FUNCTION

TWO GROUP TELEGRAPHER'S MODEL

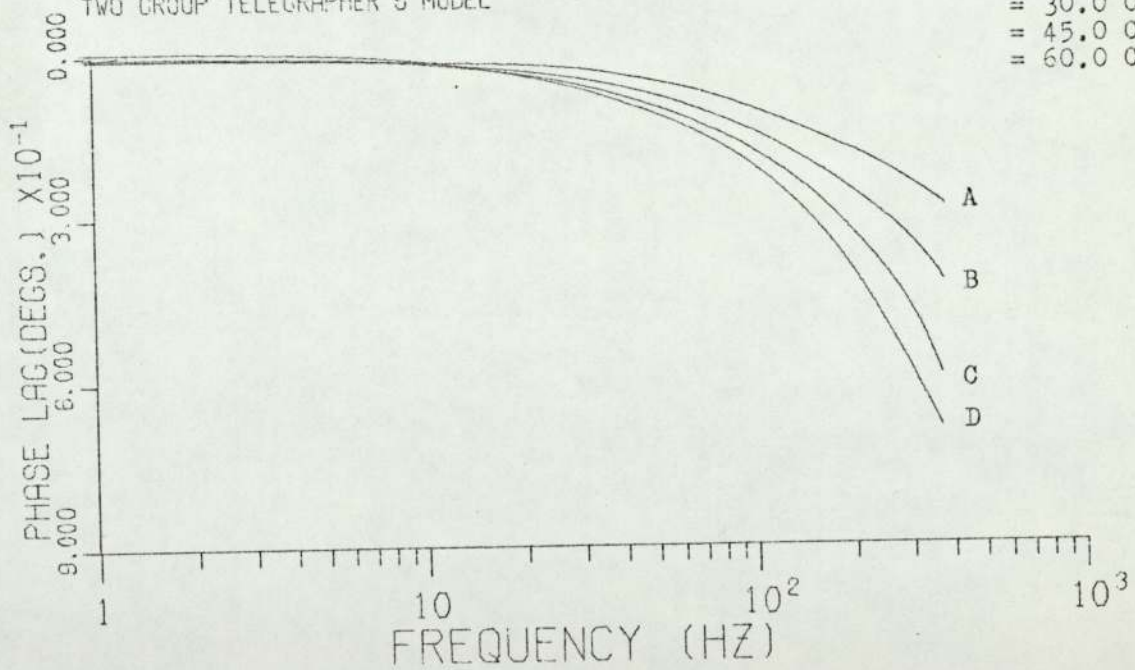
- R = 0.5 CMS.
- H = 15.0 CMS(A)
- = 30.0 CMS(B)
- = 45.0 CMS(C)
- = 60.0 CMS(D)



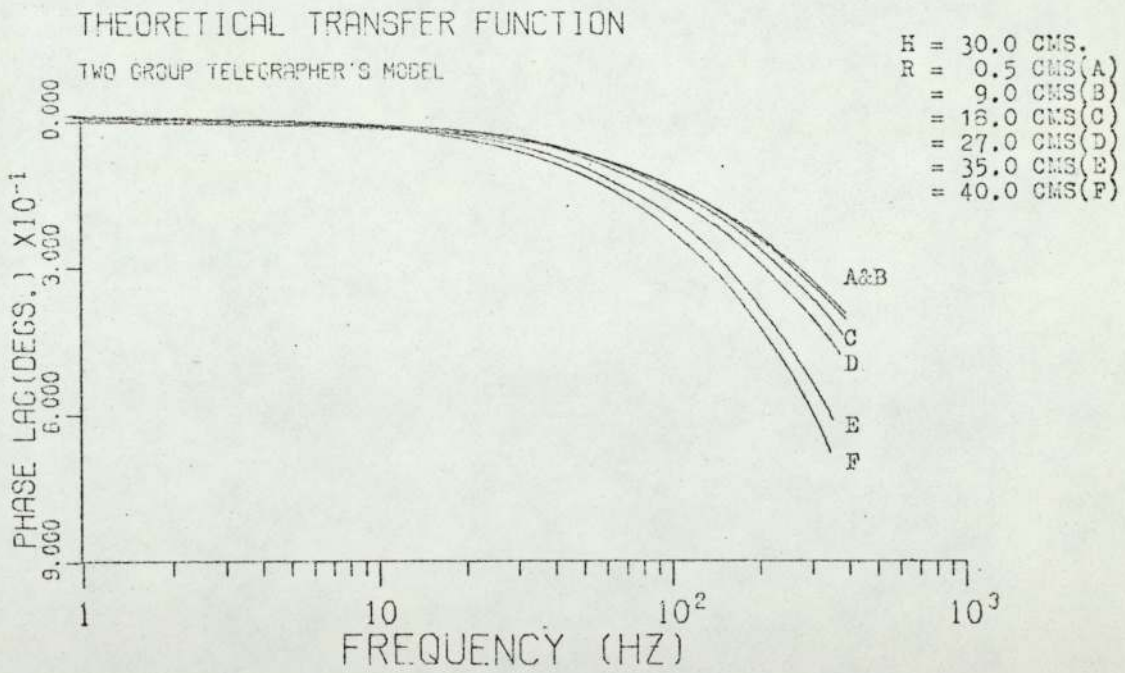
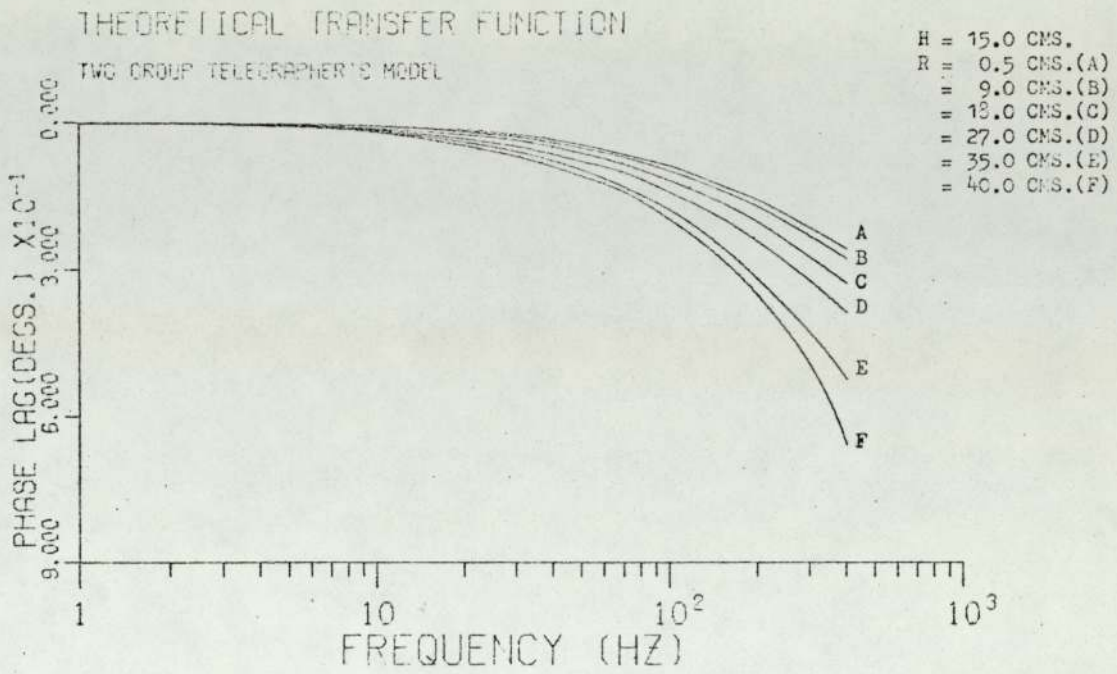
### THEORETICAL TRANSFER FUNCTION

TWO GROUP TELEGRAPHER'S MODEL

- R = 9.0 CMS.
- H = 15.0 CMS(A)
- = 30.0 CMS(B)
- = 45.0 CMS(C)
- = 60.0 CMS(D)



FIGS.(5.8) and (5.9) THEORETICAL PHASE RESPONSE FOR DIFFERENT AXIAL POSITIONS

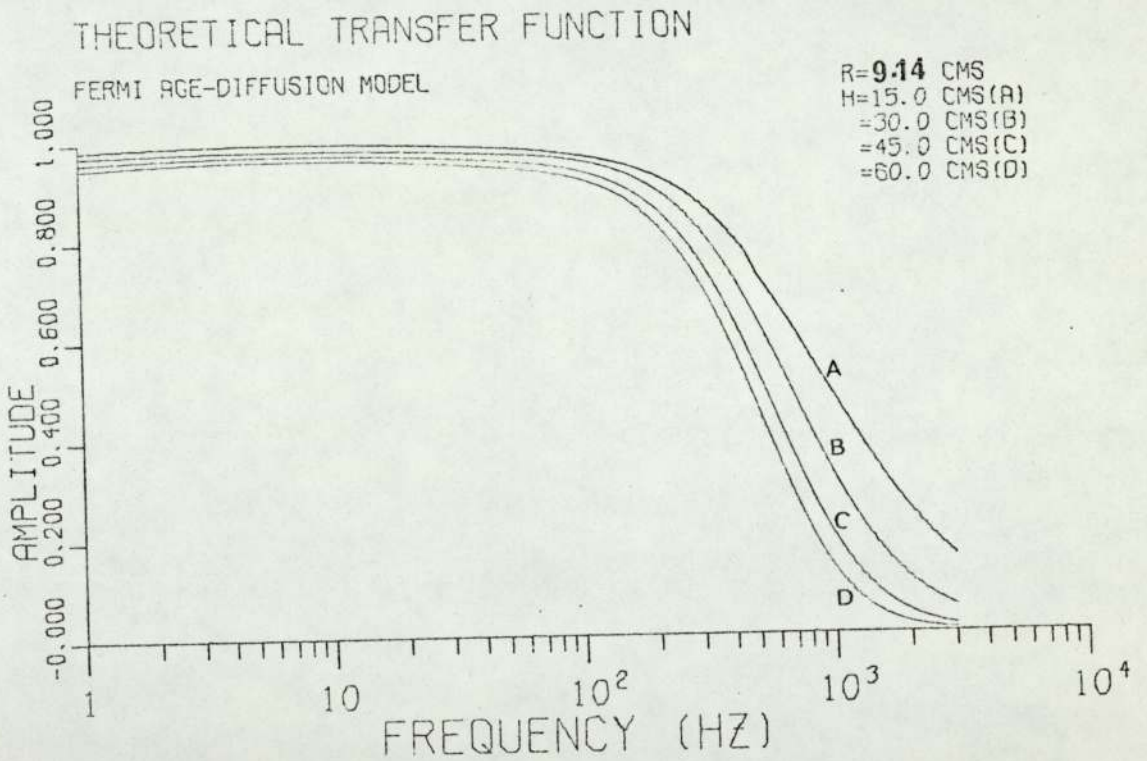
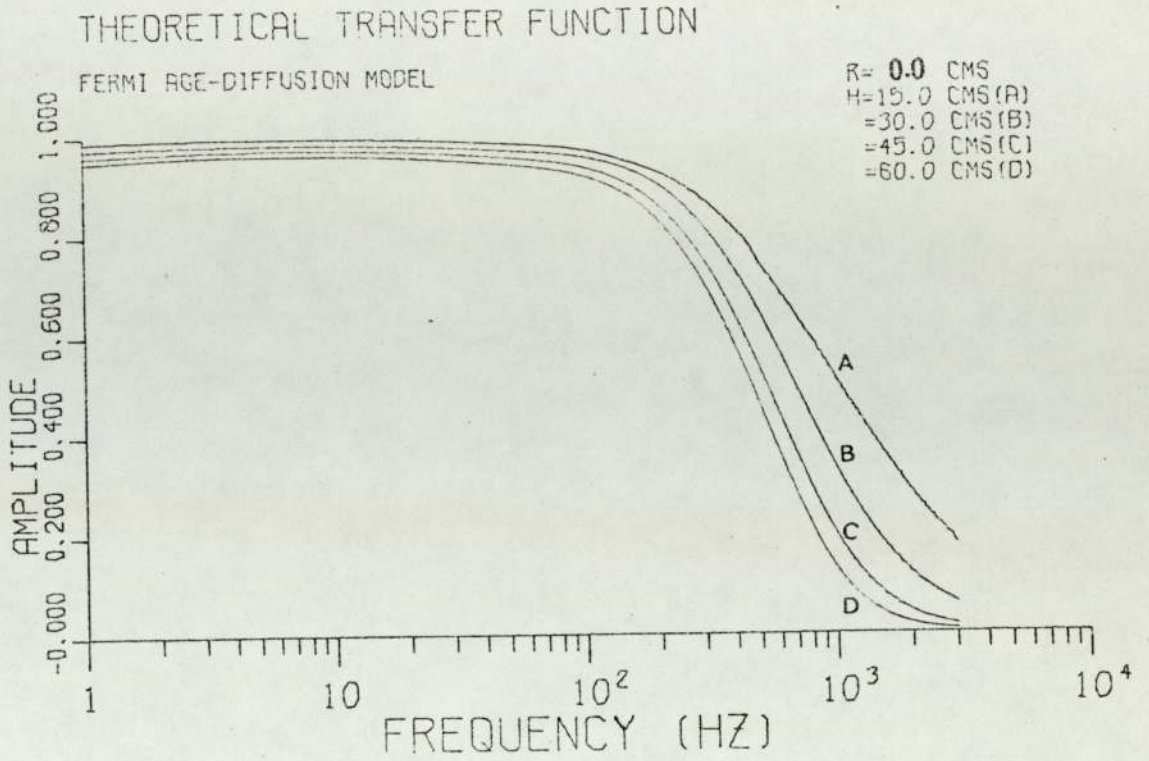


FIGS. (5.10) and (5.11) THEORETICAL PHASE RESPONSE FOR DIFFERENT RADIAL POSITIONS

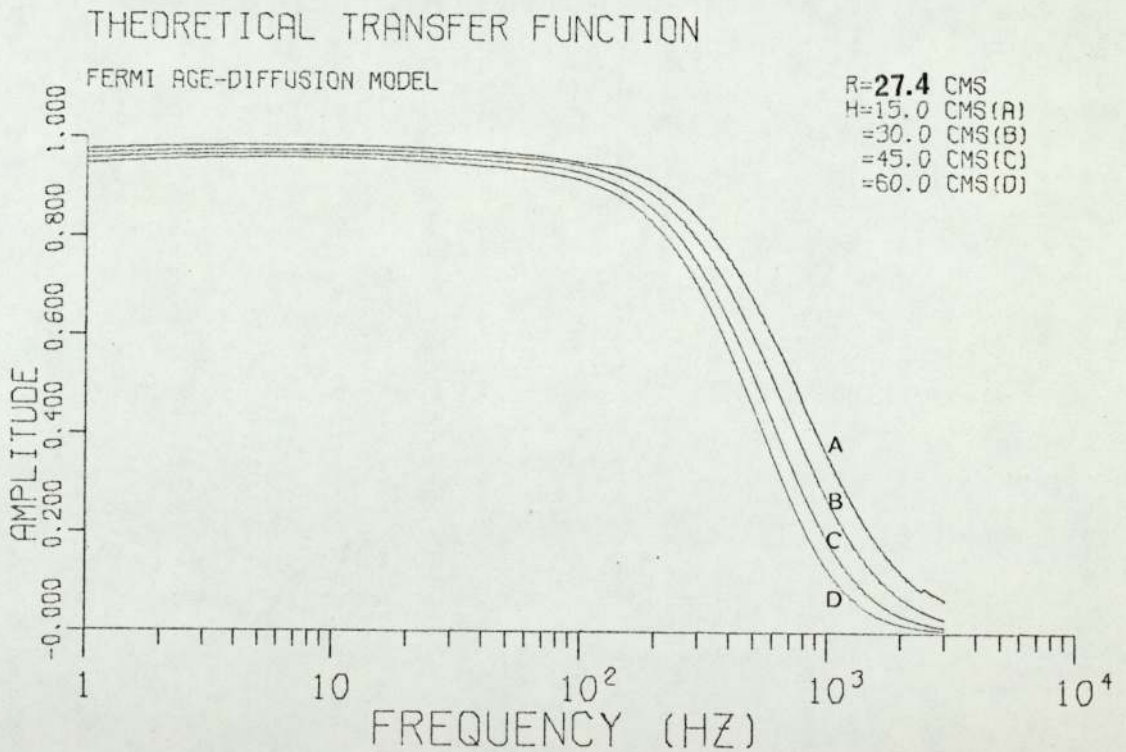
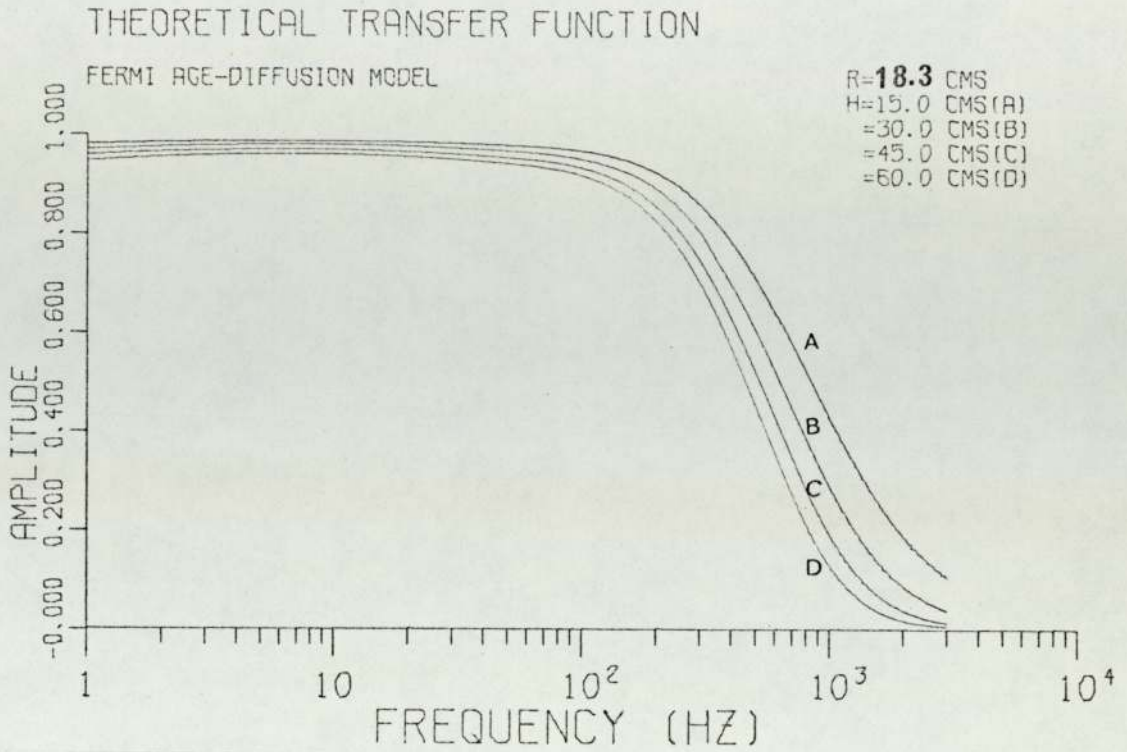
The code was used to calculate the transfer function for a homogeneous cylinder of 81.3 cms. high and 39.0 cms. radius which are the extrapolated dimensions of the subcritical assembly used to test the validity of the theoretical models. Calculations were performed for a wide range of output locations and for frequencies ranging from 0 up to 3000 Hz.

Figures (5.12) to (5.15) show the amplitude response for different axial positions. Here, as in the previous theoretical model, the amplitude remains constant for frequencies of up to nearly 100 Hz. It can also be noticed how the spatial differences become more pronounced for points closer to the artificial neutron source. This effect is even more noticeable for the radial distribution as shown in Figures (5.16) to (5.19). It is also shown here, as in the complex source method, how the spatial differences are rather smaller than those corresponding to an axial distribution. These spatial differences practically disappear at the higher end of the nuclear system (away from the source). This smearing out effect could be due to the following causes:

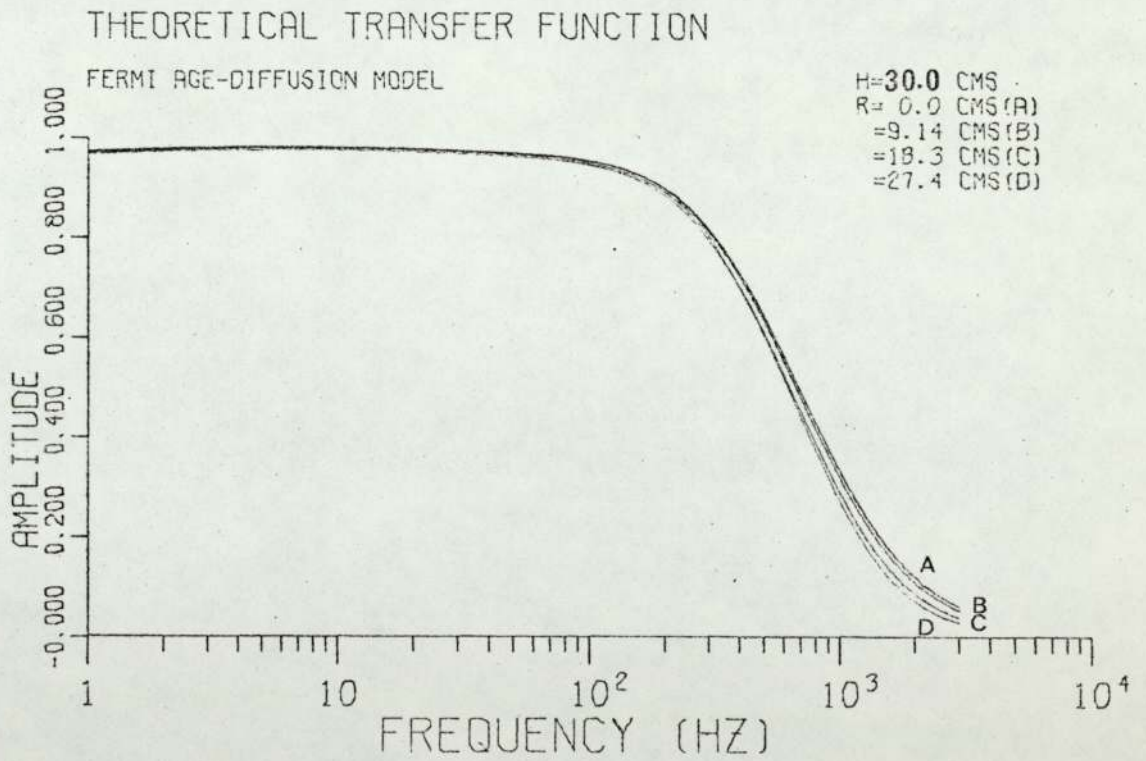
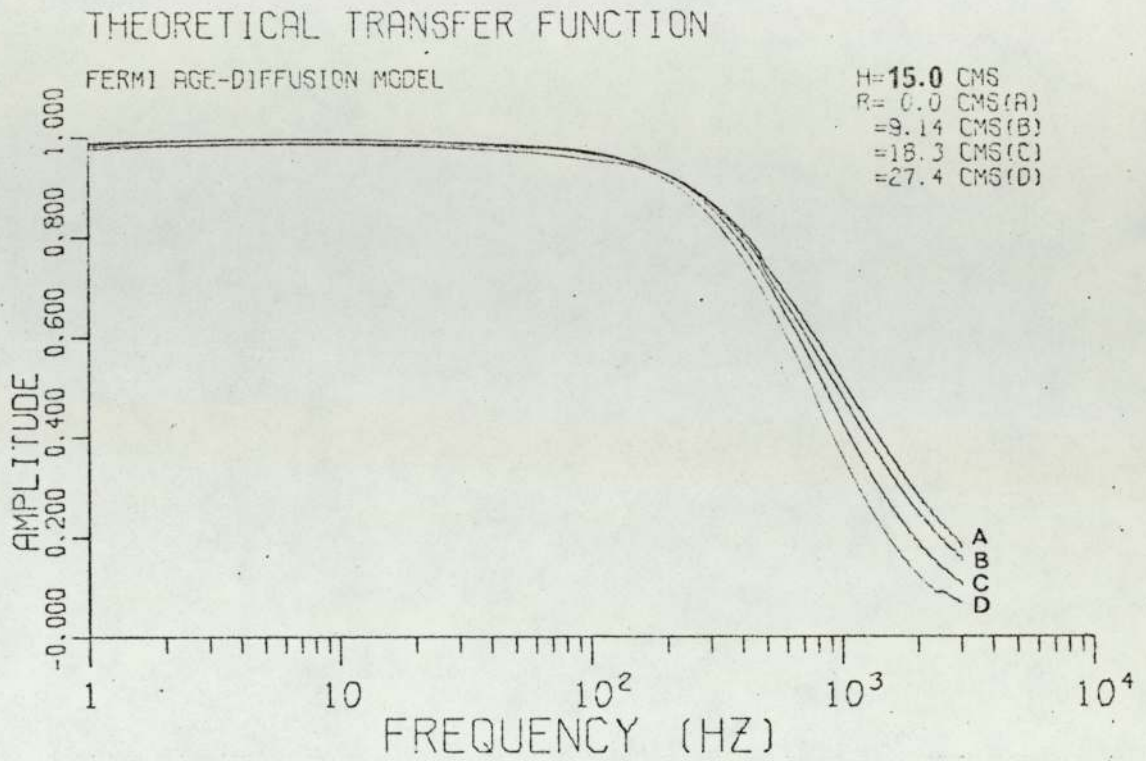
- (1) A point source.
- (2) In the lower planes (e.g.,  $H = 15$  cms.), the on axis points are much closer to the source than those near the edge of the core.
- (3) In the higher planes, the distances from the source are almost equal. Furthermore, the flux probably does not depend much on direct source neutrons but comes mainly from neutron leakage from lower parts of the core.



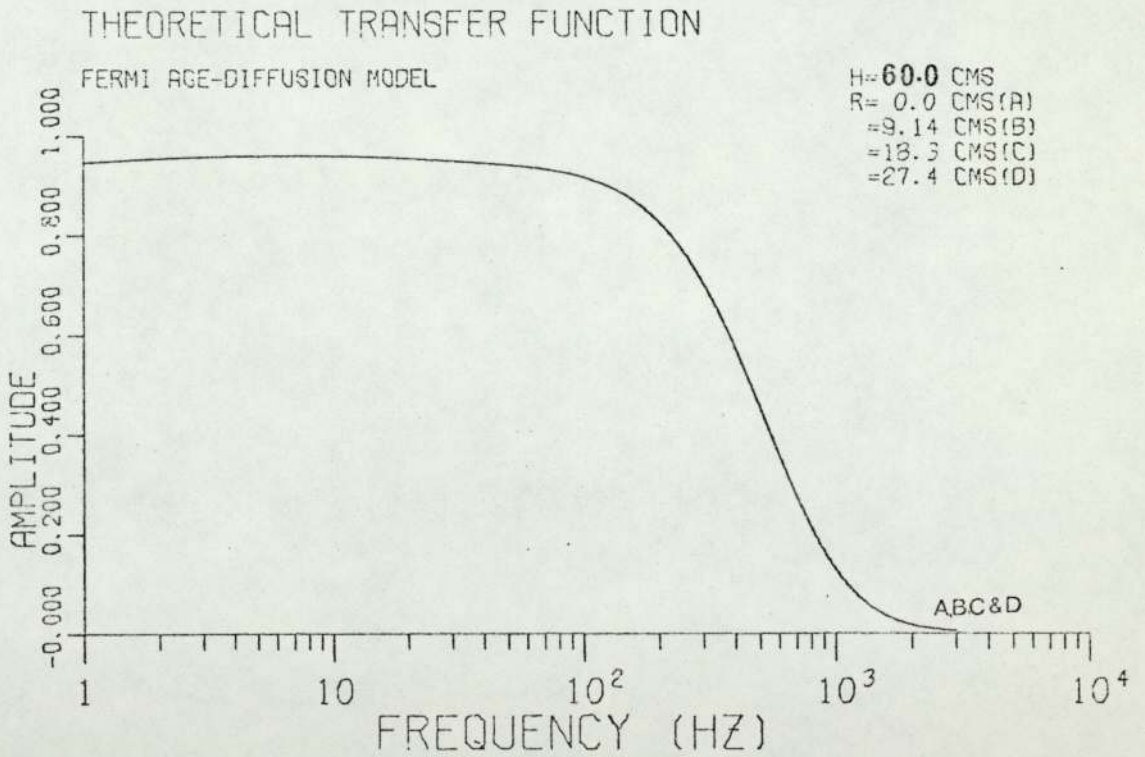
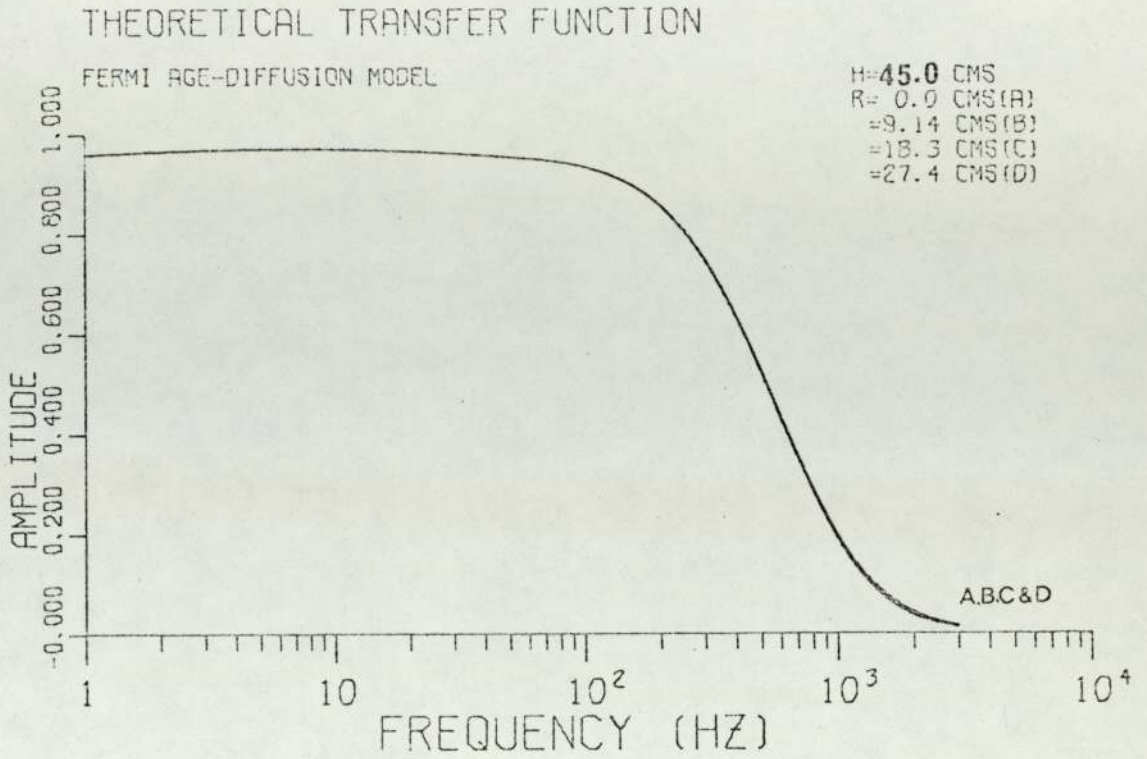
FIGS.(5.12) and (5.13) THEORETICAL AMPLITUDE RESPONSE FOR DIFFERENT AXIAL POSITIONS



FIGS.(5.14) and (5.15) THEORETICAL AMPLITUDE RESPONSE FOR DIFFERENT AXIAL POSITIONS



FIGS.(5.16) and (5.17) THEORETICAL AMPLITUDE RESPONSE FOR DIFFERENT RADIAL POSITIONS



FIGS. (5.18) and (5.19) THEORETICAL AMPLITUDE RESPONSE FOR DIFFERENT RADIAL POSITIONS

This smearing out effect was also noticeable in the experimental measurements and to a smaller extent in the other theoretical model . The fact that it was less noticeable could be explained by considering that both in the complex source method calculations and in the experimental measurements, the source at the base of the core had a broad distribution rather than being a point source due to the spreading out of the source neutrons inside the graphite pedestal.

Similar effects were also found in the phase response of the nuclear system as summarized in Figures (5.20) to (5.23). Here, however, the phase shift at a particular frequency is considerably greater than in the complex source treatment. This discrepancy between both theoretical methods is considered in the next section, where a comparison between them is made.

### 5.3 Comparison between theoretical methods.

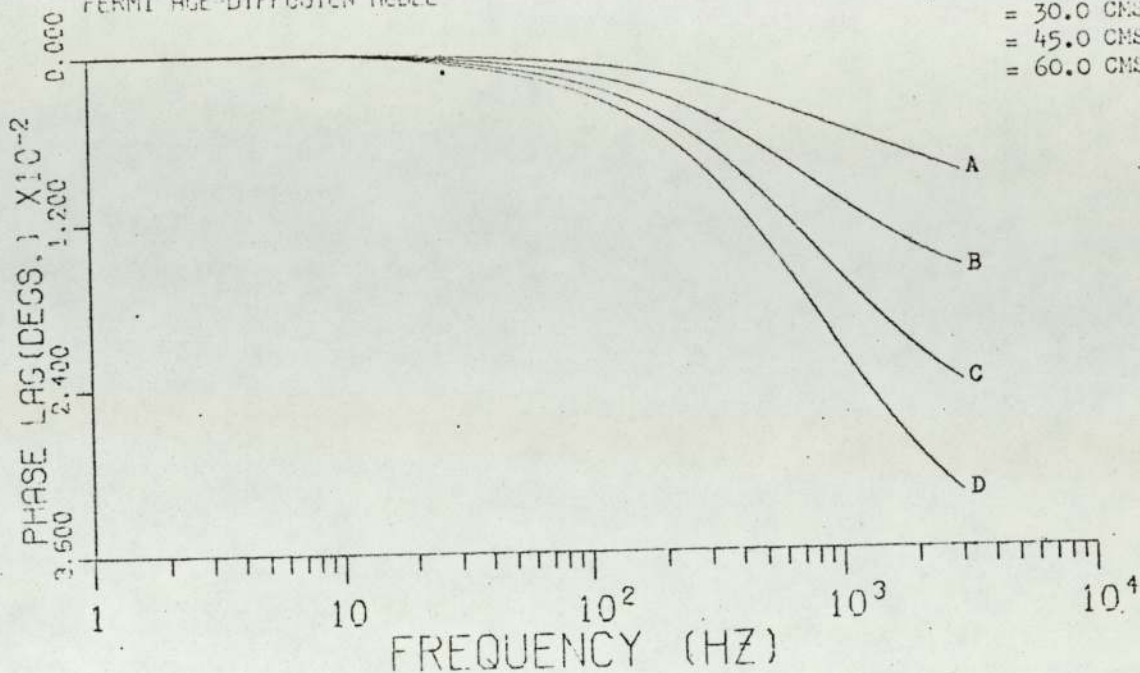
It was shown in the previous sections how the amplitude and phase responses of the nuclear system as given by the two theoretical models approximately follow the same trend. However, in order to establish a quantitative difference between the results obtained with both methods, a direct comparison between them is necessary.

A numerical comparison between the amplitudes as given by both theoretical models is given in tables 2, 3, 4 and 5. The tables, which present values corresponding to the central axis of the subcritical assembly, also show the corresponding experimentally obtained values.

THEORETICAL TRANSFER FUNCTION

FERMI AGE-DIFFUSION MODEL

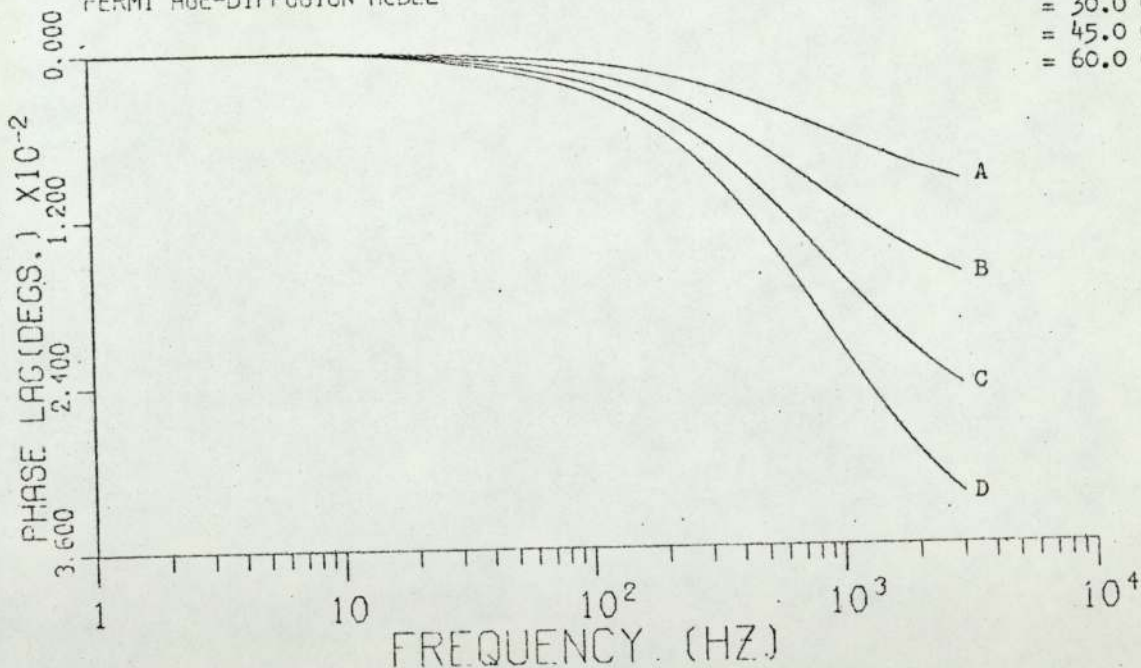
- R = 0.0 CMS.
- H = 15.0 CMS. (A)
- = 30.0 CMS. (B)
- = 45.0 CMS. (C)
- = 60.0 CMS. (D)



THEORETICAL TRANSFER FUNCTION

FERMI AGE-DIFFUSION MODEL

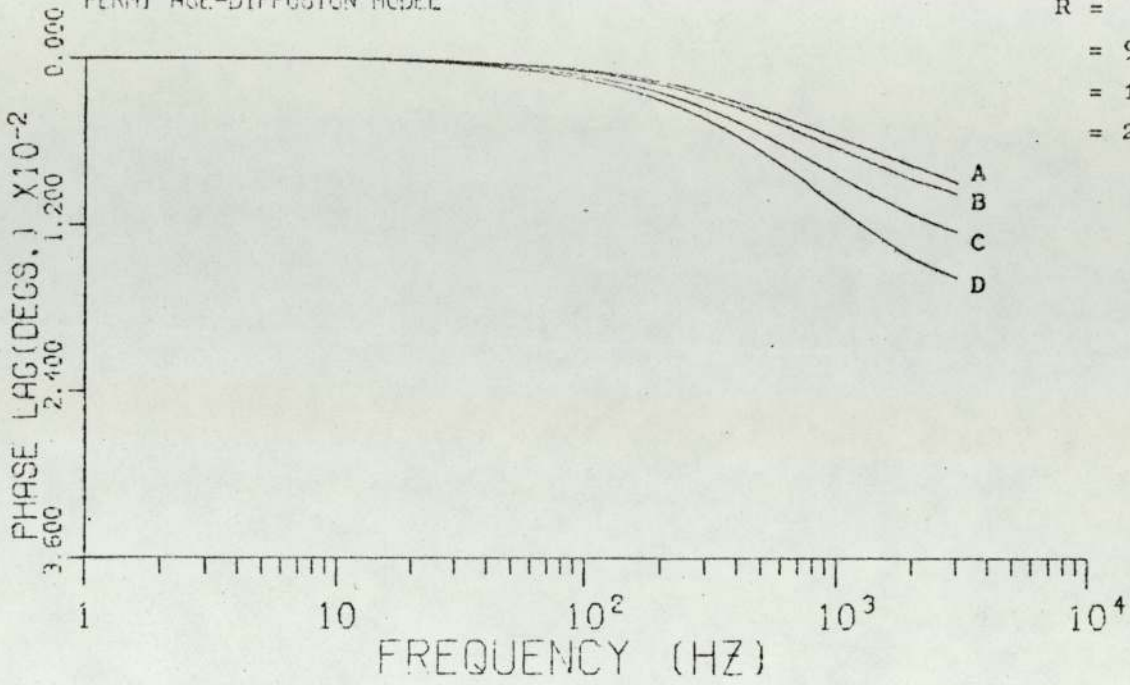
- R = 9.14 CMS.
- H = 15.0 CMS. (A)
- = 30.0 CMS. (B)
- = 45.0 CMS. (C)
- = 60.0 CMS. (D)



FIGS. (5.20) and (5.21) THEORETICAL PHASE RESPONSE FOR DIFFERENT AXIAL POSITIONS

THEORETICAL TRANSFER FUNCTION

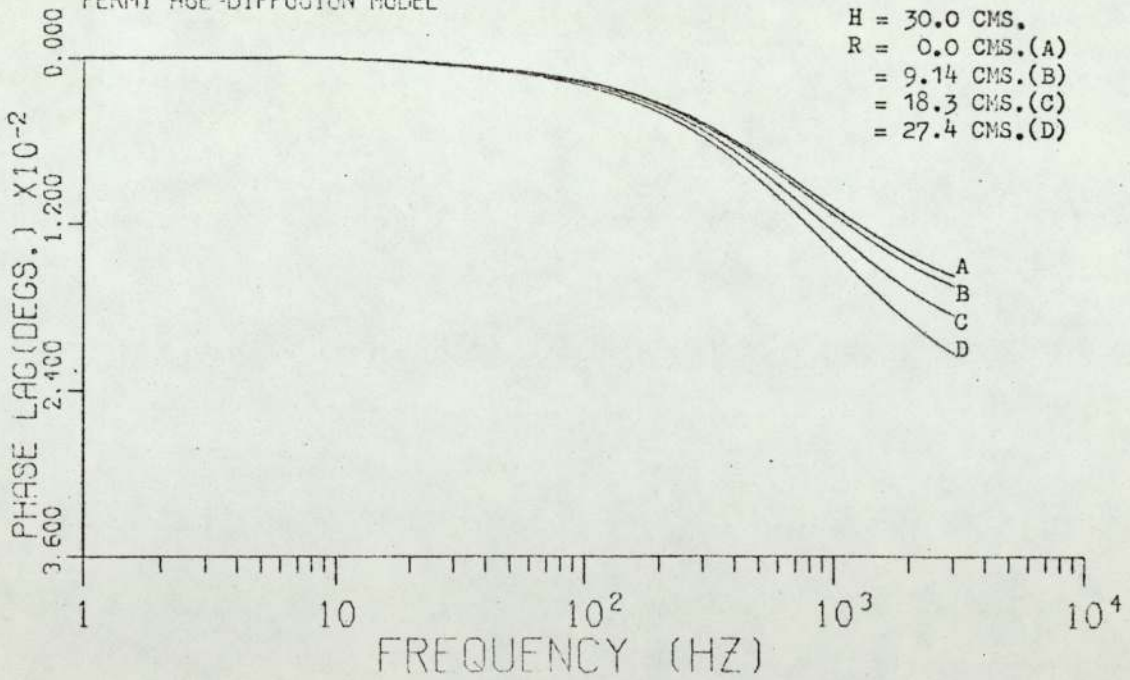
FERMI AGE-DIFFUSION MODEL



H = 15.0 CMS.  
R = 0.0 CMS. (A)  
= 9.14 CMS. (B)  
= 18.3 CMS. (C)  
= 27.4 CMS. (D)

THEORETICAL TRANSFER FUNCTION

FERMI AGE-DIFFUSION MODEL



H = 30.0 CMS.  
R = 0.0 CMS. (A)  
= 9.14 CMS. (B)  
= 18.3 CMS. (C)  
= 27.4 CMS. (D)

FIGS. (5.22) and (5.23) THEORETICAL PHASE RESPONSE FOR DIFFERENT RADIAL POSITIONS

TABLE 2

Numerical values of the Amplitude as given by the different theoretical models and experiments. (H=15 cms.)

Frequency (Hz)	Fermi Age - Diffusion	Telegrapher's	Experimental
0	1.0	1.0	--
1	0.990	0.988	0.976
10	0.989	0.987	0.960
50	0.983	0.980	0.946
100	0.968	0.972	0.929
150	0.943	0.940	0.895
200	0.920	0.916	0.868
250	0.893	0.889	0.844
300	0.864	0.860	0.834
400	0.804	0.800	0.800
500	0.733	--	0.730
750	0.604	--	0.628
1000	0.505	--	0.523
1500	0.368	--	0.449
3000	0.176	--	0.226

TABLE 3

Numerical values of the Amplitude as given by the different theoretical models and experiments. (H=30 cms.)

Frequency (Hz)	Fermi Age - Diffusion	Telegrapher's	Experimental
0	1.0	1.0	--
1	0.975	0.976	0.960
10	0.924	0.976	0.950
50	0.969	0.969	0.935
100	0.953	0.951	0.902
150	0.928	0.918	0.874
200	0.894	0.890	0.834
250	0.854	0.849	0.801
300	0.811	0.808	0.793
400	0.721	0.709	0.721
500	0.635	--	0.631
750	0.453	--	0.490
1000	0.328	--	0.397
1500	0.186	--	0.264
3000	0.056	--	0.094

TABLE 4

Numerical values of the Amplitude as given by the different theoretical models and experiments. (H=45 cms.)

Frequency (Hz)	Fermi Age - Diffusion	Telegrapher's	Experimental
0	1.0	1.0	--
1	0.961	0.967	0.954
10	0.960	0.966	0.940
50	0.954	0.954	0.930
100	0.932	0.928	0.892
150	0.897	0.894	0.847
200	0.852	0.861	0.818
250	0.800	0.820	0.768
300	0.244	0.741	0.740
400	0.629	0.627	0.632
500	0.522	--	0.542
750	0.318	--	0.393
1000	0.195	--	0.292
1500	0.081	--	0.141
3000	0.012	--	0.032

TABLE 5

Numerical values of the Amplitude as given by the different theoretical models and experiments. (H=60 cms.)

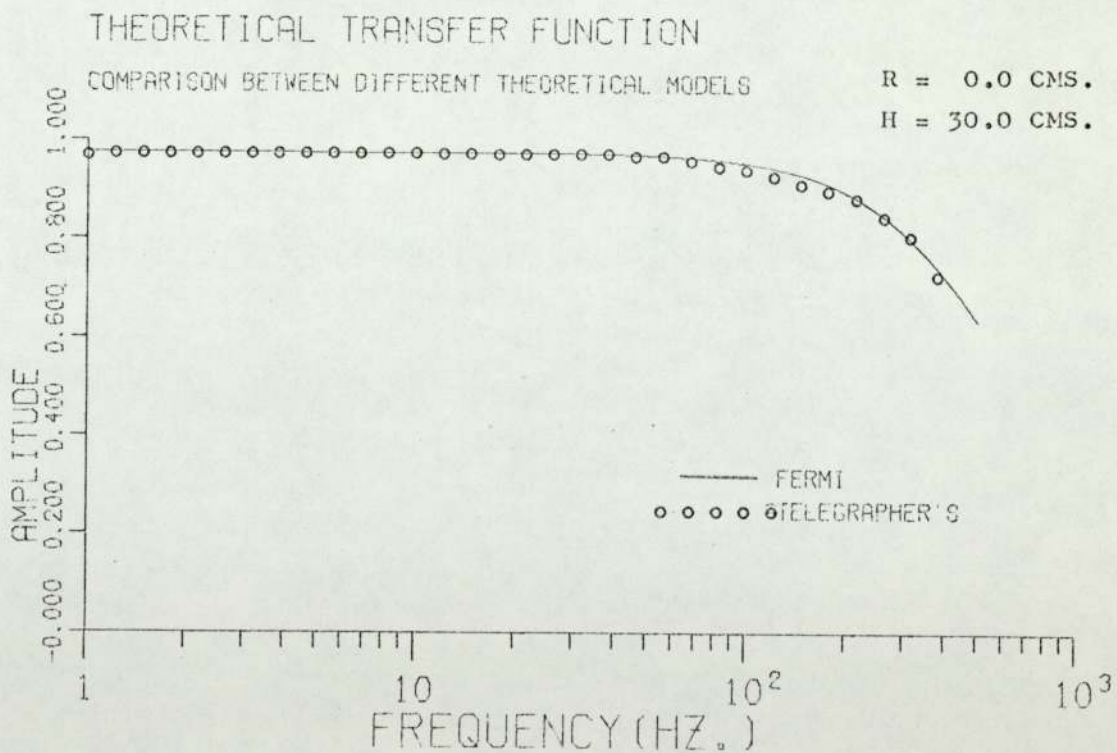
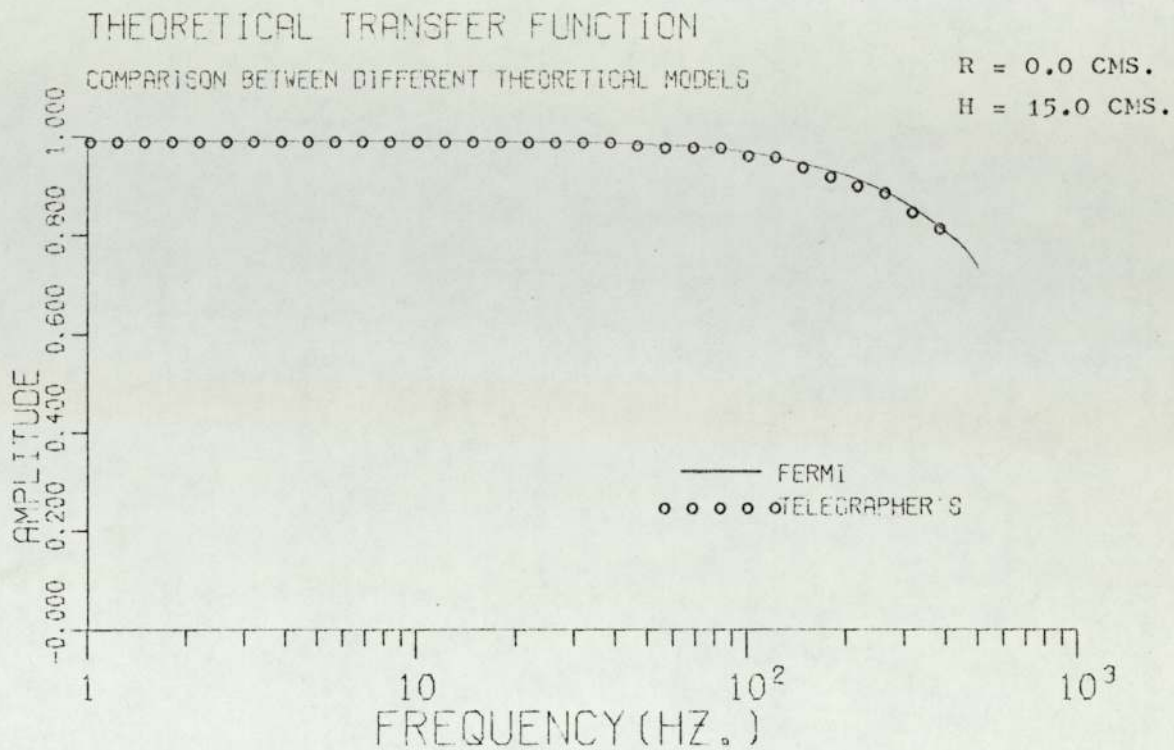
Frequency (Hz)	Fermi Age - Diffusion	Telegrapher's	Experimental
0	1.0	1.0	--
1	0.951	0.950	0.933
10	0.949	0.950	0.928
50	0.940	0.938	0.890
100	0.914	0.910	0.858
150	0.874	0.878	0.819
200	0.822	0.834	0.766
250	0.761	0.766	0.732
300	0.696	0.702	0.707
400	0.567	0.569	0.612
500	0.449	--	0.516
750	0.239	--	0.343
1000	0.126	--	0.222
1500	0.039	--	0.097
3000	0.003	--	0.015

Figures (5.24) to (5.27) show a graphical comparison between the amplitude responses as given by both theoretical models. It can be clearly seen how the agreement is remarkably close. This sort of agreement was found all over the nuclear system. This is not the case, however, for the phase responses where both theoretical models give quite different answers as shown in Figures (5.28) to (5.31). It can be noticed from these figures how at the bottom end of the system, both theoretical models give a very similar answer for a frequency range of up to approximately 200 Hz but beyond this point the discrepancy between both models becomes significant. This effect gets worse in the upper end of the system. For instance, at a plane located 60 cms. above the bottom of the core, the phase lag given by the Fermi-Diffusion treatment is twice as big as that given by the Telegrapher's equations.

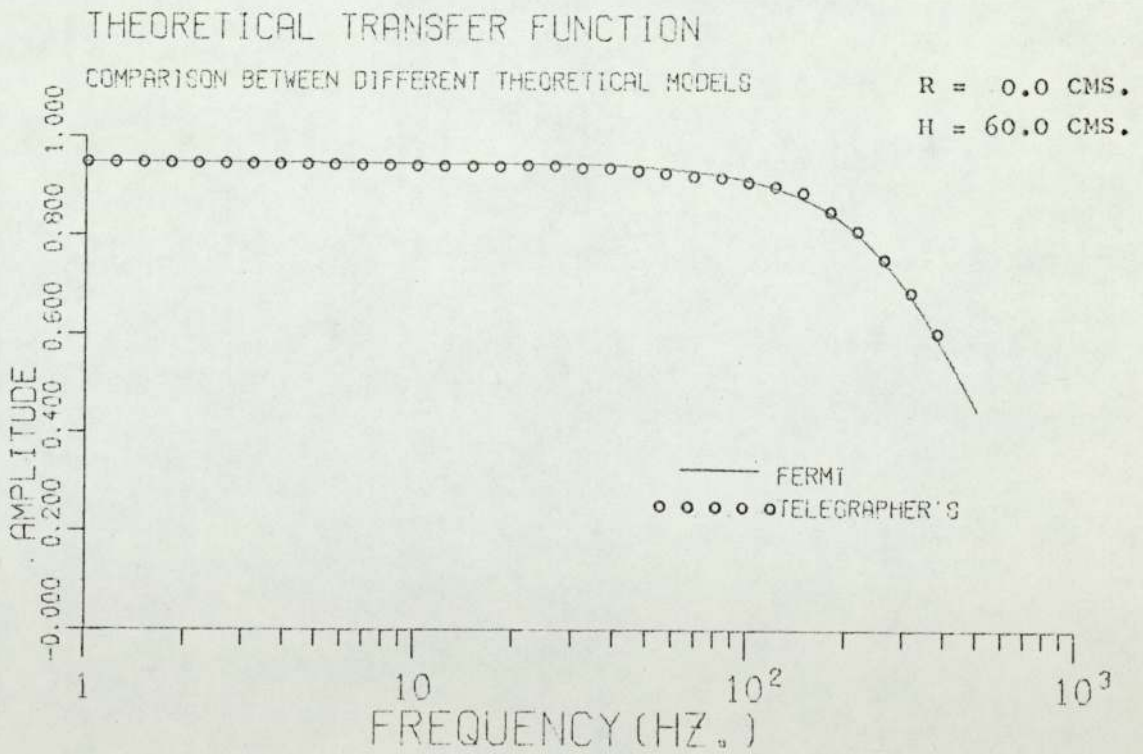
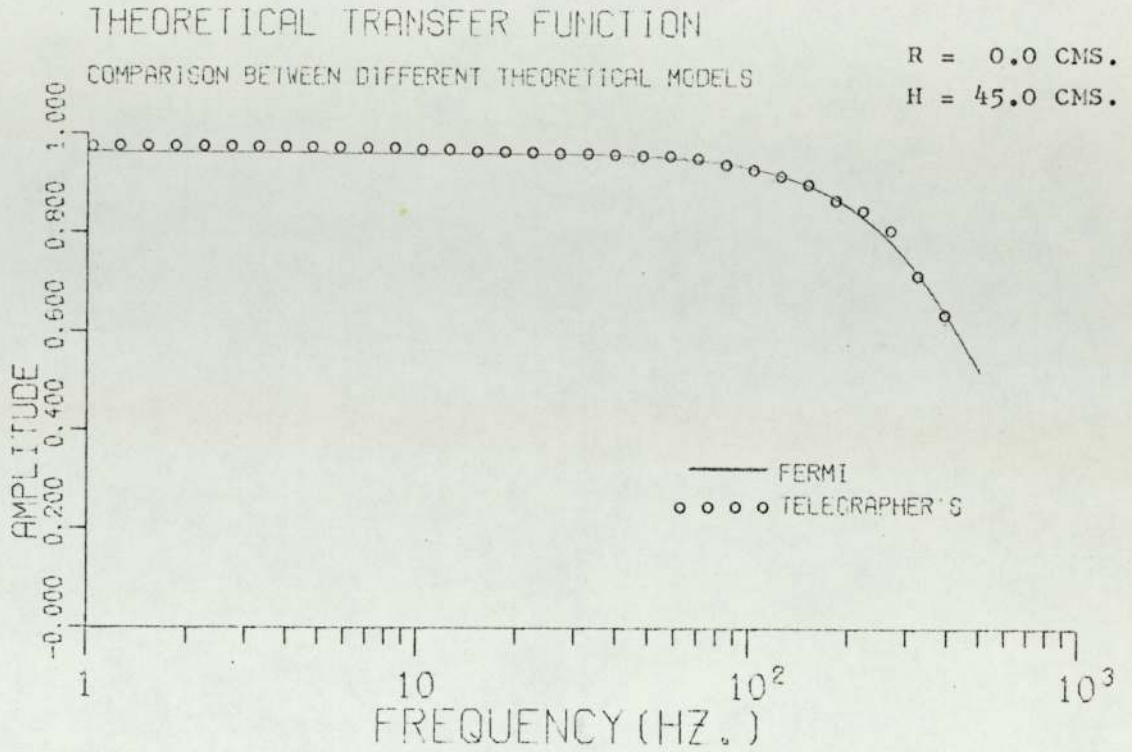
The explanation of this discrepancy could be due to the fact that an artificially high thermal lifetime of 84 microseconds was used for the Fermi Age calculations.

The nuclear system is made up of two regions with quite different thermal neutron lifetimes, on one hand the lifetime for thermal neutrons in the core is around 40 microseconds while in the reflector it is 210 microseconds. Therefore, we should expect the thermal lifetime for the system as a whole to have an intermediate value between these.

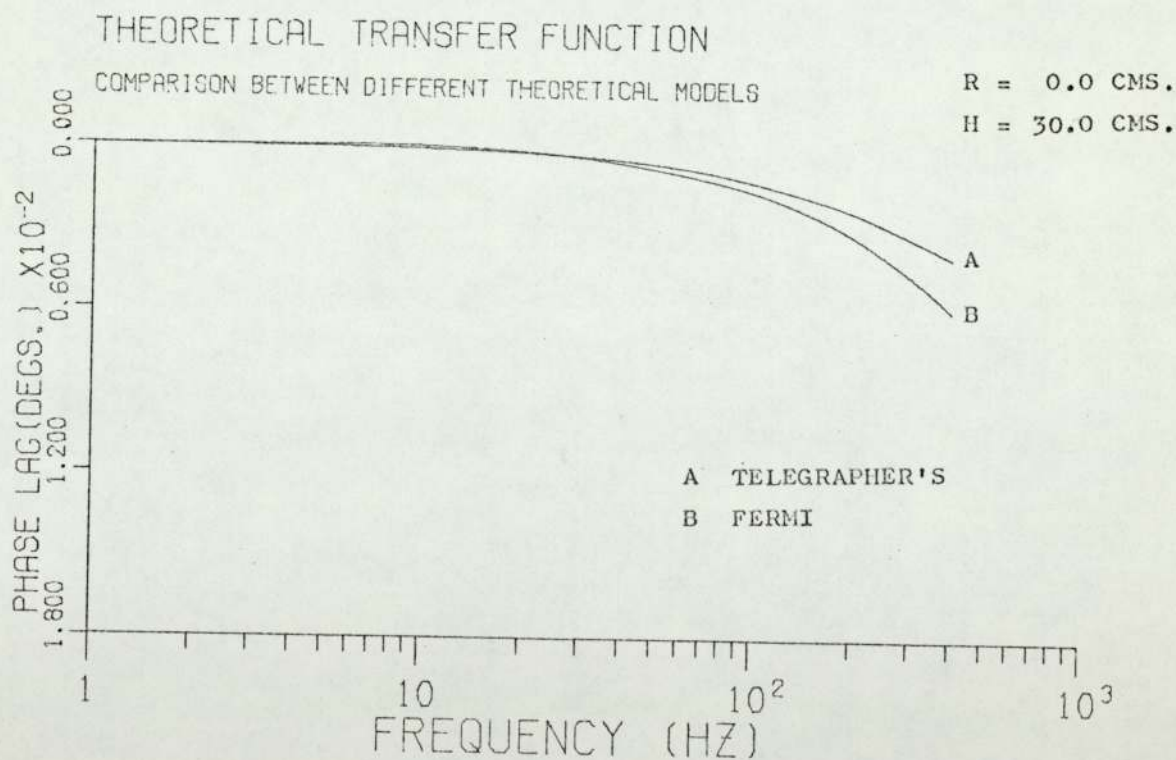
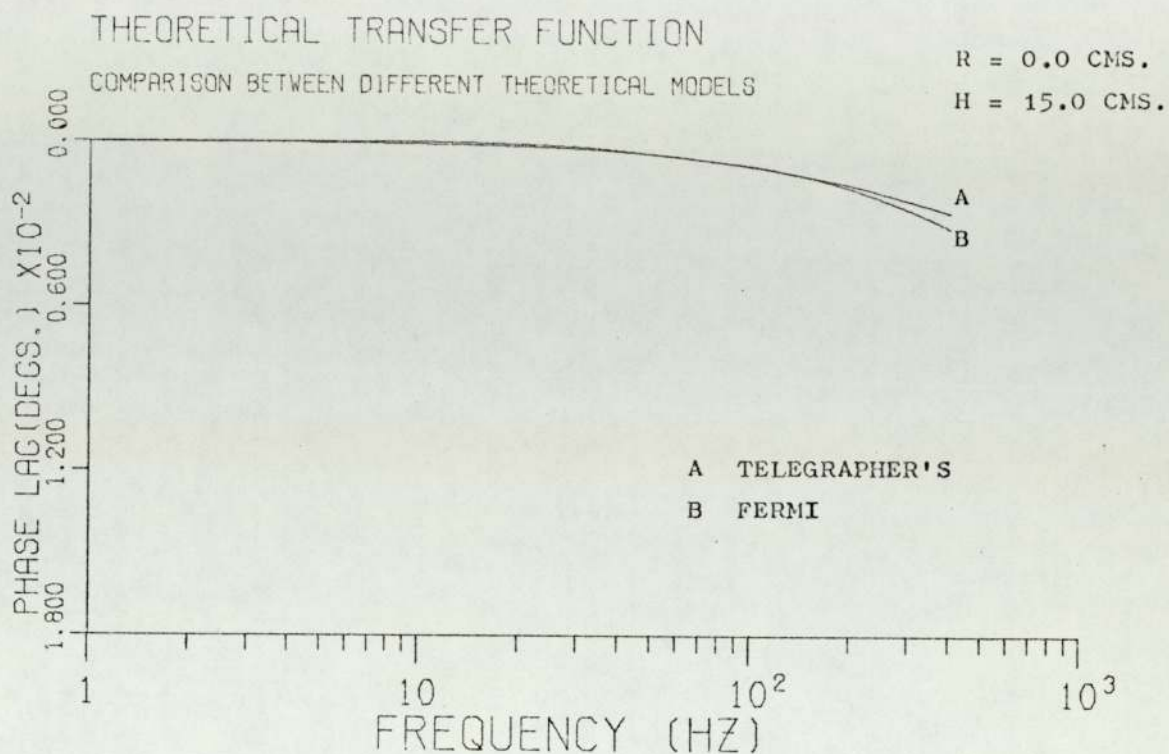
Simple perturbation theory shows that the statistical weight of a neutron is proportional to  $\phi^2$ .



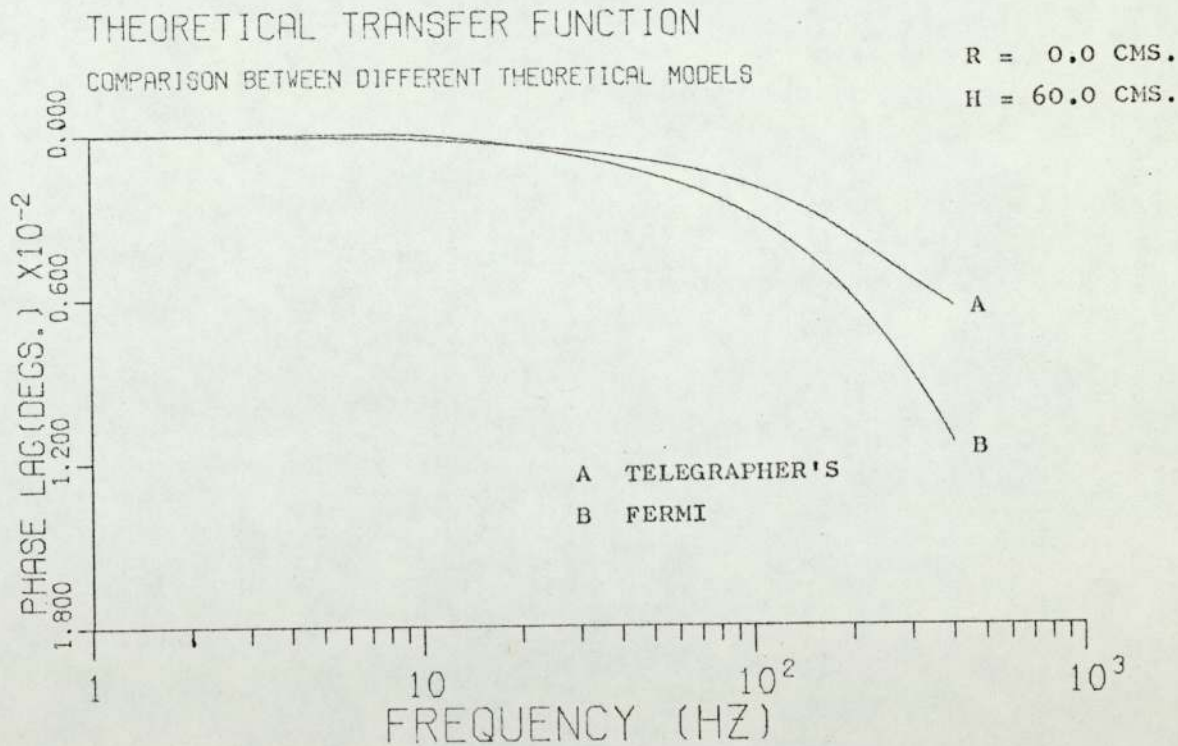
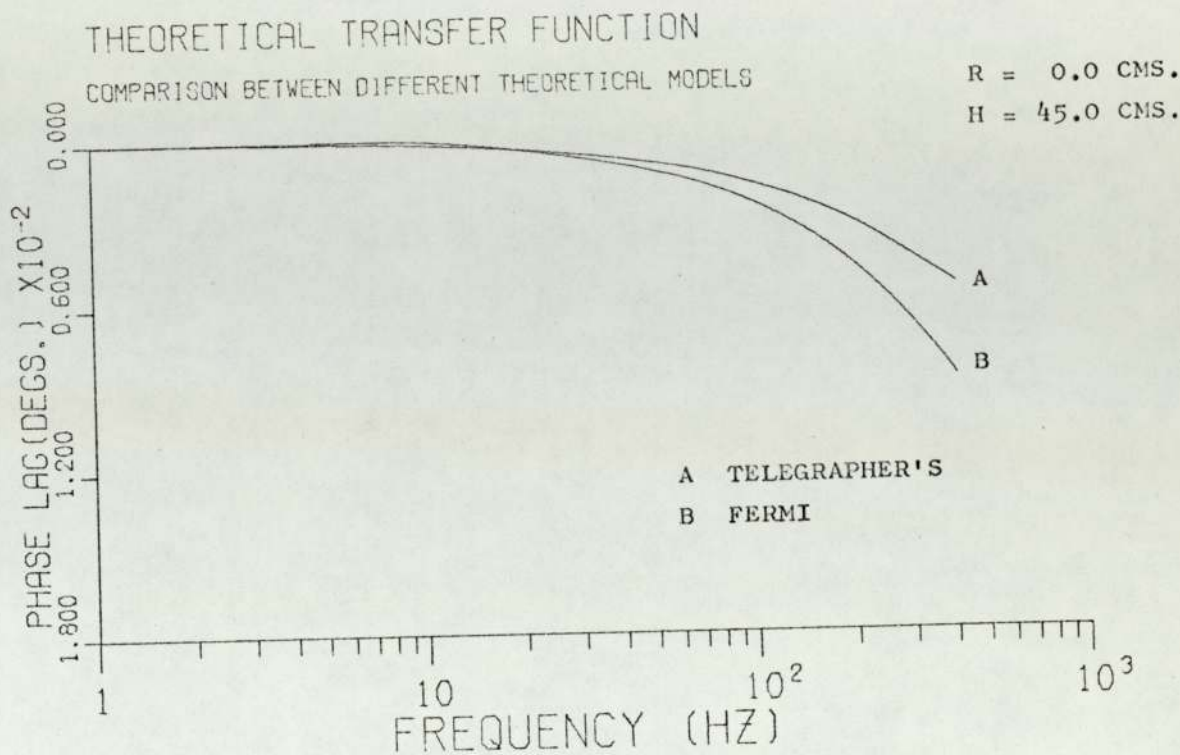
FIGS.(5.24) and (5.25) COMPARISON BETWEEN THE AMPLITUDE RESPONSES OF THE DIFFERENT THEORETICAL MODELS



FIGS.(5.26) and (5.27) COMPARISON BETWEEN THE AMPLITUDE RESPONSES OF THE DIFFERENT THEORETICAL MODELS



FIGS. (5.28) and (5.29) COMPARISON BETWEEN THE PHASE RESPONSES OF THE DIFFERENT THEORETICAL MODELS



FIGS.(5.30) and (5.31) COMPARISON BETWEEN THE PHASE RESPONSES OF THE DIFFERENT THEORETICAL MODELS

This suggests that the effective thermal neutron lifetime of the system as a whole could be calculated as follows,

$$l_{\text{eff}} = \frac{l_c \int_{\text{core}} \phi^2 dV + l_r \int_{\text{reflector}} \phi^2 dV}{\int_{\text{core+reflector}} \phi^2 dV} \dots\dots (5.1)$$

Based on experimental measurements of the relative fluxes inside the core and the reflector, and applying equation (5.1), a value of 78 microseconds was found for the thermal neutron lifetime of the subcritical facility. The experimental determination of the relative fluxes was performed using indium foils.

This value of 78  $\mu$ secs. is not quite the same as 84  $\mu$ secs. used in the present calculations. However, with a thermal lifetime of 84  $\mu$ secs. a good agreement between the amplitude responses of both theoretical models was achieved. Furthermore, this value also gives a good agreement with the experimentally measured amplitude response.

The sensitivity of the Fermi-Diffusion method to different values of the thermal neutron lifetime is shown in Figure (5.32). Here, the -3dB amplitude value was calculated for different values of the lifetime and for different output locations inside the system. It can be seen, for instance, how the -3dB point varies from 1320 Hz to 320 Hz for an output position of coordinates H=15 cms., R=0.0 cms., when the thermal lifetime is varied from 30 to 150 microseconds.

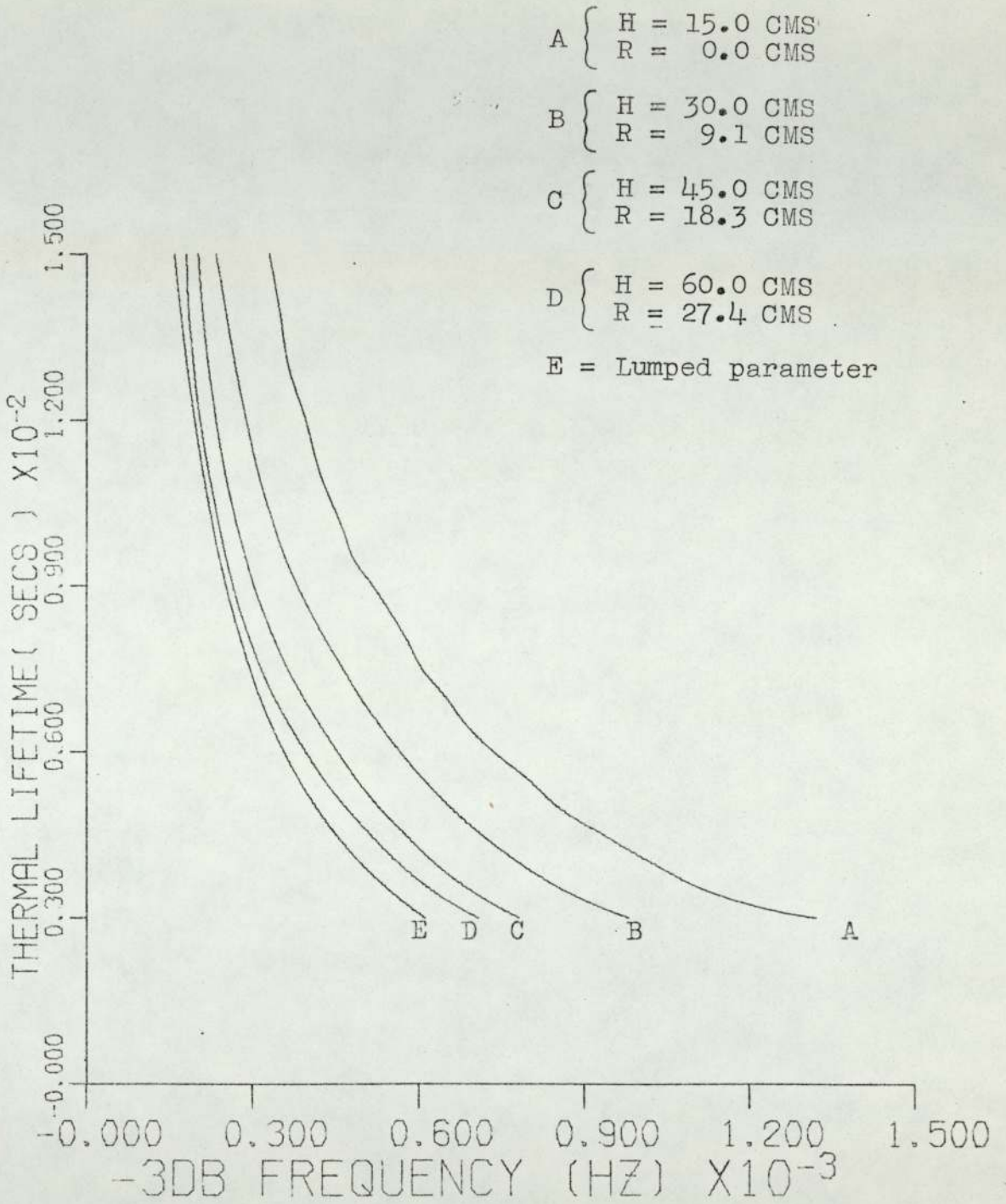


FIG. (5.32) VARIATION OF THE -3dB AMPLITUDE WITH THERMAL LIFETIME

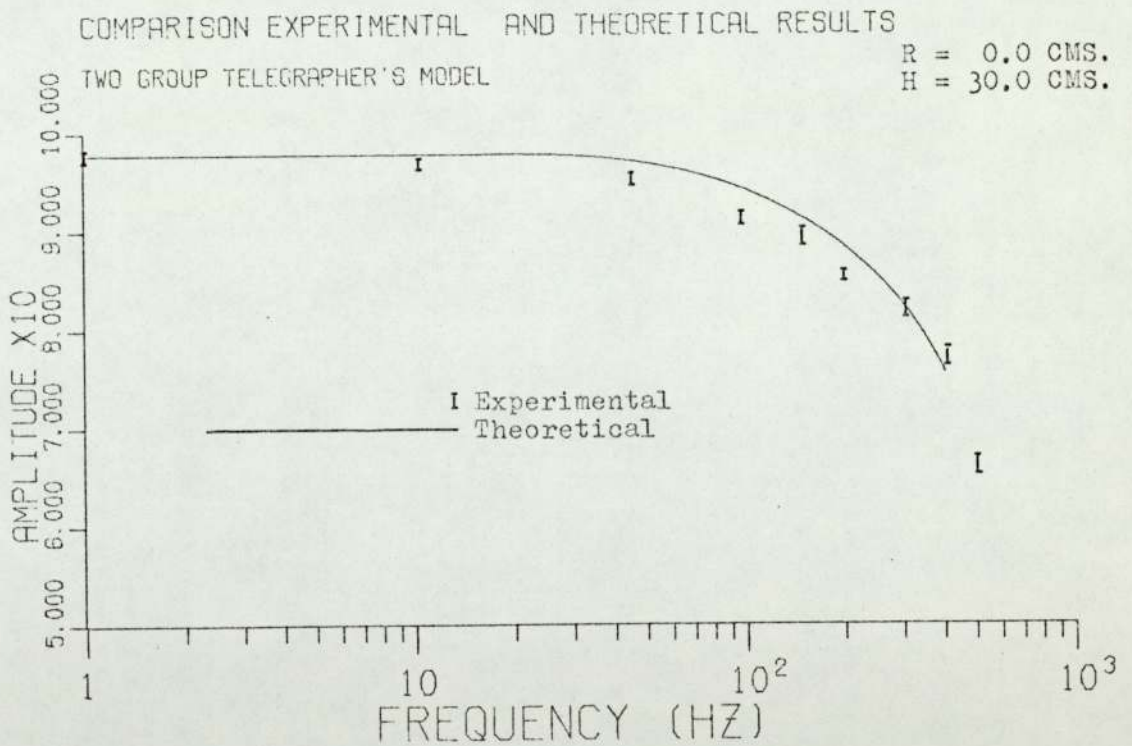
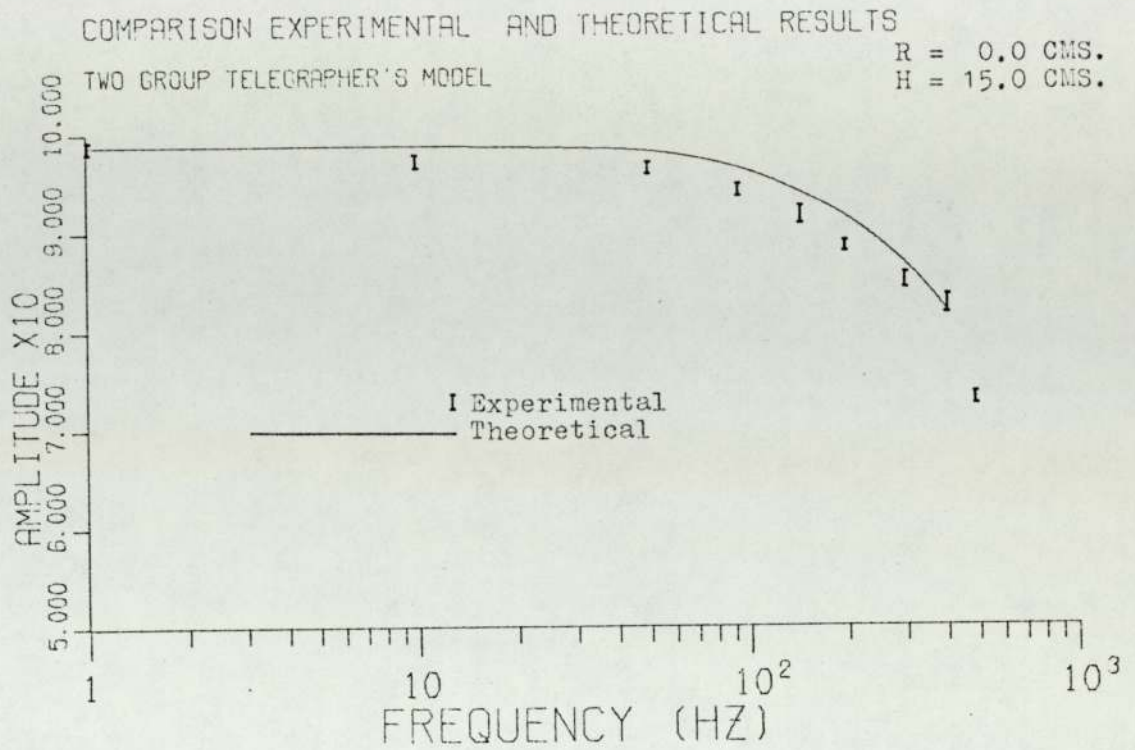
Another fact that proves that the Fermi-Age method does not represent properly the thermal neutron lifetime in an heterogeneous system is that Kylstra (66) had to assume a thermal lifetime of 200  $\mu$  secs. to obtain good agreement between the theoretical calculations and the experimental ones corresponding to a natural uranium, light-water subcritical assembly.

#### 5.4 Comparison between theoretical and experimental results.

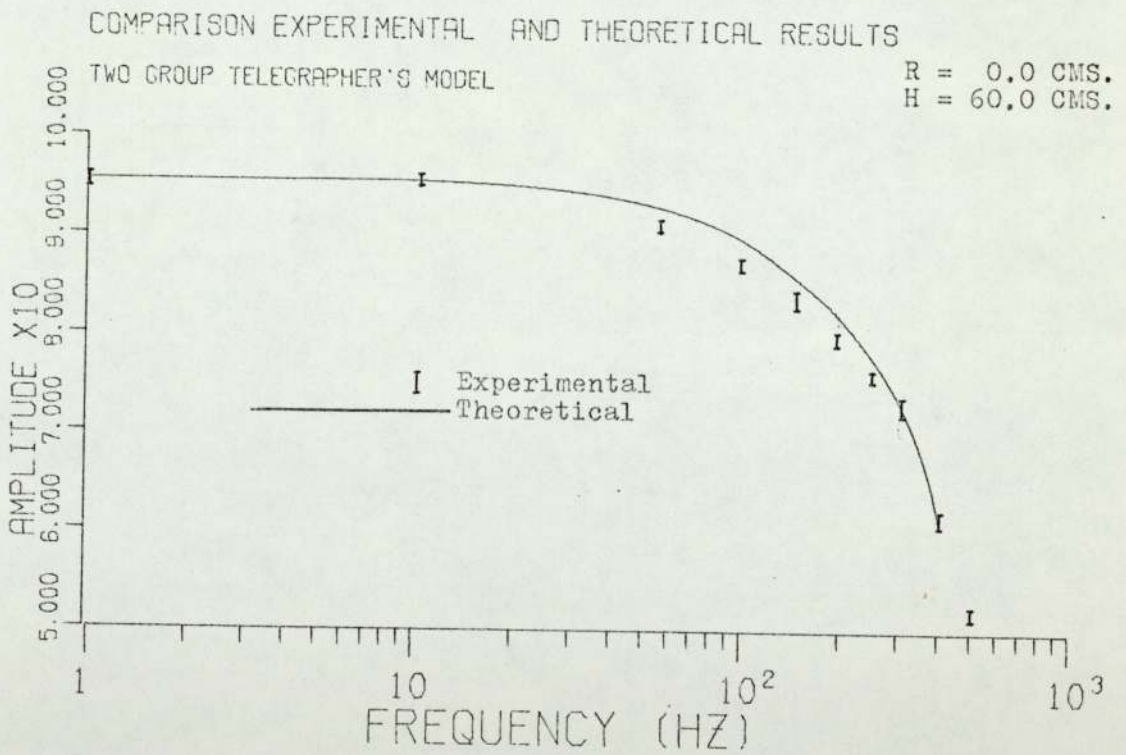
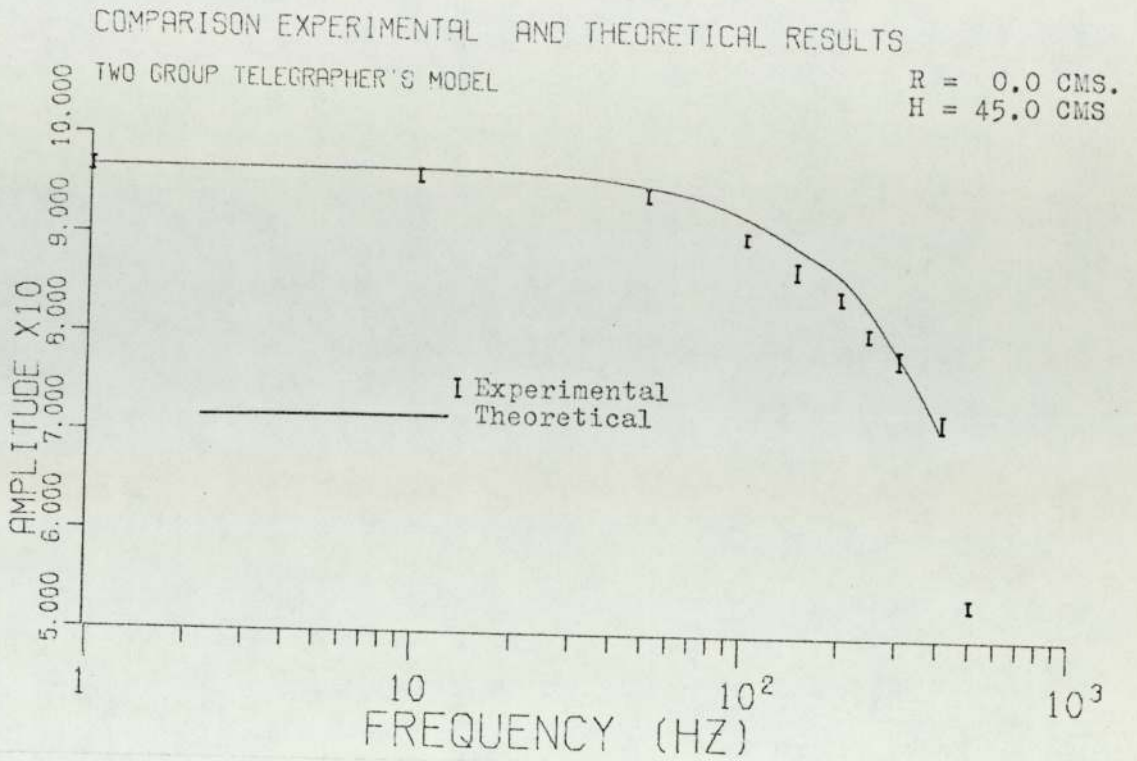
In this section, the results obtained with both theoretical models are compared with those obtained experimentally.

For convenience in producing the curves for the comparison between experimental and theoretical results the two sets of data were normalized to the experimental result at 1Hz. However, the theoretical and experimental values of 1 Hz agree to within 1.8% or better as shown in tables 2, 3, 4 and 5 and so these comparisons are almost identical to plotting the unnormalized values.

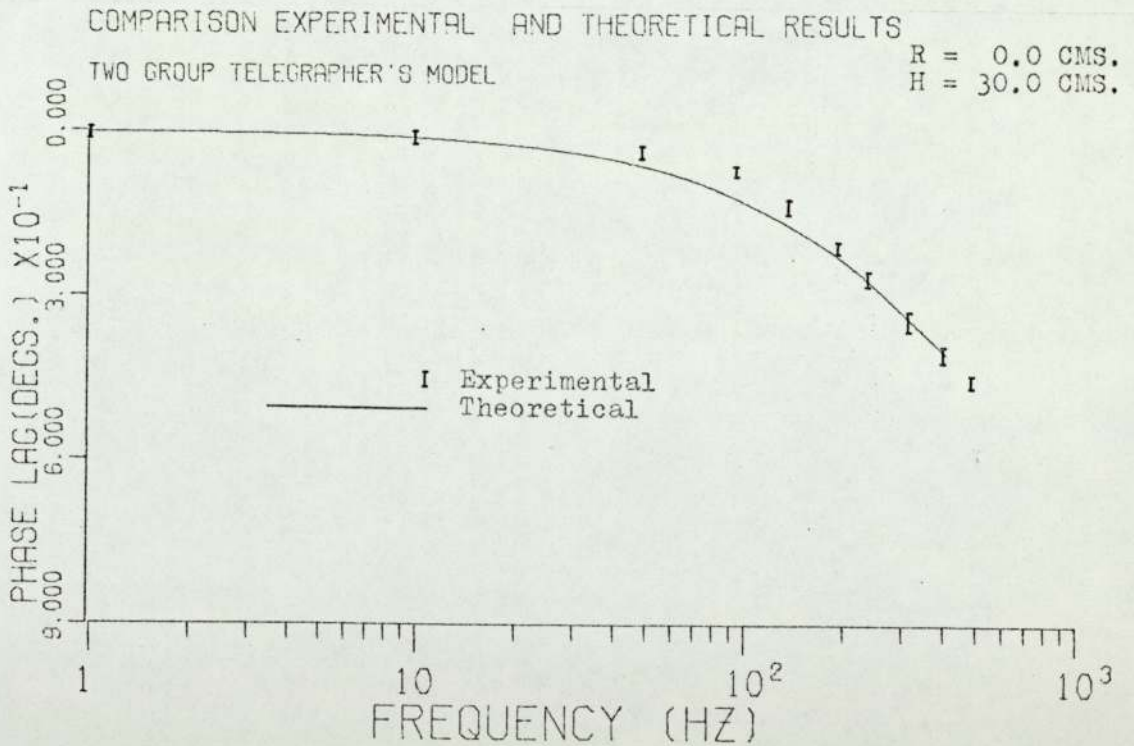
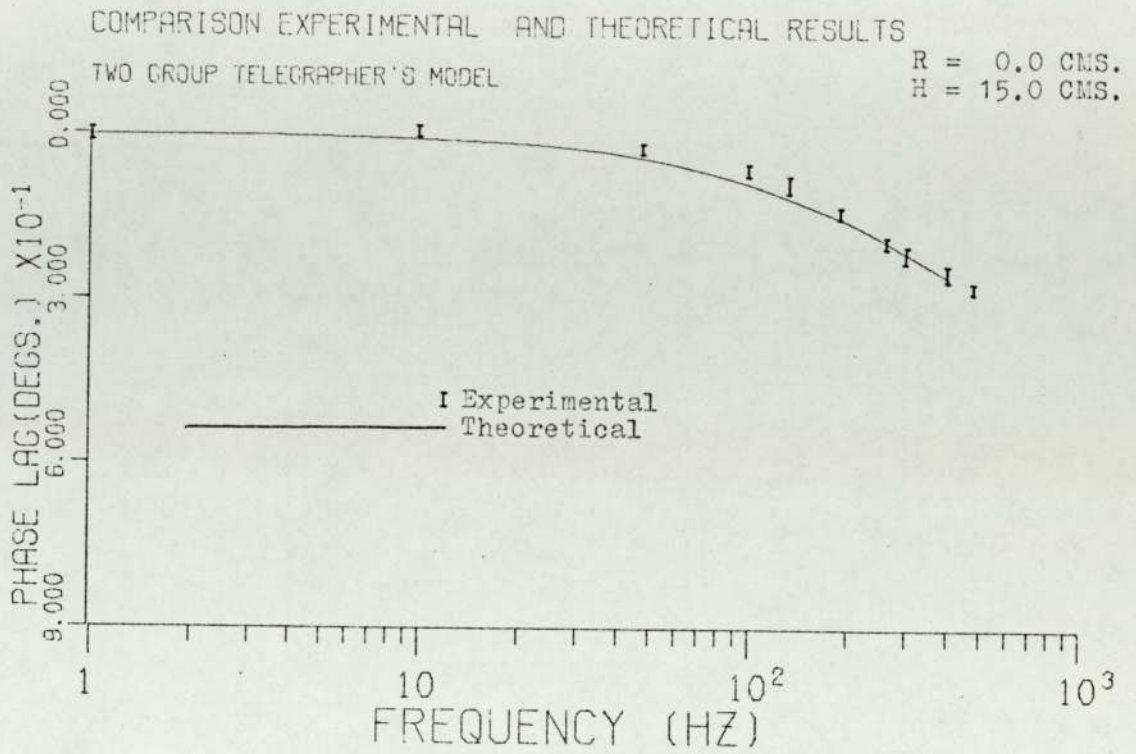
In Figures (5.33) to (5.36), the amplitude response of the nuclear system as given by the two group Telegrapher's model approximation is compared with that obtained experimentally. The agreement between the experimental and theoretical data is fairly good for the range of frequencies in which the computer program SNAP was able to find a solution. Also, a very good agreement was found between the experimental and theoretical phase responses as shown in Figures (5.37) to (5.40). As many measurements were taken in every position for every



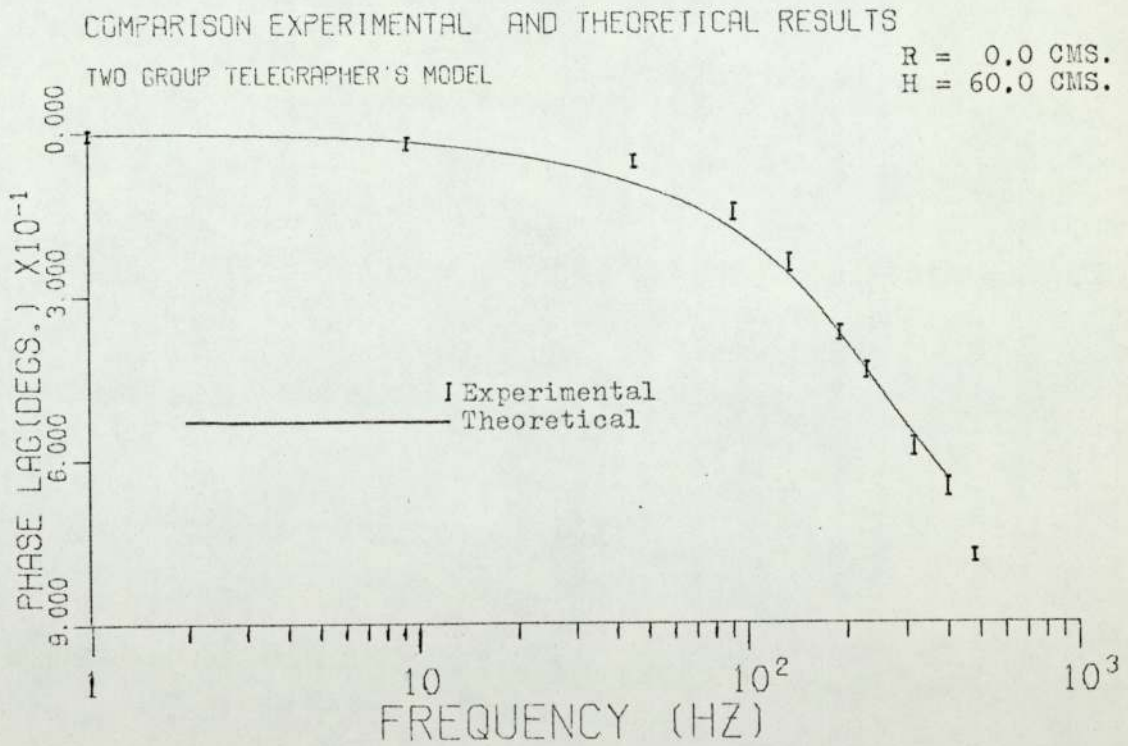
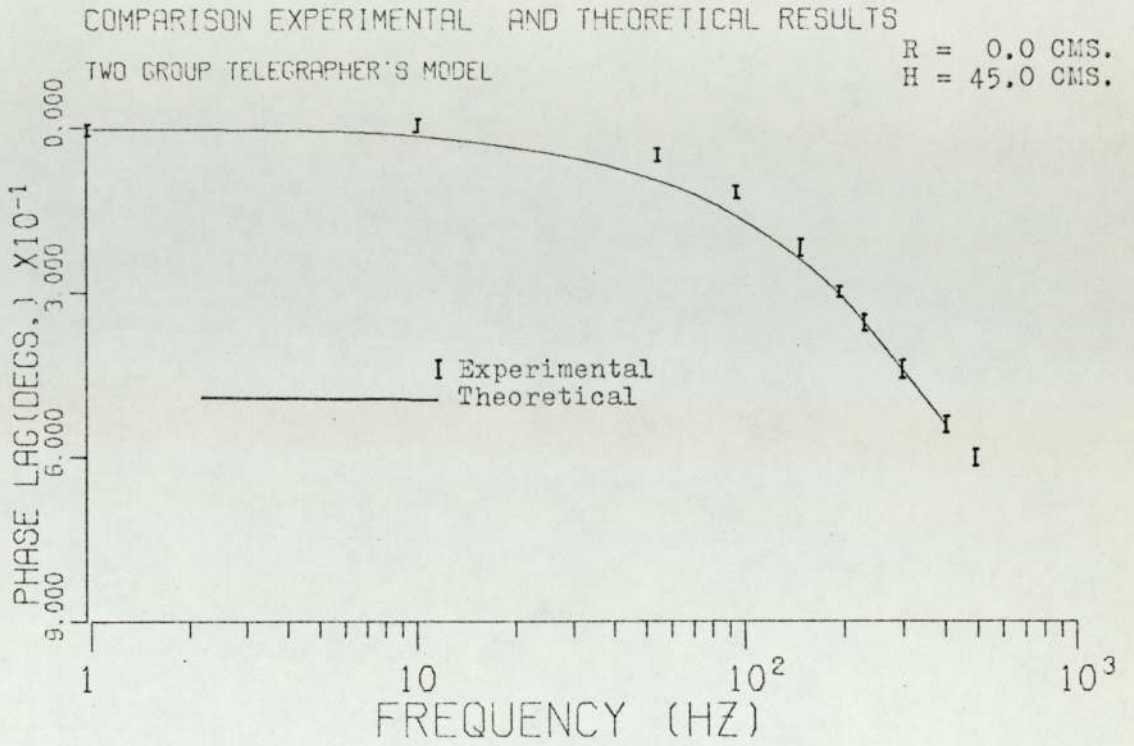
FIGS.(5.33) and (5.34) COMPARISON BETWEEN EXPERIMENTAL AND THEORETICAL RESULTS



FIGS. (5.35) and (5.36) COMPARISON BETWEEN EXPERIMENTAL AND THEORETICAL RESULTS



FIGS. (5.37) and (5.38) COMPARISON BETWEEN EXPERIMENTAL AND THEORETICAL RESULTS



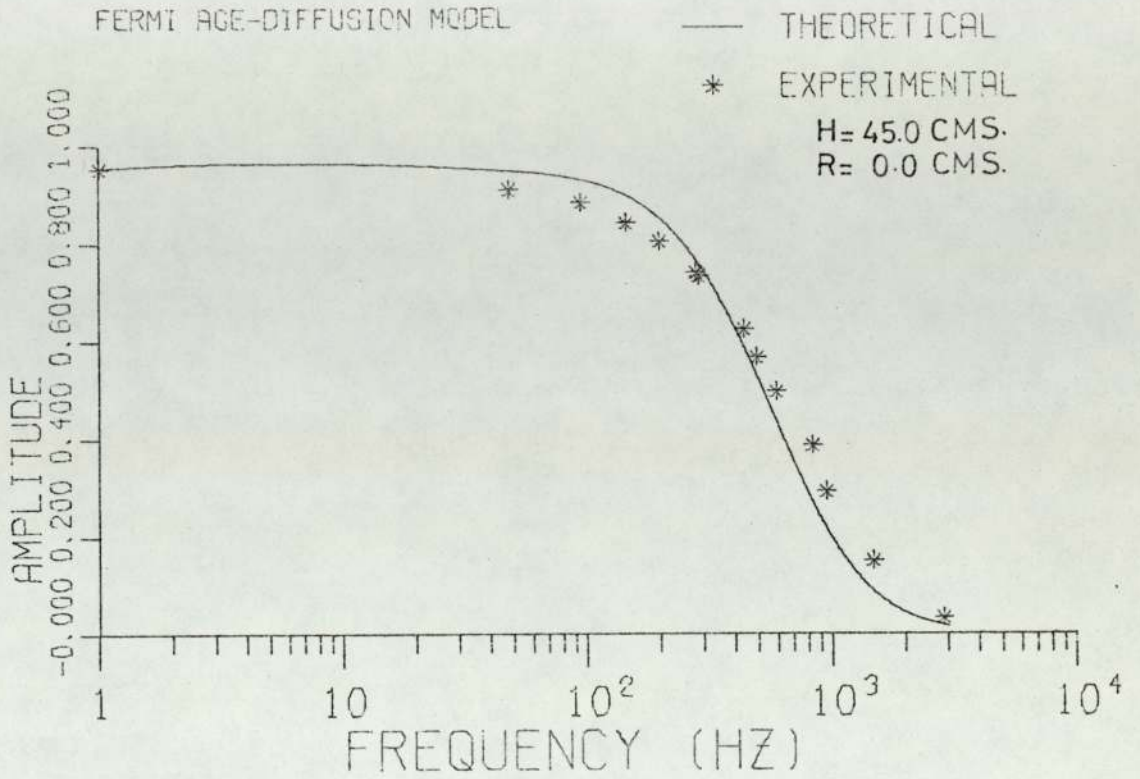
FIGS.(5.39) and (5.40) COMPARISON BETWEEN EXPERIMENTAL AND THEORETICAL RESULTS

frequency of interest, the error bars in the graphs represent the spread in the values of both the amplitude and phase lag. The points related to harmonics of the fundamental generally show a larger spread in values than those obtained from the fundamental.

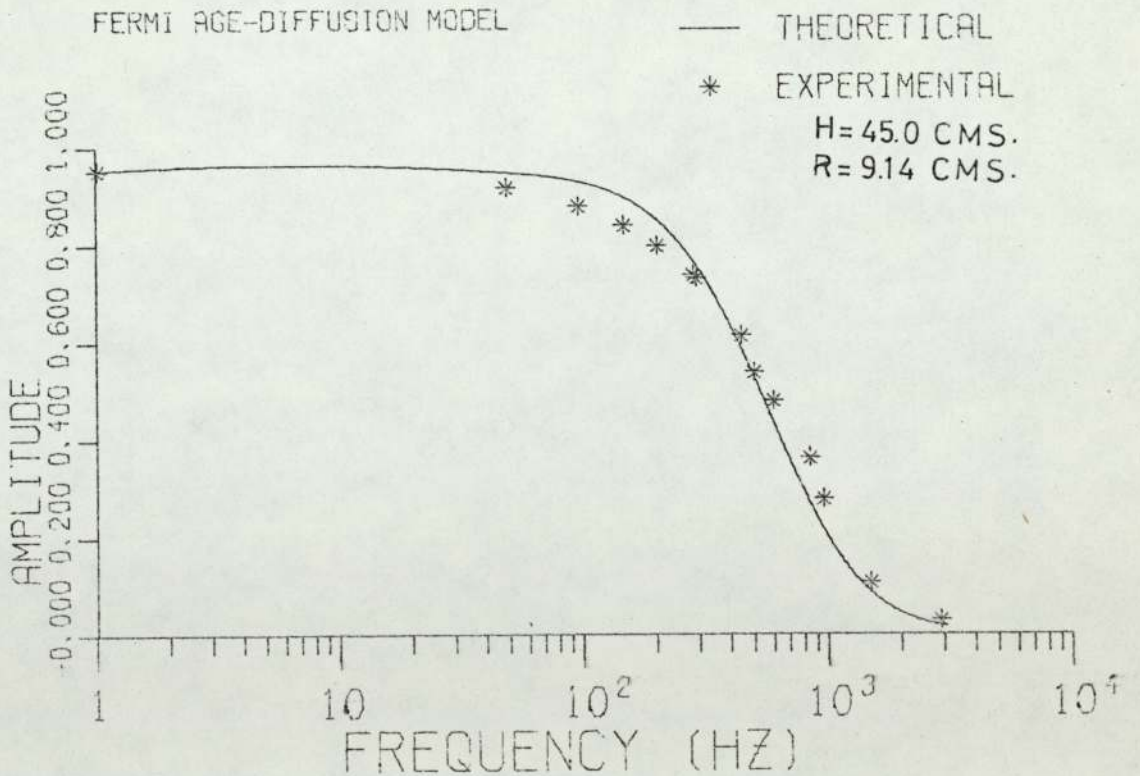
As a conclusion, it can be said that the complex source method when used to solve the two-group Telegrapher's equations is able to predict fairly accurately the transfer function in the present nuclear system for a frequency range of up to 400 Hz.

With respect to the Fermi Age - Diffusion method, the amplitude response is compared with that obtained experimentally in Figures (5.41) to (5.44). It can clearly be seen how the agreement is fairly good over the entire range of frequencies. This agreement, however, was found to be worse for the points located in the low end of the assembly which are near to the outer edge of the system. This effect can be seen in the next set of Figures (5.45) to (5.48) which correspond to calculations and measurements performed in a plane located 15 cms. high from the bottom of the subcritical assembly. These Figures show how the agreement gets worse at the high frequency end for the points located near the edge of the system. This effect, which has only been noticed in the low end of the assembly, could be due to the effect of source neutrons coming from neutrons scattered inside the graphite pedestal and the water reflector without having passed through the core of the system, thus giving an effectively broad neutron source.

COMPARISON EXPERIMENTAL AND THEORETICAL RESULTS

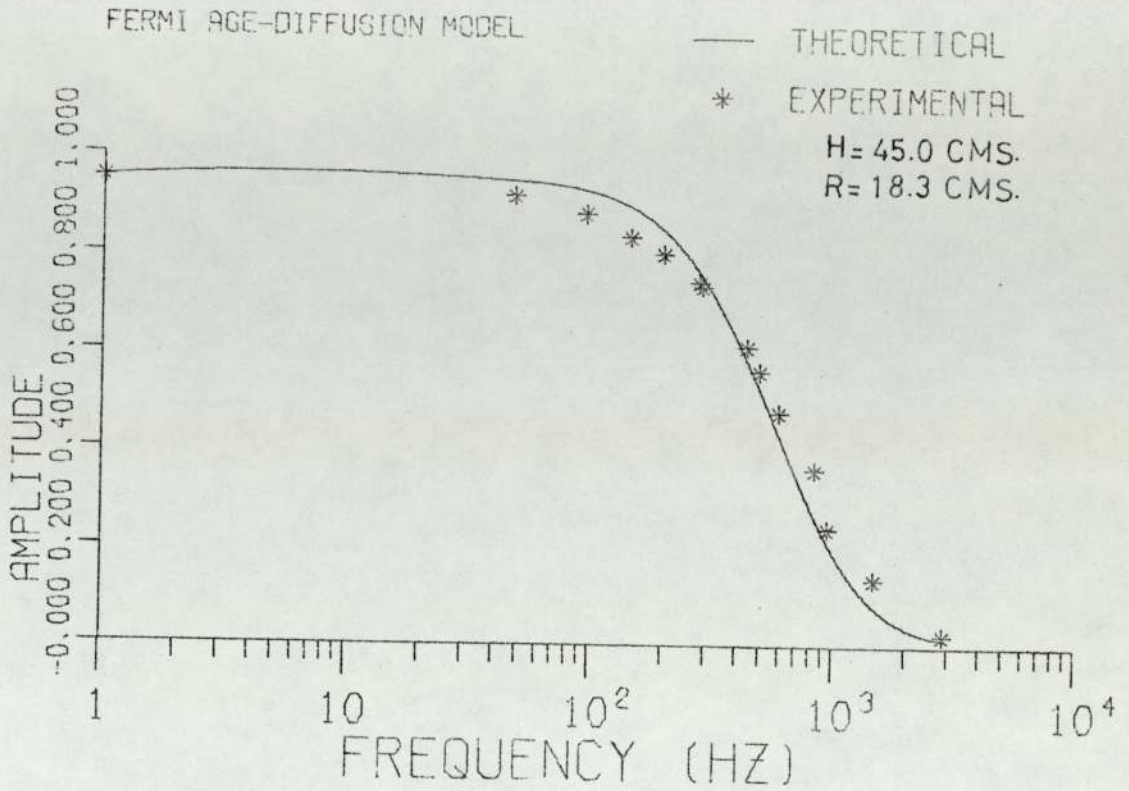


COMPARISON EXPERIMENTAL AND THEORETICAL RESULTS

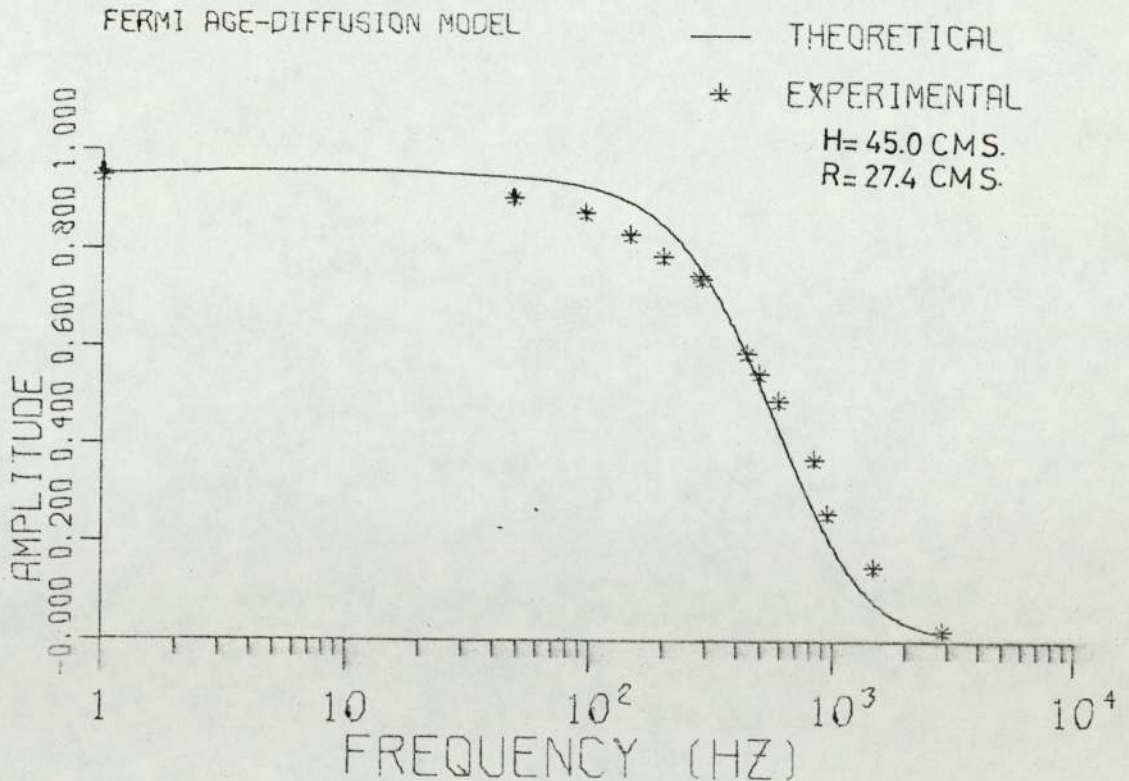


FIGS. (5.41) and (5.42) COMPARISON BETWEEN EXPERIMENTAL AND THEORETICAL RESULTS

COMPARISON EXPERIMENTAL AND THEORETICAL RESULTS

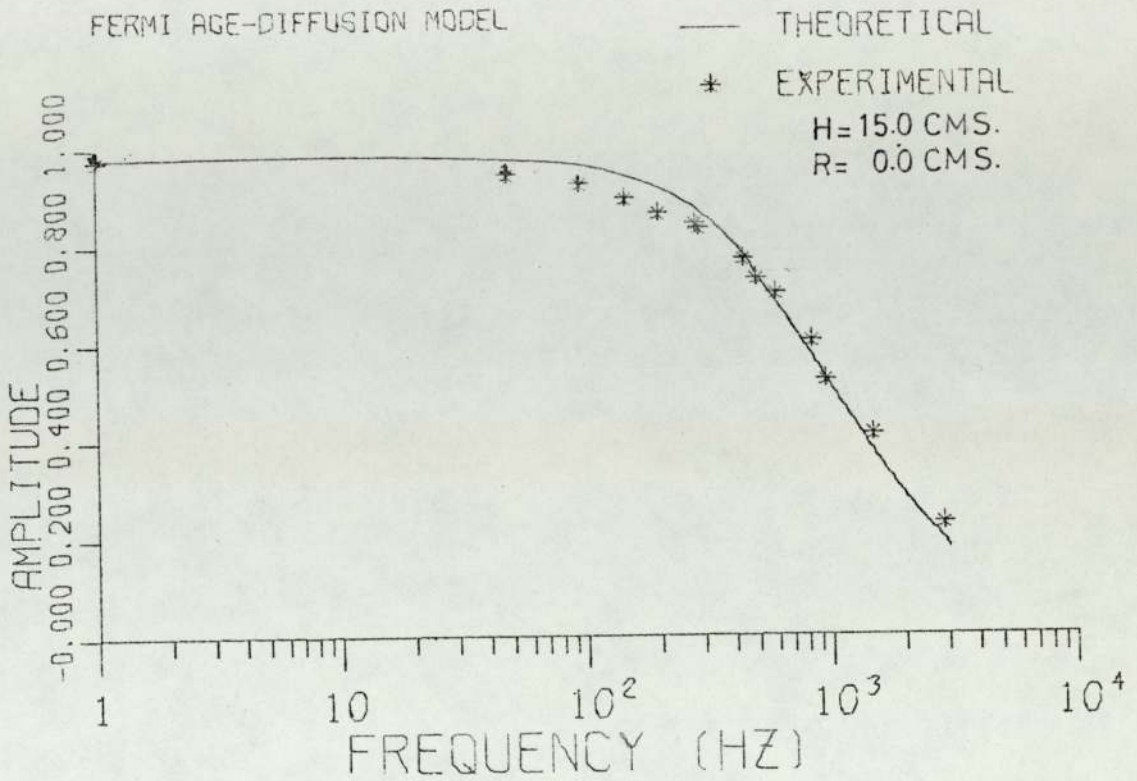


COMPARISON EXPERIMENTAL AND THEORETICAL RESULTS

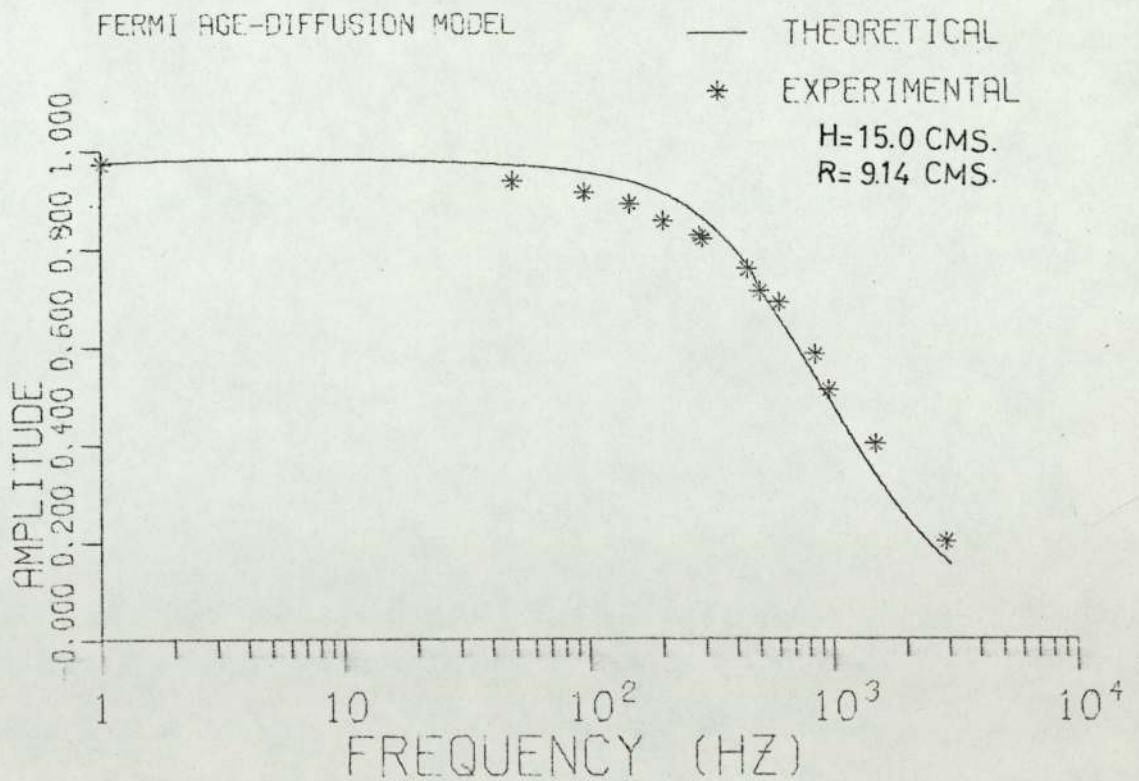


FIGS. (5.43) and (5.44) COMPARISON BETWEEN EXPERIMENTAL AND THEORETICAL RESULTS

COMPARISON EXPERIMENTAL AND THEORETICAL RESULTS

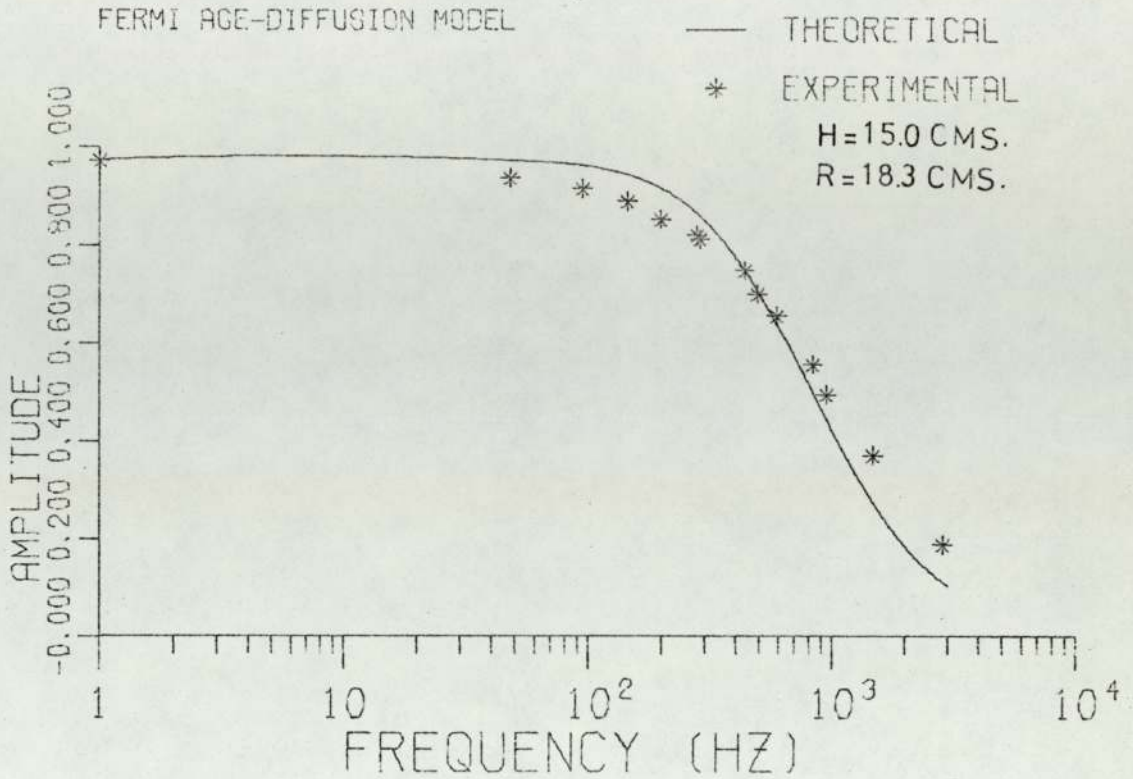


COMPARISON EXPERIMENTAL AND THEORETICAL RESULTS

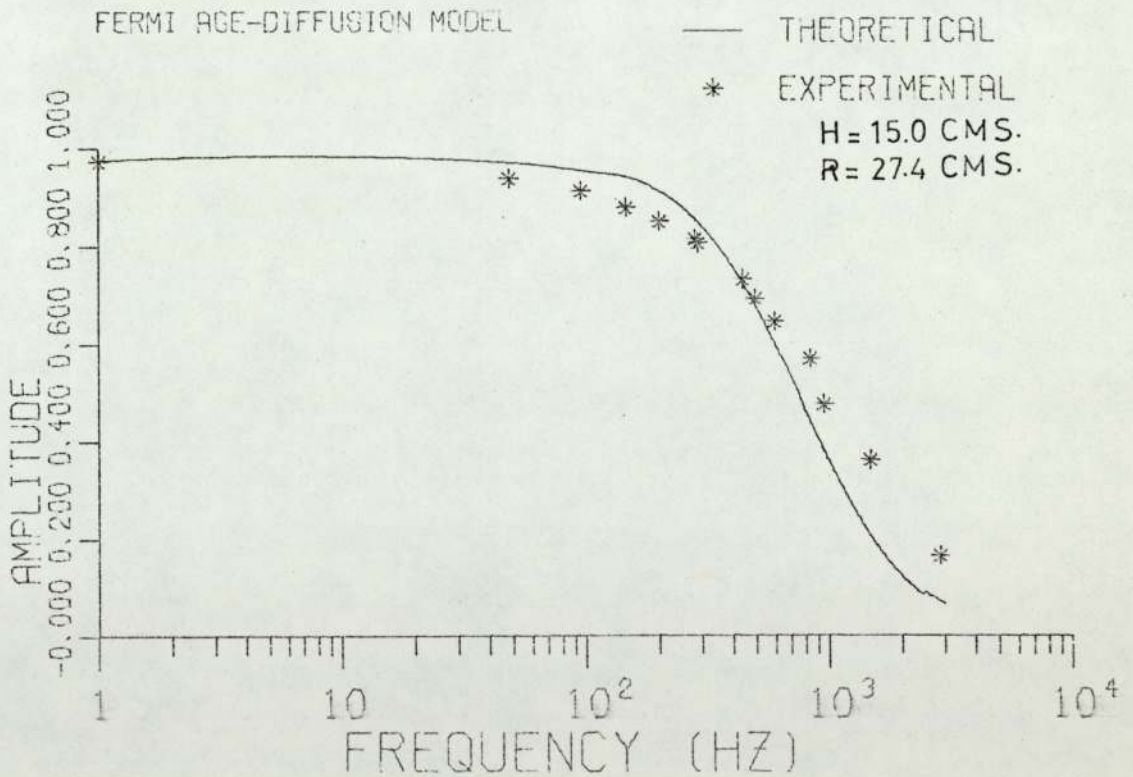


FIGS. (5.45) and (5.46) COMPARISON BETWEEN EXPERIMENTAL AND THEORETICAL RESULTS

COMPARISON EXPERIMENTAL AND THEORETICAL RESULTS



COMPARISON EXPERIMENTAL AND THEORETICAL RESULTS



FIGS.(5.47) and (5.48) COMPARISON BETWEEN EXPERIMENTAL AND THEORETICAL RESULTS

The thermal neutron lifetime used for this set of calculations was 84 microseconds. The neutron velocity is inversely proportional to the lifetime ( $l = \Sigma_a/V$ ) and therefore a long lifetime is equivalent to assuming a low neutron velocity. This implies a slow propagation of the neutron wave (velocity  $\sim v/\sqrt{3}$ ) which consequently leads to large phase lags. Therefore, a good agreement between experimental and calculated phase shifts was not obtained. This was not the case, however, of the complex source method where relativistic neutron velocities were used both in core and reflector. Neutron wave propagation velocities should therefore be similar to those in the real system and consequently phase shifts should be correctly predicted.

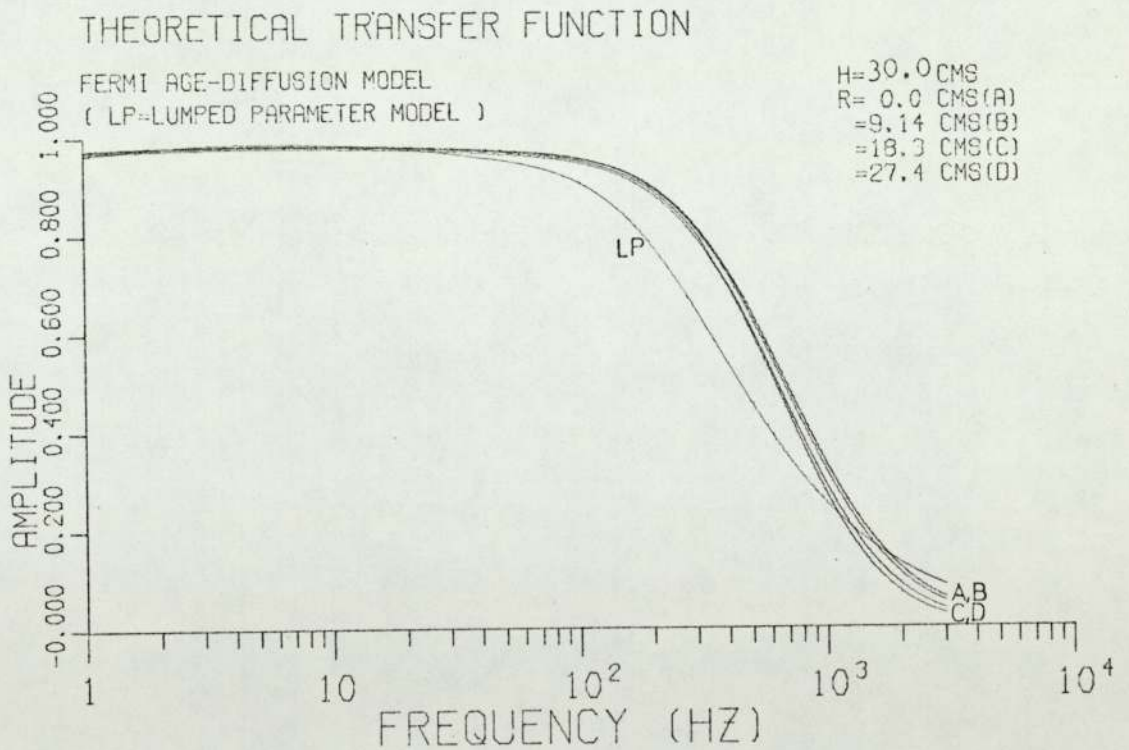
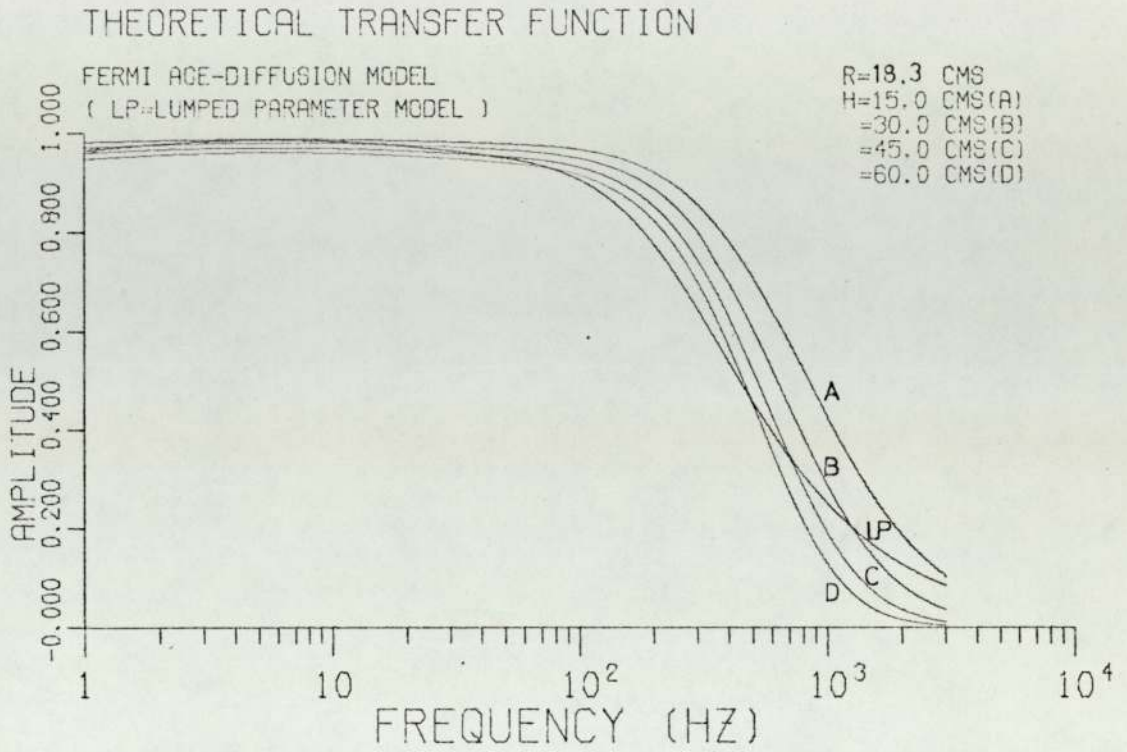
It can be concluded that the Fermi Age - Diffusion theoretical model is able to predict with a fairly good accuracy the source transfer function in the present nuclear system for frequencies of up to 3000 Hz provided that an appropriate value of the thermal neutron lifetime is selected.

### 5.5 Lumped parameter approximation.

It has been shown all throughout the present work how a spatial effect is always present and therefore it has got to be considered in the determination, both theoretical and experimentally, of the source transfer function of a nuclear system. It is possible, however, to refer to the space-independent transfer function when this term is applied to the reactivity transfer function. Since reactivity is an integral or whole-reactor parameter,

specification of the reactivity effect of an input does not uniquely specify the input in a space-dependent situation. Therefore, there is no such thing as a space-dependent reactivity transfer function(23).

A comparison between the lumped parameter and space-dependent source transfer function can be seen in Figures (5.49) and (5.50). Here, the lumped parameter distribution was obtained by using the two-group Telegrapher's equations corresponding to a lumped parameter nuclear system(22). These figures show how for an axial and a radial spatial distribution, the lumped parameter approximation does not predict at all wee the system transfer function.



FIGS.(5.49) and (5.50) COMPARISON BETWEEN LUMPED PARAMETER AND SPACE DEPENDENT TRANSFER FUNCTION

CHAPTER 6

GAMMA MEASUREMENTS

Most studies of fluctuations and correlations in neutron distributions are based upon the direct detection of neutrons. One exception is an attempt made to observe neutron fluctuations by monitoring the Cerenkov radiation (67). Cerenkov detectors were also used by E. Kenney (68) and W.K. Lehto et al (69, 70) to perform reactor noise measurements by monitoring prompt gamma rays emitted in fission events. Both Kenney (68) and Lehto (69 to 71) based their experiments on theoretical studies of gamma noise performed by Gelinias and Osborn (72). Further studies on gamma-ray noise measurements were performed by Bärns and Markkanen (73).

The results obtained by these workers clearly verify the applicability of gamma observation techniques in reactor noise measurements as a substitute and complement to noise measurements via neutron detection. Due to the small mean free path of thermal neutrons in a Nuclear System, especially a water moderated one, a neutron detector "sees" neutrons essentially only in that volume which the detector itself occupies physically in the system plus one mean free path around. In the case of photons, which have much greater mean free paths, the gamma detector is capable of receiving gammas that have travelled considerable distances through the core. This, of course, implies that the capability to observe spatially dependent effects is reduced. Making a

conservative estimate, the volume of the system which is seen by a gamma detector is about 50 times greater than that corresponding to a similar size neutron detector. Therefore, it follows that a gamma detector does not necessarily have to be placed into the core, thereby, the perturbations commonly induced by neutron-detecting devices can be avoided.

Furthermore, neutron detectors are not feasible when used to measure shut-down reactivities of power reactors due both to possible radiation damage and to the mechanical difficulties involved in the insertion of detectors inside the core.

The previous considerations suggested the idea of trying to find whether it was possible to determine experimentally the subcritical assembly transfer function by detecting the high energy prompt-gamma radiation generated by neutron interactions within the core.

The prompt gamma-ray spectrum contains a significant number of photons with energies above  $\sim 5$  Mev, while the fission-product spectrum contains very few (74). Meinschein et al (75) reported that there is a negligible delayed gamma-ray emission due to fission product decay in the time interval between  $10^{-4}$  and 1 sec. after fission. Delayed gamma emission in shorter time intervals (less than  $10^{-4}$  secs. after fission) behaves as prompt (72) and it is also a negligible fraction of the total gamma energy emitted per fission event (75). Long lived fission products can be troublesome in the sense that they are the source of considerable background due to low energy pile-up.

Also, Chapman et al (76) show that fission-product gamma radiation for energies greater than 5 Mev is considerably less than that arising promptly from fission.

Thus, by suitable photon-energy discrimination and adequate shielding (to reduce low energy pile-up), it appears that it may be possible to obtain information regarding neutron fluctuations by detecting high energy prompt photons emitted by fission. Furthermore, the high velocity of photons and its long mean free path in water compared with thermal neutrons, suggest that the frequency response might be less distorted than in the case of a neutron detector situated outside the core.

#### 6.1 Experimental arrangement.

Three different NaI(Tl) scintillators were used in turn for the present measurements. Two of them were used for outside measurements and the other one was located inside the core of the subcritical assembly. The counting rate obtained from the latter (size 12.7 mm. diameter x 19 mm. thickness) proved to be too small and it was impossible to obtain any reliable information from it.

The other two detectors (sizes 44.5 mm. x 38 mm. and 101.6 mm. x 101.6 mm.) were used for measurements outside the system. They were placed horizontally along a radius from the core centre and measurements were taken in different axial positions. In order to monitor the neutron population inside the system, a neutron detector was used simultaneously with a gamma detector. The latter was always placed in the centre of the system

and in the same plane as the gamma detector.

Low energy pile-up was minimized by shielding the detectors and the lower discriminator end was fixed at 5 Mev.

A comprehensive description of the experimental arrangement is given in Chapter 2.

## 6.2 Results and Conclusions.

The frequency response characteristics of the Nuclear System corresponding to the gamma measurements were evaluated by means of the computer program DATACOR. The code is described in Chapter 3 and is listed in Appendix 2 .

Fig. (6.1) shows a typical output of DATACOR for a NaI(Tl) scintillator detector placed outside the reflector at a height of 30 cms. It can be clearly seen how the frequency response starts falling off at a much lower frequency than the corresponding neutron one.

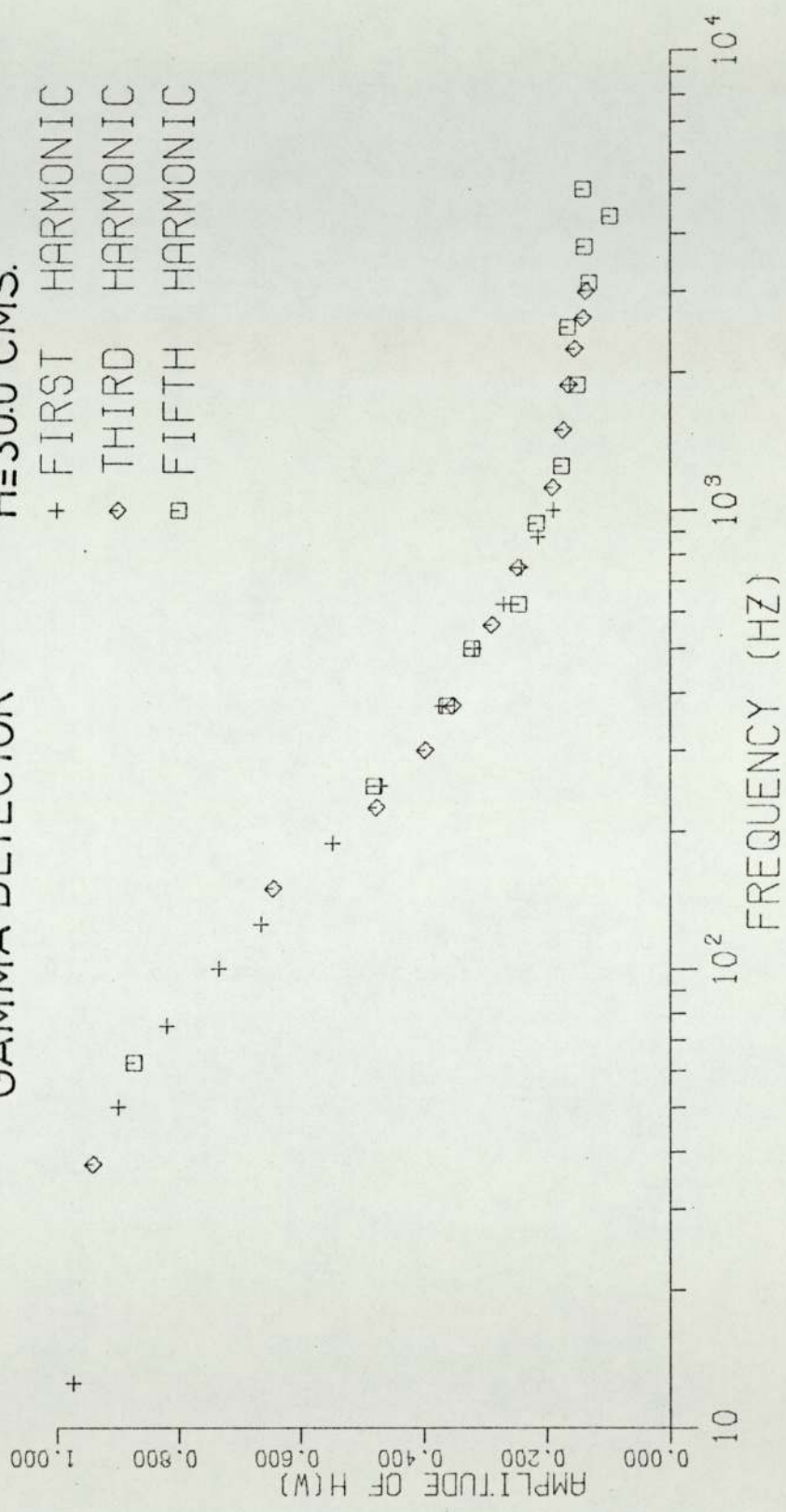
A comparison between the neutron and gamma detector responses can be seen in Figs. (6.2) and (6.3). Here, the neutron detector has been fixed in the far end of the reflector and the gamma detector was located in the same plane but outside the system. The difference in response between the two detection systems could be partially due to spatial effects.

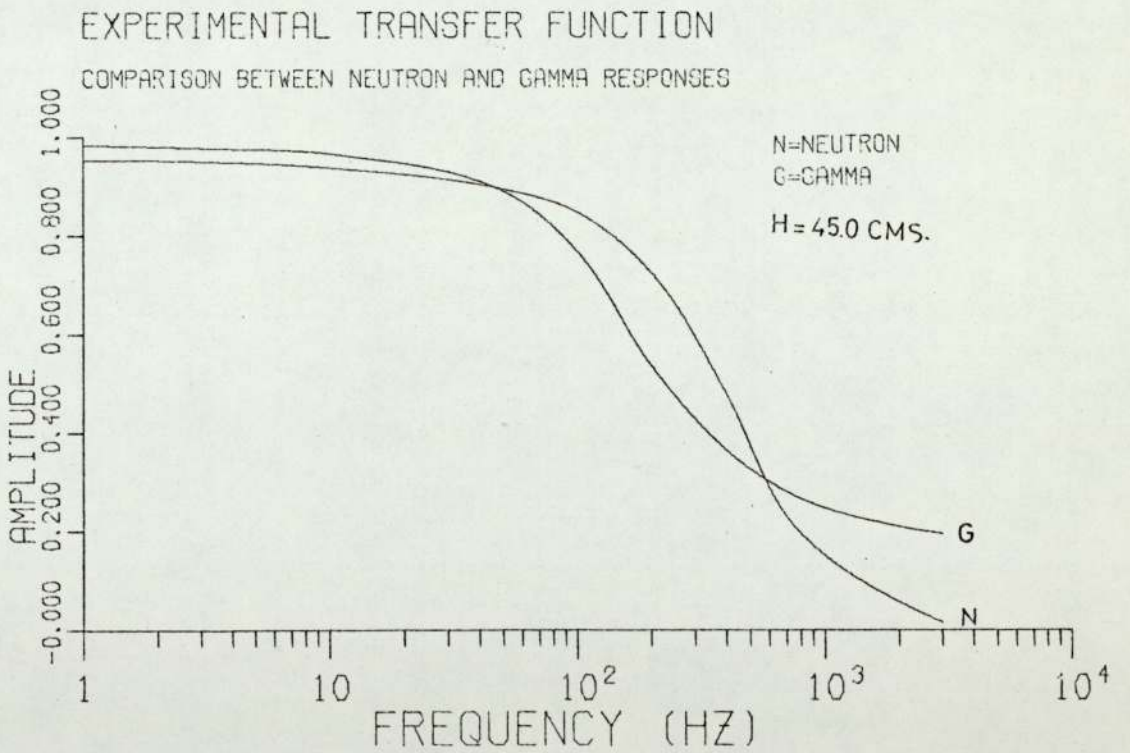
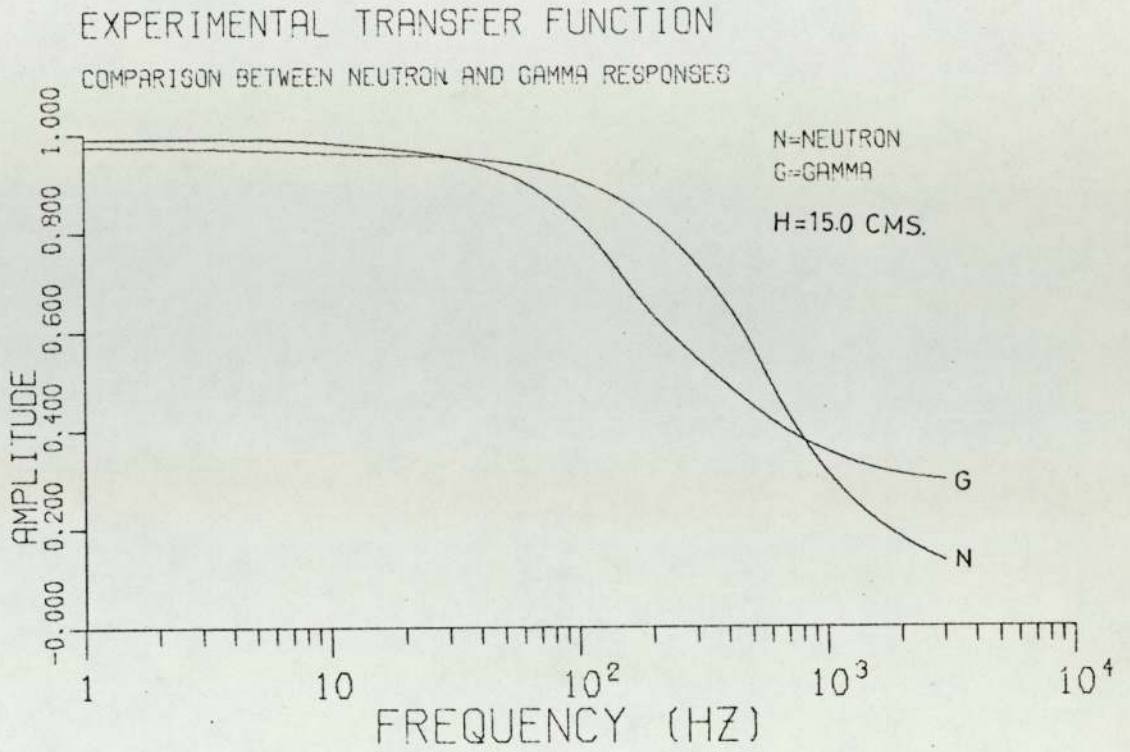
The spatial effects observed with the gamma detector can be seen in Fig. (6.4) which represents the system response to a gamma detector located in different axial positions outside the system.

The poor agreement between the neutron and gamma

# EXPERIMENTAL TRANSFER FUNCTION

GAMMA DETECTOR      H=30.0 CMS.  
+ FIRST HARMONIC  
◇ THIRD HARMONIC  
□ FIFTH HARMONIC





FIGS.(6.2) AND (6.3) COMPARISON BETWEEN NEUTRON AND GAMMA RESPONSES

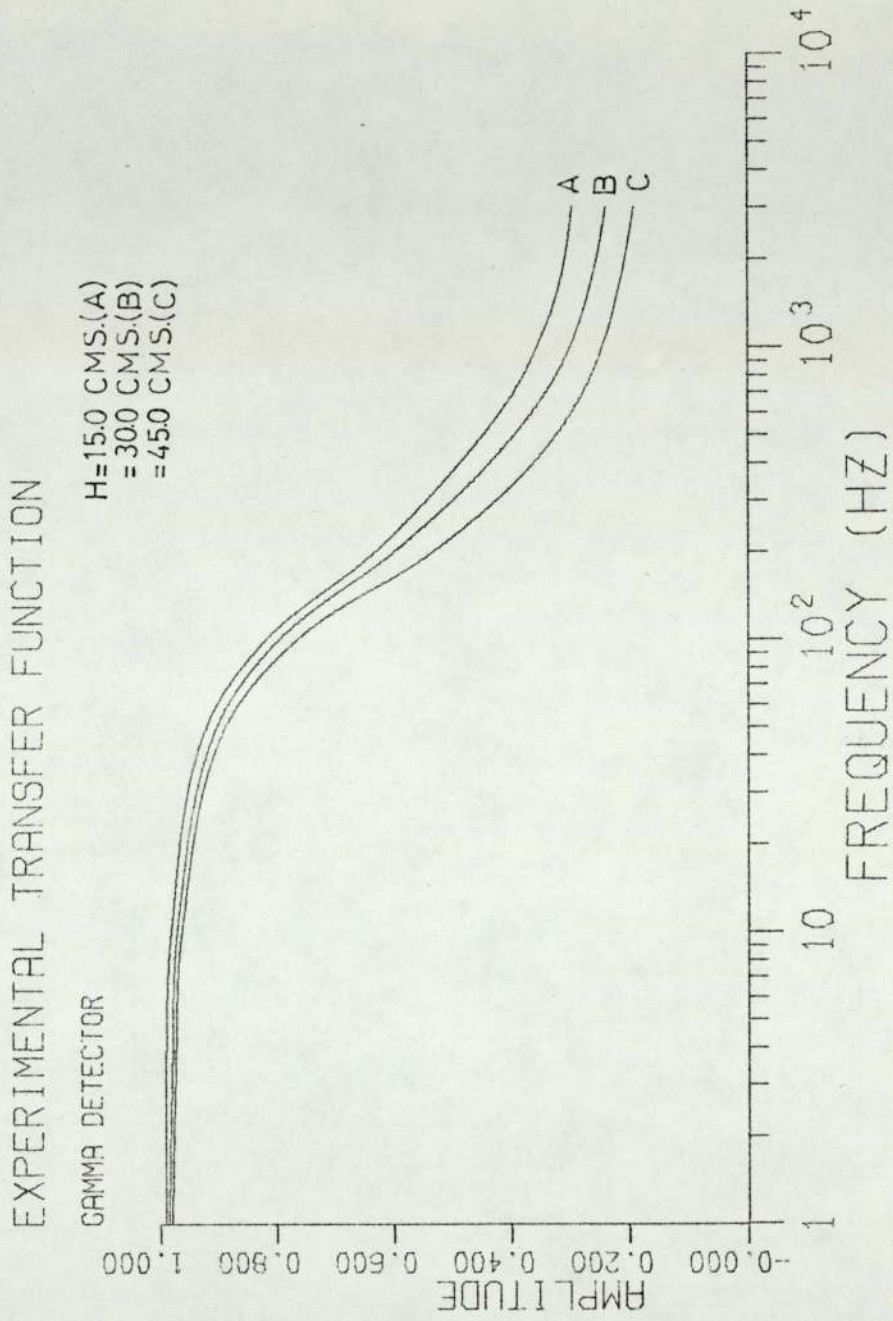


FIG. (6.4) EXPERIMENTAL AMPLITUDE RESPONSE FOR DIFFERENT AXIAL POSITIONS

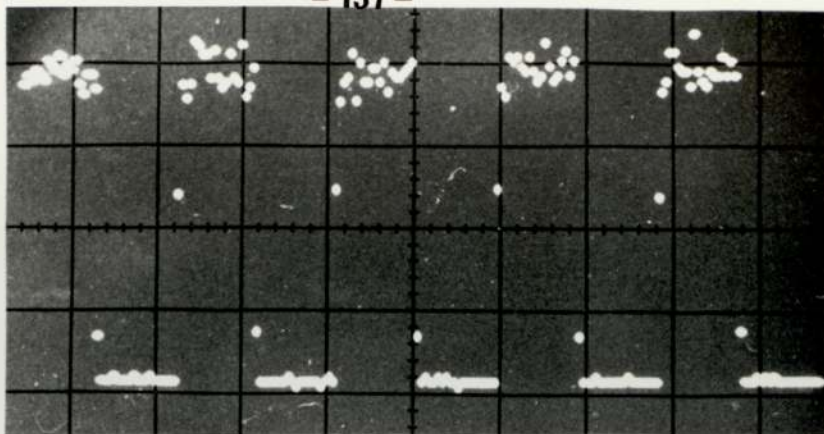
responses was immediately observed when comparing the shapes of the time dependent detector waveforms recorded by the P.H.A. as shown in Figs. (2.19) to (2.25) in Chapter 2. It can be clearly seen that both detectors have a similar time dependent output only for the very lowest range of frequencies. For frequencies greater than 10 Hz. and up to 250 Hz., the gamma response seems to be made up of two exponentials. For frequencies greater than 250 Hz., the frequency response is completely distorted compared with the neutron response and is not symmetrical about the mean level.

The fact that the neutron and gamma responses were completely different, suggested the possibility of gamma rays being produced in the target assembly either by fast neutron interactions or by excitation by deuterons.

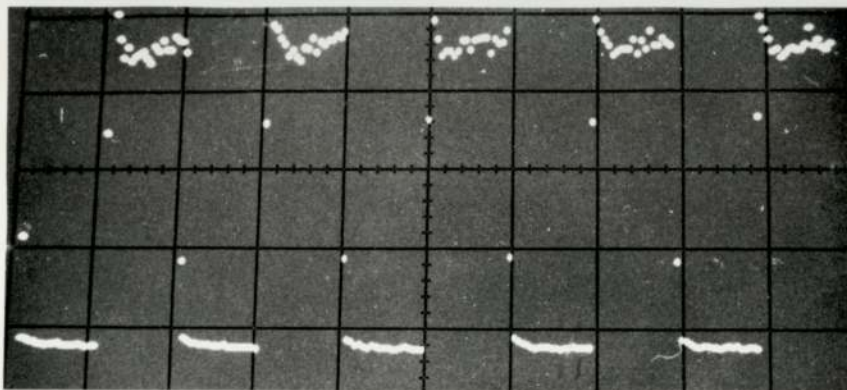
The possibility of gamma rays being produced by direct excitation by deuterons was eliminated when no gammas were observed on replacing the tritium target by a bare copper disc of exactly the same geometry.

In order to prove the feasibility of gamma rays being produced by fast neutron interactions inside the target assembly, the flight tube was removed from the subcritical assembly and measurements were taken with the detector placed as near as possible to the target. These measurements proved that a high intensity of gamma rays with energies of up to 10 Mev were produced inside the flight tube and target assembly as a consequence of fast neutron interactions with the constituent materials.

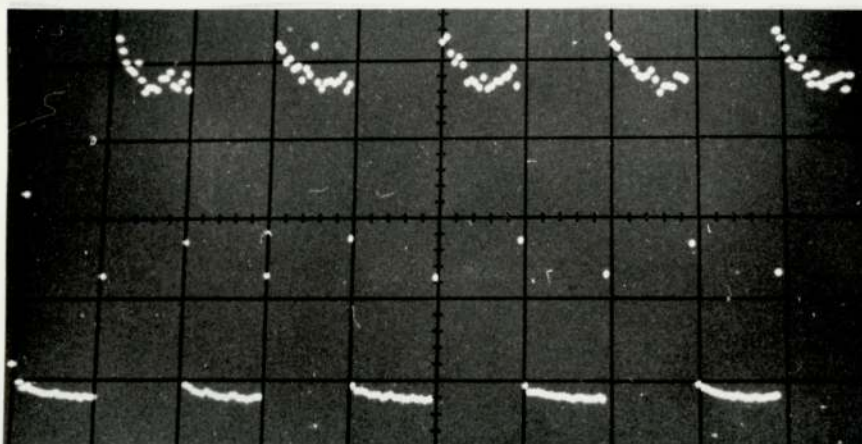
Figures (6.5) to (6.8) show the time variation of gamma rays output from the target assembly for different frequencies. By combining these waveforms with those corresponding to the prompt fission neutrons (as shown in Chapter 2), the shape of the resultant gamma ray waveforms observed when measured after passing through the subcritical assembly could be qualitatively explained. However, the physical process which produces the asymmetric variation in gamma ray output from the target assembly is still uncertain.



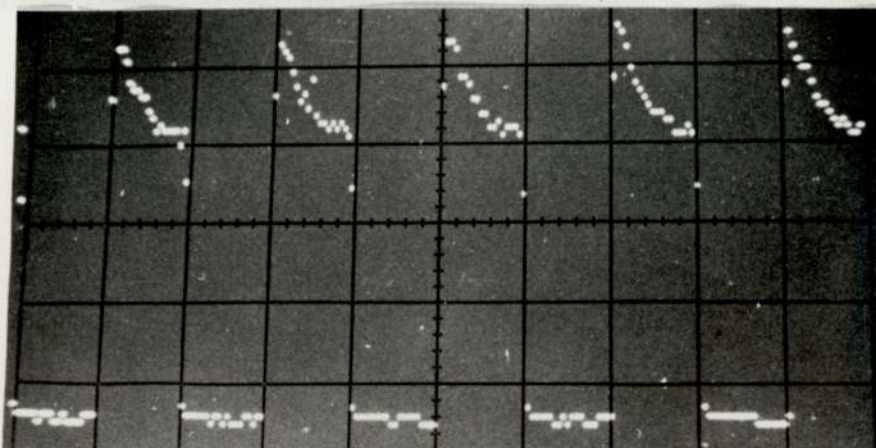
1 Hz



250 Hz



500 Hz



1000 Hz

FIGS. (6.5) to (6.8) GAMMA DETECTOR RESPONSE AT DIFFERENT FREQUENCIES

## CHAPTER 7

### CONCLUSIONS AND RECOMMENDATIONS

In this Chapter, a summary of the conclusions reached and some possible extensions to the present work, are presented.

#### 7.1 Conclusions.

The use of two different theoretical approaches towards the determination of the spatially dependent transfer function has clearly shown how a spatial effect must always be included in any theoretical model to correctly describe the transfer function of a nuclear system. Furthermore, both theory and experiment have shown that even a small system such as the one used in the experimental work can not be regarded as a point reactor or a lumped parameter model. It was found, however, that agreement between lumped and spatial transfer functions is obtained at one or two frequencies at a particular position.

Comparison between experimental and theoretical results has shown that both theoretical methods are able to predict with a fairly good accuracy the source transfer function. However, both methods have their advantages and disadvantages which could be summarized as follows:

(1) The complex source method when solved by SNAP is unable to give information for frequencies beyond 400 Hz. This might be overcome by using either a different code or modifying the method of solution used by SNAP. Also,

the size of the code (200 K of core plus three discs) limits its use to very powerful computers. On the other hand, its predictions are reasonably accurate over the range of frequencies where the code is able to find a solution. Another advantage is that SNAP can be used with practically any geometry, including reflectors, and so for a wide variety of reactor systems.

(2) The Fermi Age - diffusion method does not present any problem regarding any limiting frequency. Also, a numerical solution such as that performed by the computer program FERMI for an homogeneous cylindrical geometry does not require a powerful computer. On the other hand, this method possesses the limitations in accuracy inherent to any single region reactor calculation, mainly the inability to allow for reflector except as a reflector savings. Furthermore, the numerical solution of the equation describing the spatial dependent transfer function is only worthwhile attempting for simple geometries.

With respect to the experimental side of the present work, a great deal of improvement has been achieved regarding the pulsing system of the S.A.M.E.S. accelerator. The new pulsing system eliminates the uncertainty of the beam being in phase with the starting command of the P.H.A. Furthermore, the possibility of the ion source not being always extinguished when the radiofrequency is switched off has been eliminated for normal rates of gas inlet to the source.

Also, the electronic networks developed to

simultaneously use two detectors can be used in any further experiments where two detector correlations are required. Furthermore, the expansion of the networks to monitor any even number of detectors is quite straight forward.

With respect to the determination of the transfer function via photon observation, the results shown in Chapter 6 are somewhat disappointing. It is believed, however, that further research in the topic will give rise to more useful conclusions.

## 7.2 Recommendations for future work.

An extension of the present work should be possible on the following lines:

- (1) Further research in transfer functions via photon observation.
- (2) Effect of different reflectors on the neutron lifetime and therefore on the transfer function.
- (3) Improvement to the Fermi Age model by expanding it to a two-region geometry. This could eliminate the uncertainties regarding the thermal neutron lifetime.

APPENDIX 1

NUCLEAR INSTRUMENTS AND METHODS 109 (1973) 617-618; © NORTH-HOLLAND PUBLISHING CO.

IMPROVEMENTS TO A METHOD OF EXTERNALLY PULSING AN ACCELERATOR

A. GIL RAMOS and P. N. COOPER

Department of Physics, University of Aston in Birmingham, Gosta Green, Birmingham B4 7ET, England

Received 12 February 1973

A simplified method of producing a square beam current waveform from a SAMES 150 kV accelerator has been devised. Square light pulses are transmitted to the high voltage terminal by an optical link using semiconductor devices. The transmitted

signal controls a high voltage power transistor which extinguishes the ion source if when in the conducting state. Operating frequencies are from 1 Hz to 2 kHz.

In a previous communication<sup>1)</sup> a method was described for producing a square wave modulation of the ion current from a SAMES type J accelerator. This note describes certain simplifications and improvements

that have been made to the modulation system. Since this no longer includes a modified version of the pulsing unit designed by SAMES the method is now more readily adaptable to other accelerators.

The modulated light beam is still used to transmit the signal to the high voltage terminal. Since the light emitting diode type MGA 100 is now obsolete it has been replaced by the more efficient type 1A48. Also modifications have been made to the driving circuit so that the transmitted light pulse follows the shape of the driving pulse instead of producing a short light signal coincident with the leading edge. The revised circuit is given in fig. 1. Driving signals are taken directly from the output of a dividing circuit constructed from SN 7490N and SN 7493N integrated circuits.

When run for long periods the bistable circuit,

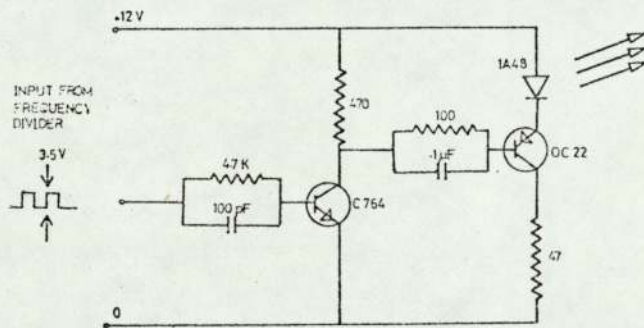


Fig. 1. Light pulse transmitter.

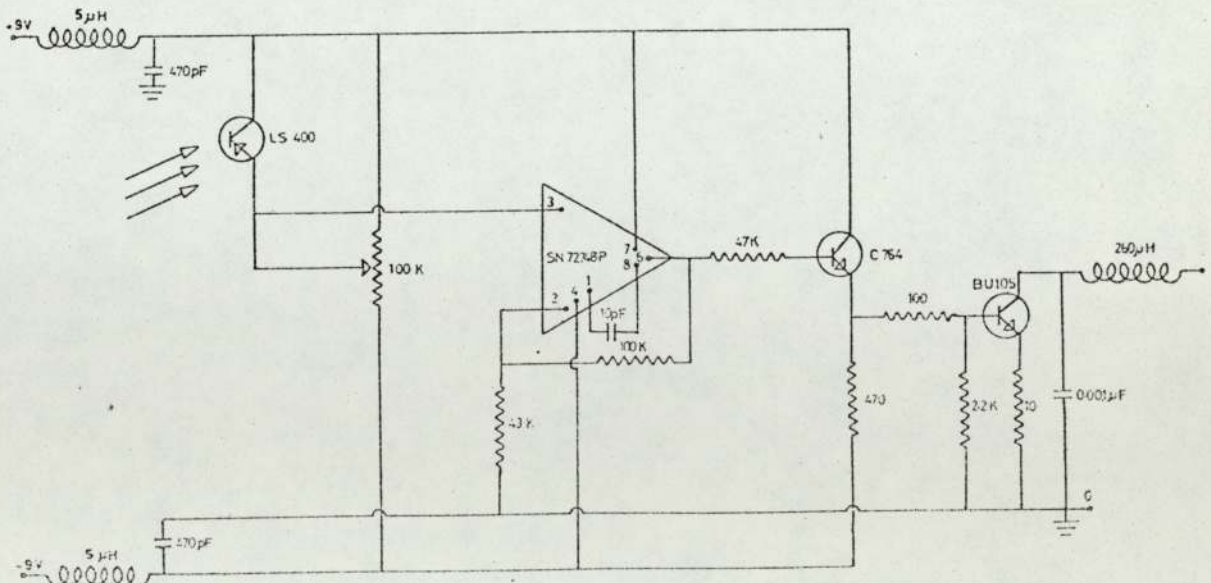


Fig. 2. Receiver and pulser.

originally used to drive the switching pentode, was found to be over-sensitive to supply voltage variations and consequently did not always respond to the trigger pulse. To overcome this the bistable circuit and the switching pentode were replaced by a single high voltage npn transistor type BU105. The base of this was driven by a square wave voltage signal derived from the transmitted light signal and the circuit for achieving this is shown in fig. 2. It was found necessary to include adequate screening and filtering against the intense radio frequency signals produced by the ion-source oscillator. One advantage of this method is that the beam pulse is in phase with the transmitted pulse whereas previously the phases could differ by  $180^\circ$ , depending on the initial state of the bistable circuit.

When the base of the BU105 is made positive the transistor conducts. In this mode it is used in one of two ways to shut off the ion source radio frequency. The first method, which was used in the original SAMES pulsing unit, is to reduce the voltage of the oscillator screen grid to near earth. This leaves the full high tension on the anode and on the coupling straps

to the ion source bottle. In consequence the plasma, under certain combinations of gas pressure and high tension voltage, may not always extinguish completely, thus giving some ion current during the off period of the cycle. An alternative method, which has proved consistently reliable, is to use the BU105 to short the high tension supply to the whole oscillator to ground. A  $2\text{ k}\Omega$  100 W wirewound resistor was inserted into the high tension lead between the power pack and the BU105 to act as a current limiter.

This method of pulsing can be easily adapted to any desired rectangular waveform where the on period differs from the off period, simply by applying the appropriate waveform to the input of the transmitter. For an applied square wave the system has been found to operate reliably in the range of frequencies 1 Hz to 2 kHz.

#### Reference

- 1) P. N. Cooper and L. Doukas, Nucl. Instr. and Meth. 92 (1971) 581.



```
BACK1(I) := BACK(I);
BACK2(I) := BACK(I + (M+N+1)/2);
'END';
'END';
'ELSE';
'BEGIN';
'FOR' I := M STEP 1 'UNTIL' (M+N+1)/2 - 1 'DO';
'BEGIN';
BACK1(I) := BACK(I + (M+N+1)/2);
BACK2(I) := BACK(I);
'END';
'END';
'END' OF PROCEDURE BACKORDER;

'PROCEDURE' BACKGRDUP(BACK);
'ARRAY' BACK;
'BEGIN';
TRUBACK := 0;
'IF' K EQ 0 'THEN';
UNIBACK1 := 0;
UNIBACK2 := 0;
'FOR' I := M STEP 1 'UNTIL' (M+N+1)/2 - 1 'DO';
TRUBACK := TRUBACK + BACK(I);
UNIBACK := 2 * TRUBACK / I;
'IF' DETNUM EQ 2 'THEN';
'BEGIN';
SPACE(10);
WRITETEXT('BACKGROUNDZCORRESPONDENTZTDETECTORZ');
'IF' K EQ 0 'THEN';
'BEGIN';
UNIBACK1 := UNIBACK1 + UNIBACK;
WRITETEXT('A');
'END';
'ELSE';
'BEGIN';
UNIBACK2 := UNIBACK2 + UNIBACK;
WRITETEXT('B');
'END';
'END';
NEWLINE(1);
SPACE(10);
WRITETEXT('BACKGROUNDZTIMEZZ=');
PRINT(T1/2, 3, 2);
WRITETEXT('MINS. ');
NEWLINE(1);
SPACE(10);
WRITETEXT('TOTALZBACKGROUNDZXXXZ=');
PRINT(TRUBACK, 6, 2);
NEWLINE(1);
SPACE(10);
WRITETEXT('BACKGROUNDZPELZMINUTEZZ=');
PRINT(UNIBACK, 5, 2);
NEWLINE(2);
'END' OF PROCEDURE BACKGRDUP;

'PROCEDURE' DATAORDER(TIME1, TIME2, TIME);
'ARRAY' TIME1, TIME2;
'ARRAY' TIME;
```

```
'BEGIN'  
  'IF' 'CL.DEN?' EQ '12' THEN'  
    'BEGIN'  
      'FOR' I:=M' STEP'L' UNTIL '(X+N+1)/2-1' DO'  
        'BEGIN'  
          TRUE1(I):=TRUE(I);  
          TRUE2(I):=TRUE(I+(X+N+1)/2);  
        'END';  
      'END';  
    'ELSE'  
    'BEGIN'  
      'FOR' I:=M' STEP'L' UNTIL '(X+N+1)/2-1' DO'  
        'BEGIN'  
          TRUE1(I):=TRUE(I+(X+N+1)/2);  
          TRUE2(I):=TRUE(I);  
        'END';  
      'END';  
    'END' OF PROCEDURE DATAORDER;
```

```
'PROCEDURE' ARRANGE(TRUE, CONVAL);  
'ARRAY' TRUE;  
'ARRAY' CONVAL;  
'BEGIN'  
  'FOR' I:=0' STEP'1' UNTIL'NUMBER-1' DO'  
    CONVAL(I):=0;  
  'FOR' I:=0' STEP'1' UNTIL'NUMBER-1' DO'  
    'FOR' J:=1' STEP'NUMBER' UNTIL '(X+N+1)/2-1' DO'  
      CONVAL(I):=CONVAL(I)+TRUE(J);  
    'FOR' I:=0' STEP'1' UNTIL'NUMBER-1' DO'  
      CONVAL(I):=CONVAL(I)/TIMCHAN;  
    'FOR' I:=0' STEP'1' UNTIL'NUMBER-1' DO'  
      CONVAL(I):=CONVAL(I)/60;  
    WRITETEXT('THE FOLLOWING VALUES CORRESPOND TO EACH CHANNEL'  
      CONTENT FOR ONE CYCLE AND PER SECOND');  
    NEWLINE(2);  
    WRITETEXT('TOTAL MEASUREMENT TIME==');  
    PRINT(T2/2, 3, 2);  
    WRITETEXT('MINS. ');  
    NEWLINE(2);  
  'END' OF PROCEDURE ARRANGE;
```

```
'PROCEDURE' CORRECT(CONVAL, CONVAL1, CONVAL2);  
'ARRAY' CONVAL, CONVAL1, CONVAL2;  
'BEGIN'  
  TRANSFERT:=0.0000125;  
  DEADT:=0.000001;  
  T:=1/(NUMBER*FREQ);  
  FACTOR:=TRANSFERT/T;  
  'FOR' I:=0' STEP'1' UNTIL'NUMBER-1' DO'  
    CONVAL1(I):=CONVAL(I)/((1-FACTOR)/(1+CONVAL(I)*DEADT)+FACTOR*  
      ((1-EXP(-CONVAL(I)*TRANSFERT))/(CONVAL(I)*TRANSFERT)));
```

AGAIN:

```
'FOR' I:=0' STEP'1' UNTIL'NUMBER-1' DO'  
  CONVAL2(I):=CONVAL1(I)/((1-FACTOR)/(1+CONVAL1(I)*DEADT)+FACTOR*  
    ((1-EXP(-CONVAL1(I)*TRANSFERT))/(CONVAL1(I)*TRANSFERT)));  
  SPACE(3);  
  'FOR' I:=0' STEP'1' UNTIL'NUMBER-1' DO'  
    'IF' ABS((CONVAL2(I)-CONVAL1(I))/CONVAL2(I)) 'GE' 0.001 THEN'
```

```
'BEGIN'  
'FOR' I:=0 STEP 1 UNTIL NUMBER-1 DO  
    CONVAL(I):=CONVAL2(I);  
    'GOTO' AGAIN;  
'END';  
'END' OF PROCEDURE CORRECT;  
  
'PROCEDURE' AVERAGE(CONVAL);  
'ARRAY' CONVAL;  
'BEGIN'  
    SUM:=0.0;  
    'FOR' I:=0 STEP 1 UNTIL NUMBER-1 DO  
        SUM:=SUM+CONVAL(I);  
        AVERAGE:=SUM/NUMBER;  
        MAXI:=0.0;  
        J:=0;  
        'FOR' I:=0 STEP 1 UNTIL NUMBER-1 DO  
            'BEGIN'  
                MAX:=CONVAL(I)-AVERAGE;  
                'IF' MAX>0 THEN  
                    'BEGIN'  
                        MAXI:=MAXI+MAX;  
                        J:=J+1;  
                    'END';  
            'END';  
        MAXIAV:=MAXI/J+AVERAGE;  
        AMPLITUDE:=(MAXIAV-AVERAGE)/AVERAGE;  
'END' OF PROCEDURE AVERAGE;  
  
'PROCEDURE' AVERAGEHEAD;  
'BEGIN'  
    NEWLINE(2);  
    SPACE(5);  
    WRITETEXT(' AVERAGE VALUE PER CYCLE PER SECOND = ');  
    PRINT(AVERAGE,7,2);  
    NEWLINE(1);  
    SPACE(5);  
    WRITETEXT(' AVERAGE MAXIMUM VALUE = ');  
    PRINT(MAXIAV,7,2);  
    NEWLINE(1);  
    SPACE(5);  
    WRITETEXT(' AMPLITUDE = (MAX-AVER)/AVER = ');  
    PRINT(AMPLITUDE,4,3);  
'END' OF PROCEDURE AVERAGEHEAD;  
  
'PROCEDURE' TABULATE(CONVAL);  
'ARRAY' CONVAL;  
'BEGIN'  
    NEWLINE(2);  
    SPACE(3);  
    WRITETEXT(' CHANNEL ');  
    NEWLINE(1);  
    SPACE(3);  
    WRITETEXT(' NUMBER ');  
    NEWLINE(1);  
    'FOR' I:=0 STEP 1 UNTIL NUMBER-1 DO  
        'BEGIN'
```

```
NEWLINE(1);
SPACE(4);
PRINT(1,3,0);
'FOR' J:=1 'STEP' 1 'UNTIL' I+9 'DO'
PRINT(CONVAL(J),5,0);
'END';
'END' OF PROCEDURE TABULATE;
```

```
'PROCEDURE' FOURHEAD;
'BEGIN'
NEWLINE(2);
SPACE(22);
WRITETEXT('('*****FOURIERANALYSIS*****')');
NEWLINE(1);
SPACE(22);
WRITETEXT('('*****')');
NEWLINE(2);
SPACE(5);
WRITETEXT('('HARMONIC')');
SPACE(13);
WRITETEXT('('A')');
SPACE(16);
WRITETEXT('('P')');
SPACE(12);
WRITETEXT('('AMPLITUDE')');
SPACE(10);
WRITETEXT('('H(O)')');
SPACE(10);
WRITETEXT('('GAIN(DB)')');
SPACE(10);
WRITETEXT('('PHASE')');
NEWLINE(1);
'END' OF PROCEDURE FOURHEAD;
```

```
'PROCEDURE' FOURIEF (NUMBER, CONVAL, A, P);
'ARRAY' CONVAL, A, P;
'INTEGER' NUMBER;
'BEGIN'
'REAL' 'ARRAY' S, C(1:2), U(1:2);
'REAL' TEMP, PI;
'INTEGER' P, I;
PI:= 3.14159265;
C(2):=1;
S(2):= 0;
C(1):= COS(2*PI/NUMBER);
S(1):= SIN(2*PI/NUMBER);
'FOR' P:=0 'STEP' 1 'UNTIL' NUMBER/2 'DO'
'BEGIN'
U(1):= 0;
U(2):= 0;
'FOR' I:=NUMBER-1 'STEP'-1 'UNTIL' 1 'DO'
'BEGIN'
U(1):=CONVAL(I)+2*C(I)*U(1)-U(2);
U(2):=U(1);
C(I):= -C(I);
'END';
A(P):= 2*(CONVAL(P)+U(1)*C(P)-U(2))/NUMBER;
P(P):= 2*(U(1)*S(P))/NUMBER;
TEMP:= C(1)*C(P)-S(1)*S(P);
```

```
      SC2:= C(1)*SC(2)+SE(1)*C(2);
      C(2):= TEMP;
    'END';
  'END' OF PROCEDURE FOURIER;
```

```
'PROCEDURE' FOUREXIT(A,B);
'ADDPAY' A,B;
'BEGIN'
  I:=0;
  SPACE(7);
  PRINT(1,2,0);
  SPACE(2);
  PRINT(A(1),5,2);
  SPACE(6);
  PRINT(P(1),5,2);
  SPACE(6);
  PRINT(A(1),5,2);
  NEWLINE(1);
  'FOR' I:=1 'STEP' 1 'UNTIL' 7 'DO'
  'BEGIN'
    C:= 3.14159265*I/(2.0*A(1));
    AMP:= SQRT(A(1)*A(1)+P(1)*P(1));
    NDBX:=AMP*C;
    GAIN:=10*LN(NDBX*NDBX)/LOG;
    PHASE:=ARCTAN(A(1)/P(1));
    'IF' A(1) 'GT' 0 'AND' P(1) 'LT' 0 'OR' A(1) 'LT' 0 'AND' P(1) 'LT' 0
    'THEN'
      PHASE:=PHASE+3.14159265;
    'IF' PLOT 'EQ' 0 'THEN'
      'GOTO' P6;
    'IF' FREQ 'GE' 10 'THEN'
      'BEGIN'
        'IF' I 'EQ' 1 'THEN'
          'BEGIN'
            PLOTCDSS((LN(FREQ)/LOG)*3-3,NDBX*4,0.100);
            HGPWHERE(X,Y);
            HGPL0T(X,10.0+Y,0,4);
            'IF' GAIN 'GT' -20 'THEN'
              PLOTCDSS((LN(FREQ)/LOG)*3-3,(GAIN+20)/5.0,0.100);
              HGPWHERE(Y,Y);
              HGPL0T(Y,Y-10.0,0,4);
            'END';
            'IF' I 'EQ' 3 'THEN'
              'BEGIN'
                PLOTCDSS((LN(3*FREQ)/LOG)*3-3,NDBX*4,0.110);
                HGPWHERE(Y,Y);
                HGPL0T(X,10.0+Y,0,4);
```

```
'IF 'GAIN'GT '-20' THEN'  
PLOT(X, ((LN(3*FREQ)/LOG)*3-3, ((GAIN+20)/5.0, 0.110));  
HCPWHERE(X, Y);  
HCPLLOT(X, Y-10.0, 0, 4);  
  
'END';  
'IF 'I'EQ' 5 ' THEN'  
'BEGIN'  
  
PLOTSQUARE((LN(5*FREQ)/LOG)*3-3, NORM*4, 0.100);  
HCPWHERE(X, Y);  
HCPLLOT(X, 10.0+Y, 0, 4);  
  
'IF 'GAIN'GT '-20' THEN'  
  
PLOTSQUARE((LN(5*FREQ)/LOG)*3-3, ((GAIN+20)/5.0, 0.100);  
HCPWHERE(X, Y);  
HCPLLOT(X, Y-10.0, 0, 4);  
  
'END';  
  
P6:  
  
'END';  
SPACE(7);  
PRINT(I, 2, 0);  
SPACE(8);  
PRINT(A(I), 5, 2);  
SPACE(6);  
PRINT(B(I), 5, 2);  
SPACE(6);  
PRINT(C(P), 5, 2);  
SPACE(7);  
PRINT(NORM, 1, 5);  
SPACE(6);  
PRINT(GAIN, 2, 3);  
SPACE(7);  
PRINT(PHASE, 2, 3);  
NEWLINE(1);  
  
'END';  
'END' OF PROCEDURE FOURFIT;  
  
'PROCEDURE' LINEFITIN(DATA);  
'ARRAY' DATA;  
'BEGIN'  
STEP:=YMAX/NYE;  
YMAX:=YMAX+STEP;  
'FOR' I:=1 'STEP' 1 'UNTIL' NYE 'DO'  
'BEGIN'  
SPACE(15);  
PRINT(YMAX-I*STEP, 2, 0);  
SPACE(1);  
WRITE('(' I ')');
```

```
      'FOR' 'I':=1 'STEP' 1 'UNTIL' 'R0' 'DO'  
      'IF' 'DATA(LI)' 'GE' ('CHAN-185100') 'THEN'  
      'WRITE' 'TEXT' ('(' 'X' ')')  
      'ELSE'  
      'SPACE' (1);  
      'NEWLINE' (1);  
    'END';  
  'SPACE' (23);  
  'WRITE' 'TEXT' ('(' '0' ')') ;  
  'SPACE' (3);  
  'WRITE' 'TEXT' ('(' 'I' ')') ;  
  'FOR' 'I':=1 'STEP' 1 'UNTIL' 'R' 'DO'  
  'WRITE' 'TEXT' ('(' '-----I' ')') ;  
  'NEWLINE' (1);  
  'WRITE' 'TEXT' ('(' 'CHANNELNUMBER' ')') ;  
  'SPACE' (11);  
  'FOR' 'I':=0 'STEP' 10 'UNTIL' 'R0' 'DO'  
  'BEGIN'  
    'PRINT' (1, 0, 0);  
    'SPACE' (5);  
  'END';  
'END' OF PROCEDURE LINEPRIN;
```

```
'PROCEDURE' OF ENPLOT;  
'EXTERNAL';
```

```
'PROCEDURE' CLOSEPLOT;  
'EXTERNAL';
```

```
'PROCEDURE' HOPLOT(X, Y, A, R);  
'REAL' X, Y;  
'INTEGER' A, R;  
'EXTERNAL';
```

```
'PROCEDURE' HOPSCALE(X, N, S, XMIN, DY, K);  
'VALUE' N, S, XMIN, DY, K;  
'ARRAY' X;  
'REAL' S, XMIN, DY;  
'INTEGER' N, K;  
'EXTERNAL';
```

```
'PROCEDURE' HGRANISV(X, Y, PCB, N, S, THETA, XMIN, DY, GAP, NH);  
'VALUE' X, Y, N, S, THETA, XMIN, DY, GAP, NH;  
'INTEGER' N, NH;  
'ARRAY' PCB;  
'REAL' X, Y, S, THETA, XMIN, DY, GAP;  
'EXTERNAL';
```

```
'PROCEDURE' STRAPP(A, N, S);  
'ARRAY' A;  
'INTEGER' N;  
'STRING' S;  
'EXTERNAL';
```

```
'PROCEDURE' HCPLOCVIS(X,Y,PCD,NO,S,THETA,MIN,MAX);  
'REAL' X,Y,S,THETA;  
'INTEGER' NO,MIN,MAX;  
'ARRAY' PCD;  
'EXTERNAL';
```

```
'PROCEDURE' HCPSYMBL(X,Y,HT,PCD,TH,N);  
'VALUE' X,Y,HT,TH,N;  
'ARRAY' PCD;  
'REAL' X,Y,HT,TH;  
'INTEGER' N;  
'EXTERNAL';
```

```
'PROCEDURE' HCPWHDR(X,Y);  
'REAL' X,Y;  
'EXTERNAL';
```

```
'PROCEDURE' PLOTROSS(X,Y,SIZE);  
'REAL' X,Y,SIZE;  
'BEGIN'  
  'REAL' S;  
  S:=SIZE/2.0;  
  
  HCPLOT(X,Y,3,0);  
  
  HCPLOT(X+S,Y,2,0);  
  
  HCPLOT(X-S,Y,1,0);  
  
  HCPLOT(X,Y,1,0);  
  
  HCPLOT(X,Y+S,1,0);  
  
  HCPLOT(X,Y-S,1,0);  
  
  HCPLOT(X,Y,1,0);  
  
'END';
```

```
'PROCEDURE' PLOTORF(X,Y,SIZE);  
'REAL' X,Y,SIZE;  
'BEGIN'  
  'REAL' S;  
  S:=SIZE/2.0;  
  
  HCPLOT(X,Y,3,0);  
  
  HCPLOT(X,Y+S,2,0);  
  
  HCPLOT(X-S,Y,1,0);  
  
  HCPLOT(X,Y-S,1,0);  
  
  HCPLOT(X+S,Y,1,0);  
  
  HCPLOT(X,Y+S,1,0);  
  
'END';
```

'END';

'PROCEDURE' PLOTSQUARE(X,Y,SIZE);

'REAL' X,Y,SIZE;

'BEGIN'

REAL S;

S:=SIZE/2.0;

HGPLOT(X,Y,3,0);

HGPLOT(X,Y+S,2,0);

HGPLOT(X-S,Y+S,1,0);

HGPLOT(X-S,Y-S,1,0);

HGPLOT(X+S,Y-S,1,0);

HGPLOT(X+S,Y+S,1,0);

HGPLOT(X,Y+S,1,0);

'END';

'PROCEDURE' PLOTBULK;

'BEGIN'

J3:=J3+1;

HGPLOCAXIS(0.0,0.0,FR,-J1,9.0,0.0,1,4);

HGPAXISV(0.0,0.0,AM,J2,4.0,90.0,0.0,0.0,0.5,2);

HGPLOCAXIS(0.0,-10.0,FR,-J1,9.0,0.0,1,4);

HGPAXISV(0.0,-10.0,BA,J7,4.0,90.0,-20.0,4.0,0.5,2);

PLOTROSS(6.0,4.0,0.100);

PLOTROMB(6.0,3.6,0.110);

PLOTSQUARE(6.0,3.2,0.100);

PLOTROSS(6.0,-6.0,0.100);

PLOTROMB(6.0,-6.4,0.110);

PLOTSQUARE(6.0,-6.8,0.100);

STRAFF(TEXT1,J4,('FIRST HARMONIC'));

STRAFF(TEXT2,J5,('THIRD HARMONIC'));

STRAFF(TEXT3,J6,('FIFTH HARMONIC'));

STRAFF(TEXT4,J8,('EXPERIMENTAL TRANSFER FUNCTION'));

HGPSYMBL(0.75,5.0,0.3,TEXT4,0.0,J8);

HGPSYMBL(6.25,3.9,0.2,TEXT1,0.0,J4);

```
HGRSYMBL(6.25,3.5,0.2,TEXT0,0.0,15);  
HGRSYMBL(6.25,3.1,0.2,TEXT3,0.0,16);  
HGRSYMBL(0.75,-5.0,0.2,TEXT4,0.0,17);  
HGRSYMBL(6.25,-6.1,0.2,TEXT1,0.0,14);  
HGRSYMBL(6.25,-6.5,0.2,TEXT2,0.0,15);  
HGRSYMBL(6.25,-6.9,0.2,TEXT3,0.0,16);  
  
'END' OF PROCEDURE PLOTBULK;
```

```
DETNUM:=READ;  
PLOT:=READ;  
PRIN:=READ;  
M:=READ;  
N:=READ;  
L:=READ;  
YKIN:=0.0;  
NG:=1;  
NNE:=00;  
NXE1:=00;  
'IF' DETNUM 'EQ' 2 'THEN'  
NYE:=25  
'ELSE'  
NYE:=50;  
LOC:=LN(10);  
J1:=14;  
J2:=17;  
J3:=0;  
J4:=15;  
J5:=15;  
J6:=15;  
J7:=15;  
J8:=30;  
J9:=10;  
J10:=10;  
'IF' PLOT 'EQ' 0 'THEN'  
'GOTO' LEVEL1;  
  
OPENPLOT;  
  
HGPlot(-5.0,10.0,0,4);  
  
STPAR(08,J1,('FREQUENCY(HZ)'));  
STPAR(09,J2,('AMPLITUDEDEPTH(L)'));  
STPAR(0A,J7,('GAIN(DBS)'));  
  
LEVEL1:
```

```
T1:=READ;  
'IF' T1 'GT' 0 'THEN'  
INDEX1:=READ;  
T2:=READ;  
'IF' T2 'LT' 0 'THEN' 'GOTO' FIN;  
NUMBER:=READ;  
FREQ:=READ;
```

```
TINCHAN:=TO/NUMBER;
'IF 'DETNUM 'EQ' 2 'THEN'
TINCHAN:=TINCHAN/2;
'BEGIN'
'REAL' 'ARRAY' BACK, THREE: W3;
'REAL' 'ARRAY' BACK1, BACK2, TEXT1, TEXT2: (N+1)/2-1;
'REAL' 'ARRAY' CONV1, CONV11, CONV111: NUMBER-1;
'REAL' 'ARRAY' A, P0: NUMBER/2;
'IF 'T1 'LT' 0 'THEN'
'GOTO' LEVEL3;
'IF 'PLOT 'EQ' 0 'THEN'
'GOTO' LEVEL2;
'IF 'J3 'EQ' 0 'THEN'
'GOTO' LEVEL2;
'ELSE'
'BEGIN'
HCPLOT(0.0,0.0,3,0);
'IF 'DETNUM 'EQ' 2 'THEN'
HCPLOT(-26.0,0.0,0,4)
'ELSE'
HCPLOT(-15.0,0.0,0,4);
'END';
LEVEL2:
'IF 'PLOT 'EQ' 0 'THEN'
'GOTO' P1;
PLOTBULK;
'IF 'DETNUM 'EQ' 2 'THEN'
'BEGIN'
STABR(TEXT5,J9,('DETECTOR 74'));
HGPSYMP(0.75,4.3,0.25,TEXT5,0.0,J9);
HGPSYMP(0.75,-5.7,0.25,TEXT5,0.0,J9);
'END';
P1:
'FOR' I:=1 'STEP' 1 'UNTIL' N 'DO' BACK(I):=READ;
PAPERTRFL;
'IF 'DETNUM 'EQ' 2 'THEN'
'BEGIN'
BACKORDER(BACK1,BACK2,BACK);
K:=0;
BACKGROUP(BACK1);
K:=K+1;
BACKGROUP(BACK2);
'END'
```

```
'ELSE'  
PACKORDER(PACK);  
LEVEL3:  
  'IF'DETNUM'EQ'2'THEN'  
  Q:=DEP2:=FRAD;  
  'FOR'I:=1'STEP'1'UNTIL'N'DO'TRUEC1:=FRAD;  
  YMAX:=TRUEC1;  
  'FOR'I:=N+1'STEP'1'UNTIL'N'DO'  
  'BEGIN'  
    P:=YMAX-TRUEC1;  
    'IF'P'LE'0'THEN'  
    YMAX:=TRUEC1;  
  'END';  
  P:=(YMAX+100)/'100*100;  
  YMAX:=P;  
  NEWLINE(1);  
  SPACE(10);  
  WRITETEXT('('THEZFOLLOWINGZVALUESZCORRESPONDZTOZTHEZFROUGH  
  ZDATA')');  
  NEWLINE(1);  
  SPACE(10);  
  WRITETEXT('('FREQUENCYZZZ=')');  
  PRINT(CNFCQ,4,0);  
  WRITETEXT('('FMTZ')');  
  NEWLINE(1);  
  SPACE(10);  
  WRITETEXT('('CHANNEL')');  
  NEWLINE(1);  
  SPACE(10);  
  WRITETEXT('('NUMBER')');  
  'IF'DETNUM'EQ'2'THEN'  
  'BEGIN'  
  SPACE(30);  
  WRITETEXT('('DETECTORZA')');  
  DATAORDER(TRUE1,TRUE2,TRUE);  
  NEWLINE(1);  
  'FOR'I:=1'STEP'10'UNTIL'(M+N+1)/2-1'DO'  
  'BEGIN'  
    NEWLINE(1);  
    SPACE(12);  
    PRINT(I,3,0);  
    'FOR'J:=1'STEP'1'UNTIL'I+9'DO'  
    PRINT(TRUE1[J],6,0);  
  'END';  
  NEWLINE(2);  
  SPACE(46);  
  WRITETEXT('('DETECTORZB')');  
  NEWLINE(1);  
  'FOR'I:=1'STEP'10'UNTIL'(M+N+1)/2-1'DO'  
  'BEGIN'  
    NEWLINE(1);  
    SPACE(10);  
    PRINT(I+(M+N+1)/2,3,0);  
    'FOR'J:=1'STEP'1'UNTIL'I+9'DO'  
    PRINT(TRUE2[J],6,0);  
  'END';
```

```
'IF'PLOT'EQ'0'THEN'  
'GOTO'P2;  
PAGE'END';  
SPACE(50);  
WRITETEXT('('-----DETECTORZA-----')');  
NEWLINE(2);  
'FOR'1:=0'STEP'1'UNTIL'79'DO'  
'BEGIN'  
    DATA1(I+1):=TIME1(I);  
    DATA2(I+1):=TIME2(I);  
'END';
```

```
LINEPRINT(DATA1);
```

```
YMAX:=YMAX-STEP;  
NEWLINE(2);  
SPACE(50);  
WRITETEXT('('-----DETECTORZB-----')');  
NEWLINE(2);
```

```
LINEPRINT(DATA2);
```

P2:

```
PAGE'END';  
WRITETEXT('('DETECTORZA')');  
NEWLINE(1);
```

```
ADVANCE(TIME1,CONVAL);
```

```
TABULATE(CONVAL);
```

```
NEWLINE(2);  
WRITETEXT('('THEY FOLLOWING VALUES HAVE BEEN CORRECTED FOR  
DRAUGHT TIME AND CORRECT TRANSFER TIME')');
```

```
CORRECT(CONVAL,CONVAL1,CONVAL2);
```

```
'FOR'1:=0'STEP'1'UNTIL'NUMBER-1'DO'  
CONVAL1(I):=CONVAL2(I);
```

```
TABULATE(CONVAL);
```

```
NEWLINE(2);  
WRITETEXT('('BACKGROUND HAS BEEN SUBTRACTED')');
```

```
'FOR'1:=0'STEP'1'UNTIL'NUMBER-1'DO'  
CONVAL1(I):=CONVAL1(I)-(CONIBACK1/60);
```

```
TABULATE(CONVAL);
```

```
AVERAGE(CONVAL);
```

```
AVERHEAD;
```

```
FOUR HEAD;
```

```
FOUR IPT (CONVAL,CONVAL,1,1);
```

```
FOUR PRINT(A,P);  
'IF'PLOT'EQ'0'THEN'  
'GOTO'P2;
```

```
HCPLLOT(0.0,0.0,3,0);
HCPLLOT(-11.0,0.0,0,4);
'IF'T1'GT'0'THEN'
PLOTBULK;
  STRAFF(TEXT6,J10,('DETECTONZE')));
  HCPSYMBL(0.75,4.3,0.25,TEXT6,0.0,J10);
  HCPSYMBL(0.75,-5.7,0.25,TEXT6,0.0,J10);
```

P3:

```
PAPERTRHEAD;
WRITETEXT('('DETECTONZE')));
NEELINE(1);
ARRANGE(TRUE2,CONVAL);
TABULATE(CONVAL);
WRITETEXT('('THEFOLLOINGIVALUESHAVERBEENCORRECTED
FORZDRADTIMEANDZKROLYTTRANSFERTIME')));
CORRECT(CONVAL,CONVAL1,CONVAL2);
'FOR'I:=0'STEP'1'UNTIL'NUMBER-1'DO'
CONVAL1I:=CONVAL2II);
TABULATE(CONVAL);
NEELINE(2);
WRITETEXT('('BACKGROUNDZHASZBEENSUBTRACTED')));
NEELINE(2);
'FOR'I:=0'STEP'1'UNTIL'NUMBER-1'DO'
CONVAL1I:=CONVAL1I-(CONIRACK2/60);
TABULATE(CONVAL);
AVERAGE(CONVAL);
AVGZHEAD;
FOURZHEAD;
FOURPIER(NUMBER,CONVAL,A,B);
FOUREXIT(A,B);
'IF'PLOT'EQ'0'THEN'
'GOTO'P4;
HCPLLOT(0.0,0.0,3,0);
HCPLLOT(11.0,0.0,0,4);
```

P4:

```
'END'
'ELSE'
```

```
'BEGIN'  
NEWLINE(1);  
'FOR' 'I':=0 'STEP' '10' 'UNTIL' 'N' 'DO'  
'BEGIN'  
  NEWLINE(1);  
  SPACE(10);  
  PRINT(1,3,0);  
  'FOR' 'J':=1 'STEP' '1' 'UNTIL' 'I+9' 'DO'  
  PRINT(TRUEIJJ,6,0);  
'END';  
NEWLINE(1);  
'FOR' 'I':=0 'STEP' '1' 'UNTIL' 'NUMBER-1' 'DO'  
CONVAL(11)=0;  
'FOR' 'I':=0 'STEP' '1' 'UNTIL' 'NUMBER-1' 'DO'  
'FOR' 'J':=1 'STEP' 'NUMBER' 'UNTIL' 'N' 'DO'  
CONVAL(11)=CONVAL(11)+TRUEIJJ;  
'IF' 'PRINT' 'P0' '0' 'THEN'  
'GOTO' 'P5';  
PARENTHESIS;  
'FOR' 'I':=K 'STEP' 'L' 'UNTIL' '79' 'DO'  
DATA(1+11)=TRUEI11;  
NEWLINE(4);
```

LINEFFIN(DATA);

P5:

```
PARENTHESIS;  
'FOR' 'I':=0 'STEP' '1' 'UNTIL' 'NUMBER-1' 'DO'  
CONVAL(11)=CONVAL(11)/TIMCHAN;  
WRITETEXT(' (' 'THE' 'FOLLOWING' 'VALUES' 'CORRESPOND' 'TO' 'EACH' 'CHA'  
NNGLE' 'CONTENT' 'Z' 'FOR' 'ONE' 'CYCLE' 'AND' 'PER' 'SECOND' ') ');  
NEWLINE(2);  
WRITETEXT(' (' 'TOTAL' 'XMAS' 'EXPERIMENT' 'TIME' 'Z' '=' ') ');  
PRINT(T9,3,2);  
WRITETEXT(' (' 'MIN. ') ');  
NEWLINE(2);  
'FOR' 'I':=0 'STEP' '1' 'UNTIL' 'NUMBER-1' 'DO'  
CONVAL(11)=CONVAL(11)/60;
```

TABULATE(CONVAL);

CORRECT(CONVAL,CONVAL1,CONVAL2);

```
'FOR' 'I':=0 'STEP' '1' 'UNTIL' 'NUMBER-1' 'DO'  
CONVAL(11)=CONVAL(11)-(UNIBACK/60);  
NEWLINE(3);  
WRITETEXT(' (' 'THE' 'FOLLOWING' 'VALUES' 'HAVE' 'BEEN' 'CORRECTED'  
FOR' 'DRAG' 'TIME' 'Z' 'AND' 'THE' 'NO' 'Z' 'TRANSFER' 'TIME' ') ');  
NEWLINE(2);  
WRITETEXT(' (' 'BACK' 'GROUND' 'HAS' 'BEEN' 'SUBTRACTED' ') ');  
NEWLINE(2);
```

TABULATE(CONVAL);

AUTOPRINT(CONVAL);

AVENHEAD;

FINISHHEAD;

```

FOURIER(NUMBER, CONVAL, A, B);
FOURMIT(A, B);
'END';
'END';
PAPERTHRO3;
'GOTO' LEVEL1;
FIN;

'IF' PLOT' NE' 0' THEN'
CLOSEPLOT;

'END';

```

2.- INPUT EXAMPLE:

```

2
1
1
0
399
1
20
12
3
40
250
229 214 186 226 201 204 220 216 196 215
201 194 228 183 216 194 191 211 205 181
200 218 216 196 202 203 189 209 183 210
244 198 222 179 246 227 209 204 194 193
199 230 179 201 195 226 196 202 204 195
202 189 200 219 203 220 220 204 205 206
...
...
UP TO 400 VALUES
...
12
16900 13452 09856 07366 05375 04122 03393 02623 02240 01888
01689 01509 01300 01136 01102 01040 00933 00881 00850 00813
01975 07006 11560 14254 15906 16923 17140 17623 17792 17949
17856 17653 17207 17387 17879 18001 17961 17803 18143 18150
16833 13197 09315 07242 05367 04227 03300 02626 02235 01830
01645 01435 01337 01269 01084 01037 00900 00934 00902 00805
02069 06309 11510 14143 16000 16752 17167 17467 17637 17725
..
..
UP TO 400 VALUES
..
-1
-1
****

```

3-LINEPRINTER OUTPUT EXAMPLE

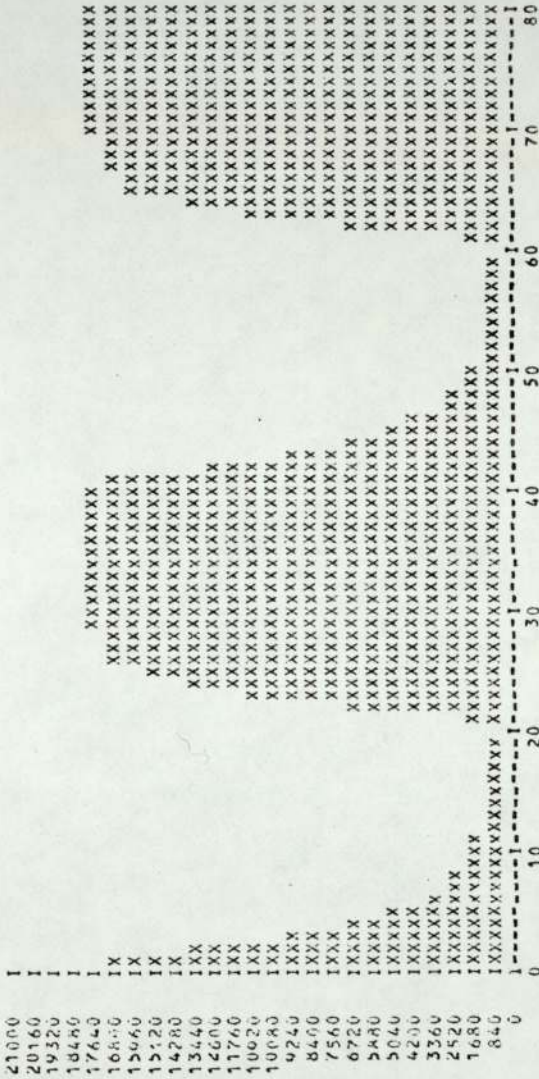
BACKGROUND CORRESPONDENT TO DETECTOR A  
 BACKGROUND TIME = 10.00 MINS.  
 TOTAL BACKGROUND = 41155.00  
 BACKGROUND PER MINUTE = 4115.50

BACKGROUND CORRESPONDENT TO DETECTOR B  
 BACKGROUND TIME = 10.00 MINS.  
 TOTAL BACKGROUND = 44070.00  
 BACKGROUND PER MINUTE = 4407.00

THE FOLLOWING VALUES CORRESPOND TO THE ROUGH DATA  
 FREQUENCY = 250.00 HTZ

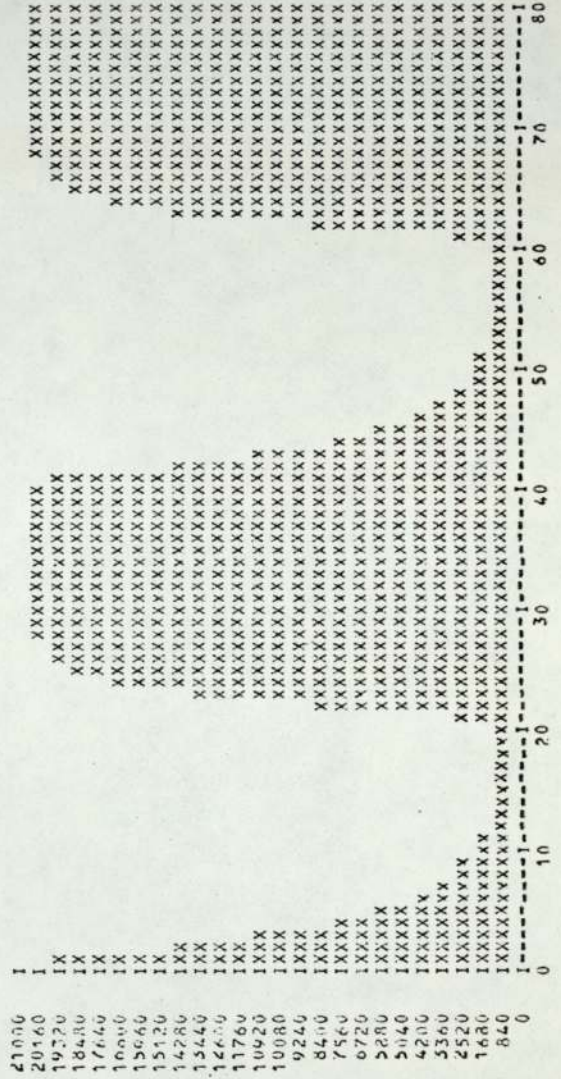
CHANNEL NUMBER	DETECTOR A										DETECTOR B																													
	0	10	20	30	40	50	60	70	80	90	100	110	120	130	140	150	160	170	180	190	200	210	220	230	240	250	260	270	280	290	300	310	320	330	340	350	360	370	380	390
	16910	15453	9856	7366	5375	4122	3328	2628	2240	1888	16910	15453	9856	7366	5375	4122	3328	2628	2240	1888	16910	15453	9856	7366	5375	4122	3328	2628	2240	1888	16910	15453	9856	7366	5375	4122	3328	2628	2240	1888
	1689	1500	1300	1136	1102	1040	933	881	858	813	1689	1500	1300	1136	1102	1040	933	881	858	813	1689	1500	1300	1136	1102	1040	933	881	858	813	1689	1500	1300	1136	1102	1040	933	881	858	813
	1975	7006	11560	14254	15006	16928	17140	17628	17702	17949	1975	7006	11560	14254	15006	16928	17140	17628	17702	17949	1975	7006	11560	14254	15006	16928	17140	17628	17702	17949	1975	7006	11560	14254	15006	16928	17140	17628	17702	17949
	17856	17653	17907	17887	17879	18001	17901	17808	18143	18150	17856	17653	17907	17887	17879	18001	17901	17808	18143	18150	17856	17653	17907	17887	17879	18001	17901	17808	18143	18150	17856	17653	17907	17887	17879	18001	17901	17808	18143	18150
	16053	13197	9815	7243	5367	4227	3300	2696	2235	1830	16053	13197	9815	7243	5367	4227	3300	2696	2235	1830	16053	13197	9815	7243	5367	4227	3300	2696	2235	1830	16053	13197	9815	7243	5367	4227	3300	2696	2235	1830
	1645	1435	1337	1269	1084	1037	900	934	902	805	1645	1435	1337	1269	1084	1037	900	934	902	805	1645	1435	1337	1269	1084	1037	900	934	902	805	1645	1435	1337	1269	1084	1037	900	934	902	805
	2066	6890	11510	14143	16090	16752	17167	17467	17637	17725	2066	6890	11510	14143	16090	16752	17167	17467	17637	17725	2066	6890	11510	14143	16090	16752	17167	17467	17637	17725	2066	6890	11510	14143	16090	16752	17167	17467	17637	17725
	17750	17741	17798	18109	17945	18102	18142	18034	17893	18214	17750	17741	17798	18109	17945	18102	18142	18034	17893	18214	17750	17741	17798	18109	17945	18102	18142	18034	17893	18214	17750	17741	17798	18109	17945	18102	18142	18034	17893	18214
	17049	13234	9979	7334	5552	4217	3317	2634	2311	1981	17049	13234	9979	7334	5552	4217	3317	2634	2311	1981	17049	13234	9979	7334	5552	4217	3317	2634	2311	1981	17049	13234	9979	7334	5552	4217	3317	2634	2311	1981
	1641	1533	1337	1171	1044	1051	986	949	902	834	1641	1533	1337	1171	1044	1051	986	949	902	834	1641	1533	1337	1171	1044	1051	986	949	902	834	1641	1533	1337	1171	1044	1051	986	949	902	834
	2101	7005	11379	14125	15943	16731	17241	17752	17777	17970	2101	7005	11379	14125	15943	16731	17241	17752	17777	17970	2101	7005	11379	14125	15943	16731	17241	17752	17777	17970	2101	7005	11379	14125	15943	16731	17241	17752	17777	17970
	17440	17783	17998	17967	17778	17945	17997	18033	17734	17934	17440	17783	17998	17967	17778	17945	17997	18033	17734	17934	17440	17783	17998	17967	17778	17945	17997	18033	17734	17934	17440	17783	17998	17967	17778	17945	17997	18033	17734	17934
	16300	13370	9917	7170	5546	4167	3335	2644	2193	1852	16300	13370	9917	7170	5546	4167	3335	2644	2193	1852	16300	13370	9917	7170	5546	4167	3335	2644	2193	1852	16300	13370	9917	7170	5546	4167	3335	2644	2193	1852
	1626	1413	1319	1211	1140	960	964	931	907	871	1626	1413	1319	1211	1140	960	964	931	907	871	1626	1413	1319	1211	1140	960	964	931	907	871	1626	1413	1319	1211	1140	960	964	931	907	871
	2150	6963	11514	14261	16050	16628	17268	17583	17583	17803	2150	6963	11514	14261	16050	16628	17268	17583	17583	17803	2150	6963	11514	14261	16050	16628	17268	17583	17583	17803	2150	6963	11514	14261	16050	16628	17268	17583	17583	17803
	17657	17830	17890	17886	17836	17907	17741	17890	18273	18162	17657	17830	17890	17886	17836	17907	17741	17890	18273	18162	17657	17830	17890	17886	17836	17907	17741	17890	18273	18162	17657	17830	17890	17886	17836	17907	17741	17890	18273	18162
	17005	13230	9764	7389	5450	4211	3253	2643	2279	1890	17005	13230	9764	7389	5450	4211	3253	2643	2279	1890	17005	13230	9764	7389	5450	4211	3253	2643	2279	1890	17005	13230	9764	7389	5450	4211	3253	2643	2279	1890
	1587	1414	1304	1222	1069	1033	951	890	868	833	1587	1414	1304	1222	1069	1033	951	890	868	833	1587	1414	1304	1222	1069	1033	951	890	868	833	1587	1414	1304	1222	1069	1033	951	890	868	833
	2028	6936	11354	14174	16189	16678	17090	17581	17591	17797	2028	6936	11354	14174	16189	16678	17090	17581	17591	17797	2028	6936	11354	14174	16189	16678	17090	17581	17591	17797	2028	6936	11354	14174	16189	16678	17090	17581	17591	17797
	17648	17788	17900	17790	18005	17917	18002	17982	17936	18217	17648	17788	17900	17790	18005	17917	18002	17982	17936	18217	17648	17788	17900	17790	18005	17917	18002	17982	17936	18217	17648	17788	17900	17790	18005	17917	18002	17982	17936	18217
	19491	14931	11127	8180	5963	4745	3733	2975	2540	2085	19491	14931	11127	8180	5963	4745	3733	2975	2540	2085	19491	14931	11127	8180	5963	4745	3733	2975	2540	2085	19491	14931	11127	8180	5963	4745	3733	2975	2540	2085
	1626	1552	1399	1319	1245	1139	1046	1052	1073	1067	1626	1552	1399	1319	1245	1139	1046	1052	1073	1067	1626	1552	1399	1319	1245	1139	1046	1052	1073	1067	1626	1552	1399	1319	1245	1139	1046	1052	1073	1067
	2536	8835	14269	17258	18830	19644	20115	20329	20461	20789	2536	8835	14269	17258	18830	19644	20115	20329	20461	20789	2536	8835	14269	17258	18830	19644	20115	20329	20461	20789	2536	8835	14269	17258	18830	19644	20115	20329	20461	20789
	20638	20684	20719	20495	20630	20841	20845	20716	20856	20927	20638	20684	20719	20495	20630	20841	20845	20716	20856	20927	20638	20684	20719	20495	20630	20841	20845	20716	20856	20927	20638	20684	20719	20495	20630	20841	20845	20716	20856	
	19357	14850	11058	8158	6034	4806	3705	2909	2457	2151	19357	14850	11058	8158	6034	4806	3705	2909	2457	2151	19357	14850	11058	8158	6034	4806	3705	2909	2457	2151	19357	14850	11058	8158	6034	4806	3705	2909	2457	2151
	1836	1645	1439	1332	1241	1087	1104	1053	917	946	1836	1645	1439	1332	1241	1087	1104	1053	917	946	1836	1645	1439	1332	1241	1087	1104	1053	917	946	1836	1645	1439	1332	1241	1087	1104	1053	917	946
	2602	8742	14330	17070	18968	19588	20157	20468	20357	20410	2602	8742	14330	17070	18968	19588	20157	20468	20357	20410	2602	8742	14330	17070	18968	19588	20157	20468	20357	20410	2602	8742	14330	17070	18968	19588	20157	20468	20357	20410
	20683	20779	20566	20968	20539	20629	20914	20833	20664	20948	20683	20779	20566	20968	20539	20629	20914	20833	20664	20948	20683	20779	20566	20968	20539	20629	20914	20833	20664	20948	20683	20779	20566	20968	20539	20629	20914	20833	20664	20948
	19275	15112	10995	8052	6061	4621	3725	2974	2332	2079	19275	15112	10995	8052	6061	4621	3725	2974	2332	2079	19275	15112	10995	8052	6061	4621	3725	2974	2332	2079	19275	15112	10995	8052	6061	4621	3725	2974	2332	2079
	1767	1584	1453	1266	1230	1170	979	982	967	924	1767	1584	1453	1266	1230	1170	979	982	967	924	1767	1584	1453	1266	1230	1170	979	982	967	924	1767	1584	1453	1266	1230	1170	979	982	967	924

-----DETECTOR A-----



CHANNEL NUMBER

-----DETECTOR B-----



CHANNEL NUMBER

DETECTOR A  
 THE FOLLOWING VALUES CORRESPOND TO EACH CHANNEL CONTENT FOR ONE CYCLE AND PER SECOND  
 TOTAL MEASUREMENT TIME = 1.50 MINS.

CHANNEL NUMBER	29548.44	21924.89	16223.11	12128.80	9308.44	7348.00	5895.56	5003.56	4196.00
0	37594.22	29548.44	21924.89	16223.11	12128.80	9308.44	7348.00	5895.56	4196.00
10	3639.11	3246.22	2932.00	2417.33	2276.00	2104.00	2055.56	1972.00	1847.11
20	4579.11	15470.67	25475.11	35634.67	37207.56	38180.44	39115.56	39284.44	39664.00
30	39569.33	39464.44	39774.67	39752.44	39943.11	39903.56	39909.78	39990.67	40300.89

THE FOLLOWING VALUES HAVE BEEN CORRECTED FOR DEAD TIME AND MEMORY TRANSFER TIME

CHANNEL NUMBER	40005.94	31029.09	22735.22	16664.77	12374.95	9453.04	7437.96	5953.40	4225.26
0	40005.94	31029.09	22735.22	16664.77	12374.95	9453.04	7437.96	5953.40	4225.26
10	3661.11	3263.72	2946.27	2682.51	2427.03	2284.60	2111.34	2062.57	1852.77
20	4613.97	15872.07	26572.18	33225.64	37798.76	39569.22	40669.08	41729.46	42352.85
30	42245.17	42125.90	42478.77	42502.03	42453.48	42670.51	42625.48	42632.56	43078.13

BACKGROUND HAS BEEN SUBTRACTED

CHANNEL NUMBER	39937.35	30960.50	22666.63	16596.18	12306.36	9384.45	7369.37	5884.81	4156.67
0	39937.35	30960.50	22666.63	16596.18	12306.36	9384.45	7369.37	5884.81	4156.67
10	3592.52	3195.13	2877.68	2613.91	2358.44	2216.00	2042.75	1993.97	1784.18
20	4545.38	15803.48	26503.58	33137.05	37729.67	39500.63	40600.49	41660.87	42284.25
30	42176.57	42037.30	42410.17	42433.44	42384.89	42601.92	42356.89	42563.97	43009.54

AVERAGE VALUE PER CYCLE PER SECOND = 23182.81  
 AVERAGE MAXIMUM VALUE = 39951.89  
 AMPLITUDE=(MAX-AVFR)/AVER = 0.723

\*\*\*\*FOURIER ANALYSIS\*\*\*\*  
 \*\*\*\*\*

HARMONIC	A	B	AMPLITUDE	H(W)	GAIN(DB)	PHASE
0	46365.61	0.00	46365.61	0.81134	-1.816	2.770
1	5690.57	-22315.95	23948.44	0.07849	-22.104	0.065
2	74.92	1155.94	1158.37	0.58275	-4.690	2.291
3	4310.78	-3780.57	5733.71	0.06865	-23.267	-0.775
4	-354.56	361.82	506.58	0.39328	-8.106	2.013
5	2098.28	-993.68	2321.68	0.05395	-25.359	-1.261
6	-252.79	80.94	265.43	0.27729	-11.141	1.851
7	1123.55	-323.68	1169.74			

DETECTOR B  
 THE FOLLOWING VALUES CORRESPOND TO EACH CHANNEL CONTENT FOR ONE CYCLE AND PER SECOND  
 TOTAL MEASUREMENT TIME = 1.50 MINS.

CHANNEL NUMBER	43040.44	33250.67	24540.44	18064.44	13424.00	10420.00	8201.78	6335.56	5374.67	4652.46
0	43040.44	33250.67	24540.44	18064.44	13424.00	10420.00	8201.78	6335.56	5374.67	4652.46
10	4024.44	3537.33	3170.56	2936.00	2728.00	2571.11	2324.00	2310.67	2182.22	2156.89
20	5656.89	15732.44	31655.11	38228.44	41930.56	43637.78	44748.89	45432.44	45603.56	45814.22
30	45791.11	46006.67	45996.44	46200.00	45820.89	46257.33	46163.11	46024.00	46164.00	46344.00

THE FOLLOWING VALUES HAVE BEEN CORRECTED FOR DEAD TIME AND MEMORY TRANSFER TIME

CHANNEL NUMBER	46214.72	35130.99	25557.74	18612.86	13725.73	10601.36	8313.94	6606.68	5422.72	4688.43
0	46214.72	35130.99	25557.74	18612.86	13725.73	10601.36	8313.94	6606.68	5422.72	4688.43
10	4051.36	3558.12	3196.34	2950.31	2740.35	2582.08	2332.96	2319.53	2190.12	2164.61
20	5710.13	20367.68	33357.20	40723.43	44931.00	46902.25	48184.01	48975.77	49174.08	49416.39
30	49391.58	49641.70	49629.84	49866.19	49426.12	49932.78	49823.34	49661.82	49824.38	50033.48

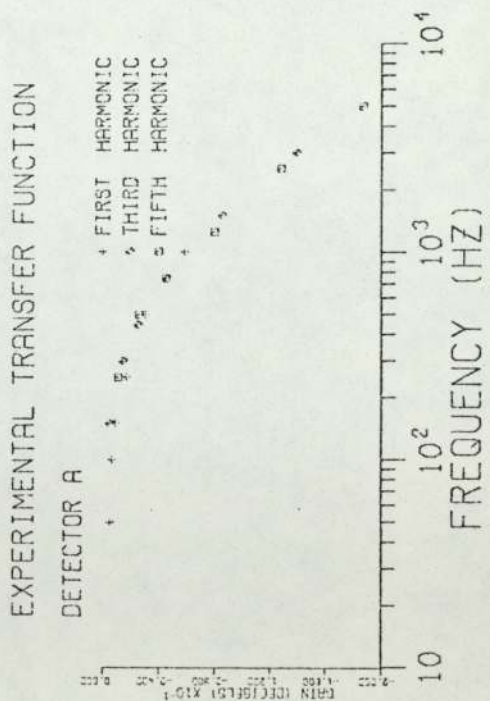
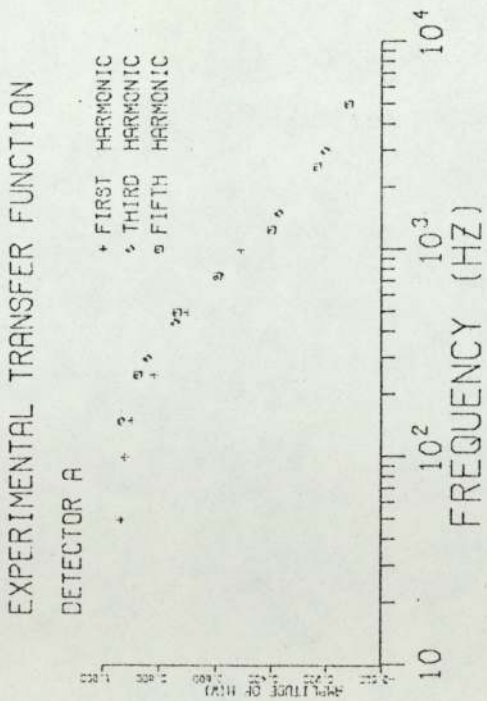
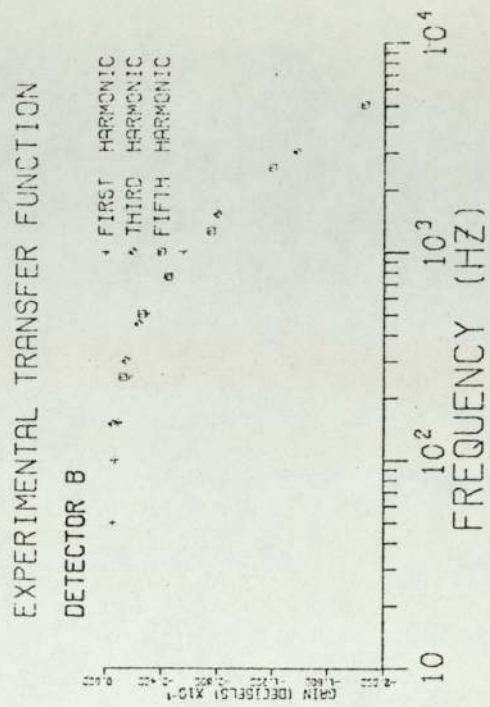
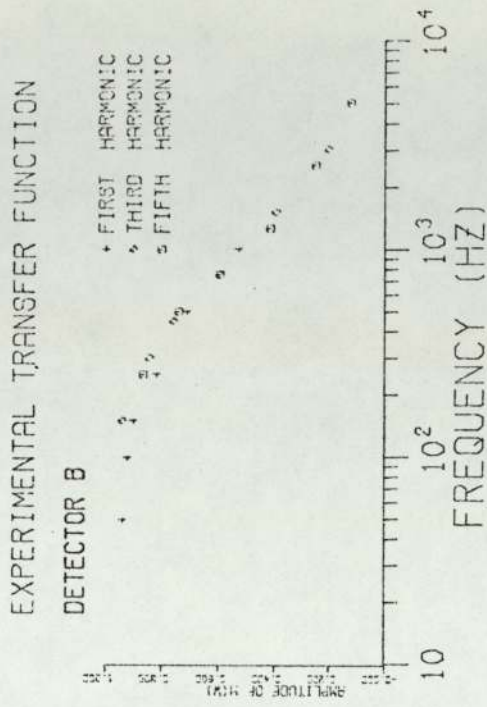
BACKGROUND HAS BEEN SUBTRACTED

CHANNEL NUMBER	40141.27	35057.54	25484.29	18539.41	13652.28	10527.91	8240.49	6533.23	5349.27	4614.98
0	40141.27	35057.54	25484.29	18539.41	13652.28	10527.91	8240.49	6533.23	5349.27	4614.98
10	3977.91	3484.67	3122.89	2876.86	2666.90	2508.63	2259.51	2246.08	2116.67	2091.16
20	5636.68	20314.23	33283.75	40549.98	44877.55	46828.80	48111.16	48902.32	49100.63	49344.94
30	49318.13	49568.25	49556.39	49792.74	49352.67	49859.33	49749.89	49588.37	49750.93	49960.03

AVERAGE VALUE PER CYCLE PER SECOND = 27125.97  
 AVERAGE MAXIMUM VALUE = 46939.73  
 AMPLITUDE=(MAX-AVER)/AVER = 0.730

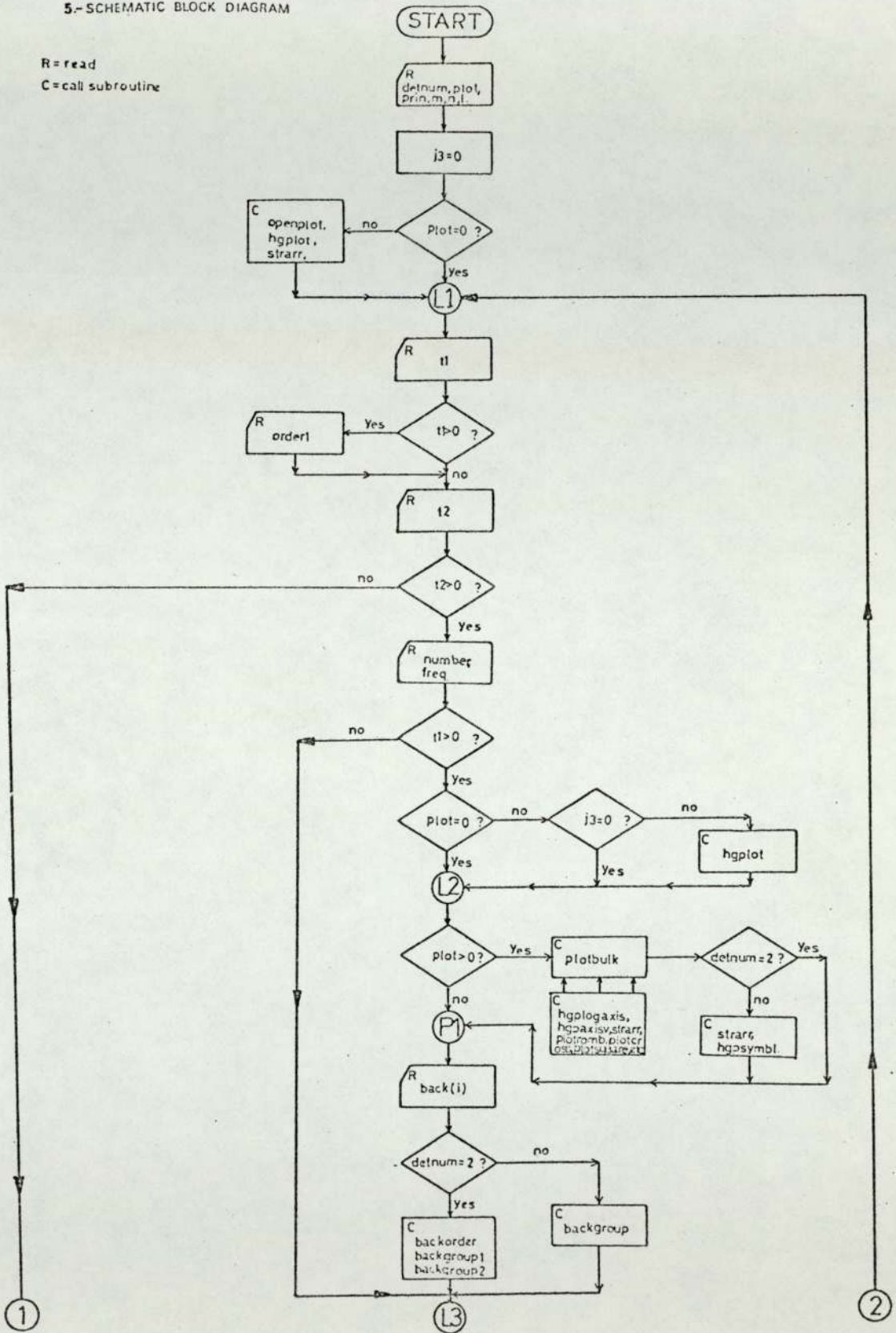
\*\*\*\*FOURIER ANALYSIS\*\*\*\*  
 \*\*\*\*\*

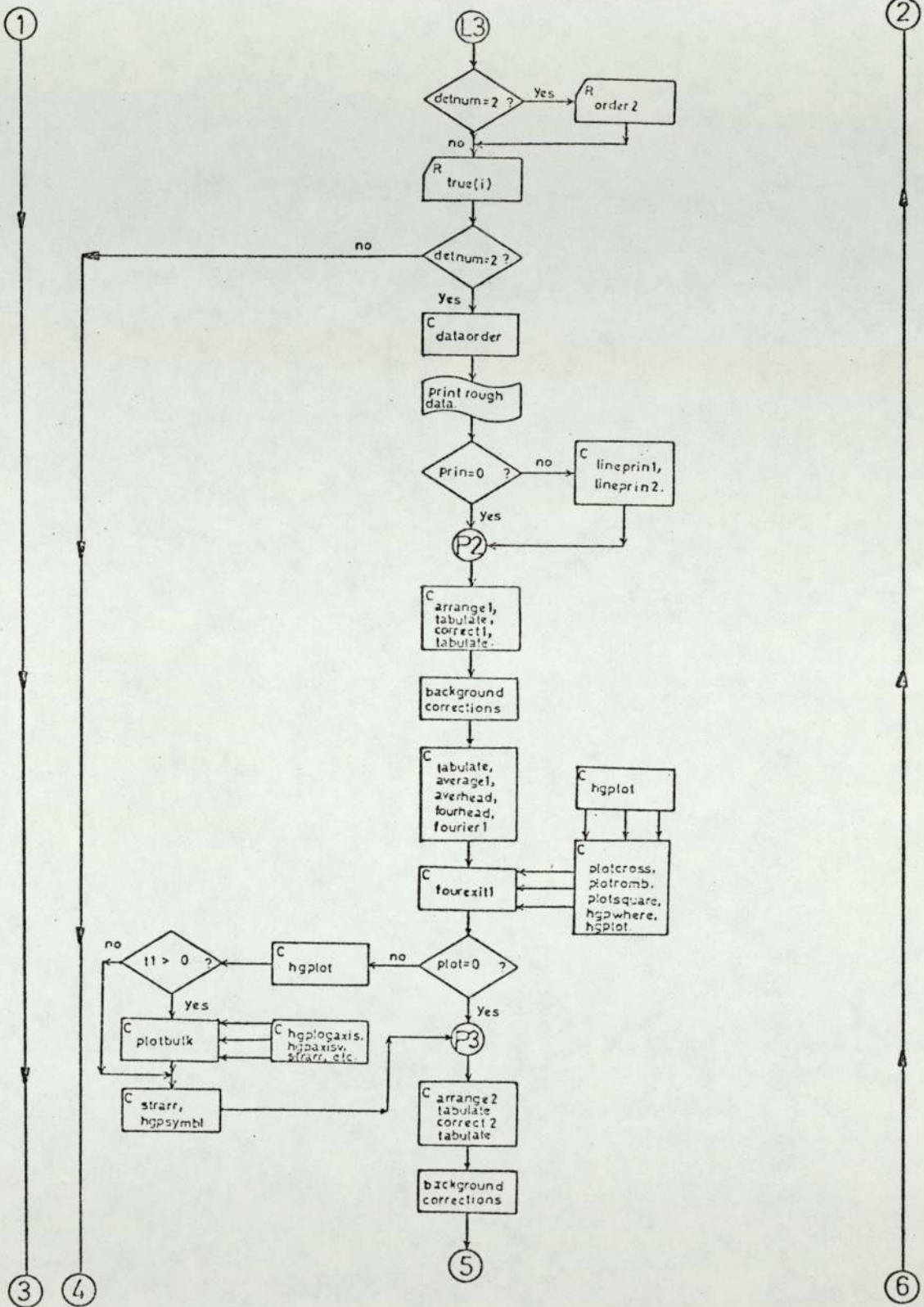
HARMONIC	A	B	AMPLITUDE	H(W)	GAIN(DB)	PHASE
0	54251.93	0.00	54251.93	0.81500	-1.777	2.796
1	9539.77	-26482.35	28148.22	0.08738	-21.171	0.136
2	204.71	1495.06	1509.01	0.59293	-4.540	2.351
3	4852.87	-4800.61	6826.14	0.08556	-21.335	-0.629
4	-434.62	597.40	738.77	0.41544	-7.630	2.094
5	2483.62	-1434.08	2869.65	0.06684	-23.499	-1.109
6	-344.52	171.33	384.77	0.29677	-10.551	1.951
7	1359.93	-542.86	1464.28			

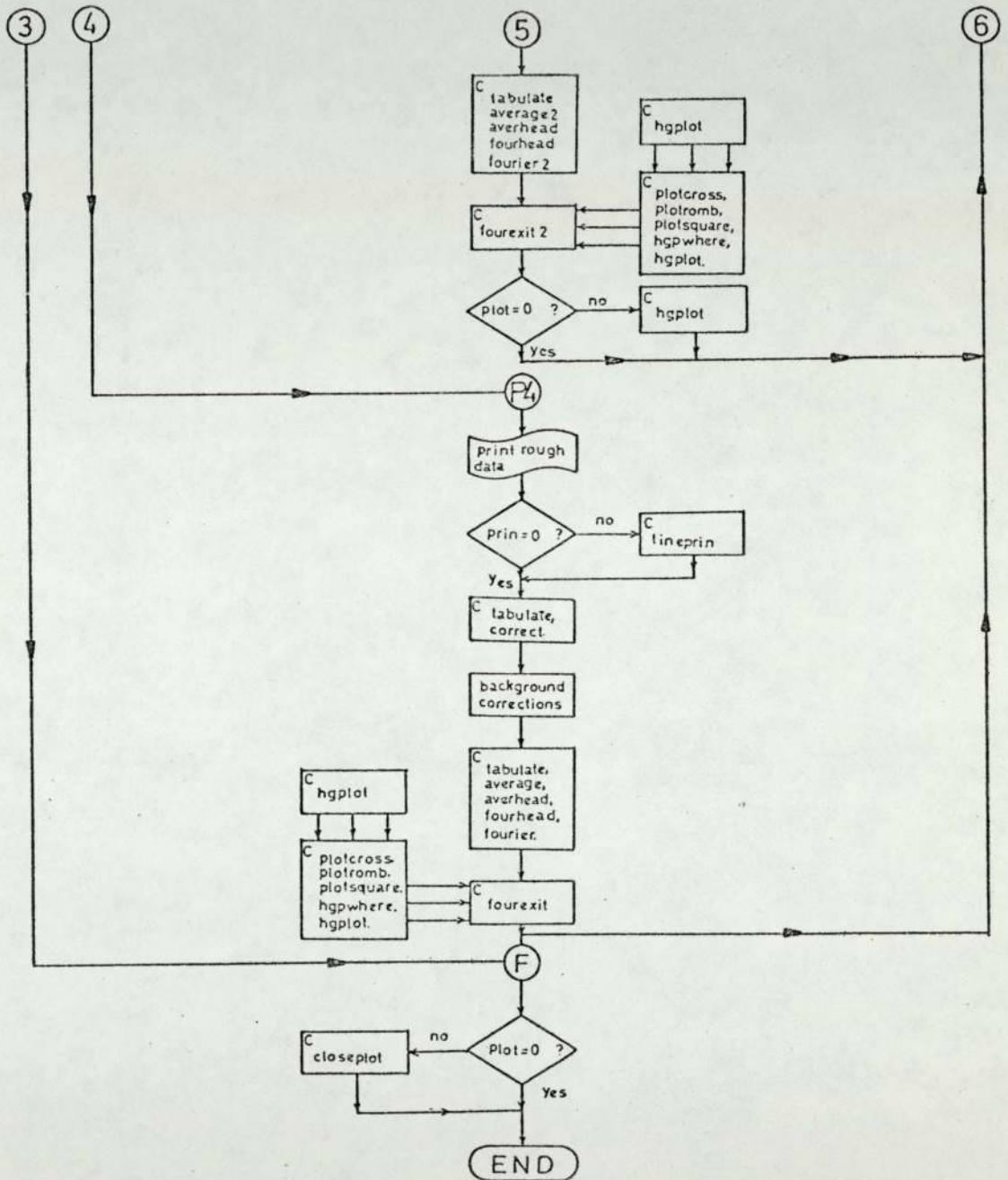


5.-SCHEMATIC BLOCK DIAGRAM

R = read  
C = call subroutine







APPENDIX 3

COMPUTER PROGRAM FERMI

1.- LISTING

```

C
C
C*****
C
C
C      THIS PROGRAM REQUIRES THE FOLLOWING INPUT:
C
C      PLOT CONTROL FOR PLOTTING GRAPH,1 YES,0 NO
C      PEXP CONTROL FOR EXPERIMENTAL COMPARISON,1 YES, 0 NO
C      EXDAT EXPERIMENTAL VALUES FOR COMPARISON, FIXED AT 14
C      NF      MAXIMUM FREQUENCY ,UP TO 5000 HZ.
C      INCR STEP IF INCREMENT IN FREQUENCY
C      R      RADIUS OF THE SYSTEM
C      C      HEIGHT OF THE SYSTEM
C      E      TOTAL ERROR ALLOWED
C      B      BETA
C      T1     TAU
C      R1     RADIAL COORDENATE DETECTOR
C      Z3     AXIAL COORDENATE DETECTOR
C      DL     DIFFUSION LENGHT
C      T      FERMI AGE
C      SL     FAST LIFETIME
C      TL     THERMAL LIFETIME
C      RKF    MULTIPLYING FACTOR
C      EE     ERROR ALLOWED FOR ROOTS OF CHARACTERISTIC EQUATION
C      DFAC   FACTOR IN DR AND DI (INCREMENT FOR CONVERGENCY)
C
C
C*****
C
C
C      INTEGER PLOT,PEXP
C      DIMENSION BE(20),DD(40),BZ(20),DIFER(500)
C      COMMON FR0(500),A1(500),A2(500),THE(500),TH2(500)
C      COMMON EXDAT(14)
C      DATA BE/ .269465,.115804,.073712,.054056,.042642,.035231,
C      1.030033,.026169,.023165,.020794,.01885129,.017241414,.01590121,
C      2.01473796,.01373584,.01285956,.0121,.01140624,.010816,.01026169
C      3/ , BZ/2.4048,5.5201,8.6537,11.7915,14.9309,18.0711,21.2116,
C      424.3525,27.4935,30.6346,33.7758,36.9171,40.0184,43.1998,46.3412,
C      549.4826,52.6241,55.7655,58.9070,62.0485/, J1,J2,J3,J4/1,2,3,4/,
C      6ZLZ,CT,PI2/8.68588964,57.29578,6.28318531/,CFAC/1.0/,J5/0/ ,
C      7CONS/0.707/,11,12,13,14/14,9,29,25/
C      71 FORMAT(F20.0)
C      701 FORMAT(I4)
C      1001 FORMAT(IH1/,110H SPACE-DEPENDENT TRANSFER FUNCTION IN A CYLINDRICAL
C      1L,HOMOGENEOUS AND MULTIPLYING NUCLEAR SYSTEM //,26
C      2H FERMI AGE-DIFFUSION MODEL,/////,32H NUCLEAR SYSTEM CHARACTERISTI
C      3CS:////10X,17HRADIUS SYSTEM = ,F5.2,3HCM,/,//,10X,17HHEIGHT SYSTEM

```

```
4 = ,F5.2,3HCM.,////,10X,22HMULTIPLYING FACTOR = ,F6.4,/,10X,20H
SDIFFUSION LENGTH = ,F6.3,3HCM.,/,10X,13HFERMI AGE = ,F6.2,4HCM2
6.,/,10X,20HTHERMAL LIFETIME = ,F9.6,5HSECS.,/,10X,17HFAST LIFE
TIME = ,F9.6,5HSECS.,/,10X,8HBETA = ,F9.6,/,10X,7HTAU = ,F8.4,
8////,22H NUMERICAL PARAMETERS: ,/,10X,15HTOTAL ERROR = ,F8.5,/,10
9X,54HERROR ALLOWED FOR ROOTS OF CHARACTERISTIC EQUATION = ,F8.5,
1/,10X,42HINCREMENT FOR CONVERGENCY IN DR AND DI = ,F8.5)
1003 FORMAT(1H/,70H THE TRANSFER FUNCTION IS BEING CALCULATED FOR THE
IFOLLOWING POSITION ,/,10X,10HRADIAL = ,F6.3,3HCM.,/,10X,9HAXIAL
2 = ,F6.3,////////,6X,4HFREQ,12X,4HREAL,12X,4HIMAG,13X,3HAMP,14X,2HDB,
315X,5HTHETA,11X,5HTHEIA,6X,5HTERMS)
1004 FORMAT(1H ,7E16.7,F7.0)
1007 FORMAT( 41H0 VALUES OF NCT1, NR, N, R3, S3,
1 ,31HF, RAR3, RA13, ARE ,/,31S, 2E20.8,
2 /,3E20.8 )
1009 FORMAT(1H ,////,27H -3DB POINT CORRESPONDS TO ,F7.3,4H HZ.)
READ(5,701)PLJT,PEXP
IF(PEXP)1111,1111,2222
2222 READ(5,71)(EXDAT(I),I=1,14)
1111 READ(5,701)NF,INCR
READ(5,71) R,C,E,B,T1,RJ, Z3,DL,T,SL,TL,RKF,EE,DFAC
IF(PLJT)5,5,9998
9998 CALL OPENPLJT
5 WRITE(6,1001) R,C,RKF,DL,T,TL,SL,B,T1,E,EE,DFAC
WRITE(6,1003)R,J,Z3
NF=NF/INCR+2
DL2=DL*DL
RJ=RJ/R
SSS=0.
J10=J1
DO 40 I=1,NF
GO TO(4000,4001,4002,4003),J10
4000 FRO(I)=0.0
J10=J2
GO TO 4004
4001 FRO(I)=1.0
J10=J3
GO TO 4004
4002 FRO(I)=INCR
J10=J4
GO TO 4004
4003 FRO(I)=INCR*(I-2)
4004 F=FRO(I)
AN=RN
RC2=SC2
RC4=SC4
NX=0.
NY=0.
W=PI2*F
WS=W*SL
WT=W*TL
S3=0.
R3=0.
S2=0.
R2=0.
S6=0.
R6=0.
AR3=0.
```

```
AS3=0.
AR2=0.
AS2=0.
CL=2.*C
DB=1.-B
TIW=W*T1
TIW2=TIW*TIW
RKD=RKF/(1.+TIW2)
RK=RKD*(1.+TIW2*DB)
SK=RKD*TIW*B
CJU=-1
IF(F)600,600,625
600 IF(NY)605,605,300
605 NY=1
B2S=(2.4/R)**2
TB17=T*B2S
DT17=1.+DL2*B2S
A17=DL2*T
B17=(T*DT17+DL2)/(A17*2.)
C17=(DT17-RKF*EXP(-TB17))/A17
Q17=B17*B17-C17
IF(Q17)10,20,20
10 RC2=B17
GJ TJ 51
20 RC2=B17-SORT(Q17)
51 SC2=0.
CRR=Z3*SORT(RC2)
GJ TJ 300
625 NY=0
300 CONTINUE
DJ 70 N=1,20
B2N=(BZ(N)/R)**2
DLBN=DL2*B2N
TB1=T*B2N
AA=1.
301 CONTINUE
IF(RJ)3,3,2
2 CALL F4J0(BZ(N)*RJ,AA)
3 CONTINUE
CJ1=1.+DLBN
CJ2=AA/BE(N)
NR=0
4 CONTINUE
EF=EE
CALL RJJTS(CJ1,DL2,TB1,T,WS,WT,RK,SK, NR,AD2,BD2,
IAN,BN,EF,CFAC,DFAC,J1,J2,J3,J4,J5)
IF(EF-9.5)302,302,2001
2001 A=0.
XK=0.
GJ TJ 101
302 CONTINUE
RC1=T*AD2-TB1
SC1=T*BD2
CALL CMPLX(J4,RC1,SC1,RC2,SC2,J5,J5)
IF(RK)303,413,303
413 RC3=1.
SC3=0.
GJ TJ 415
```

```
303 CONTINUE
    RC3=DL2+T*(C01-DL2*AD2)
    SC3=T*(WT-DL2*BD2)
415 CONTINUE
    CALL CMPLX(J1,AN,BN,RC3,SC3,RC4,SC4)
    CALL CMPLX(J2,RC2,SC2,RC4,SC4,RC5,SC5)
    RN=RC5*CU2
    SN=SC5*CU2
    M=0
    FM=0.
    NCT=0
    NCT1=0
    GT=0.
505 CONTINUE
    GP1=Z3+GT
    ZFP1=GP1*AN-CRR
    CALL CMPLX(J4,-ZFP1,-GP1*BN,R12,S12,J5,J5)
    IF(M)920,920,905
905 GP1=GT-Z3
    ZFP1=GP1*AN-CRR
    CALL CMPLX(J4,-ZFP1,-GP1*BN,R22,S22,J5,J5)
    PIT=(-1.)**M
    R12=PIT*(R12+R22)
    S12=PIT*(S12+S22)
920 CONTINUE
    CALL CMPLX(J1,RN,SN,R12,S12,DR,DI)
    S3=S3+DI
    R3=R3+DR
    ABJ=ABS(DR)
    ABA=ABS(DI)
    AR3=AR3+ABJ
    AS3=AS3+ABA
    IF(MOD(NR,2))9050,9020,9050
9020 RAR3=1.
    GJ TJ 9100
9050 RAR3=ABJ/AR3
9100 IF(AS3)9200,9010,9200
9010 RAI3=0.
    GJ TJ 405
9200 RAI3=ABA/AS3
405 CJU=CJ+1.
    6 IF(CJU)30,30,9
    9 CONTINUE
    IF(NCT-100)55,55,50
50 NCT=2
    NCT1=NCT1+1
    WRITE(6,1007)NCT1,NR,N,R3,S3,F,RAR3,RAI3
    IF(NCT1-5)55,55,70
55 IF(RAR3-E)56,56,30
56 IF(RAI3-E)57,57,30
57 GJ TJ 65
30 FM=FM+1.
    M=M+1.
    NCT=NCT+1
    GT=CL*FM.
    IF((GT-2.*Z3)*AN-10.)505,65,65
65 IF(RK)201,201,250
201 IF(FM)75,75,70
```

```
250 IF (FM)260,260,4
260 IF (NR-1)75,75,70
70 CONTINUE
75 CONTINUE
   RR5=COS(WS)
   SR5=-SIN(WS)
   CALL CMPLX(CJ1,RR5,SR5,R3,S3,R6,S6)
   IF (F)741,741,742
741 RNF=R6
742 A=R6/RNF
   XK=S6/RNF
101 CONTINUE
   DD(1)=C(J)+1.
   A1(1)=SQRT(A*A+XK*XK)
   IF (I-1)8000,8000,8004
8004 IF (SSS)8003,8003,8000
8003 DIFER(I)=CUNS-A1(I)
   IF (DIFER(I))8000,8001,8001
8001 DBLS=INCR*DIFER(I)/(A1(I-1)-A1(I))+FRQ(I-1)
   SSS=1.0
8000 A2(1)=ZLZ*ALJG(A1(I))
   THE(I)=CT*ATAN(XK/A)
   TH2(I)=180.-THE(I)
   WRITE(6,1004)F,A,XK,A1(I),A2(I),THE(I),TH2(I),DD(I)
40 CONTINUE
   WRITE(6,1009)DBLS
   IF (PLJIT)9997,9997,9996
9996 CALL PLJITER(I1,I2,I3,I4,NF,PEXP)
9997 CONTINUE
   STOP
   END
```

```
      SUBROUTINE CMPLX(NRTL,R1,S1,R2,S2,R3,S3)
      GJ TJ(1,2,3,4),NRTL
1   R3=R1*R2-S1*S2
   S3=R1*S2+R2*S1
   GJ TJ 20
2   DEM=R2*R2+S2*S2
   R3=(R1*R2+S1*S2)/DEM
   S3=(R2*S1-R1*S2)/DEM
   GJ TJ 20
3   R3=R1
   S3=S1
   CJI=SQRT(R3*R3+S3*S3)
   R2=SQRT((CJI+R3)*.5)
   IF (S3)10,10,100
10  S2=S3
   GJ TJ 20
100 S4=SQRT((CJI-R3)*.5)
   S2=SIGN(S4,S3)
   GJ TJ 20
4   SA=EXP(R1)
   R2=SA*COS(S1)
   S2=SA*SIN(S1)
20  CONTINUE
   RETURN
   END
```

```
      SUBROUTINE R-FITS(DB1,DL,TB1,T,WS,WT,RK,SK ,NR,A,B,AA,BB,E,F,F2,
1  J1,J2,J3,J4,J5)
      DIMENSION AR(500),BR(500),AAR(500),BBR(500),CJUT(500)
1005 FORMAT(1H0,15X,71H NUMBER INTERACTIONS EXCEEDED 100.DECREASE VALU
      IE OF INCREMENT DR AND DI)
      KC=0
      F3=F
      F1=F2
      IF(NR) 25,25,100
25  CONTINUE
      SKT=6.28*F3/T
      IF(RK-.05)30,30,50
30  R1=DB1/DL
      S1=WT/DL
      IF(RK)500,500,200
50  CONTINUE
      DB2=DB1
      DL2=DL
      TB2=TB1
      T2=T
      WS2=WS
      WT2=WT
      RK2=RK
      CALL GUESS(DB2,DL2,TB2,T2,WS2,WT2,RK2,R1,S1,J1,J2,J3,J4,J5)
      GO TO 200
100  CONTINUE
      S2=BR(NR)
      S1=BR(1)
      S1=-S2+S1
      IF(NR-2)90,90,95
90  R1=AR(1)
      GO TO 96
95  R1=AR(NR-1)
96  CONTINUE
      IF(MOD(NR,2))105,200,105
105  CONTINUE
      IF(S1)700,400,700
700  S1=S1+ SIGN(SKT,S1)
      GO TO 200
400  S1=S1+SKT
200  CONTINUE
      CJU=0.
201  IDY=1
      R=R1
      S=S1
      IF(F1)210,207,210
207  F1=1.
210  CONTINUE
      RC1=DB1-DL*R
      SC1=WT-DL*S
      RC2=TB1-T*R
      SC2=WS-T*S
      CALL CMPLX(J4,RC2,SC2,RC3,SC3,J5,J5)
      CALL CMPLX(J1,RC1,SC1,RC3,SC3,RC4,SC4)
      Y1=RC4-RK
      Z1=SC4+SK
      CJU=CJU+1.
      NCT=NCT+1
```

```
RC5=DL+T*RC1
SC5=T+SC1
CALL CMPLX(CJ1,RC3,SC3,RC5,SC5,YP,ZP)
CALL CMPLX(CJ2,Y1,Z1,YP,ZP,DR,DS)
R1=R+DR*F1
S1=S+DS*F1
250 CONTINUE
RE=ABS(DR/R)
IF(S) 7000,7001,7000
7001 SE=0.
GO TO 7002
7000 SE=ABS(DS/S)
7002 CONTINUE
IF(RE-E)255,255,260
255 IF(SE-E)270,270,260
260 R=R1
S=S1
IF(C)U-99.)210,210,268
268 KC=1
GO TO 600
270 CONTINUE
500 A=R1
B=S1
NR=NR+1
AR(NR)=R1
BR(NR)=S1
CALL CMPLX(CJ3,R1,S1,RC1,SC1,J5,J5)
AA=RC1
BB=SC1
AAR(NR)=RC1
BBR(NR)=SC1
CUUT(NR)=CJU
IF(NR-100)610,510,510
510 KC=1
600 IF(KC)610,610,605
605 WRITE(6,1005)
E=10.
610 RETURN
END
```

```
SUBROUTINE GUESS(OB1,DL,TB1,T,WS,WT,RK,R1,S1,J1,J2,J3,J4,J5)
IF(WS-WT)1,2,2
1 NW=1
WFAC=WT
GO TO 5
2 NW=-1
WFAC=WS
5 CONTINUE
DT=OB1-1.
IF(TB1-DT)7,8,8
7 NC=1
TFAC=DT
GO TO 10
8 NC=-1
TFAC=TB1
10 CONTINUE
IF(WFAC-TFAC)12,13,13
```

```

12 NU=NC
   GJ TJ 15
13 NU=NW
15 CONTINUE
   IF (NJ)20,20,50
20 TIG=DL+T
   RI=(-ALIG(RK)+DT+TB1)/TIG
   SI=(WS+WF)/TIG
   GJ TJ 100
50 CONTINUE
   TLF=2.*T*DL
   P1=T*DB1+DL
   Q1=WT*T
   P2=Q2
   CALL CMPLX(CJ4,-TB1,-WS,P2,Q2,J5,J5)
   P3=DB1-RK*P2
   Q3=WT-RK*Q2
   P4=Q4
   CALL CMPLX(CJ1,P1,Q1,P1,Q1,P4,Q4)
   P5=P4-2.*TLF*P3
   Q5=Q4-2.*TLF*Q3
   CALL CMPLX(CJ3,P5,Q5,P3,Q3,J5,J5)
   R1=(P1-P3)/TLF
   S1=(Q1-Q3)/TLF
100 CONTINUE
   RETURN
   END

```

```

SUBROUTINE PLITTER(I1,I2,I3,I4,NF,PEXP)
  DIMENSION X(500),Y(500)
  DIMENSION FR(2),AM(2),TEXT1(4),TEXT2(4),TEXT3(6),TEXT4(2),TEXT5(2)
  COMMON FR0(500),A1(500),A2(500),THE(500),TH2(500)
  COMMON EXDAT(14)
  DATA AM(1)/8AMPLITUDE/,AM(2)/8HE /,FR(1)/8FREQUENCY/,FR(2)/8
1HY (HZ) /,TEXT1(1)/8THEORETICAL/,TEXT1(2)/8CALIBRATION/,TEXT1(3)/8SF
2ER FUN/,TEXT1(4)/8CONTIN /,TEXT2(1)/8FERMI AG/,TEXT2(2)/8HE-DIF
3FUS/,TEXT2(3)/8HIDDEN MIDE/,TEXT2(4)/8HL /,TEXT3(1)/8COMPARIS
4/,TEXT3(2)/8H IN EXPER/,TEXT3(3)/8HMENTAL /,TEXT3(4)/8HAND THEU/,T
5EXT3(5)/8HRETICAL /,TEXT3(6)/8HRESULTS /,TEXT4(1)/8THEORETICAL/,TEXT
64(2)/8CAL /,TEXT5(1)/8EXPERIMENT/,TEXT5(2)/8HNTAL /
  CJEFF=EXDAT(1)/A1(2)
  DO 1 I=1,NF-1
    X(I)=ALOG10(FR0(I+1))*1.25
    Y(I)=A1(I+1)*2.5
  2 Y(I)=Y(I)*CJEFF
  1 CONTINUE
  CALL HGPLUT(-5.0,10.0,0,4)
  CALL HGPLJGAXIS(0.0,0.0,FR,-11,5.0,0.0,0,4)
  CALL HGPAxisV(0.0,0.0,AM,I2,2.5,90.0,0.0,0.2,0.5,2)
  IF(PEXP)5,5,6
  6 CALL HGPSYMBL(0.0,3.5,0.125,TEXT3,0.0,47)
  CALL HGPSYMBL(3.5,3.04,0.12,TEXT4,0.0,11)
  CALL HGPSYMBL(3.5,2.74,0.12,TEXT5,0.0,12)
  CALL HGPLUT(3.0,3.1,3,0)
  CALL HGPLUT(3.3,3.1,2,0)
  CALL HGPLUT(3.1,2.8,3,0)

```

```
CALL HGPILOT(3.2,2.8,2,0)
CALL HGPILOT(3.15,2.85,3,0)
CALL HGPILOT(3.15,2.75,2,0)
GO TO 7
5 CALL HGPSYMP(0.00,3.5,0.15,TEXT1,0.0,13)
7 CALL HGPSYMP(0.00,3.1,0.1,TEXT2,0.0,14)
CALL HGPCURVE(X,Y,NF-1,0,0.0,0,0)
IF(PEXP)3,3,4
4 CALL PLOTDCROSS
3 CALL CLOSEPLOT
RETURN
END
```

```
SUBROUTINE PLOTDCROSS
DIMENSION X(14),Y(14),EXFR(14),XX(15),YY(15)
COMMON FPO(500),A1(500),A2(500),THE(500),TH2(500)
COMMON EXDAT(14)
DATA EXFR/1.0,47.8,95.0,145.00,198.0,277.0,285.0,435.0,490.0,594.0
1,831.0,950.0,1470.0,2850.0/
S=0.05
DO 1 I=1,14
X(I)=ALOG10(EXFR(I))*1.25
Y(I)=EXDAT(I)*2.5
XX(I)=X(I)
YY(I)=Y(I)
CALL HGPILOT(X(I),Y(I),3,0)
CALL HGPILOT(X(I)+S,Y(I),2,0)
CALL HGPILOT(X(I)-S,Y(I),1,0)
CALL HGPILOT(X(I),Y(I),1,0)
CALL HGPILOT(X(I),Y(I)+S,1,0)
CALL HGPILOT(X(I),Y(I)-S,1,0)
CALL HGPILOT(X(I),Y(I),1,0)
1 CONTINUE
XX(15)=3.15
YY(15)=2.8
CALL ASTSYMBOL(XX,YY,15,1,0.03,0)
RETURN
END
FINISH
```

2.- EXAMPLE INPUT DATA(FORMATS DO NOT CORRESPOND)

1	1						
0.9767	0.9425	0.9227	0.8926	0.8625	0.8400	0.8292	
0.7683	0.7287	0.6987	0.6437	0.5352	0.4490	0.2265	
2000	50						
39.0	81.3	0.04	0.0065	12.7	0.0	15.0	
1.9	40.6	0.000013	0.000084	0.845	0.845	0.5	

3.- LINEPRINTER OUTPUT EXAMPLE

SPACE-DEPENDENT TRANSFER FUNCTION IN A CYLINDRICAL, HOMOGENEOUS AND  
MULTIPLYING NUCLEAR SYSTEM

FERMI AGE-DIFFUSION MODEL

NUCLEAR SYSTEM CHARACTERISTICS:

RADIUS SYSTEM = 39.00CM.  
HEIGHT SYSTEM = 81.30CM.  
MULTIPLYING FACTOR = 0.8450  
DIFFUSION LENGTH = 1.900CM.  
FERMI AGE = 40.60CM<sup>2</sup>.  
THERMAL LIFETIME = 0.000084SECS.  
FAST LIFETIME = 0.000013SECS.  
BETA = 0.006500  
TAU = 12.7000

NUMERICAL PARAMETERS:

TOTAL ERROR = 0.04000  
ERROR ALLOWED FOR ROOTS OF CHARACTERISTIC EQUATION = 0.00100  
INCREMENT FOR CONVERGENCY ON DR AND DI = 0.50000

THE TRANSFER FUNCTION IS BEING CALCULATED FOR THE FOLLOWING POSITION

RADIAL = 0.000CM.  
AXIAL = 15.000

FREQ	REAL	IMAG	AMP	DB	THETA	THETA	TERMS
0.000000E 00	0.100000E 01	0.5080423E-01	0.1001290E 01	0.1119500E-01	0.2908367E 01	0.1770916E 03	20.
0.100000E 01	0.9891722E 00	0.4928005E-01	0.9903990E 00	-0.8379605E-01	0.2852088E 01	0.1771479E 03	20.
0.500000E 02	0.9262644E 00	-0.2728222E-01	0.9830031E 00	-0.1480026E 00	-0.1590391E 01	0.1815904E 03	16.
0.100000E 03	0.630052E 00	-0.1011503E 00	0.9683029E 00	-0.2797756E 00	-0.5096141E 01	0.1859961E 03	14.
0.150000E 03	0.9285429E 00	-0.1667151E 00	0.9433996E 00	-0.5061688E 00	-0.1017871E 02	0.1901787E 03	10.
0.200000E 03	0.8914060E 00	-0.2280843E 00	0.9201235E 00	-0.7230776E 00	-0.145237E 02	0.1943524E 03	10.
0.250000E 03	0.8482712E 00	-0.2805833E 00	0.8934713E 00	-0.9763679E 00	-0.1830270E 02	0.1983027E 03	10.
0.300000E 03	0.8016451E 00	-0.3240481E 00	0.8646631E 00	-0.1263061E 01	-0.2201000E 02	0.2020100E 03	10.
0.350000E 03	0.7535545E 00	-0.3590911E 00	0.8347400E 00	-0.1568975E 01	-0.2547919E 02	0.2054792E 03	10.
0.400000E 03	0.7055053E 00	-0.3864163E 00	0.8043976E 00	-0.1890585E 01	-0.2871022E 02	0.2087102E 03	10.
0.450000E 03	0.6586675E 00	-0.4070719E 00	0.7743062E 00	-0.2221745E 01	-0.3171701E 02	0.2117170E 03	10.
0.500000E 03	0.6065410E 00	-0.4131243E 00	0.7338690E 00	-0.2687629E 01	-0.3425938E 02	0.2142594E 03	13.
0.550000E 03	0.5640334E 00	-0.4233355E 00	0.7052281E 00	-0.3033408E 01	-0.3689008E 02	0.2168901E 03	13.
0.600000E 03	0.5240900E 00	-0.4297271E 00	0.6777431E 00	-0.337698E 01	-0.3935001E 02	0.2193500E 03	13.
0.650000E 03	0.4880706E 00	-0.4343469E 00	0.6533329E 00	-0.3697043E 01	-0.4166672E 02	0.2216667E 03	15.
0.700000E 03	0.4533104E 00	-0.4350671E 00	0.6283102E 00	-0.4036518E 01	-0.4382357E 02	0.2238236E 03	15.
0.750000E 03	0.4210385E 00	-0.4337804E 00	0.6045154E 00	-0.4371853E 01	-0.4583398E 02	0.2258540E 03	15.
0.800000E 03	0.3936449E 00	-0.4332050E 00	0.5853400E 00	-0.4651836E 01	-0.4773919E 02	0.2277392E 03	17.
0.850000E 03	0.3659126E 00	-0.4290300E 00	0.5638832E 00	-0.4976186E 01	-0.4954028E 02	0.2295403E 03	17.
0.900000E 03	0.3402268E 00	-0.4238801E 00	0.5435405E 00	-0.5293562E 01	-0.5124837E 02	0.2312484E 03	17.
0.950000E 03	0.3164224E 00	-0.4179589E 00	0.5242359E 00	-0.5609630E 01	-0.5287188E 02	0.2328719E 03	17.
1.000000E 04	0.2943681E 00	-0.4114334E 00	0.5058953E 00	-0.5918787E 01	-0.5441743E 02	0.2344174E 03	17.
0.105000E 04	0.2739397E 00	-0.4044563E 00	0.4884955E 00	-0.6222789E 01	-0.5589008E 02	0.2358901E 03	17.
0.110000E 04	0.2549864E 00	-0.3971513E 00	0.4719611E 00	-0.6521877E 01	-0.5729797E 02	0.2372980E 03	17.
0.115000E 04	0.2373798E 00	-0.3896139E 00	0.4562343E 00	-0.6816242E 01	-0.5864746E 02	0.2386475E 03	17.
0.120000E 04	0.2236176E 00	-0.3840409E 00	0.4444010E 00	-0.7044499E 01	-0.5978881E 02	0.2397888E 03	19.
0.125000E 04	0.1943221E 00	-0.3762885E 00	0.4301611E 00	-0.7327377E 01	-0.6101679E 02	0.2410168E 03	19.
0.130000E 04	0.1811941E 00	-0.3685024E 00	0.4165995E 00	-0.7605626E 01	-0.6219600E 02	0.2421960E 03	19.
0.135000E 04	0.1689742E 00	-0.3607235E 00	0.4038741E 00	-0.7879383E 01	-0.6332929E 02	0.2433293E 03	19.
0.140000E 04	0.1576051E 00	-0.3529875E 00	0.3913469E 00	-0.8148761E 01	-0.6441968E 02	0.2444197E 03	19.
0.145000E 04	0.1469991E 00	-0.3453342E 00	0.3795986E 00	-0.8413508E 01	-0.6546880E 02	0.2454688E 03	19.
0.150000E 04	0.1469991E 00	-0.3377606E 00	0.3683707E 00	-0.8674297E 01	-0.6648107E 02	0.2464811E 03	19.
0.155000E 04	0.1371621E 00	-0.3303218E 00	0.3576673E 00	-0.8930414E 01	-0.6744993E 02	0.2474499E 03	19.
0.160000E 04	0.1279329E 00	-0.3229022E 00	0.3474058E 00	-0.9183260E 01	-0.6839214E 02	0.2483921E 03	19.
0.165000E 04	0.1193093E 00	-0.3158050E 00	0.3375907E 00	-0.9432190E 01	-0.6930373E 02	0.2493037E 03	19.
0.170000E 04	0.1112562E 00	-0.3087675E 00	0.328001E 00	-0.9677225E 01	-0.7018472E 02	0.2501847E 03	19.
0.175000E 04	0.1037238E 00	-0.3018814E 00	0.3192037E 00	-0.9918642E 01	-0.7103772E 02	0.2510377E 03	19.
0.180000E 04	0.9667800E-01	-0.295157E 00	0.310856E 00	-0.1015637E 02	-0.7186384E 02	0.2518638E 03	19.
0.185000E 04	0.9007573E-01	-0.2886044E 00	0.3023345E 00	-0.1039025E 02	-0.7266644E 02	0.2526664E 03	19.
0.190000E 04	0.8389361E-01	-0.2822064E 00	0.2944123E 00	-0.1062088E 02	-0.7344397E 02	0.2534440E 03	19.
0.195000E 04	0.7809915E-01	-0.2759681E 00	0.2868063E 00	-0.1084823E 02	-0.7419845E 02	0.2541985E 03	19.
0.200000E 04	0.7266779E-01	-0.2698645E 00	0.2795061E 00	-0.1107218E 02	-0.7493074E 02	0.2549307E 03	19.

4. GRAPHPLOTTER OUTPUT EXAMPLE

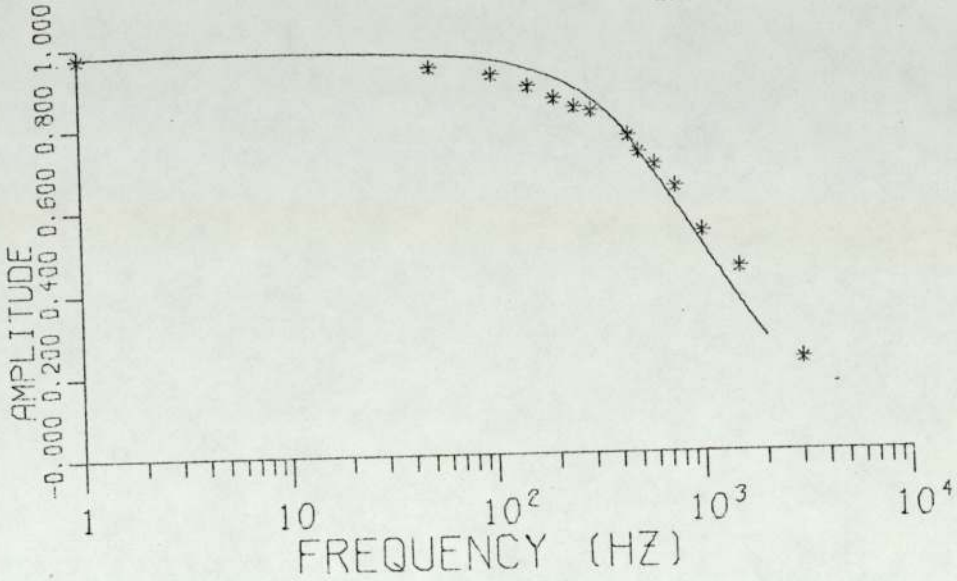
A - PEXP=1

COMPARISON EXPERIMENTAL AND THEORETICAL RESULTS

FERMI AGE-DIFFUSION MODEL

— THEORETICAL

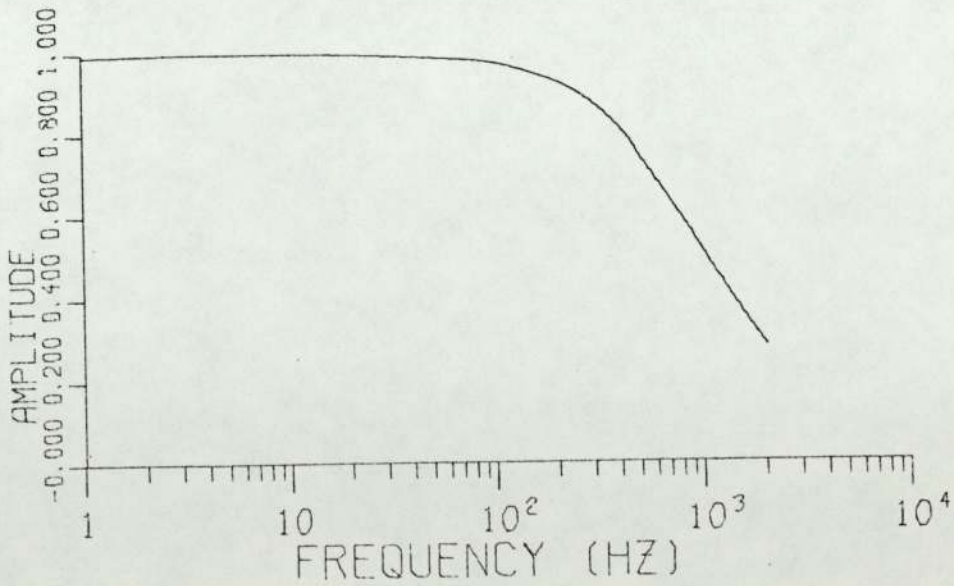
\* EXPERIMENTAL



B - PEXP=0

THEORETICAL TRANSFER FUNCTION

FERMI AGE-DIFFUSION MODEL



REFERENCES

- (1) - Manley, J.H., et al., Phys.Rev., 61, 152, 1942.
- (2) - Beckurts, K.H., Reactor Physics Research with Pulsed Neutron Sources, Nuc.Inst. and Methods, 11, 144-168, 1961.
- (3) - Lopez, W.M., and Beyster, J.R., Measurements of Neutron Diffusion Parameters in Water by the Pulsed Neutron Method, Nuc.Sci. and Engineering, 12, 190-202, 1962.
- (4) - Starr, E., and Devilliers, J.W.L., Measurements of the Diffusion Parameters of Carbon Block, Trans.Am.Nucl.Society, 7(1), 45, 1964.
- (5) - Miley, G.H., and Doshi, P.E., Reactor-Pulse Propagation through Graphite, Trans.Am.Nucl. Society, 7(1), 45-46, 1964.
- (6) - Ghatak, A.K., and Honeck, H.C., Approach to Equilibrium of a Neutron Pulse in Graphite, Trans.Am.Nucl.Society, 7(1), 46-47, 1964.
- (7) - Garelis, E., and Russell, J.L., Theory of Pulsed Neutron Source Measurements, Nucl.Sci. and Engineering, 16, 263-270, 1963.
- (8) - Brown, J.R., et al., Measurements of Subcritical Reactivity Using a Pulsed-Neutron Source, Trans.Am.Nucl.Society, 6(2), 284-285, 1963.
- (9) - Weinberg, A.M., and Schwinger, H.C., Theory of Oscillating Absorber in a Chain Reactor, Phys.Rev., 74, 851, 1948.

- (10) - Weinberg, A.M., and Wigner, E.P., The Physical Theory of Neutron Chain Reactors, University of Chicago Press, P 235, 1958.
- (11) - Raievski, V., and Horowitz, I., Determination of the Mean Free Path of Thermal Neutrons by Measurement of the Complex Diffusion Length, Proc.Int.Conf. on Peaceful Uses of Atomic Energy, U.N., New York, Geneva, 5(42), 1955.
- (12) - Uhrig, R.E., Neutron Waves in a Subcritical Assembly, Trans.Am.Nucl. Society, 2(2), 1959.
- (13) - Uhrig, R.E., Oscillatory Techniques in a Subcritical Assembly, Proc. 1961 Univ.Conf. on Subcritical Assemblies, Rep. TID 7619, 1962.
- (14) - Perez, R.B., and Uhrig, R.E., Propagation of Neutron Waves in Moderating Media, Nucl.Sci. and Engineering 17, 90-100, 1963.
- (15) - Perez, R.B., and Uhrig, R.E., Development of Techniques of Neutron-Wave and Neutron Pulse Propagation, Proc.Symp.Neutron Noise, Waves and Pulse Propagation, AEC Symposium Series 9, U.S.AEC, 1, 1967.
- (16) - Mortensen, G.A., and Smith, H.P., Neutron Wave Propagation Using the P1 Approximation, Nucl.Sci. and Engineering, 22, 321-327, 1965.
- (17) - Moore, M.N., The Dispersion Law of a Moderator, Nuclear Sci. and Engineering, 26, 3, 354, 1966.
- (18) - Williams, M.M.R., The Dispersion Law of a Neutron Wave in a Finite System, J.of Nucl.Energy, 22, 153, 1968.

- (19) - Wood, J., An Interpretation of the Neutron Wave Experiment, J.of Nucl.Energy, 23, 17, 1969.
- (20) - Brehm, R.L., Analysis of Neutron-Wave Type Experiments, Proc.Symp.Neutron Noise and Pulse Propagation, AEC Symposium Series 9, U.S.AEC, 69, 1967.
- (21) - Kunaish, H.H., Consistent P3 Theory of Neutron-Wave Propagation, Proc.Symp.Neutron Noise, Waves and Pulse Propagation, AEC Symposium Series 9 U.S.AEC, 87, 1967.
- (22) - Doukas, L., Reactivity Investigations Using a Periodic Neutron Source in a Subcritical Assembly, Ph.D. Dissertation, Dept.of Physics, U.of Aston in Birmingham, Nov. 1971.
- (23) - Cohn, C.E., et al., Calculating Space Dependent Reactor Transfer Functions Using Static Techniques, Nucl.Sci. and Engineering, 26, 198-206, 1966.
- (24) - Schultz, M.A., Control of Nuclear Reactors and Power Plants, McGraw Hill, New York, 1961.
- (25) - Glasstone, S., and Edlund, M.C., The Elements of Nuclear Reactor Theory, C.Van Nostrand Co., Inc., 1963.
- (26) - Kylstra, C.D., and Uhrig, R.E., Measurements of the Spatially Dependent Transfer Functions, TID-7679, Proc.Symp. Noise Analysis in Nuclear Systems, Gainesville, Florida, Nov. 1963.
- (27) - Keepin, G.R., Physics of Nuclear Kinetics, Addison and Wesley Inc., 1965.

- (28) - Cooper, P.N., The Physical Design of an Organic Moderated Reactor, AERE-RS/L225, 1958.
- (29) - Twim-Danso, L., Investigation on Neutron Diffusion Parameters in Liquid Moderators and Liquid Moderated Multiplying Assemblies, Ph.D., Dissertation, Dept.of Physics, University of Aston in Birmingham, 1969.
- (30) - Cooper, P.N., and Doukas, L., External Pulsing of an Accelerator, Nuc.Inst. and Methods, 92, 1971, 581.
- (31) - Hanna, N.N., et al., J.Nucl.Eng., 22, 587, 1968.
- (32) - Millar, P., Electronic Eng., 25, 446-506, 1953.
- (33) - Gil Ramos, A., and Cooper, P.N., Improvements to a Method of Externally Pulsing an Accelerator, Nucl.Inst.and Methods, 109, 1973, 617-618.
- (34) - Price, W.J., Nuclear Radiation Detection, McGraw-Hill, 1964.
- (35) - Neutron Cross Section Evaluation Group, Nucleonics, 19, 73, 1961.
- (36) - Mills, W.R., et al., Rev.Sci.Instr., 33, 866, 1962.
- (37) - Abson, W., et al., Proc.Inst.Elect.Eng., 105B, 349, 1958.
- (38) - Batchelor, R., et al., Rev.Sci.Instr., 26, 1037, 1955.
- (39) - Neutron Cross-Sections, BNL Supplement N<sup>o</sup>2, 325, 1964.
- (40) - Day, R.B., Physics Review, 102, 767, 1956.
- (41) - Neutron Cross-Sections, B.N.L., 325, 1958.
- (42) - Aitken, J.H., and Dixon, W.R., Nuclear Physics, 67, 395, 1965.

- (43) - Mann, H.M., and Antenna, J.L., IEEE, Trans.Nucl. Sci., NS. 11, N<sup>2</sup>3, 201, 1964.
- (44) - Grodstein, G.W., National Bureau of Standards, Circular NBS-583.
- (45) - Boas, M.L., Mathematical Methods in the Physical Sciences, John Wiley & Sons, Inc., 287, 1966.
- (46) - Stephenson, G., Mathematical Methods for Science Students, Longmans, 240, 1966.
- (47) - Goertzel, G., Mathematical Methods for Digital Computers, John Wiley & Sons, Inc., 258, 1960.
- (48) - Scheid, F., Theory and Problems of Numerical Analysis, McGraw Hill, 293, 1968.
- (49) - Hildebrand, F.B., Numerical Analysis, McGraw Hill, New York, 1955.
- (50) - Hamming, R.W., Numerical Methods for Scientists and Engineers, McGraw Hill, 68, 1962.
- (51) - Goertzel, G., An algorithm for the Evaluation of Finite Trigonometric Series, Amer.Math.Monthly, Vol. 65, 34, 1958.
- (52) - Mifsud, C.J., Collected Algorithms from CACM, CACM Library Algorithm 157.
- (53) - Abbott, J.M., The Graphplotter, GP/117/1, Computer Centre, University of Aston, March 1971.
- (54) - Subroutine UAD1; Computer Centre Subroutines Package, University of Aston.
- (55) - Bridges, D.N., and Clement, J.D., An investigation on space-dependent reactor transfer functions with temperature feedback, Nucl.Sci. and Engineering, 47, 421-434, 1972.

- (56) - Jeffers, D.E., Spatial Transfer functions of a two core reactor, ATKE, 16-23, (129-131), 1970.
- (57) - Meghreblian, R.V., and Holmes, D.K., Reactor Analysis, McGraw-Hill Co., New York, 351, 1960.
- (58) - McCallien, C.W.J., 'SNAP', a two dimensional neutron diffusion code, TRG Report 1990(R), UKAEA, Reactor Group, Warrington, Lancashire.
- (59) - McCallien, C.W.J., Squifid and Snap: Some programming details, Risley Computer Section, UKAEA, RCN7/70, Sept.1971.
- (60) - McCallien, Private communication, 1974.
- (61) - Munday, P.J., 'SNAP', TNPG/MTS.Int. 1779, The Nuclear Power Group Ltd., Radbroke Hall, Knutsford, Cheshire, Feb.1971.
- (62) - Munday, P.J., 'SNAP 2', TNPG/MTS.Int.1779, The Nuclear Power Group Ltd., Radbroke Hall, Knutsford, Cheshire, May,1971.
- (63) - Hassitt,A., CRAM; A Computer Program to solve the Multigroup Diffusion Equations, TRG Report 229(r), Reactor Engineering Laboratory, Risley, 1962.
- (64) - McCallien, C.W.J., The Solution of Reactor Diffusion Problems, The Computer Journal, Vol.13, N 4, Nov.1970.
- (65) - Kylstra, C.D., and Uhrig, R.E., Spatially Dependent Transfer Functions for Nuclear Systems, Nucl.Sci.and Engineering, 22, 191-205, 1965.
- (66) - Kylstra, C.D., Spatially Dependent Transfer Function for Nuclear Systems by Cross Correlation Methods; Ph.D. dissertation, University of Florida, Dec.1963.

- (67) - Chang-hwa-shen, Noise Analysis of Pennsylvania State University Reactor, M.Sc.Thesis, Pennsylvania State University, 1964.
- (68) - Kenney, E., Neutron Noise, waves and Pulse Propagation, CONF-660206, USAEC Symposium Series 9, 1967.
- (69) - Carpenter, J.M., and Lehto, W.K., Nucl.Appl., 3, 750, 1967.
- (70) - Lehto, W.K., and Carpenter, J.M., Reactor Noise Measurements using gamma rays, Nucl.Sci.and Eng., 32, 142-145, 1967.
- (71) - Lehto, W.K., and Carpenter, J.M., Determination of Reactor Kinetic Parameters by Photon Observation, Nucl.Sci. and Eng., 33, 225-237, 1968.
- (72) - Gelinas, R.J., and Osborn, R.K., Reactor Noise Analysis by Photon Observation, Nucl.Sci. and Eng., 24, 184-192, 1966.
- (73) - Bars, B., and Markkanen, E., Reactor Parameters from Neutron and Gamma-ray Noise Measurements, Nucl.Sci. and Eng., 48, 202-210, 1972.
- (74) - Reactor Physics Constants, ANL-5800, second ed., p.630, ANL, 1963.
- (75) - Meinschein, F.C., et al., Gamma Rays associated with Fission, Second U.N. International Conference on Peaceful uses of Atomic Energy, A/Conf. 15/P/670, June 1958.

- (76) - Chapman, G.T. et al., Pulse Height Spectra of  
Gamma Rays emitted by the Stainless Steel Clad  
Bulk Shielding Reactor II(BSR-KK), ORNL - 3609,  
1964.